A Cab for Insulin

Characterising Cab45 in Pancreatic β-Cells

Mark Germanos

In fulfilment of the requirements of the degree

Doctor of Philosophy

Faculty of Medicine and Health

The University of Sydney

2022

Table of Contents

(This page is intentionally left blank)

Declaration

I declare that this thesis is less than 80,000 words, exclusive of references and appendices. I certify that the ideas and interpretations presented in this thesis are the product of my own intellect. This project was truly a collaborative one, and the following statements detail the individuals who contributed to generating results that have been presented. All have given permission to present their work here.

Prof. Nabil Seidah conducted the work presented in Figure 10.

Dr. Belinda Yau and Dr. Sheyda Naghiloo performed imaging for Figure 12A.

Dr. Louise Cottle performed imaging for Figure 12C.

Dr. Belinda Yau performed the islet isolation in Figure 13A and A/Prof. Melkam Kebede ran the Western blot.

Dr. Belinda Yau performed the subcellular fractionation protocol in Figure 14A and I performed the Western blotting.

Dr. Jerome Cattin and Dr. Belinda Yau performed staining and imaging in Figure 14B, and Belinda conducted the colocalisation analysis.

Matthew Taper reproduced experiments that I had initially conducted, but with extended time points, under my supervision in Figure 16. Matthew performed all of the analysis.

Dr. Jerome Cattin with A/Prof. Michael Ailion performed stable transfection, colocalisation, and secretion experiments in Figure 17.

A/Prof. Cedric Asensio generated the Cab45KO INS1 cells used in Section 3.3.1.

Dr. Mark Larance performed label free quantification proteomics on Cab45KO INS1 cells. Dr. Sheyda Naghiloo generated subsequent figures presented in Figure 18.

Dr. Belinda Yau produced the results that are presented in Figures 19 and 20A.

Amy Wilson generated some data for the overnight rescue of insulin SG content presented in Figure 22.

Matthew Taper performed the transfection experiments presented in Figure 23 under my supervision. I acquired the images and together we performed the analysis.

Yousun An, Amy Wilson and Dr. Belinda Yau performed insulin secretion assays in Cab45KO INS1 cells presented in Figures 24 and 25.

Jason Tong performed the Fura-2 experiments in Cab45KO INS1 cells presented in Figure 26. In doing so, I followed and learned the protocol and conducted the Fura-2 experiments presented in Figure 33.

Dr. Jerome Cattin with A/Prof. Michael Ailion performed the siRNA depletion of Cab45 from INS1 cells and PC1/3 secretion experiments in Figure 27.

Most of the work on Cab45KO MIN6 cells in section 3.3.2 was performed by myself with some secretion experiments performed by Dr. Belinda Yau and Matthew Taper. Dr. Sheyda Naghiloo conducted imaging on these cells.

Characterisation of βCab45 mice was performed with Dr. Belinda Yau. Belinda also handled the islet isolations and preparation of islets for GSIS assays in Figure 41, performing several of the assays as well. Since her absence on maternity leave, Dr. Amanda Brandon has been very helpful in stepping in to help with the OGTTs.

Of course, my supervisor A/Prof. Melkam Kebede as well as long-term postdoc Dr. Belinda Yau have both contributed immensely to the strategy and implementation of this project, and the interpretation of findings.

Now, all of those who have contributed work to this project have been acknowledged.

- ***Mark Germanos***

Acknowledgements

In classic Mark Germanos style, I have left this to the very last minute. In fact, I am currently in the negative of minutes that I have left right now so I will do this from the top of my head. This is an extremely common occurrence so if you are a potential employer reading this I would exercise caution if you are considering my hiring.

To all of my family, friends, and colleagues, you all mean the world to me. It's taken a long time to get to this point but we made it! Dr. G!! This would not have been possible without you all.

Firstly, thanks to those who showed me the ropes and made this project happen. Melkam, thank you for believing in my intelligence even when I made it seem clear that I had none. With your tutelage, I have become one of the smartest minds to have ever graced this earth. Belinda, similarly, thank you for your patience in dealing with my general incompetence in the lab. With your guidance, I have become one of the most prolific data generators that this world has ever seen. All jokes aside, you both pushed me to push myself and learn how to perform in an arena that was completely unfamiliar at first, and for that learning experience I am forever grateful.

Sheyda, thank you for making me feel welcome, comfortable, and at home when I first joined the lab. The warmth extends to everyone who has come through the Kebede lab (Sunny, Nick, Matt, Andy, Amy, and newcomers Gab and Cara, among others), and CPC Level 5 West over the years. Also, thanks to Peter Thorn for being a great co-supervisor, and the David James laboratory for opening the doors to their lab meetings and providing us with fantastic examples of how to do science early on in development when I was just a baby scientist. I am still a baby but hopefully I can chew my own food now at least. I would also like to extend my gratitude to John and Ruth Fell who have helped me develop as a coach and trainer - there is no way this would have been achieved without your ongoing support throughout my undergraduate and postgraduate degrees.

Now, my family, I did this all for you. You were what kept me going when things got hard. Dad, you have been a steady rock for all of these years, and I hope to someday repay you for all your hard work. Mum, thanks for all of the reassuring conversations that we have had. Victor, you have an abnormally large heart (trust me I'm a Dr. now), and it is inspiring how you are able to wear it on your sleeve. Rada, also with an abnormally large heart that remains more so the inside (like me), never stop reminding us to fight for what we believe in and for what is right. And to each of our cousins and the rest of our family, thank you for leading the way and showing us how it's done.

My mates, cheers for being legends and for holding it down in your own lives. We came up together and have been on some wild adventures, and couldn't ask for a better group of blokes to share this experience with. And my incredible girlfriend Kitty, props to you for being almost as cool as the rest of my friends. I would not replace a single one of you for anyone in this world except for maybe you Kitty but only with one of the boys if the opportunity ever arises. Nah I'm just playing. That opportunity will never arise :(. Nah but actually, Kitty, you are the light of my life and you give me something to look forward to every time I wake up and every time I come home, except for the times that you come to the lab and do my work for me.

My people, I want to thank you all for being so patient, during both the times that I lost focus and the times that I gained it back. You all know that life is a bit complicated for me. I've been steady grinding since the day I looked around at primary school and realised that things were different for our family. To complete a task of this magnitude fulfils a desire that I have always had - to work at a high level and get the most out of myself. But just because we're done it doesn't mean we're going to stop. I'll always be putting in work. It's easy when you're surrounded by the best people.

(This page is intentionally left blank)

Publications

Chapter 1.2 of this thesis is published as Germanos et al., 2021. I conceptualised the manuscript with A/Prof. Melkam Kebede and Dr. Belinda Yau, and wrote the manuscript with all co-authors.

List of Abbreviations

2.8G	**2.8 mM glucose**
3G	**3 mM glucose**
16.7G	**16.7 mM glucose**
18G	**18 mM glucose**
6/J	**C57BL6/J**
ABR	**Australian Bioresources**
ADF	**Actin depolymerizing factor**
ATP	**Adenosine triphosphate**
AUC	**Area under the curve**
BCA	**Bicinchoninic acid**
BSA	**Bovine serum albumin**
Cab_{308}Myc	**Myc-tagged Cab45 mutant missing amino acids 309-361**
Cab45	**Calcium binding protein of 45 kDa**
CD	**Cation dependent**
CgA	**Chromogranin A**
CgB	**Chromogranin B**
CI	**Cation independent**
cKO	**Conditional knockout**
CPE, CPH	**Carboxypeptidase H/E**
CRE	**Ins1-Cre**
CREC	**Calumenin, Reticulocalbin, ERC-55, Cab45**
CRISPR	**Clustered regularly interspaced short palindromic repeats**
DAPI	**4,6'-diamidino-2-phenylindole, dihydrochloride**
db/db	**$C57BLKS^{db}$**
DMEM	**Dulbecco's Modified Eagle Medium**
EDTA	**Ethylenediaminetetraacetic acid**
EGTA	**Ethylene glycol-bis(β-aminoethyl ether)-N,N,N′,N′-tetraacetic acid**
ELISA	**Enzymes-linked immunosorbent assay**
EM	**Electron microscopy**
ER	**Endoplasmic reticulum**
FAT/CD36	**Fatty acid translocase**
FBS	**Foetal bovine serum**
FLOX	**SDF4-floxed**
Fura-2AM	**Fura-2-acetoxymethyl ester**
GRP	**Green fluorescent protein**
GSIS	**Glucose stimulated insulin secretion**
GWAS	**Genome wide association studies**
HA	**Hemagglutinin**

HAs	**Homology arms**
HEPES	**4-(2-hydroxyethyl)-1-piperazineethanesulfonic acid**
HET	**Heterozygous knockout**
HFHSD	**High fat high sucrose diet**
HG	**High glucose**
hGH	**Human growth hormone**
hIAPP	**Human islet amyloid polypeptide**
HREC	**Human research ethics committees**
HTRF	**Homogeneous time resolved fluorescence**
IAPP	**Islet amyloid polypeptide**
iAUC	**Incremental area under the curve**
Ins1	**Insulin-1 gene**
Ins2	**Insulin-2 gene**
IP_3	**Inositol 1,4,5-triphosphate**
IP_3R	**Inositol trisphosphate receptor**
ISG	**Immature secretory granule**
KCl	**Potassium chloride**
KD	**Knockdown**
KO	**Homozygous knockout**
KS/J	**C57BLKS/J**
KSIS	**Potassium chloride-stimulated insulin secretion**
LFQ	**Label free quantification**
LG	**Low glucose**
LIMK	**LIM kinase**
M6PR	**Mannose 6 phosphate**
mIAPP	**Mouse islet amyloid polypeptide**
MIP	**Mouse insulin promoter**
MSG	**Mature secretory granule**
NAADP	**Nicotinic acid adenine dinucleotide phosphate**
NHMRC	**National Health and Medical Research Council**
NOD	**Non-obese diabetic**
ob/ob	**C57BL6/J^{ob}**
OGTT	**Oral glucose tolerance test**
PAL	**Peptidyl-α-hydroxyglycine α-amidating lyase**
PAM	**Peptidyl-glycine alpha-amidating monooxygenase**
PBS	**Phosphate buffered saline**
PBST	**Phosphate buffered saline + 0.1% Tween 20**
PC	**Proprotein convertase**
PFK1	**1-phosphofructokinase**
PHM	**Peptidylglycine alpha-hydroxylating monooxygenase**

PM	**Plasma membrane**
PVDF	**Polyvinylidene difluoride**
RFP	**Red fluorescent protein**
rIAPP	**Rat islet amyloid polypeptide**
RIP	**Rat insulin promoter**
RIPA	**Radioimmunoprecipitation assay**
RPMI	**Roswell Park Memorial Institute**
RT	**Room temperature**
RyRs	**Ryanodine receptors**
SDC	**sodium deoxycholate**
SDF4	**Stromal cell derived factor 4**
SDS	**Sodium dodecyl sulphate**
SDS-PAGE	**Sodium dodecyl sulphate-polyacrylamide gel electrophoresis**
SEM	**Standard error of the**
SERCA2B	**Sarco/endoplasmic reticulum Ca^{2+}-ATPase**
SG	**Secretory granule**
SgII	**Secretogranin II**
SgIII	**Secretogranin III**
siCab45	**siRNA to Cab45**
siCtrl	**non-targeting siRNA control**
SPCA1	**Secretory pathway Ca^{2+} ATPase 1 (SPCA1)**
SSH1	**Protein phosphatase slingshot homologue 1**
T1D	**Type 1 diabetes**
T2D	**Type 2 diabetes**
TBS	**Tris buffered saline**
TBST	**Tris buffered saline + 0.1% Tween 20**
TCA	**Trichloroacetic acid**
TGN	**Trans-Golgi network**
Tris	**Tris(hydroxymethyl)aminomethane**
UniPort	**Universal Protein Resource**
V-ATPase	**Vacuolar H^{+}-ATPase**
VMAT2	**Vesicular monoamine transporter type-2**
VNUT	**Vesicular nucleotide transporter**
WFS1	**Wolfram syndrome 1**
WT	**Wild-type**
ZnT	**Zn^{2+} transporter**

(This page is intentionally left blank)

List of Figures

(This page is intentionally left blank)

Abstract

The pancreatic β-cell is purpose-built for the production and secretion of insulin, the only hormone that can remove glucose from the blood. Insulin is kept inside miniature membrane-bound storage compartments known as secretory granules, and these specialised organelles can readily fuse with the plasma membrane upon cellular stimulation to release insulin into the circulation. At this point in time, the mechanisms that govern the generation of insulin secretory granules are poorly defined. This is pertinent to understanding the molecular pathogenesis of type 2 diabetes, where a reduced population and/or compromised quality of secretory granules can contribute to the failure of β-cells to release enough insulin for the control of circulating glucose. Recently, a soluble 45 kDa Ca^{2+}-binding protein that localises to the Golgi apparatus, Cab45, has emerged as a promising candidate that could contribute to the initial stages of secretory granule biogenesis. In the constitutively secreting HeLa cell line, Cab45 sorts secretory cargo into vesicles from the Golgi apparatus. Its mode of action can be described as an aggregative mechanism that has preference for certain cargo, providing a means by which large volumes of protein can be directed through specific trafficking routes. This is a suitable mechanism for a cell such as the β-cell, which dedicates much of its energy to synthesising insulin and other secretory cargoes, but manages to consistently traffic this cargo with high accuracy. Presented here is the first investigation of Cab45 function in cell models that participate in regulated secretion. Cab45 expression is invariably correlated to β-cell function in both humans and in animal models of type 2 diabetes, and its experimental depletion impairs the function of all models that have been studied.

Chapter 1: Literature Review

1.1 Introduction

Glucose homeostasis and type 2 diabetes. In a healthy state, following the ingestion of a meal, the concentration of glucose in the blood increases and is sensed by pancreatic β-cells which respond by secreting insulin. Glucose-stimulated insulin secretion (GSIS) is biphasic, with an initial rapid first phase reaching a high peak that precedes a sustained low-amplitude second phase that can last for several hours (Curry, Bennett, and Grodsky 1968; Henquin et al. 2006; Z. Wang and Thurmond 2009). Circulating insulin binds to receptors expressed on target 'insulin-sensitive' tissues (muscle, fat and liver) to trigger coordinated cascades of signalling that regulate whole-body glucose homeostasis and return euglycaemia (**Figure 1A**) (James, Stöckli, and Birnbaum 2021). Gradual disruption to this axis, proceeding through several stages of pathogenesis, underlies the onset of type 2 diabetes (T2D) which is defined as a chronically elevated circulating blood glucose level. It is commonly understood that a combination of lifestyle and genetic factors contribute to its development, but precise aspects of its molecular aetiology are yet to be uncovered.

Insulin resistance and hyperinsulinaemia. Prolonged exposure of insulin-sensitive tissues to environmental stressors (i.e. those that are obesogenic and oxidative) can interfere with multiple aspects of cellular function and impair the response to insulin signalling (James, Stöckli, and Birnbaum 2021). This insulin resistant state is the initiating factor that creates a relative deficiency of insulin, where its capacity to mediate glucose uptake into tissues is reduced. As a result, the β-cells of the pancreas must compensate to elevate their production and secretion of insulin, bringing about a required state of hyperinsulinaemia. β-cells achieve this in two ways, through enhancing intracellular functions and by gaining mass via increases in cell size and number (Weir and Bonner-Weir 2004). While this compensatory mechanism is necessary to prevent dysregulated glucose homeostasis, hyperinsulinaemia presents its own set of health challenges and may even occur prior to and drive the development of obesity and metabolic diseases (James, Stöckli, and Birnbaum 2021).

Development of T2D. Intriguingly, most insulin-resistant individuals do not develop T2D, consistent with the understanding that many individuals possess β-cells that have the ability to persistently compensate in the face of metabolic stress (Prentki and Nolan 2006). Indeed, early genome wide association studies (GWAS) concluded that genetic variants associated with the disease predominantly involve proteins that are important for β-cell function (Billings and Florez 2010). Those with compromised β-cell function may not be able to persistently adapt to an elevated demand for insulin when required. Instead, gradual β-cell decompensation permits the progression from a state of insulin resistance to impaired glucose tolerance (prediabetes) and eventually T2D (Weir and Bonner-Weir 2004). Importantly, those experiencing prediabetes and the early stages of T2D continue

to display hyperinsulinaemia, demonstrating an active but insufficient attempt by the β-cells to compensate (Weir and Bonner-Weir 2004). Later stages of T2D however are characterised by a reduction in circulating insulin, indicating a deterioration of β-cell function and/or mass (β-cell failure) that can eventually progress to overt insulin-dependent T2D (Weir and Bonner-Weir 2004). Through all stages of T2D, the presence of a sustained hyperglycaemia causes a host of vascular and cellular complications that underlie the morbidity and mortality associated with the disease (Harding et al. 2019).

Islets of Langerhans. Pancreatic β-cells are one of three major endocrine cell types residing within the islets of Langerhans, which are small clusters of cells scattered amongst the exocrine pancreas. β-cells make up the majority of islet cell types (~60%), followed by the glucagon-producing α-cells (~25%), and the somatostatin producing δ-cells (~10%) (Da Silva Xavier 2018) (**Figure 1B**). γ- or PP-cells producing pancreatic polypeptide make up 1-2% of the population and several other cell types such as ε-cells that produce ghrelin also exist.

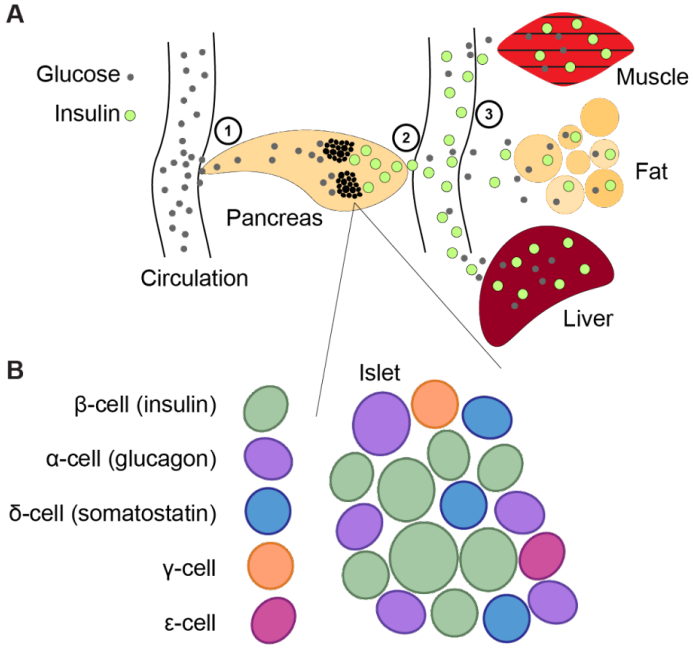

Figure 1. Systemic glucose control by pancreatic β-cells. **(A)** Basic schematic representation of systemic glucose regulation by insulin secreted from pancreatic β-cells. (1) Rise in circulating glucose sensed by the pancreatic β-cells. (2) Insulin is secreted by the pancreatic beta cells. (3) Insulin binds to receptors expressed on target tissues to facilitate glucose uptake from the circulation **(B)** Visualisation of the cell populations that compose the islets of Langerhans within the pancreas.

Successful compensation relies on the availability of biologically active insulin residing within pancreatic β-cells. The following subsection of this literature review (1.2) is re-printed (in American English, with updated section, figure and citation numbers) from a review article published in the journal *Metabolites* for the special Islet Biology and Metabolism Edition (Germanos et al. 2021). Here, the literature to date on how luminal factors within the β-cell secretory pathway facilitate the synthesis of insulin was explored.

(This page is intentionally left blank)

1.2 Inside the Insulin Secretory Granule

1.2.1 Abstract

The pancreatic β-cell is purpose-built for the production and secretion of insulin, the only hormone that can remove glucose from the bloodstream. Insulin is kept inside miniature membrane-bound storage compartments known as secretory granules (SGs), and these specialized organelles can readily fuse with the plasma membrane upon cellular stimulation to release insulin. Insulin is synthesized in the endoplasmic reticulum (ER) as a biologically inactive precursor, proinsulin, along with several other proteins that will also become members of the insulin SG. Their coordinated synthesis enables synchronized transit through the ER and Golgi apparatus for congregation at the trans-Golgi network, the initiating site of SG biogenesis. Here, proinsulin and its constituents enter the SG where conditions are optimized for proinsulin processing into insulin and subsequent insulin storage. A healthy β-cell is continually generating SGs to supply insulin in vast excess to what is secreted. Conversely, in type 2 diabetes (T2D), the inability of failing β-cells to secrete may be due to the limited biosynthesis of new insulin. Factors that drive the formation and maturation of SGs and thus the production of insulin are therefore critical for systemic glucose control. Here, we detail the formative hours of the insulin SG from the luminal perspective. We do this by mapping the journey of individual members of the SG as they contribute to its genesis.

1.2.2 Introduction

The insulin secretory granule (SG) in the pancreatic β-cell is essential for glucose homeostasis in the body. It is both the site of proinsulin conversion into insulin and C-peptide (Orci et al. 1984), as well as the storage compartment for mature insulin to be readily available for secretion upon nutrient stimuli. Insulin is first synthesized as pre-proinsulin at the endoplasmic reticulum (ER), immediately converted to proinsulin, and transported through the Golgi to the trans-Golgi network (TGN). Here, proinsulin, along with other cargo proteins, is partitioned and sorted into its destination compartment, the immature SG (ISG) (Orci et al. 1984). In the ISG, at least 99% of proinsulin is ultimately converted to insulin and C-peptide in a 1:1 molar ratio via proteolytic cleavages by the proprotein convertases PC1/3 and PC2 (Rhodes and Halban 1987; Michael et al. 1987; Davidson, Rhodes, and Hutton 1988; Smeekens et al. 1992). This coincides with several processes that facilitate SG maturation, including luminal acidification (Orci et al. 1987), selective removal of certain soluble components (Kuliawat et al. 1997), and Zn^{2+}-mediated insulin crystallization (Baker et al. 1988). Finally, in response to nutrient stimuli, these mature SGs (MSGs) are mobilized to fuse with the plasma membrane and deliver insulin to the bloodstream.

Importantly, ISGs can also undergo regulated secretion (Halban 1982), which can be heightened in situations of increased β-cell demand (Seaquist et al. 1996; Mezza et al. 2018; Boland et al. 2018) and may explain the higher circulating proinsulin to insulin ratio observed in both pre-diabetic and diabetic patients (Ward et al. 1987; Yoshino et al. 2018; Pfützner et al. 2005; Pradhan et al. 2003; Nijpels et al. 1996; Vangipurapu et al. 2015; Yang et al. 2019). The mechanism behind increased proinsulin secretion is unknown; although it has been suggested to result from defective proinsulin trafficking or processing, and/or the premature release of ISGs (Porte and Kahn 1989; Rhodes and Alarcón 1994). Interestingly, β-cells from animal models of type 2 diabetes (T2D) display a compensatory expansion of the secretory pathway, characterized by increased proinsulin biogenesis but exhibit a thorough depletion of MSGs, pointing to the existence of a bottleneck in the secretory pathway resulting in an MSG replenishment defect during β-cell failure (Alarcon et al. 2016). Therefore, there is a diversion away from SG maturation in favor of ISG secretion, limiting the compensatory capacity of the β-cell during metabolic stress.

Alongside insulin, the β-cell SG contains a cocktail of cargo proteins. These proteins drive trafficking through the regulated secretory pathway and are also released to affect systemic function (Ohsawa et al. 1989; Natori and Huttner 1996; Carmon et al. 2020; Bartolomucci et al. 2011). Luminal enzymes accompany the cargo from synthesis in the ER through to storage in the MSG but are under tight regulation to restrict their activity to the correct site (Davidson, Rhodes, and Hutton 1988). The ionic composition of the lumen controls protein behavior and is generated by a range of transmembrane channels and transporters that are stationed throughout the secretory pathway (Hutton and Peshavaria 1982; Schoonderwoert et al. 2000; Lemaire, Chimienti, and Schuit 2012; Hutton,

Penn, and Peshavaria 1983; Hur and Yoo 2015; Mitchell et al. 2001). Finally, sorting receptors can escort unwanted components away from the maturing SG to refine its contents after formation (Kuliawat et al. 1997; Klumperman et al. 1998). In this review, we will explore the major luminal components of the β-cell SG. These components will be discussed in relation to secretory pathway dysfunction, providing context to critical aspects of β-cell failure. However, first, we will start with a historical overview of the process of insulin SG formation.

Historical overview of insulin SG formation. Pioneering efforts in the 1980s elucidated the main concepts surrounding β-cell granule biogenesis. Orci first used immunogold labelling of total insulin, with an antibody that recognizes both proinsulin and insulin, to show that it is closely associated with membranes of the Golgi apparatus until the TGN, where it dissociates and concentrates into a mildly condensing core (Orci, Ravazzola, and Perrelet 1984). This core buds from the TGN into clathrin-coated ISGs, which develop into non-clathrin coated MSGs (Orci, Ravazzola, and Perrelet 1984). At the time, Halban was using pulse-chase methods to incorporate radiolabeled arginine and lysine analogues into newly synthesized proinsulin to inhibit its post-translational processing into insulin (Halban 1982). In collaboration, they inhibited proinsulin conversion and utilized autoradiography with clathrin-immunolabeling to provide the first direct evidence that proinsulin traffics from the TGN into clathrin-coated ISGs before its conversion into insulin and C-peptide (Orci et al. 1984). Moreover, proinsulin conversion was shown to be required for complete SG maturation, as these analogue-treated cells could not form an electron-dense core which is characteristic of the MSG (Orci et al. 1984). Indeed, the development of proinsulin and insulin-specific monoclonal antibodies later confirmed that proinsulin localization is most concentrated in the ISG compartment while insulin dominates the MSG compartment (Orci et al. 1987).

In 1987, Rhodes and Halban released a landmark study using radiolabeled proinsulin to follow the efficiency of its trafficking and conversion and the events of β-cell SG exocytosis (Rhodes and Halban 1987). The study found that 99% of proinsulin entered ISGs to lend itself for conversion, and that the resulting newly synthesized SGs were preferentially secreted over older SGs when exposed to glucose. Importantly, Halban had already shown that radiolabeled conversion-resistant proinsulin is released from the β-cell at the same rate as the non-resistant radiolabeled insulin product, therefore demonstrating that the ISGs housing proinsulin are also secretion-competent (Halban 1982). Collectively, foundational work from the 1980s suggested that the SG is the minimal functional unit for exocytosis, is formed through stringent processes, and is endowed with factors required for its regulated release early after formation. It would follow that delayed MSG production could result in the increased release of ISGs and hyperproinsulinemia, and thus a failure of the β-cell to respond to glucose with the secretion of insulin (Alarcon et al. 2016; Kahn and Halban 1997; Alarcón et al. 1995). Ensuing efforts centering on answering how these carriers are formed have found that an ordered system of ionic and molecular factors underlie how SG proteins are sorted, packaged, and

processed (Omar-Hmeadi and Idevall-Hagren 2020). Likewise, efforts centered around understanding the preferential nature of exocytosis have facilitated the characterization of a vast network of components which confer mobility and fusion-competence to prepare the SG for release (Thurmond and Gaisano 2020).

The MSG holds at least 50 unique soluble and transmembrane proteins (Norris, Yau, and Kebede 2021), and the biosynthesis of many are thought to be commonly regulated at the translational level following exposure of the β-cell to glucose (Magro and Solimena 2013). This enables their synchronized transit and congregation at the TGN, but from here, several proteins will traverse the ISG compartment on their way to other destinations. Due to this, the ISG intermediary was once the centerpiece of debate concerning the mode of transport that proinsulin and other regulated secretory proteins take en route to the MSG (Arvan and Halban 2004). In the early 1990s, Arvan and colleagues found that C-peptide (the fragment generated from proinsulin after its complete conversion) could be released from the β-cell in molar excess to that of insulin during non-stimulatory conditions (Arvan et al. 1991). Follow up studies characterized the kinetics of this 'constitutive-like' secretion, specifically showing that this pathway emanates from the SG compartment and temporally coincides with the maturation of ISGs into MSGs (Kuliawat and Arvan 1992). Subsequent demonstration that insulin, but not proinsulin, is capable of forming insoluble hexamers, led to the idea that insulin condensation within the core of the SG permits the excursion of C-peptide out of the maturing granule as the soluble fraction is removed (Kuliawat and Arvan 1994). Moreover, by analyzing the regulated secretion of lysosomal hydrolase cathepsin B at different time points following pulse-chase radiolabeling, it was revealed that pro-cathepsin B entered the ISG only to be removed from the ISG shortly after entry (Kuliawat and Arvan 1994). Taken together, these studies established the presence of post-Golgi sorting mechanisms that serve to facilitate SG maturation by refining its composition.

Arvan thus proposed that members of the SG were not exclusively trafficked into the regulated secretory pathway from the TGN, but rather that an assortment of proteins were delivered into ISGs through means of unregulated 'bulk-flow' - largely due to the stoichiometric infeasibility of sorting receptors existing for each cargo (Arvan and Castle 1998). Subsequent post-Golgi mechanisms served to remove and traffic non-regulated secretory proteins to other destinations and drive the maturation of the SG. The term 'sorting by retention' was used to describe the selective condensation of proteins within the maturing SG, and 'sorting by exit' was used to describe budding from the vesicle that sequesters parts of the soluble fraction to remove other proteins (Arvan and Castle 1998) (**Figure 2**). This proposal sparked a debate; in particular, proponents against bulk-flow asserted that entry of proinsulin and other key granular components into the ISG could not be through a passive, unregulated mechanism (Molinete et al. 2000). In the end, the field came to the consensus on a tripartite process where luminal TGN protein sorting was also involved in segregating proteins prior to ISG formation, termed 'sorting by entry' (Arvan and Halban 2004). Moreover, technological advances utilized by recent studies have revealed increasing levels of complexity, showing that some

transmembrane components are in fact added to the SG after formation through retrograde plasma membrane/endosomal trafficking (Hummer et al. 2020). As we explore the luminal components of the insulin SG, we will come to appreciate that SG formation is difficult to lay out as a step-by-step mechanism. Individual components will contribute to multiple steps along the pathway, collaborating through a sequence of events to generate a functional entity that can be released upon stimulus. It is becoming more apparent that correctly forming this entity is crucial for systemic glucose homeostasis.

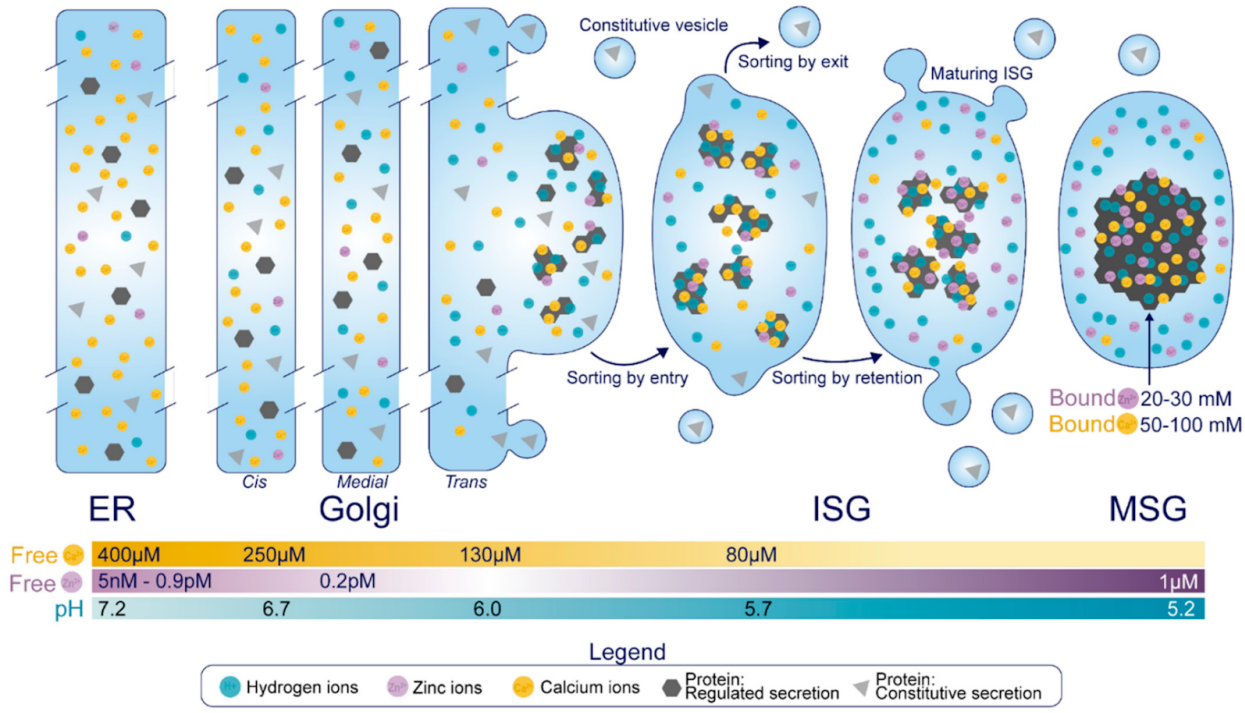

Figure 2. Overview of the β-cell secretory pathway. Following synthesis in the ER, proteins transit the Golgi apparatus to the TGN, and those destined for the regulated secretory pathway are sorted by entry into ISGs. This event relies on soluble protein aggregation which is under the control of Ca^{2+} and H^{+}, and several proteins may also interact with membrane components of the TGN that are enriched in β-cell SGs. Some non-SG proteins can also slip into ISGs but are removed as a byproduct of the sorting by exit mechanism, which specifically escorts proteins from the maturing SG via receptor mediated recognition and vesicle budding. Concurrently, Zn^{2+}, Ca^{2+}, and H^{+} taken up by the maturing SG will bind to certain proteins to enhance their condensation and prevent their exit, in a process termed sorting by retention. While the free concentration of Ca^{2+} is in the micromolar range and decreases proximal to distal along the secretory pathway, the β-cell SG holds 50–100 mM Ca^{2+} bound to luminal proteins. Similarly, the total amount of Zn^{2+} bound to luminal proteins in the SG is in the range of 20–30 mM, although its free concentration is elevated in the distal secretory pathway relative to the proximal secretory pathway. Finally, the pH of the newly formed ISG can be estimated as similar to that of a constitutive vesicle (~5.7), but this will drop to 5.2 in the MSG. Notably, these values represent the free H^{+} concentration, but there exists no indication of the amount of H^{+} that is bound to luminal proteins.

1.2.3 Luminal Components of the Insulin Secretory Granule

The luminal components of the insulin SG can be functionally segregated into four groups. These are cargo molecules, luminal enzymes and chaperones, ions (and their transporters and channels), and sorting receptors.

1.2.3.1 Cargo Molecules

The primary cargoes of SGs in the pancreatic β-cell are insulin, islet amyloid polypeptide (IAPP), the granins [chromogranin A (CgA), chromogranin B (CgB), secretogranin II (SgII), secretogranin III (SgIII), and VGF (non-acronymic)], and each of their precursors and derivatives. In addition to those covered in this review, the insulin SG also contains amines such as dopamine and serotonin (Ericson, Håkanson, and Lundquist 1977; Ekholm, Ericson, and Lundquist 1971; Lundquist, Ekholm, and Ericson 1971), as well as nucleotides like ATP (Sakamoto et al. 2014), which can be taken up by SG-localized pumps but as of yet, have ill-defined intragranular and post-exocytotic roles (Henquin 2021). In this section, we will demonstrate what is known about the trafficking and processing of each individual cargo protein. These events are heavily dependent on the differential ionic composition of each compartment, where Ca^{2+}, H^{+} and Zn^{2+} supplied by localized uptake pumps exist in an ascending concentration gradient proximal to distal (**Figure 2**).

Insulin. Insulin is synthesized as pre-proinsulin on the rough ER, and upon translocation has its N-terminal 24-residue signal sequence cleaved to form proinsulin (Liu et al. 2012). Proinsulin undergoes folding in the ER where it acquires three disulfide bonds and dimerizes prior to ER exit (Huang and Arvan 1995). En route to the TGN, proinsulin forms hexamers in the presence of Zn^{2+} (Huang and Arvan 1995), and importantly, proinsulin hexamers remain soluble (Kuliawat and Arvan 1994). Zn^{2+} binds to a histidine corresponding to residue 10 on the B chain of mature insulin (His-B10), and while the precise cisternal location of this event is undetermined, there is evidence of a Zn^{2+}-dependent rate limiting step for proinsulin trafficking around the TGN/ISG compartment (Haataja et al. 2013).

After entry into the ISG, proinsulin is converted to insulin and C-peptide via ordered cleavage at two sites of dibasic amino acid residues by the subtilisin-related proprotein convertases, first by PC1/3 and then by PC2 (**Figure 3A**). The 31–32 Arg-Arg site is located at the C-peptide/B-chain junction and the 64–65 Lys-Arg site is located between the C-peptide/A-chain junction. Molecular modelling suggests that the co-ordination of Zn^{2+} by His-B10 works to position these sites along the exposed radial surface of the proinsulin hexamer (Kiselar et al. 2011), enabling accessibility for the two processing enzymes. PC1/3 preferentially cleaves the B-chain junction on the carboxyl side of Arg32, generating a proinsulin intermediate split between residues 32 and 33 (split 32,33 proinsulin) (Davidson, Rhodes, and Hutton 1988; Smeekens et al. 1992). PC2 preferentially cleaves the A-chain junction on the carboxyl side of Arg65 to generate the split 65,66 proinsulin intermediate (Davidson, Rhodes, and Hutton 1988; Smeekens et al. 1992). Following conversion by each of the subtilisin-related prohormone convertases, the exoprotease carboxypeptidase H/E (CPE) acts to trim the revealed dibasic residues to create the 'des' intermediates, des 31, 32, or des 64,65 proinsulin, with numbers denoting the excised residues (Davidson and Hutton 1987). A second round of endoprotease and CPE activity will generate insulin and C-peptide in a 1:1 molar ratio (Michael et al. 1987; Davidson, Rhodes, and Hutton 1988). The insulin molecule consists of an A-chain and a B-chain, linked together by two disulfide bridges and maintained in hexameric oligomers through the co-ordination of two-Zn^{2+} by three of the six His-B10s (Baker et al. 1988; Weiss, Steiner, and Philipson 2014). Continual uptake of H^+ and Zn^{2+} into the developing SG affects the charge state of hexameric insulin and facilitates its packing into extremely insoluble crystals (Norrman and Schluckebier 2007). The low percentage of unprocessed/incompletely processed proinsulin can pack with crystalline insulin to some extent (Steiner 1973) and C-peptide can co-precipitate with insulin in pH conditions mimicking the MSG (Landreh et al. 2012). C-peptide can also undergo further exoproteolytic cleavage to generate des 27–31 C-peptide, accounting for roughly 10% of the total C-peptide content (Verchere et al. 1996). Upon exocytosis, exposure to the neutral extracellular pH is likely to dissipate the insulin crystal rapidly (Gold and Grodsky 1984), allowing monomeric insulin to circulate and signal via the insulin receptor expressed on target tissues.

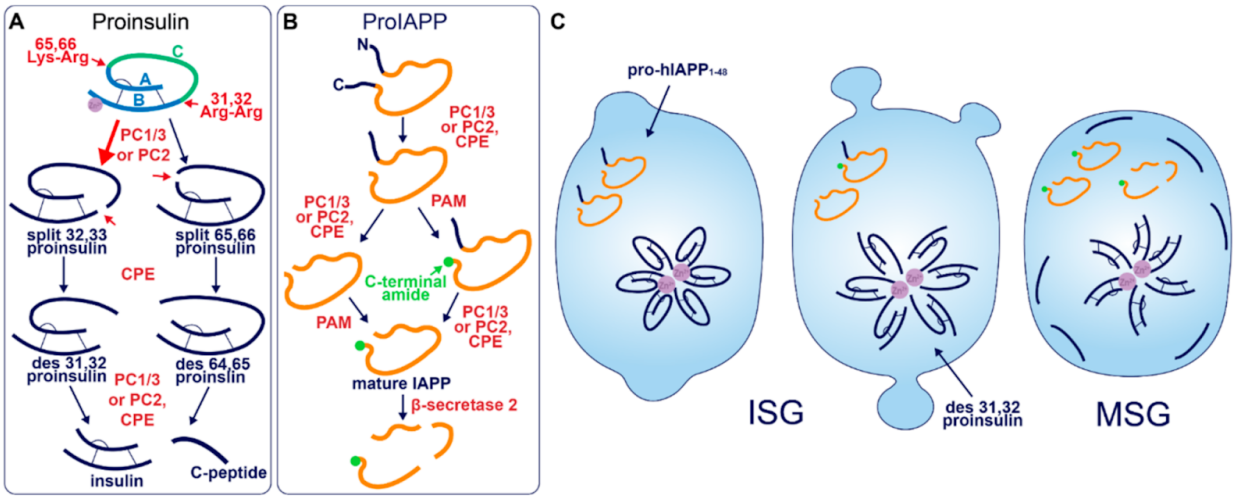

Figure 3. Prohormone Processing in the β-cell. (A) Sequence of proinsulin processing. After entry into the ISG, proinsulin is converted to insulin and C-peptide via cleavage at two sites of dibasic amino acid residues. The 31–32 Arg-Arg site is located at the C-peptide/B-chain junction and the 64–65 Lys-Arg site is located between the C-peptide/A-chain junction. Cleavage at one dibasic site by endoprotease PC1/3 or PC2 produces the split proinsulin molecules, which precedes C-terminal trimming of exposed residues by exoprotease CPE to produce the des proinsulin molecules. One round of endo/exoprotease activity is followed by the same action at the other dibasic site. **(B)** Sequence of proIAPP processing. The C-terminal proregion of proIAPP is cleaved in the TGN prior to ISG entry. Next, in no particular order, within the maturing ISG the N-terminal proregion of proIAPP is removed and the exposed C-terminal glycine residue is amidated to produce IAPP. IAPP may then be further processed into smaller fragments by β-secretase 2. **(C)** Processing events and products during secretory granule maturation in the human β-cell SG. des 31,32 proinsulin is the major proinsulin intermediate in human β-cells and is elevated in the circulation of those with T2D along with $proIAPP_{1–48}$.

A human mutation of His-B10 to aspartate (mAsp-B10) underlies familial hyperproinsulinemia (Chan et al. 1987) and represents a condition where mutant proinsulin is presumed to be excluded from wild-type proinsulin hexamers. While expression of this mutant in mice does not affect its intracellular conversion to insulin, there is an enrichment of non-crystallized SGs, and the constitutive release of proinsulin is increased by ~15% (Carroll et al. 1988). These phenotypes could indicate that mAsp-B10 proinsulin is correctly targeted into the ISG, but there is an increased constitutive-like release in the absence of Zn^{2+}-facilitated hexamarization prior to its conversion into insulin. Indeed, while contributing to the maturation of the SG, constitutive-like secretion is estimated to account for only 0.6% of the release of non-converted proinsulin (Halban and Irminger 2003). This situation could represent an extreme example of protein exit out of the ISG, displaying the secretory capacity of the constitutive-like pathway. An alternative (and not mutually exclusive) explanation is that mAsp-B10 proinsulin leaks directly into the constitutive pathway from the TGN, however mAsp-B10 proinsulin degradation is also enhanced (Carroll et al. 1988) suggesting that its transit to the PM occurs through the constitutive-like pathway (a route that travels via the

endo-lysosomal system (Kuliawat and Arvan 1994)). Nonetheless, these studies have highlighted that Zn^{2+}-facilitated hexamarization is a primary mechanism of proinsulin sorting and consequent SG maturation.

Early studies investigating human proinsulin and rat proinsulin isomers I and II in primary islets revealed that they are differentially processed. Human proinsulin tends to be cleaved first at the B-chain junction to produce des 31,32 proinsulin (Sizonenko et al. 1993) (Figure 3C), whereas the rat isomers tend to be cleaved first at the A-chain junction to produce des 64,65 proinsulin (Sizonenko and Halban 1991). This is thought to be due to the amino acid located four residues prior to the cleavage site (P4 position (Schechter and Berger 1967)), where the presence of a basic lysine or arginine residue enhances substrate recognition and/or enzymatic activity (Kaufmann, Irminger, and Halban 1995). Both rat isomers contain a basic arginine at P4 in the A-chain site, and both rat proinsulin I and human proinsulin contain a basic lysine at P4 in the B-chain site (Halban 1994). As a result, rat proinsulin I is more rapidly converted into insulin, and the accumulation of processing intermediates from this isomer is reduced due to the existence of basic residues at P4 in both cleavage sites (Sizonenko and Halban 1991).

Processing of human proinsulin follows a sequence favoring the prior activity of PC1/3 on the B-chain junction, followed by PC2, which has a far better affinity for des 31,32 proinsulin than intact proinsulin (Rhodes, Lincoln, and Shoelson 1992). Although this points to the existence of sequential cleavage through the action of both endoproteases, multiple lines of evidence indicate that PC1/3 works alone to produce mature insulin from both rat and human proinsulin isomers. While each enzyme possesses the catalytic ability to cleave at both dibasic sites (Kaufmann et al. 1997), PC1/3 achieves this far more efficiently than PC2 (Irminger et al. 1994; Neerman-Arbez, Sizonenko, and Halban 1993; Neerman-Arbez, Cirulli, and Halban 1994) and processing intermediates of proinsulin accumulate when PC1/3 expression is low (Neerman-Arbez, Sizonenko, and Halban 1993). The situation is different in mice, seemingly requiring the activity of both endoproteases; while the deletion of PC1/3 from mice results in an extremely pronounced block in proinsulin conversion (Zhu et al. 2002), knockout of PC2 also significantly hampers insulin maturation despite the presence of PC1/3 (Furuta et al. 1998). Finally, a recent study that re-characterized the expression of PC1/3 and PC2 in human islet β-cells found an abundance of PC1/3 and an absence of PC2, suggesting that PC1/3 is sufficient for humans to produce insulin (Ramzy, Asadi, and Kieffer 2020). Interestingly, humans with T2D had upregulated PC1/3 and an induction of PC2 expression. The authors of this study speculated that aberrant PC2 expression could cause a processing defect that underlies the pathological state, although, it may be the case that PC2 expression is invoked by metabolic stress as a compensatory response to assist PC1/3 in proteolytic activities. Indeed, the catalytic rate of PC2 on des 31,32 proinsulin exceeds that of PC1/3 on intact proinsulin (Rhodes, Lincoln, and Shoelson 1992). Simple overexpression of either PC1/3 or PC2 has been shown to enhance proinsulin conversion in rat insulinoma INS1 cells (Irminger, Meyer, and Halban 1996), hence, induction of PC2

activity could support proinsulin conversion when PC1/3 is overwhelmed especially considering that the A-chain junction is not preferred by PC1/3 (Davidson, Rhodes, and Hutton 1988; Bailyes, Bennett, and Hutton 1991).

Both PC1/3 and PC2 endoprotease activities are sensitive to pH and Ca^{2+}. In-vitro assays using enzymes isolated from rat islets have shown that PC1/3 requires millimolar levels of Ca^{2+} and a pH close to 5.5 for activity whereas PC2 can exert activity at a micromolar levels of Ca^{2+} and over a broader pH range, although its pH optimum is also 5.5 (Davidson, Rhodes, and Hutton 1988). In cells however, PC1/3 undergoes fast maturation into an active enzyme upon entry into the SG (Shennan et al. 1995). Due to the stringent regulation of PC2 by the molecular chaperone 7B2 (Muller, Zhu, and Lindberg 1997; Zhu et al. 1996; Hwang and Lindberg 2001), the low pH requirement for its autocatalytic activation (Shennan et al. 1995; Lamango et al. 1999), as well as its substrate-specificity to des 31,32 proinsulin (Rhodes, Lincoln, and Shoelson 1992), its activity is likely to be restricted to later stages of SG maturation. Therefore, it appears that early PC1/3 activity at both sites could render PC2 redundant, as has been demonstrated in animal models (Irminger et al. 1994; Neerman-Arbez, Sizonenko, and Halban 1993; Neerman-Arbez, Cirulli, and Halban 1994) but not quite yet in humans. Crucially, compensatory upregulation of the endoproteases may be futile, considering the premature ISG release that occurs in β-cell failure. It has been known for some time that des 31,32 intermediates are the predominant species of circulating proinsulin that is elevated in human T2D (Ostrega et al. 1995; Clark et al. 1992), therefore fast endoprotease activity is critical for systemic metabolic homeostasis. Therapeutic compounds that alter the ionic composition of the SG to bolster endoprotease activation and activity could be effective in treating T2D.

Despite a common outcome, nuances in the generation of insulin are clear between species. Their awareness may be important for translating data from model organisms to the context of human β-cell function.

Islet Amyloid Polypeptide. IAPP is a 37 amino-acid peptide stored in the MSG that is co-secreted with insulin in a 1:100 molar ratio (Lukinius et al. 1989; Nakazato et al. 1990; Stridsberg, Sandler, and Wilander 1993), and can function to suppress insulin secretion and control various aspects of energy homeostasis (Ohsawa et al. 1989). Additionally, known as amylin, IAPP and its precursors and derivatives are notorious for forming fibrils that distribute extracellularly throughout islets as amyloid deposits, a pathological feature of human T2D (Hull et al. 2004). Early observations report the occurrence of islet amyloid deposits in >90% of diabetic patients (P. Westermark and Grimelius 1973; P. Westermark and Wilander 1978) but later studies have shown a variable prevalence depending on duration of disease and ethnicity, especially when sample size is increased (H.-L. Zhao et al. 2003). The question of how IAPP remains non-pathogenic in healthy conditions and how it transitions to a pathogenic molecule has kept researchers occupied for some time. Appropriately, most work on IAPP has been focused on its secretory dynamics, processing, and amyloidogenic properties (Per Westermark, Andersson, and Westermark 2011; Haataja et al. 2008; Raleigh et al. 2017) rather than its luminal sorting. To this end, not much is known about its behavior in the early secretory pathway or the determinants of its trafficking fate.

Akin to proinsulin, human pro-IAPP is a 67 amino-acid (aa) peptide derived from pre-proIAPP that forms an intramolecular disulfide bridge in the ER and is subject to endoproteolytic processing (J. Wang et al. 2001; Marzban, Soukhatcheva, and Verchere 2005; Marzban, Trigo-Gonzalez, and Verchere 2005; Marzban et al. 2004) (**Figure 3B**). It is thought that PC1/3 acts first on a C-terminal proregion in the TGN (Marzban, Trigo-Gonzalez, and Verchere 2005) which is followed by CPE action to generate a 48-residue processing intermediate. A subsequent round of PC1/3 or PC2 and CPE action on the N-terminal proregion generates a 38 aa peptide with a C-terminal Gly termed amylin free acid (Y.-C. Chen, Taylor, and Verchere 2018). A fourth enzyme, peptidyl-glycine alpha-amidating monooxygenase (PAM), is probably responsible for amidation at the C-terminal 38 glycine residue which may or may not occur prior to cleavage of the N-terminal pro-region, to generate the mature C-terminally amidated form of IAPP (Y.-C. Chen, Taylor, and Verchere 2018). Finally, a fifth membrane-bound enzyme that localizes to the β-cell SG, β-secretase 2, can process IAPP further into smaller fragments (Rulifson et al. 2016).

Early reports demonstrated that PC2 can cleave at both the N- and C-terminal proregions of pro-mouse IAPP (mIAPP) in addition to PC1/3 cleavage occurring only at the C-terminal site (J. Wang et al. 2001; Marzban, Soukhatcheva, and Verchere 2005; Marzban, Trigo-Gonzalez, and Verchere 2005; Marzban et al. 2004). However, both rat and human islets appear not to express PC2 at detectable levels normally (Ramzy, Asadi, and Kieffer 2020). Indeed, pro-human IAPP (hIAPP) can be fully processed by PC1/3 in PC2 null mice (Courtade et al. 2017); however, pro-rat IAPP (rIAPP) can be processed at both sites by PC2 but only at one site by PC1/3 (Marzban et al. 2004). These differences are likely due to the modified sequence at the C-terminal site (**Figure 4**), where the position of Ala and Val residues may determine whether PC1/3 can cleave: i.e., KR↓VA (Val at P1′

and Ala at P2′) in rIAPP compared to KR↓AV (Ala at P1′ and Val at P2′) in hIAPP and KR↓AA (Ala at P1′ and P2′) in mIAPP. Likewise, it has also been suggested that a Val common to both hIAPP and rIAPP at the N-terminal site allows cleavage by PC1/3 (Ramzy, Asadi, and Kieffer 2020), which is not experienced by mIAPP (J. Wang et al. 2001) that contains Met at this residue. Thus, PC1/3 may be sufficient for full pro-IAPP processing in humans due to the sequence variations that lie between species.

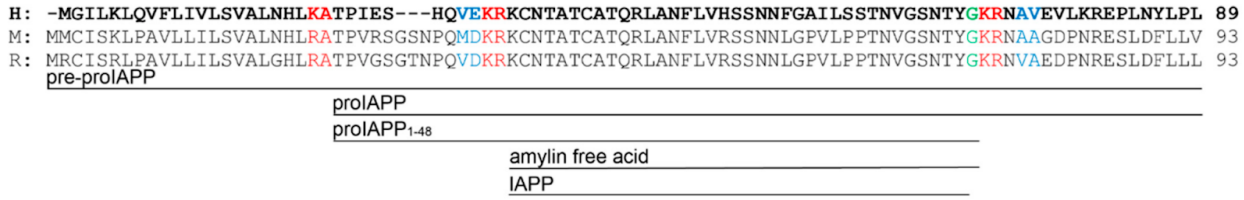

Figure 4. IAPP precursor/product amino acid sequence in human (H), mouse (M), and rat (R). The green glycine residue is amidated after the C-terminal cleavage site is processed. Red residues denote dibasic sites of endoproteolytic processing. Blue residues indicate a modified sequence between species at cleavage sites that could account for their differential specificity to PC enzymes.

IAPP resides in the soluble fraction of the MSG, and hIAPP is extremely fibrillogenic whereas rIAPP and mIAPP are not fibrillogenic at all (P. Westermark et al. 1990). It has been shown *in-vitro* that pro-hIAPP products become increasingly more amyloidogenic with further cleavages (Yonemoto et al. 2008), however, it is thought that the presence of ionic and molecular factors in the MSG periphery inhibits hIAPP oligomer formation in healthy conditions (Jaikaran, Nilsson, and Clark 2004; P. Westermark et al. 1996; Brender et al. 2010; Khemtémourian et al. 2011; Janciauskiene et al. 1997; Kudva et al. 1998). An extensive body of literature has covered the molecular mechanisms of hIAPP pathogenicity in T2D (Per Westermark, Andersson, and Westermark 2011; Haataja et al. 2008; Raleigh et al. 2017). Considering that hIAPP is likely not a driver of SG biogenesis or function but instead plays the role of chaotic passenger, we will focus here on how secretory pathway dysfunction could precede hIAPP-mediated β-cell damage.

A current working hypothesis to explain the initiation of islet amyloid formation is that hIAPP-related peptides undergo dysregulated fibrillogenesis at some point inside the β-cell secretory pathway, potentially due to overproduction during compensation/failure (K. H. Johnson et al. 1989), but this only occurs within a small subset of islet β-cells (Per Westermark, Andersson, and Westermark 2011; Haataja et al. 2008; Raleigh et al. 2017; Gurlo et al. 2010; Lin et al. 2007; Yagui et al. 1995). If pro-hIAPP overproduction is the fuel, then disruption of organellar membranes from within the cell is the spark that results in β-cell death and the deposition of extracellular amyloid. Through regular exocytosis from neighboring β-cells, released hIAPP can then add to the size of the initial deposit. An alternative (and not mutually exclusive) hypothesis suggests that release of the

48-residue pro-hIAPP (pro-hIAPP1–48) intermediate can initiate extracellular amyloid formation by a specific interaction with heparin sulfate proteoglycans in the extracellular matrix (H. Wang and Raleigh 2014). Interestingly, large ordered fibrils that make up the bulk of the visually identified IAPP deposition are thought to be relatively inert on a cytotoxic level (Raleigh et al. 2017), although interruption of islet cytoarchitecture could impair coordinated islet function. Rather, it is the presence of medium-sized disordered oligomers that are thought to exert most of the cellular damage (Janson et al. 1999). Fitting with this, recent experimental focus has instead been placed on the mechanism of medium-sized oligomer formation and cytotoxicity (Brender et al. 2008; Brender, Salamekh, and Ramamoorthy 2012).

Not surprisingly, the N-terminal prosequence of hIAPP is detectable in islet amyloid deposits (P. Westermark et al. 1989; G. T. Westermark et al. 2000). This observation resembles what is observed with proinsulin in that incompletely processed hIAPP may be released from the β-cell during T2D, and indeed, elevated serum pro-hIAPP has been observed in glucose intolerant and T2D patients (Zheng et al. 2010). If one considers that ISGs released during β-cell failure are a source of hIAPP processing intermediates (**Figure 3C**), we could look to luminal factors that might explain the propensity of these molecules to become pathogenic. Indeed, insulin, Zn^{2+}, H^{+}, Ca^{2+}, C-peptide, and proinsulin have been assessed individually or in combination, *in-vitro*, along with hIAPP, in various studies to reason that a delicate balance of cofactors is required to inhibit hIAPP oligomerization (Jaikaran, Nilsson, and Clark 2004; P. Westermark et al. 1996; Brender et al. 2010; Khemtémourian et al. 2011; Janciauskiene et al. 1997; Kudva et al. 1998; Xu et al. 2021). In healthy cells, regulated exocytosis of MSGs could maintain this balance as components are released in an appropriate molar ratio. Conversely, during β-cell compensation and failure, release of the incompletely formed ISG might not replicate this outcome, and cytotoxic hIAPP oligomers could form in the extracellular microenvironment adjacent to the plasma membrane to induce membrane damage.

Dysregulated hIAPP oligomerization exacerbates the progression of T2D, so preventing β-cell death at the hands of hIAPP could limit T2D severity. Abnormal SG composition or the premature release of ISGs may be contributing factors, highlighting the importance of correctly forming the insulin SG.

Granins. The granin family of proteins (CgA, CgB, SgII, SgIII, and VGF) are ubiquitously expressed across neurons and endocrine cells and are considered major contributors to the biogenesis of regulated SGs from within the lumen (**Figure 5**). Their effectiveness has been displayed by several groups with findings that expression of just a single granin in cells that do not have a regulated secretory pathway is able to produce SGs that are capable of regulated release (Carmon et al. 2020; Elias et al. 2012; Montero-Hadjadje et al. 2009; Inomoto et al. 2007; Huh, Jeon, and Yoo 2003). Granins are synthesized as soluble cargo precursor proteins, which are highly acidic and hydrophilic, but are prone to aggregation under mild acidity (pH < 6.4) and high Ca^{2+} (>1 mM) conditions (Bartolomucci et al. 2011; Chanat and Huttner 1991). It has been shown that both of these ionic requirements must be met for granin aggregation (Chanat and Huttner 1991; Yoo and Albanesi 1991), which can be achieved at the initiating site of SG biogenesis in the TGN (**Figure 2**) where ion pumps maintain a high luminal Ca^{2+} concentration and contribute to a substantial lowering of the pH through enhanced H^{+} uptake (Schoonderwoert et al. 2000; Sun-Wada et al. 2006; Taupenot, Harper, and O'Connor 2005). Moreover, several granins have been shown to interact with each other, and, lacking transmembrane domains themselves, some can also interact with lipid species on the luminal aspect of the secretory pathway membrane to provide a link between soluble and membrane fractions. In this way, their physical abundance, coordinated aggregation within the TGN, and binding to specific components on the membrane has been proposed to drive the segregation and sorting of peptide hormones and other proteins into the regulated secretory pathway (Natori and Huttner 1996), meeting the requirements of a 'refined bulk-flow' sorting by entry mechanism (Arvan and Halban 2004).

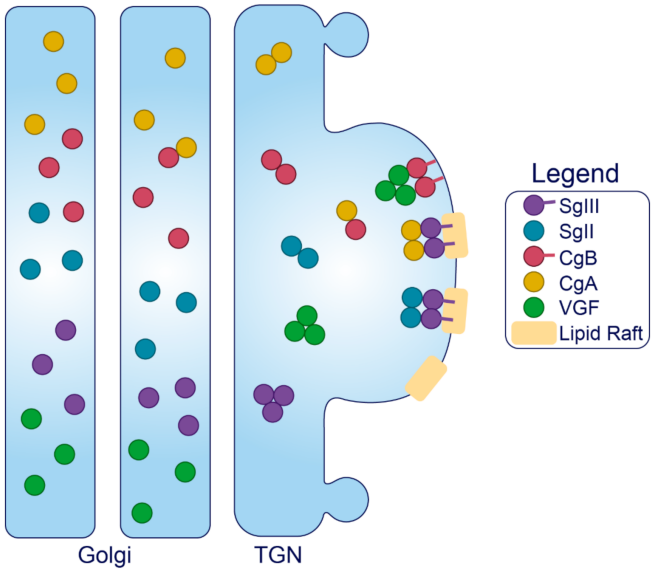

Figure 5. Trafficking of the granins. Upon exposure to mild acidity (pH < 6.4) within the Golgi apparatus, the granins will bind Ca^{2+}, which triggers their aggregation and interaction with other granin members. In the TGN, several of these members will interact with target molecules in the membrane to drive the formation of SGs at distinct sites from within the lumen.

Sphingolipid–cholesterol lipid rafts accumulate in microdomains of the TGN (Klemm et al. 2009; Orci et al. 1981), and these rafts can alter the distribution of transmembrane components to create sorting stations that are essential for granule biogenesis (von Blume and Hausser 2019; Y. Wang, Thiele, and Huttner 2000). These rafts are also enriched in vesicles of the regulated secretory pathway (T. Y. Wang and Silvius 2000; Kreutzberger et al. 2020; Hussain et al. 2018), indicating that SG membranes originate from the sorting domains where granins and other SG constituents aggregate and bind. Importantly, saturated fatty acid and cholesterol intake can change the composition of lipid species distributed among cell membranes to influence trafficking and SG morphology (Bogan, Xu, and Hao 2012; Payet et al. 2013). Therefore, dietary status could affect interactions between the granins and secretory pathway membranes, but this requires investigation. Finally, since granins can bind Ca^{2+} at a high capacity with low affinity (Yoo and Albanesi 1991), they are also thought to equip the SG with the ability to store and release Ca^{2+} (Yoo et al. 2001; Yoo and Lewis 1995).

It should be noted that most of the literature on granins has reported on their role in neuronal/neuroendocrine cell lines, which although share features in common with the β-cell, have secretory pathways adapted to the specific needs of neural transmission. In these settings, we can draw insight from molecular interactions that govern trafficking and behavior of the granins themselves, but specific effects of granin depletion on SG biogenesis/secretion are often subject to cell-specific variation and thus will only be discussed with respect to the β-cell.

Granins can possess multiple sorting determinants and may be targeted to several SG sub-populations (**Figure 5**). SgIII is membrane-associated, and contains an N-terminal lipid-binding region that is required for its sorting into SGs of AtT-20 cells (Hosaka et al. 2004) and for its interaction with cholesterol in INS1 and AtT-20 SGs (Hosaka et al. 2002). This suggests that SgIII is sorted into the regulated secretory pathway through an interaction with TGN cholesterol (Hosaka et al. 2004). N-terminal residues (48–111) of CgA can bind to SgIII to follow SgIII sorting into the regulated secretory pathway of AtT-20 cells, where it also exists in association with SG membranes (Hosaka et al. 2002). Importantly, CgA also associates with INS1 granule membranes but only in the presence of SgIII (Hosaka et al. 2004). These results collectively indicate that SgIII is an adaptor for CgA in β-cells, with both granins associated at least to some degree with the SG membrane, and that correct trafficking relies on the presence of an N-terminal region on SgIII that binds cholesterol. This has been further demonstrated in PC12 cells, where SgIII was specifically shown to sort large aggregates of CgA into SGs (Han et al. 2008). Very little is known about the trafficking determinants of SgII aside from an understanding that both the N- and C-termini contain information for sorting (Courel et al. 2008), and that it may interact with SgIII on the SG membrane (Sun et al. 2013; Hotta et al. 2009). While SgII also regulates granule biogenesis in other secretory cells (Courel et al. 2010), interactions have not been published in β-cell models, and in general, insight into SgII function in the β-cell is lacking.

Like SgIII, CgB can interact with cellular membranes via a highly conserved N-terminal 22 residue disulfide-bonded loop (Glombik et al. 1999; Pimplikar and Huttner 1992). This loop is essential for CgB sorting to SGs but is not required for its aggregation within the TGN, indicating that CgB aggregates are not routed by default to SGs but are sorted through mediation of exposed N-terminal loops with the TGN membrane (Glombik et al. 1999); although, the corresponding membrane component is yet to be found. Several observations suggest that CgB trafficking is not entirely synchronous with insulin. In addition to the insulin SG, CgB also occupies distinct granules that do not contain insulin and conversely, insulin can occupy SGs devoid of CgB (Giordano et al. 2008). Additionally, CgB is present with SgII in nucleoplasmic vesicles of bovine chromaffin cells where they may have a role in regulating nuclear Ca^{2+} homeostasis (Yoo et al. 2007), although this has not been studied in the β-cell. In the β-cell, CgB co-localizes and co-immunoprecipitates with VGF (Bearrows et al. 2019), and it has been shown *in-vitro* that CgA and CgB can form dimers at pH 7.5 and heterotetramers at pH 5.5 (Yoo and Lewis 1996), suggesting that CgB could traffic with either VGF or CgA. However, VGF does not immunoprecipitate with CgA (Bearrows et al. 2019). Little else is known about the determinants of VGF trafficking, although a predicted alpha helix loop in its C-terminus may be required for direction into INS1 SGs (Garcia et al. 2005).

A handful of studies have investigated the consequences of granin depletion in β-cells albeit with varying success, possibly due to the method of study. Transient gene silencing seems to outcompete stable knockouts for studying function, and this is probably due to the circumvention of compensatory changes that occur during development. For example, whole body CgB knockout (KO) provided an insulin secretory defect that was unable to be explained aside from a small decrease in the number of docked SGs (Obermüller et al. 2010), whereas adenoviral knockdown (KD) of CgB in INS1-832/3 insulinoma cells and isolated mouse islets resulted in marked insulin secretory defects that could be explained by a defect to SG biogenesis (Bearrows et al. 2019). Similarly, islets from whole body CgA KOs actually have enhanced insulin secretion with no defects to SG generation (Wollam et al. 2017), whereas siRNA KD of CgA in the human β-cell line, EndoC-βH1, resulted in reduced basal and glucose-stimulated insulin secretion (GSIS) as well as cellular insulin content (Thomsen et al. 2018). CgA KO mice had compensatory doubling in CgB expression and tripling in SgII expression (Wollam et al. 2017), which may explain the absence of a secretory phenotype in CgA KOs. Islets from whole-body SgIII KO mice have impaired GSIS but only when subject to a high-fat-high-sucrose diet. This is associated with reduced insulin and increased proinsulin content, but there were no reported ultrastructural granule abnormalities (Maeda et al. 2018). Interestingly, in this study, CgA levels failed to increase when SgIII KO mice were put on diet but did so in the islets of wild-type mice (Maeda et al. 2018). As discussed previously, SgIII is a known adaptor for CgA and therefore its absence could result in CgA mis-sorting and thus the failure of compensatory upregulation. Finally, VGF depletion has also been assessed via KD of its mRNA in INS1-832/3 cells and a tamoxifen-inducible KO from mouse islets (Stephens et al. 2017). This study noted reduced

GSIS in both models, associated with a loss of total and docked SGs, and a reduction to their size in line with an increased cellular proinsulin-to-insulin ratio and delays to proinsulin conversion (Stephens et al. 2017). This study concluded that VGF depletion caused a granule replenishment defect, hampering the secretion of newly synthesized granules during the sustained second phase of GSIS (Stephens et al. 2017).

In summary, the granins are critical components of ISG formation, driving the formation of regulated carriers from within the lumen through aggregating and binding to distinct sites of the TGN membrane. Their ubiquity across cells of the neuroendocrine system implies an essential role for SG function, where their combined abundance and aggregative nature may confer unique characteristics to the SG.

1.2.3.2 Luminal Enzymes and Chaperones

Several enzymes and chaperones undergo processing in the secretory pathway and are targeted to the β-cell SG to generate the diverse intragranular cocktail. PC1/3, PC2, CPE, the PC2 binding partner 7B2, PAM, furin, chaperonin 60, and β-secretase 2 are members of this functional group that have activity in the β-cell. Active furin is widespread across the trans Golgi network, cell surface and endosomes, however it traverses the ISG before being sorted out of the maturing granule (Dittié et al. 1997). β-secretase 2 is a transmembrane aspartic protease that was previously mentioned for its role in mature IAPP proteolysis (Rulifson et al. 2016). Chaperonin 60, a heat shock related protein, has also been found to co-localize and co-immunoprecipitate with proinsulin and PC1/3 (Arias et al. 2000); however, the functional significance of this protein has not been investigated. Since we have already discussed the activity of CPE, PC1/3 and PC2 on proinsulin and proIAPP conversion, here we will restrict their discussion to trafficking and activation.

Carboxypeptidase E. CPE, also known as CPH, exists in both soluble and membrane-associated forms in β-cells (Docherty and Hutton 1983). An alpha-helix in the C-terminus of CPE anchors through cholesterol rich lipid rafts of the secretory pathway membrane, leaving six residues protruding to the cytoplasm (Dhanvantari et al. 2002; Fricker, Das, and Angeletti 1990) (**Figure 6**). Importantly, penetration through the membrane only occurs at or below pH 6 (Fricker, Das, and Angeletti 1990), conditions reflecting the late Golgi and SG compartments but not the proximal Golgi or ER (Demaurex et al. 1998) (**Figure 2**). Several lines of evidence have also demonstrated that membrane-bound forms of CPE can aggregate at this pH with at least 1 mM Ca^{2+} (Song and Fricker 1995), and co-immunoprecipitate in these conditions with both pro-opiomelanocortin and insulin *in-vitro* (Rindler 1998). This aggregation appears to occur independently from membrane binding, since treatment with Triton X-100 at pH < 6 to interfere with aggregation does not dissociate CPE from the membrane (Song and Fricker 1995). Collectively, pH-dependent lipid-raft insertion and aggregation provide a means by which CPE is concentrated along the TGN membrane for targeting to the SG. Moreover, it has been shown that CPE interacts with SgIII in both INS1 and AtT-20 cells (Hosaka et al. 2005), providing more control over targeting. Following SG entry, CPE is cleaved by an endoprotease at its C-terminus to generate the soluble, major enzymatic form of CPE (Guest et al. 1995) (**Figure 6**). Immunostaining reveals its predominant localization to the SG at steady state (Chu et al. 2011), where its enzymatic activity operates in a narrow pH optimum between 5.0 and 5.5 (Greene, Das, and Fricker 1992).

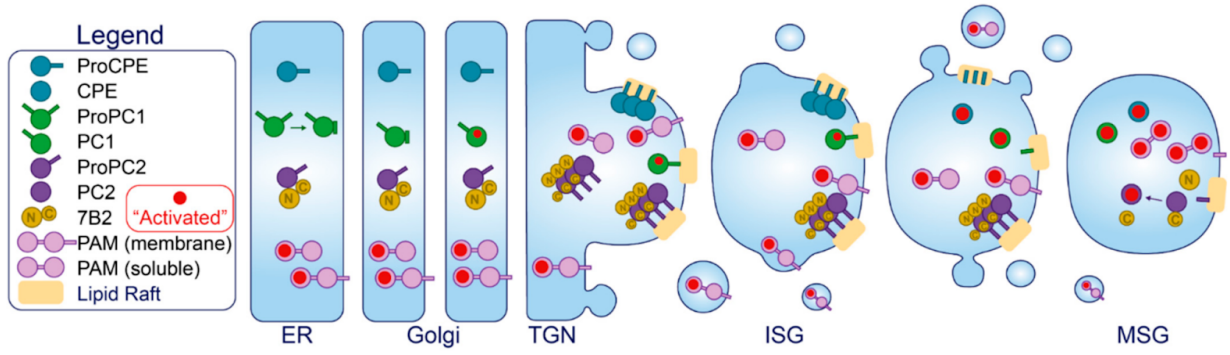

Figure 6. Enzyme suppression and activation. The major processing enzymes of the insulin SG are synthesized as inactive precursors in the ER. Through mechanisms unique to each member, their activity (indicated in red) is suppressed during transit. Activation is principally driven by ionic changes; several enzymes require certain conditions for trafficking into the ISG and conformational activation, and all members require a low pH for optimal enzymatic activity. This will naturally play out through the TGN and the maturing SG as the luminal composition is modified.

PC1/3. The trafficking and activation of PC1/3 is considerably less complicated than PC2. In the ER, pre-proPC1/3 undergoes cotranslational signal peptide removal to generate a 94 kDa pro-form of PC1/3 (Benjannet et al. 1993; A. Zhou and Mains 1994). This precursor harbors enzymatic activity but only toward its own N-terminal pro-region, which is cleaved in the ER (Benjannet et al. 1993; A. Zhou and Mains 1994) and thought to remain associated with the catalytic site of mature 87 kDa PC1/3 to prevent activity in the early secretory pathway (Boudreault, Gauthier, and Lazure 1998) (**Figure 6**). This will later dissociate after a second cleavage by PC1/3 (Boudreault, Gauthier, and Lazure 1998); however, the location of this event (TGN or ISG) is not settled yet. Moreover, the C-terminal region partially inhibits PC1/3 activity (Jutras et al. 1997; Rabah et al. 2007), and befittingly, PC1/3 can process certain substrates prior to its entry and complete activation inside the SG (Benjannet et al. 1991; Thomas et al. 1991). The C-terminal region also contains a predicted alpha helix required for sorting into the regulated secretory pathway (Jutras, Seidah, and Reudelhuber 2000), likely through an interaction with membrane lipid rafts (Blázquez, Docherty, and Shennan 2001). Following entry into the SG, the inhibitory C-terminal region is cleaved (possibly by itself) to generate fully active 74 and 66 kDa products (Jutras et al. 1997; Rabah et al. 2007; Y. Zhou and Lindberg 1994) (**Figure 6**), providing a relatively simple activation mechanism in the SG. 87 kDa PC1/3 exhibits a pH optimum between 5.5 and 6.5 (Y. Zhou and Lindberg 1993), respective conditions reflecting the SG and the TGN (**Figure 2**). Both 74 and 66 kDa products exhibit pH optima between 5.0 and 5.5 (Davidson, Rhodes, and Hutton 1988; Y. Zhou and Lindberg 1994), reflecting the MSG. All forms also have a high Ca^{2+}-dependence (Y. Zhou and Lindberg 1993, 1994), so the luminal ionic composition must be optimized for PC1/3 activity.

PC2 and 7B2. In the ER, pre-proPC2 undergoes cotranslational signal peptide cleavage to generate a 76 kDa proPC2. Unlike proPC1/3, its inhibitory N-terminal pro-region is not cleaved and remains associated with the catalytic subunit until it reaches the SG (Muller et al. 2000). ProPC2 traffics through the secretory pathway together with its chaperon 7B2 (Lee and Lindberg 2008); after synthesis and folding, proPC2 can bind pro7B2 in the ER where it accelerates proPC2 trafficking to the Golgi (Muller, Zhu, and Lindberg 1997; Benjannet et al. 1995, 1998). Pro7B2 is proteolytically cleaved at Arg152 (a furin cleavage site) in the TGN to generate a 21 kDa N-terminal (7B2-NT) and a 5 kDa C-terminal peptide (7B2-CT) (Hwang and Lindberg 2001; Paquet et al. 1994), both of which remain associated with proPC2 (Lamango et al. 1999). While the 7B2-NT appears to maintain proPC2 folding and trafficking, 7B2-CT is a well-established PC2 inhibitor *in-vitro* (Braks, Van Horssen, and Martens 1996) (**Figure 6**).

Both proPC2 and 7B2-NT can aggregate under pH- and Ca^{2+}- conditions mimicking the TGN (Shennan, Taylor, and Docherty 1994; Linard et al. 1995). Residues 45–84 in proPC2 have been shown to mediate its association with TGN membranes (Blázquez et al. 2000). Here, proPC2 likely interacts with sphingolipids in the TGN membrane since sphingolipid depletion causes re-routing of transfected mature PC2 to the constitutive pathway (Blázquez et al. 2000). ProPC2 also requires 7B2 for direction (Rovère et al. 2000), so 7B2 depletion will cause proPC2 to traffic constitutively (Barbero and Kitabgi 1999). Therefore, in the absence of 7B2-peptides, unfolded, improperly aggregated PC2 could route constitutively (Lee and Lindberg 2008; Barbero and Kitabgi 1999). In the SG, proPC2 does not undergo full autocatalytic maturation until the luminal pH drops to 5.2 (Lamango et al. 1999; Muller et al. 2000), conditions reflecting the MSG (**Figure 2**), and once fully mature PC2 cleaves and removes the inhibitory 7B2-CT fragment (Zhu et al. 1996). Thus, although PC2 is active *in-vitro* over a broad range of pHs and Ca^{2+} (Davidson, Rhodes, and Hutton 1988), its fully active form is restricted to the MSG within cells.

PAM. PAM is a bifunctional enzyme consisting of two contiguous catalytic domains, peptidylglycine alpha-hydroxylating monooxygenase (PHM) and peptidyl-α-hydroxyglycine α-amidating lyase (PAL) (Perkins, Husten, and Eipper 1990) (**Figure 6**). Sequential action of PHM followed by PAL functions to amidate glycine at the carboxyl terminus of peptides (Bradbury, Finnie, and Smyth 1982), which removes charge to confer full biological activity to the peptide (Merkler 1994). Cargoes that have already been processed by PC1/3, PC2 and CPE to yield C-terminal glycine residues are generally subject to this reaction (Bousquet-Moore, Mains, and Eipper 2010). While PHM is active over a broad acidity range (Eipper et al. 1991), the stability of the intermediate formed by PHM declines at pH levels >6.0 (Bundgaard and Kahns 1991) and the pH optimum for PAL is around 5.0. At least 50% of all biologically active peptides require amidation for full biological activity (Kyun-Hwan and Baik L 2001), and thus far, PAM is the only enzyme identified to be responsible for this reaction *in-vivo*. In both human and mouse islets, PAM co-localizes with insulin, glucagon, and somatostatin (Thomsen et al. 2018; Y.-C. Chen et al. 2020), and while insulin is not a target of PAM, IAPP is a potential target (Y.-C. Chen, Taylor, and Verchere 2018) and CgA was recently verified as a PAM substrate in β-cells (Thomsen et al. 2018). PAM depletion can affect insulin content and GSIS which may be mediated by its downstream targets including CgA (Thomsen et al. 2018); however, PAM haploinsufficiency in mice does not accelerate diet- or IAPP-induced diabetes (Y.-C. Chen et al. 2020). Notably, T2D-associated PAM risk alleles exist that are associated with reduced insulinogenic index (Thomsen et al. 2018; Y.-C. Chen et al. 2020), thus, PAM activity appears to have relevance to β-cell function.

Several isoforms of PAM differentially expressed between tissues (Kumar, Mains, and Eipper 2016) are produced by alternative mRNA splicing; some are soluble and others are type-I transmembrane enzymes (Oyarce and Eipper 1993). Human β-cells only express soluble isoforms whereas mouse β-cells only express transmembrane isoforms (Y.-C. Chen et al. 2020). Isoform differences are due to the presence/absence of specific regions, including a C-terminal transmembrane region, a linker region between the two contiguous enzymes PHM and PAL, as well as each of the two enzymes themselves (Kumar, Mains, and Eipper 2016). Both forms are enzymatically active although integral membrane PAM will presumably have more restricted access to substrates (Husten and Eipper 1994).

Both soluble and integral forms of PAM traffic simultaneously through the early secretory pathway, but then diverge upon entry into the ISG (Milgram, Eipper, and Mains 1994). The enzymatic domains of PAM contain information for direction toward the regulated secretory pathway since expressed soluble PHM or PAL traffic correctly into ISGs (Milgram, Johnson, and Mains 1992), however, the transmembrane/cytosolic aspect of integral membrane PAM can override luminal trafficking information for transit via an independent route (Milgram, Eipper, and Mains 1994; Milgram, Mains, and Eipper 1993). While both forms enter the ISG efficiently and are retained to some degree within maturing SGs, they can both exit the ISG through the constitutive-like pathway in

unstimulated conditions (Milgram, Eipper, and Mains 1994). Integral membrane PAM exits the SG to a greater extent (Milgram, Eipper, and Mains 1994), and has been shown to cycle through the PM where it may be retrieved to the TGN (Milgram, Mains, and Eipper 1996) or the MSG (El Meskini et al. 2001; Marx and Mains 2002).

Since human β-cells only express PAM3 (Y.-C. Chen et al. 2020), a soluble isoform, its trafficking is relatively simple. The situation is more complicated in mouse β-cells which express transmembrane isoforms PAM1 and PAM2 (Y.-C. Chen et al. 2020), and thus, are subject to additional trafficking fates and require endoproteolytic cleavage within the SG to generate soluble PAM to access substrates more readily [212]. In addition to a low pH (Eipper et al. 1991; Husten and Eipper 1994), Zn^{2+} and Ca^{2+} (Chufán et al. 2009), PAM requires Cu^{2+} (Kulathila et al. 1994) and ascorbate (Bradbury, Finnie, and Smyth 1982) for activity.

Collectively, enzymes control the intragranular landscape by modifying proteins and altering their properties, operating as the focal regulatory units of the SG lumen. This culminates in the main transformative event of the granule interior—the crystallization of proteolytically generated insulin—which creates an extremely dense proteinaceous core. Though deploying enzymes that require such specific conditions for activity, it appears that the β-cell strikes a balance between rapid processing and orderly aggregation to ensure the safe generation of a functional product.

1.2.3.3 Ions, Transporters, and Channels

Transporters and channels embedded into the secretory pathway membrane control the composition of the luminal milieu to facilitate cargo sorting and processing. They also control the release of ions from the SG store to regulate cytosolic events. In this section, we will discuss the coordinated function of transporters and channels that modulate important features of the intergranular lumen.

Activation: H^+. Foundational studies from the Hutton lab established the low pH of the β-cell SG (Hutton 1982) and found activity of an ATP-dependent pump responsible for translocating H^+ into the granule lumen (Hutton and Peshavaria 1982). The vacuolar H^+-ATPase (V-ATPase) localizes to the β-cell SG (Sun-Wada et al. 2006) and is the major component responsible for endoprotease activation and cargo processing in regulated secretory cells (Schoonderwoert et al. 2000; Taupenot, Harper, and O'Connor 2005). Due to the influx of positive charge, a complimentary influx or efflux of anions or cations, respectively, would be required to maintain a normal electrochemical gradient across the SG membrane and this is normally achieved by the counterregulatory actions of Cl^- transporters (Barg et al. 2001; Deriy et al. 2009; Li et al. 2009; Maritzen et al. 2008; Jentsch et al. 2010). Moreover, other transporters can utilize the proton gradient generated by V-ATPase to exchange H^+ for cytosolic materials. For example, vesicular monoamine transporter type-2 (VMAT2) can exchange intragranular H^+ for cytosolic monoamines, thus functioning to regulate the luminal pH (Blackmore et al. 2001).

V-ATPase is widely distributed throughout the endo-lysosomal system and the plasma membrane. It consists of two complexes, V_1 (cytosolic) and V_0 (membrane-associated) (**Figure 7**), which, respectively, contain eight and nine subunits (Holliday 2014). ATP hydrolysis by V_1 provides energy for V_0 to rotate and pump 2–4 H^+ molecules from the cytosol into luminal or extracellular spaces (Maxson and Grinstein 2014), and this can be controlled by several factors. Dissociation of V_1 from V_0 is the primary mechanism of pump regulation (Lafourcade et al. 2008) and is sensitive to glucose exposure (Kane 1995). Complex assembly is affected by the membrane lipid composition; the β-cell SG contains an abundance of enriched lipid species, and sphingolipids are thought to stabilize assembly and facilitate ATP hydrolysis (Chung, Lester, and Dickson 2003). Localization and density of the pump is obviously limiting for compartmental acidification, thus, regarding the β-cell SG, an abundance of V-ATPase is critical for luminal protein processing.

In addition, H^+ pumping is sub-optimally coupled to ATP hydrolysis (Kettner et al. 2003; Cross and Müller 2004), providing room for further V-ATPase modulation. This may contribute to the establishment of a secretory pathway H^+ gradient or allow V-ATPase to respond to environmental stimuli. In yeast, V-ATPase efficiency is associated with the a-subunit of the V_0 domain, which is also likely to determine its cellular localization (Kawasaki-Nishi et al. 2001). Subunit a is situated in an ideal position to modulate the pump. It is embedded into the membrane adjacent to a proteolipid ring formed by the c subunits of V_0 (through which H^+ passes) and extends toward the cytosol to interact with V_1 (Holliday 2014). Yeast co-express two homologs to the mammalian a-subunit and these have been shown to affect both the localization and activity of V-ATPase (Kawasaki-Nishi et al. 2001).

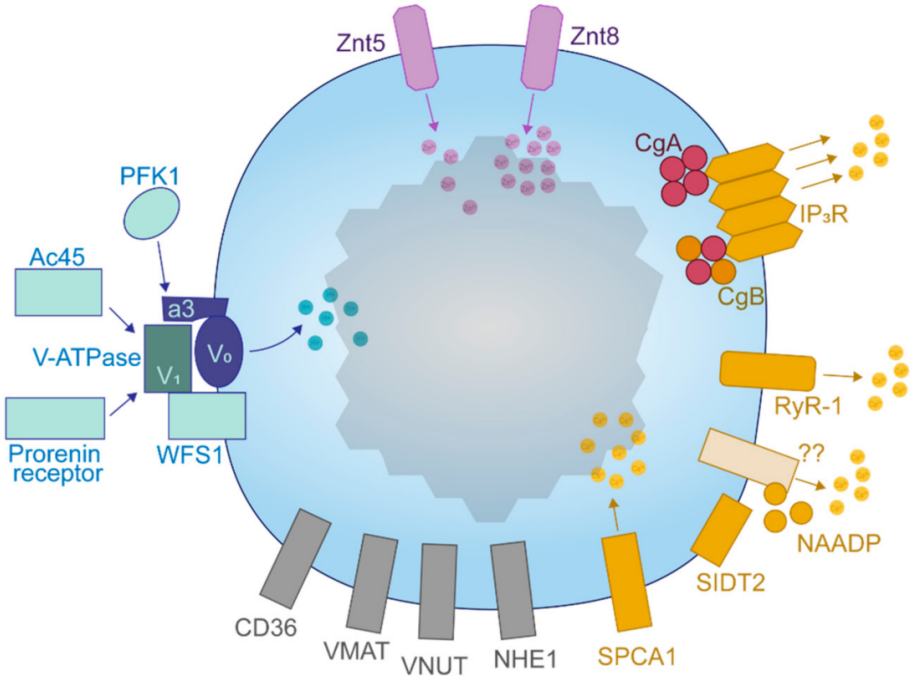

Figure 7. Channels and transporters of the insulin SG. An array of transmembrane components controls the luminal composition of the insulin SG and transform the SG into a responsive store that is utilized by the beta cell for cytosolic signaling.

Four isoforms of subunit a exist in mammals (a1–a4) making it the most diverse member of the V-ATPase complex, suggesting that this component can endow compartmental specificity regarding the localization and efficiency of the pump. a1 appears to localize to the Golgi, a2 to both lysosomes and the Golgi and a3 is mostly expressed on β-cell SGs (Sun-Wada et al. 2006). Interestingly, the a4 subunit has been shown to interact with 1-phosphofructokinase (PFK1) in the human kidney (Y. Su et al. 2003), coupling nutrient sensing to V-ATPase activity (Banerjee and Kane 2020). SGs with low pH are required for GSIS (Stiernet et al. 2006); therefore, glucose-mediated acidification could facilitate both SG maturation and release.

Accessory subunits Ac45 and the prorenin receptor, encoded by ATP6ap1 and ATP6ap2 genes, respectively, are also associated with the V-ATPase to assist SG acidification in β-cells (Louagie et al. 2008; Dai et al. 2015; Binger et al. 2019; Brouwers et al. 2021). Ac45 is subject to processing by furin (Louagie et al. 2008; Brouwers et al. 2021) and the prorenin receptor interacts with and may act downstream of the GLP1 receptor (Dai et al. 2015; Binger et al. 2019). A V-ATPase interactor, Wolfram syndrome 1 (WFS1), resides in β-cell ER and SG membranes (Hatanaka et al. 2011) and has been shown to bind the V1A subunit via an N-terminal region to assist SG acidification (Gharanei et al. 2013). To conclude, the V-ATPase and/or its regulatory subunits are potential targets for enhancing insulin production during high demand.

Crystallization: Zn^{2+}. Insulin SGs hold high levels of Zn^{2+}, with some estimates approaching 30 mM (Hutton, Penn, and Peshavaria 1983; Vinkenborg et al. 2009). Zn^{2+} can alter the structure of its bound proteins, cofactor for enzyme activity and also serve as an extracellular signaling molecule (Bafaro et al. 2017). Measurement of insulin and Zn^{2+} released during GSIS reveals that the total amount of Zn^{2+} in the SG is at least double that which is expected based on the stoichiometric composition of the insulin hexamer (Lubag et al. 2011), probably due to the existence of an additional Zn^{2+} that displaces water within crystallized hexamers (Lemaire, Chimienti, and Schuit 2012). Co-secreted Zn^{2+} has autocrine (Slepchenko et al. 2015; Slepchenko, James, and Li 2013) and potentially paracrine (H. Zhou et al. 2007; Hardy et al. 2011) effects on other islet cells, and may also travel to the liver to inhibit insulin receptor endocytosis and thus hepatic insulin uptake (Tamaki et al. 2013). One study using computer modelling has also suggested that Zn^{2+} could maintain insulin in an oligomeric state during secretion, and that this would limit the availability of Zn^{2+} and monomeric insulin to act as anti-fibrillogenic agents against hIAPP-related proteins (Nedumpully-Govindan and Ding 2015). Early estimates, however, report that exposure to the extracellular environment would likely dissipate the insulin-zinc hexamer seconds after complex dilution outside of the β-cell (Gold and Grodsky 1984), allowing monomeric insulin to circulate and signal. Notably, reductions in circulating and pancreatic Zn^{2+} levels are implicated in those with excess fat and T2D (Banaszak, Górna, and Przysławski 2021; Rutter et al. 2016), and Zn^{2+} supplementation can enhance insulin secretion to better control glycemia during the insulin resistant state (Cooper-Capetini et al. 2017). Thus, intracellular changes in Zn^{2+} could drive aspects of β-cell dysfunction.

Secretory pathway Zn^{2+} uptake is under the control of the Zn^{2+} transporter (ZnT) family. ZnTs dimerize to localize and function and likely do so as H^+/Zn^{2+} antiporters (Bafaro et al. 2017; Daniels, Jagielnicki, and Yeager 2020), so therefore the establishment of a luminal proton gradient by V-ATPase may be permissive for Zn^{2+} uptake. ZnT5 and Znt7 localize to the β-cell Golgi apparatus whereas ZnT5 and ZnT8 are in the SG (Lemaire, Chimienti, and Schuit 2012) (**Figure 7**). ZnT3 has been shown to colocalize with insulin in INS1 cells (Smidt et al. 2016), however it appears to be absent in β-cells from mouse islets (Bellomo, Meur, and Rutter 2011). ZnT8 is the most abundantly expressed β-cell ZnT but has minimal expression in other tissues (Lemaire, Chimienti, and Schuit 2012).

The current literature on ZnT8-mediated Zn^{2+} homeostasis is deep and interesting, owing to the existence of multiple T2D susceptibility loci covering the SLC30A8 gene (Barragán-Álvarez et al. 2021; Rutter and Chimienti 2014; Davidson, Wenzlau, and O'Brien 2014). Importantly, loss of function mutations at residue 325 tend to favor a reduced risk of T2D, and opposite deleterious effects are seen with a gain of function at this residue. These may be mediated by changes to proinsulin conversion and insulin secretion, raising the question of whether Zn^{2+} is important for β-cell SG biogenesis. Surprisingly, guinea pigs express a proinsulin molecule that lacks histidine at the B10 residue and thus cannot bind Zn^{2+}, similar to the human mutation discussed in Section 1.2.3.1, yet

they can generate SGs, process proinsulin, and secrete insulin (Zimmerman, Kells, and Yip 1972). However, despite the inability of insulin to bind Zn^{2+}, the presence of Zn^{2+} in these settings is not changed as is the case with altered ZnT8 transporter activity.

Studies of the effect of ZnT8 depletion in β-cell lines and rodent models have provided results that are difficult to synthesize thus far (Rutter and Chimienti 2014; Davidson, Wenzlau, and O'Brien 2014; O'Halloran et al. 2013). In general, experimental depletion of ZnT8 does not lead to major impairments in proinsulin processing or insulin content; however, SGs tend to be void of electron-dense spheres, appearing instead as electron-dense rods or as pale ISGs. This agrees with the expression of other ZnT members through the secretory pathway and on the SG, providing sufficient Zn^{2+} to sustain intragranular functions albeit with impaired insulin crystallization (Lemaire, Chimienti, and Schuit 2012; Lemaire et al. 2009). Assessment of insulin secretion in various ZnT8-deficient models has shown a mixed bag of results, with reports contrasting between mildly reduced, unchanged, or mildly enhanced effects (Rutter and Chimienti 2014; Davidson, Wenzlau, and O'Brien 2014; O'Halloran et al. 2013). Recognition of variable factors such as the mode of deletion, and mouse age, sex, and genetic background are hoped to assist in study design to clear up the matter (Rutter and Chimienti 2014). Indeed, a study published in 2020 revealed both positive and negative age-dependent consequences of ZnT8 deletion in mice (Syring et al. 2020). Moreover, assessing the importance of Zn^{2+} for SG biogenesis is complicated by the presence of multiple ZnTs. For example, an investigation comparing the effects of a whole-body single ZnT7 KO to a double ZnT7/ZnT8 KO, revealed that the double KO could provide a significant secretory defect not seen by ZnT7 KOs alone or by previous reports in ZnT8 KOs (Syring et al. 2016)].

Several lines of evidence indicate that ZnT8-mediated Zn^{2+} import affects proinsulin processing, which could explain, at least in part, the protective or deleterious impacts of SLC30A8 mutations. It has been shown that humans with the arginine risk variant of ZnT8 at residue 325, thought to be a gain-of-function mutation (Merriman et al. 2016), display increased circulating proinsulin compared to the protective tryptophan variant (Kirchhoff et al. 2008). Moreover, mice overexpressing the arginine 325 variant have an increased β-cell proinsulin content and release (Tumarada et al. 2017). Conversely, in INS1E cells expressing the loss-of-function tryptophan 325 variant, cyclosporin A-induced β-cell dysfunction was attenuated when compared to the gain-of-function arginine 325 variant (Kim et al. 2011). Finally, humans heterozygous for a ZnT8 variant truncated at residue 138, which impairs transporter synthesis and thus results in ZnT8 haploinsufficiency, are equipped with increased proinsulin conversion and circulating insulin, and improved glucose tolerance (Tumarada et al. 2017; Dwivedi et al. 2019). Since ZnTs are likely to function as H^{+}/Zn^{2+} exchangers (Bafaro et al. 2017; Daniels, Jagielnicki, and Yeager 2020), enhanced flux through ZnT8 could buffer the reduction in luminal pH during SG maturation to limit endoprotease activity. Accelerated packing of the granule matrix in the presence of high Zn^{2+} could also reduce the accessibility of proinsulin to the endoproteases for conversion. In the case of reduced

ZnT8 activity or haploinsufficiency, the presence of adequate Zn^{2+} supplied by the single copy of ZnT8 or other ZnTs in the secretory pathway would probably maintain hexameric proinsulin transit and cofactor for CPE activity, while the event of insulin crystallization does not appear to be necessary for regulated release. Therefore, in the setting of β-cell compensation, a ready supply of mature insulin could help to control circulating glucose. Importantly, SLC30A8 risk-alleles are particularly noted to confer T2D susceptibility to lean individuals (Davidson, Wenzlau, and O'Brien 2014; Cauchi et al. 2008), so in this case, limited proinsulin conversion in newly synthesized granules that are preferentially secreted could reduce the insulin response to glucose. Nonetheless, there is still plenty to be learned about the impact that Zn^{2+} has inside the insulin SG. While the consequence of SLC30A8 gene variants have been of interest, little is known about Znt8 structure and mechanism, and the factors that regulate it.

Modulation: Ca^{2+}. Ca^{2+} is concentrated within the secretory pathway relative to the cytosol, where it controls luminal protein sorting and processing among other activities. Travelling proximal to distal, the amount of free Ca^{2+} decreases whereas the total amount of Ca^{2+} increases (**Figure 2**), in line with several proteins harboring an increased affinity to Ca^{2+} when the pH is reduced (Yoo and Albanesi 1991; Gerdes et al. 1989). Quantitatively, the β-cell SG can hold between 50 to 100 mM Ca^{2+} (Hutton, Penn, and Peshavaria 1983), although measurement of the free concentration yields values of around 50 μM (~0.05% of the total amount) (Mitchell et al. 2001). Therefore, the SG compartment, endowed with transporters and channels for Ca^{2+}, should possess a high capacity to buffer cytosolic Ca^{2+}. This dynamic reservoir can be utilized during β-cell stimulation to sequester and release Ca^{2+}, modulating the cytosolic signals that underlie insulin secretion. Indeed, it has been shown that depletion of Ca^{2+} from the SG compartment impairs exocytosis (Scheenen et al. 1998). β-cell SGs have been shown to take up Ca^{2+} during nutrient exposure (Mitchell et al. 2001), and Ca^{2+} release from the SG is required for insulin secretion (Mitchell, Lai, and Rutter 2003). Ca^{2+}-dependent effector proteins are in proximity to the SG and sites of exocytosis (Thurmond and Gaisano 2020), and therefore localized Ca^{2+} released from the SG could facilitate its own trafficking and exocytosis.

Several transporters and channels act in concert to coordinate luminal and cytosolic events that are regulated by Ca^{2+} (**Figure 7**). The secretory pathway Ca^{2+} ATPase 1 (SPCA1) is an uptake pump that regulates a Ca^{2+}-dependent secretory protein sorting mechanism at the TGN in constitutively secreting cells (von Blume et al. 2012, 2011). In INS1 cells, SPCA1 may sequester cytosolic Ca^{2+} into secretory pathway compartments during glucose stimulation, accounting for around 20% of the total SG Ca^{2+} uptake (Mitchell, Tsuboi, and Rutter 2004). Its depletion thus enhances insulin secretion (Mitchell, Tsuboi, and Rutter 2004). In these cells, SPCA1 was shown to fractionate strongly with insulin suggesting its localization throughout the early and late secretory pathway (Mitchell, Tsuboi, and Rutter 2004).

Ryanodine receptors (RyRs) respond directly to cytosolic Ca^{2+} to release Ca^{2+} from intracellular stores but are inactive at low and high concentrations of Ca^{2+}. RyR-1 was identified as the lone RyR subtype expressed on the β-cell SG, but it is also expressed on the ER where RyR-2 also locates (Mitchell, Lai, and Rutter 2003). Pharmacological inhibition of SG RyR-1 reduces Ca^{2+} efflux and impairs GSIS (Mitchell, Lai, and Rutter 2003).

NAADP is a potent signaling molecule produced during β-cell glucose metabolism (Masgrau et al. 2003) that binds to unidentified NAADP-sensitive sites to elicit Ca^{2+} release from intracellular stores, including the SG, during GSIS (Mitchell et al. 2001; Chang et al. 2016). SIDT2 is located on insulin SGs and may mediate this mechanism (Chang et al. 2016). Whole-body SIDT2 KO mice are glucose intolerant and have an insulin secretory defect (Gao et al. 2013). The requirement of either NAADP or RyR-1-mediated Ca^{2+} release for GSIS suggests that the SG is an important reservoir of Ca^{2+} that is utilized during secretory functions.

After initial confusion (Blondel et al. 1994; Ravazzola, Halban, and Orci 1996), it was recently verified that all three subtypes of the IP_3R are expressed on β-cell SGs at a level two-fold higher than the ER (Hur and Yoo 2015). IP_3Rs require tetramerization and binding of each member to inositol 1,4,5-triphosphate (IP_3) in order for the channel to open and release Ca^{2+} from stores, and these tetramers can be formed by any combination of IP_3R subtypes (Taylor and Konieczny 2016). In the absence of IP_3, Ca^{2+} inhibits the IP_3R, although, Ca^{2+} must bind to the IP_3R with IP_3 for the channel to open (Taylor and Tovey 2010). IP_3Rs localized on non-β-cell SGs have been estimated to be more sensitive than those of the ER (Huh, Kim, and Yoo 2007), although one study reported that β-cell SGs do not release Ca^{2+} in response to IP_3 (Mitchell et al. 2001). Several caveats are apparent in this study; low levels of Ca^{2+} were incubated with permeabilized mouse insulinoma MIN6 cells exposed to IP_3 despite a high requirement for maximal IP_3R activation (Marshall and Taylor 1993), and the membrane glutamine receptor (mGlu5) is unable to raise cytosolic Ca^{2+} in conjunction with its function to generate IP_3 (Storto et al. 2006) as would be seen during glucose stimulation (Takahashi, Yokoi, and Seino 2019). Therefore, the role of IP_3R-mediated Ca^{2+} release from the insulin SG should be reevaluated.

On the inside, both CgA and CgB can interact with the intraluminal loop of all three IP_3R subtypes at pH 5.5 to stabilize IP_3 binding and channel rigidity (Yoo and Lewis 1995; Huh, Kim, and Yoo 2007; Yoo and Lewis 2000; Yoo and Jeon 2000; Yoo et al. 2000). These granins possess an extremely high capacity to bind Ca^{2+} with low affinity at the acidic pH of the MSG (Yoo and Albanesi 1991; Yoo et al. 2001), and it has been suggested that IP_3R conformational changes can alter that of CgA and CgB to release bound Ca^{2+} through the IP_3R channel (Yoo et al. 2000; Yoo 2010). The relative abundance of IP_3R isoforms and their tetrameric composition as well as that of the interacting granin species are thought to underlie SG Ca^{2+} balance, such that equal amounts of IP_3 can stimulate varying amounts of Ca^{2+} release (Yoo 2000). Therefore, the distribution of components within the SG during maturation, idling, and in primed states could modulate SG Ca^{2+} release. Indeed, CgB can undergo redistribution to the MSG periphery upon glucose stimulation (Giordano et al. 2008). Since intragranular acidification is essential for chromogranin-IP_3R interactions, it appears that the utility of the SG as an IP_3-sensitive Ca^{2+} store is reliant on its proper maturation. In conclusion, a host of components are responsible for handling Ca^{2+} for use both inside and outside of the SG.

Other transporters. SGs in the β-cell also contain a truncated form of the NHE1 Na^+/H^+ exchanger (Moulin et al. 2007), fatty acid translocase (FAT/CD36) (Noushmehr et al. 2005; Nagao et al. 2020), and a vesicular nucleotide transporter (VNUT) (Geisler et al. 2013). A role for NHE1 has not yet been determined. CD36, which is predominantly expressed on the PM, has multiple roles throughout the body (X. Su and Abumrad 2009), with a general cellular function to facilitate fatty acid uptake. In β-cells, CD36 is localized to the PM and the SG and mediates the acute and chronic effects of free fatty acids on insulin secretion (Noushmehr et al. 2005). CD36 is upregulated in the islets of obese humans with T2D, where altered lipid handling may impair the action of exocytotic proteins (Nagao et al. 2020). VNUT is a transporter required for ATP uptake into the SG lumen (Geisler et al. 2013) and its depletion results in reduced basal and glucose-stimulated ATP release and insulin secretion (Geisler et al. 2013). In addition, a Golgi-localized magnesium transporter NIPAL1 was recently shown to positively regulate insulin content and secretion in MIN6 cells (Manialawy et al. 2020), albeit through an unknown mechanism.

The activity of channels and transporters provide overarching control on SG maturation and serve as conduits that alter luminal responses based on events transpiring in the cytosol. A prime example is the ability of glucose to drive V-ATPase subunit association to enhance acidification. Together, their presence transforms the SG into a dynamic hub used for ionic signaling and buffering.

1.2.3.4 Sorting Receptors

Early efforts centered around identifying a 'sorting by entry' receptor for proinsulin proved futile, possibly because soluble secretory cargo destined for the β-cell MSG are not sorted through receptor-mediated recognition. CPE was once entertained as a candidate for proinsulin sorting from the TGN (Cool et al. 1997; Normant and Loh 1998), but this was contested (Irminger et al. 1997). Conversely, the mannose 6 phosphate receptor (M6PR) has been identified as a critical component of 'sorting by exit' which serves to refine the SG during maturation. It functions to target proteins modified with a mannose 6 phosphate carbohydrate group from the TGN and the ISG to the lysosome, as well as from the plasma membrane for endosomal retrieval (Klumperman et al. 1998, 1993; Dittié, Klumperman, and Tooze 1999; Puertollano et al. 2001). The M6PR specifically contributes to the sorting of the luminal lysosomal hydrolase pro-cathepsin B in β-cells (Kuliawat et al. 1997; Klumperman et al. 1998) (**Figure 8**).

Two forms of the M6PR exist, a cation independent (CI) ~300 kDa isoform and a ~46 kDa isoform that dimerizes and requires cationic binding (CD—cation dependent) to function. The CD-M6PR locates to the TGN and the ISG where it resides in proximity to clathrin-coated patches and is found on small transport vesicles but not in the MSG (Klumperman et al. 1998). Islets lacking the CD-M6PR contain four-fold more cathepsin B in the β-cell MSG (Kuliawat et al. 1997). While the CD-M6PR has a defined role in cathepsin B sorting, a role for the CI-M6PR in the β-cell SG has not yet been determined. To conclude here, little is known about other luminal components that are actively removed from the ISG.

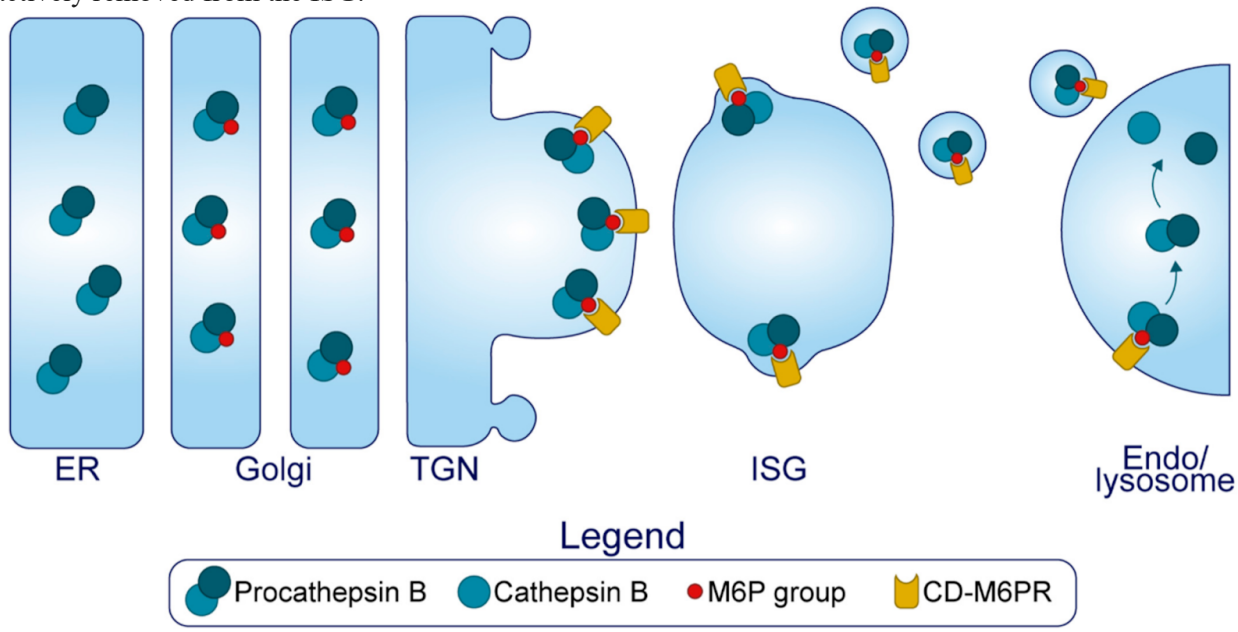

Figure 8. Granule refinement. The cation dependent mannose 6 phosphate receptor (M6PR) binds to certain proteins modified with a mannose 6 phosphate group (namely, procathepsin B) in the TGN, and this complex enters the ISG. During maturation, this complex will exit the SG via small transport vesicles and traffic to the endolysosomal system. A byproduct of this process may be the removal of soluble components in the general vicinity of the budding vesicle.

1.2.4 Concluding Remarks

At its essence, insulin synthesis requires the entry of proinsulin and its processing enzymes into ISGs, followed by enzyme activation and then the complete execution of enzymatic activity. Each of these steps are facilitated by ions that are supplied by channels and transporters, which exert influence on luminal proteins by altering their behavior. First, ion-facilitated granin aggregation and binding to distinct lipid rafts of the TGN membrane may provide the luminal driving force to generate SGs, forming what is currently an ill-defined path of entry for protein to flow through. This is evidenced by observations that granin depletion can limit the biogenesis of nascent SGs. Several resident enzymes of the SG also aggregate specifically in the TGN and bind to lipid rafts to provide a common pathway for sorting, however the trafficking route that key proteins such as proinsulin and proIAPP take are yet to be fully defined. Sorting by entry into the ISG is efficient but may not be entirely specific, so the presence of sorting receptors and active ion uptake transporters provide the ISG with two simultaneous quality control mechanisms for refinement—sorting by exit and sorting by retention. Here, proteins specifically recognized by sorting receptors, and some unwitting bystanders, are escorted from the SG via small transport vesicles, but MSG-destined proteins will bind luminal ions to reduce their solubility and prevent their egression via these carriers. It is currently unclear how important the two post-Golgi sorting mechanisms are for generating insulin itself, but irregular SG maturation could impair overall SG composition and function and encourage the pathological formation of hIAPP oligomers. As the lumen is progressively modified by continual ion uptake, enzymes will begin to exert activity on proinsulin and other peptides to form the complete intragranular cocktail, which will develop into an extremely insoluble ion-bound crystal core surrounded by a halo of soluble components. Here, human T2D-associated Znt8 variants are the exemplar of how ionic alterations can affect parameters of SG maturation, and conceptually illustrate how seemingly small differences can precipitate the chronic disease. Once mature, the SG functions as an intracellular signaling compartment in addition to its role in holding and releasing insulin.

In T2D there is a loss of insulin SGs, GSIS is impaired, and the secretion of proinsulin and its processing intermediates is elevated. Recent subcellular evidence links these phenotypes to a diversion away from SG maturation toward premature ISG secretion, suggesting that MSG formation is a primary limiting factor for insulin secretion in T2D. It is therefore conceivable that defects within the secretory pathway could predispose individuals to the disease by creating an upstream bottleneck to MSG production, delaying the synthesis of MSGs. This might be fine in the healthy state when production is not limiting but could compromise secretion when insulin content is depleted during the chronic condition.

Currently, there is an abundance of knowledge about the distal stages of exocytosis, but a gap in our understanding of events that occur through the late Golgi and the maturing SG. Here, we have provided a comprehensive summary of what happens inside the lumen during the formative hours of the insulin SG. In doing so, it becomes clear that generating a SG that is rich in insulin is quite arduous, and therefore, prone to perturbations that may affect the capacity of the β-cell to adapt to chronic demand.

1.3 Cab45

As discussed, Ca^{2+}-dependent cargo aggregation within the TGN is crucial for ISG generation in specialised secretory cells. A soluble Golgi-resident Ca^{2+}-binding protein of 45 kDa, Cab45, has recently been uncovered as the centrepiece of a novel secretory cargo sorting pathway in HeLa cells (von Blume et al. 2012; Crevenna et al. 2016). HeLa cells only participate in constitutive secretory functions, and the role of Cab45 in specialised secretory cells (i.e. cells equipped with a regulated secretory pathway) such as the pancreatic β-cell is unknown. Genome-wide association studies (GWAS) have implicated several Cab45 coding variants both positively and negatively associated with diseases including T2D or markers of metabolic disease such as fasting glucose, fasting insulin, and several indicators of body composition (HuGeAMP 2022). Its mRNA transcript is also upregulated in islets of the leptin-deficient C57BL/6J$^{ob/ob}$ mouse (Diabetes Wisconsin 2022), a model where β-cells undergo successful compensation during obesity and insulin resistance, suggesting a potential function in insulin SG production or downstream exocytosis. The subject of this thesis is the characterisation of Cab45 in β-cell lines and primary rodent islets in relation to this potential function. In doing so, this is also the first study of Cab45 in specialised secretory cells.

Cab45 is part of the CREC (Calumenin, Reticulocalbin, ERC-55, Cab45) family of proteins that all contain multiple low affinity Ca^{2+}-binding EF-hands and mostly localise to various sites along the secretory pathway of mammalian cells (Honore and Vorum 2000; Honoré 2009). Low affinity high capacity Ca^{2+}-binding gives CREC family proteins the ability to sense changes in local calcium concentrations over a large dynamic range, and considerable sequence variability outside of the EF hand motifs allow each member to carry out diverse intracellular activities in response to calcium signalling.

1.3.1 The SDF4 Gene and Cab45 Isoforms

Cab45 is encoded by the stromal cell derived factor 4 (SDF4) gene, situated at chromosome 1.p36.33 in humans (National Center for Biotechnology Information 2022). The human SDF4 transcript is alternatively spliced to produce three known protein isoforms. These are Cab45-G, Cab45-S and Cab45-C, localising to the Golgi (von Blume et al. 2012), ER (L. Chen et al. 2014, 2016) and the cytosol (Lam et al. 2007) respectively (**Figure 9A**). Cab45-G and Cab45-S share a common translational start site in exon 2 of the mature SDF4 transcript but use alternative 3' acceptor splice junctions in exon 7 (National Center for Biotechnology Information 2022). This results in homologous amino acid sequences up to residue 304, but differ from residue 305 onwards due to a frameshift. Both contain an N-terminal signal sequence for direction into the secretory pathway (Uniprot Consortium 2022). The full-length 362 amino acid isoform Cab45-G contains six EF hands, while the Cab45-S isoform lacks a 6th EF hand and extends to 348 amino acids (Uniprot Consortium 2022). Cab45-C is an N-terminally truncated isoform due to the skipping of exons 2 and 3, resulting

in a translational start site in exon 5 that produces a 130-amino acid protein that does not contain a signal sequence (Uniprot Consortium 2022). This isoform is completely homologous to the C-terminus of Cab45-G and harbours three EF hands. The Universal Protein Resource (UniProt) database indicates the existence of a further three human isoforms with sizes of 202, 254, and 250 amino acids (Uniprot Consortium 2022), however experimental validation of these isoforms are unavailable.

The canonical Cab45-G protein is highly conserved between mammals – human Cab45-G shares 87% and 85% sequence homology with mouse and rat respectively, while rat and mouse share 95% homology. UniProt lists only two isoforms each in rat and mouse – a 361-amino acid Cab45-G isoform expressed in both, as well as a 218-amino acid isoform in mouse and a 382-amino acid isoform expressed in rat (Uniprot Consortium 2022). This is despite functional studies from one research group into the exocytotic capabilities of the 130-amino acid Cab45-C in rat pancreatic acinar cells (Lam et al. 2007) and β-cells (Zhang et al. 2009). In regards to this, evidence published for the expression of Cab45-C in rat β-cells appear questionable as antibodies show almost perfect colocalisation with insulin (indicating cross-reactivity), and this publication did not include any staining of Cab45-C alone (Zhang et al. 2009). Decent evidence however has been presented by the same group for its expression in rat pancreatic acinar cells (Lam et al. 2007). Aside from these publications, all existing functional studies related to Cab45 have employed human cell cultures, therefore, the question remains open as to which isoforms are expressed in mouse and rat cells. This is an important consideration since current β-cell research relies heavily on the rat INS1 cell line and the mouse MIN6 cell line. From here on in, Cab45-G will be referred to as Cab45 unless otherwise stated.

1.3.2 Cab45-Dependent Cargo Sorting at the *Trans*-Golgi Network

Cab45-dependent cargo sorting in HeLa cells is dependent on the control of luminal Golgi Ca^{2+} signals, which hinge on cytosolic interactions between the cofilin isoforms, actin depolymerizing factor (ADF) and cofilin-1, with filamentous (F)-actin and the TGN-localised transmembrane Ca^{2+} uptake pump SPCA1 (**Figure 9B**) (Pakdel and von Blume 2018; Blank and von Blume 2017; Kienzle and von Blume 2014). In the cytosol, ADF and cofilin-1 are under the control of LIM kinase (LIMK) and protein phosphatase slingshot homologue 1 (SSH1) (Mizuno 2013), and in the lumen, Cab45 is under the control of protein kinase Fam20C (Hecht et al. 2020). Additional components diacylglycerol and sphingomyelin assist in the generation of vesicles that Cab45-cargo complexes enter (Deng et al. 2018). Targeted depletion of ADF/cofilin-1, SPCA1, Cab45, and Fam20C have each been shown to disrupt the secretion of several exogenously and endogenously expressed proteins in HeLa cells whereas that of others are maintained, indicating that this pathway has specificity toward certain cargoes (von Blume et al. 2012, 2011, 2009; Hecht et al. 2020). Targeted depletion experiments have also gathered that these components are critical for Golgi Ca^{2+} homeostasis. Thus, the pancreatic β-cell, which contains a unique set of secretory proteins and relies on Ca^{2+} for insulin SG biogenesis and stimulus-secretion coupling, is an excellent candidate system to further explore the function of Cab45.

In the cytosol, cofilin protein localisation is heterogeneous and exists in active (dephosphorylated) and inactive (phosphorylated) states (Mizuno 2013). Active cofilin accelerates actin dynamics by binding to and severing F-actin, consequentially increasing the abundance of G-actin to be used as substrate for further actin remodelling. When inactive, cofilins cannot bind or sever F-actin, limiting the supply of G-actin. In HeLa cells it has been shown that a small pool of cofilin-1 localises to the TGN, but during periods of high secretory activity active cofilin-1 undergoes extensive redistribution to the TGN in an actin-dependent process (von Blume et al. 2011). While the molecular nature of this redirection remains to be elucidated, at the TGN, active cofilin-1 binds to the P-domain of the SPCA1 Ca^{2+} pump (Kienzle et al. 2014). Here, in contrast to its typical role as a severing protein, cofilin-1 has been demonstrated to work as a linker that recruits F-actin to SPCA1 (Kienzle et al. 2014). These interactions are required for SPCA1-mediated Ca^{2+} uptake into the TGN where it has been theorised that F-actin works to assemble SPCA1 into cholesterol-rich membrane microdomains that are preferred for pump activity (Kienzle et al. 2014). Furthermore, in a positive feedback cycle, SPCA1 activity is coupled to sphingomyelin and diacylglycerol synthesis (Deng et al. 2018), the latter of which promotes negative membrane curvature and the budding of secretory vesicles from the TGN. Sphingomyelin is also an essential component of vesicle membranes that contain cargoes of this sorting pathway, and its local enrichment at sites across the TGN containing SPCA1 promotes pump activity (Deng et al. 2018). While much is to be resolved about the nature of the F-actin-ADF/cofilin-1-SPCA1 complex, the controllers of cofilin phosphorylation, LIMK and

SSH1, have also been localised to the TGN and are implicated in secretory cargo sorting (von Blume et al. 2009). Therefore, it may be the case that the coordination of dynamic actin remodelling at the TGN by LIMK/SSH1/ADF/cofilin-1 is the means by which SPCA1 pumping activity is regulated.

In the secretory pathway lumen, the localisation and behaviour of Cab45, a soluble protein, is controlled through both phosphorylation and Ca^{2+} binding (von Blume et al. 2012; Crevenna et al. 2016; Hecht et al. 2020). In HeLa cells, Cab45 localises to the TGN and exists in both low molecular weight and large molecular weight oligomeric complexes, the latter of which are formed only in the presence of Ca^{2+} concentrations that are found in the Golgi complex (Crevenna et al. 2016). Thus, SPCA1 mediated Ca^{2+} uptake into the TGN favours the formation of Cab45 oligomers, which have been demonstrated to interact with specific secretory cargo and regulate their secretion presumably by aggregating and sorting them away from other soluble proteins (Crevenna et al. 2016). From here, Cab45 phosphorylation by Fam20C provides a higher order of control by limiting the size of Cab45 oligomers to permit entry of Cab45-cargo complexes into sphingomyelin-enriched vesicles (Hecht et al. 2020). Phosphorylation state may account for the detection of low molecular weight Cab45 despite its localisation in the high Ca^{2+} environment of the Golgi apparatus.

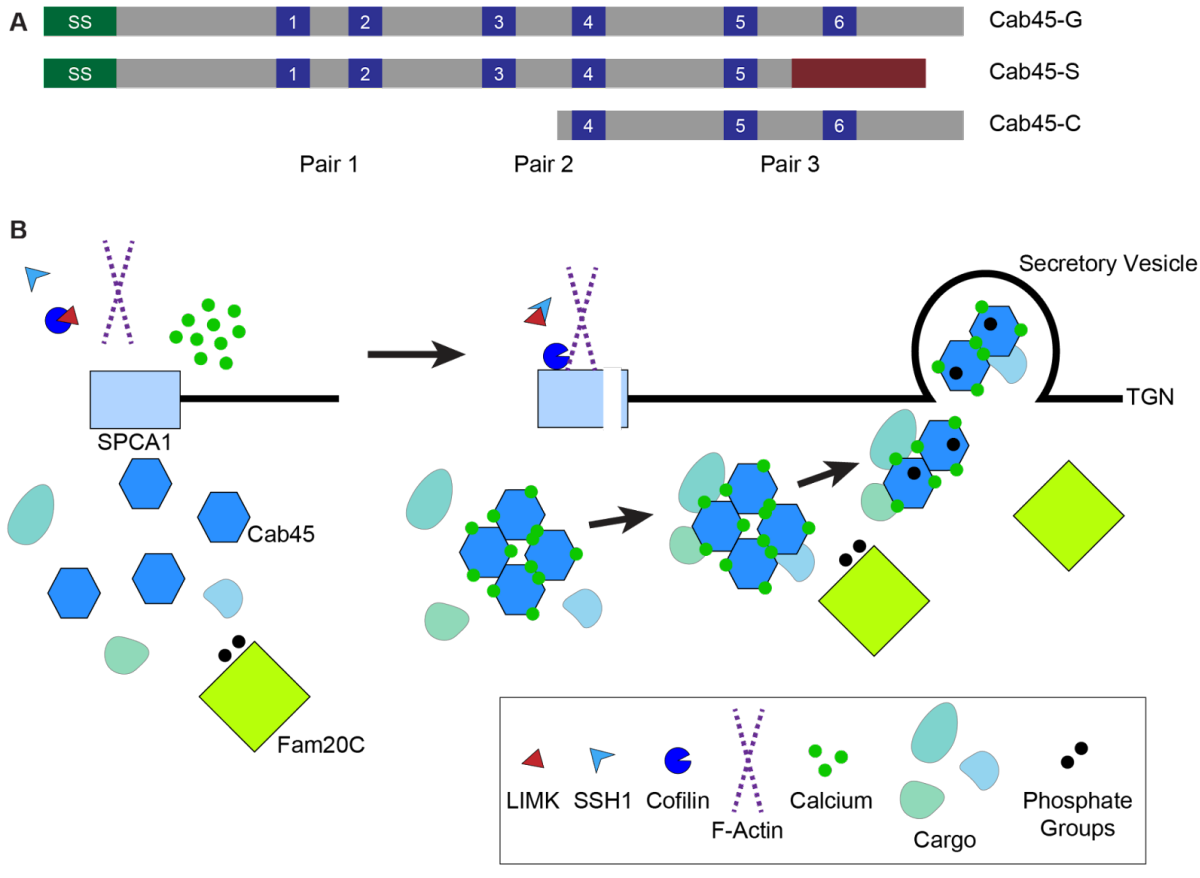

Figure 9. Cab45 isoforms and Cab45-G dependent cargo sorting. (A) Schematic representation of Cab45 protein isoforms. Green depicts the signal sequence, blue depicts the Ca^{2+}-binding EF hands, and burgundy depicts the alternate C-terminus of Cab45-S/ **(B)** Graphic depiction of Cab45-dependent secretory cargo sorting as uncovered in HeLa cells.

1.3.3 Members of Cab45-Dependent Cargo Sorting in Pancreatic β-cells

All proteins involved in Cab45-dependent cargo sorting are present in pancreatic β-cells, but only a handful of studies have enquired into their function. As mentioned earlier, SPCA1 may be present on the insulin SG in addition to the TGN, and its activity during GSIS appears to sequester cytosolic calcium to modulate the signal for insulin secretion in INS1 cells (Mitchell, Tsuboi, and Rutter 2004). Cofilin-1 has been shown to be active during the basal cellular state, resulting in a G-actin predominant environment that could be conducive to the immediate release of highly motile insulin SGs during the first phase of GSIS (Uenishi et al. 2013). During the first 15 minutes of glucose stimulation, LIMK is gradually phosphorylated, resulting in the phosphorylation and inactivation of cofilin-1 which permits cortical F-actin remodelling by other regulators (Uenishi et al. 2013). This was proposed to be a mechanism by which the first and second phase of GSIS were segregated, as motile SGs released during first phase would be restricted by the newly constructed F-actin network, which in turn is permissive for the release of a separate population of SGs during the second phase. Importantly, cofilin-1 activity is required for the second phase and therefore is likely not deactivated entirely during glucose stimulation (Uenishi et al. 2013). The distinction between pools of cofilin-1 as seen in HeLa cells are yet to be made in β-cells, and follow up studies are also required to confirm the upstream regulators of cofilin-1 activity in β-cells (Uenishi et al. 2013; Z. Wang et al. 2011).

Recent investigations revealing the adaptive plasticity of pancreatic β-cells have demonstrated that islets isolated from diabetic mice and subject to acute euglycaemic rest results in the replenishment of insulin stores and subsequent rescue of GSIS (Alarcon et al. 2016; Boland et al. 2018). This is concomitant with adaptive changes in the expression and phosphorylation of proteins involved in translation, ER to Golgi trafficking, and insulin SG biogenesis (Kang et al. 2019). Fam20C localises to the Golgi apparatus and is the major kinase responsible for phosphorylating secretory proteins, and has been positioned as a key mediator of β-cell adaptive plasticity (Kang et al. 2019). Restoration of Fam20C expression and phosphorylation at Fam20C-regulated phosphosites is observed following acute β-cell rest (Kang et al. 2019), suggesting that these sites are important for normal SG biogenesis. Notably, this study did not report that Cab45 expression or phosphorylation was regulated by acute euglycaemic rest. This could mean that Fam20C does not phosphorylate Cab45 in the β-cell, or could indicate that mouse models predisposed to β-cell failure that were used in this study have irrevertible changes in Cab45 expression or phosphorylation.

1.4 Aims and Hypotheses

The mechanism by which resident proteins are trafficked into the insulin SG are poorly defined. Cab45-dependent cargo sorting can be described as an aggregative mechanism that has preference for certain cargo, providing a means by which large volumes of protein can be directed through specific trafficking routes. Hence, Cab45 lends itself as a suitable candidate molecule for controlling protein sorting into ISGs from the TGN. This investigation began with the hypothesis that Cab45 regulates the sorting of proinsulin or other proteins into insulin SGs. The aim of this thesis was to characterise aspects related to Cab45 behaviour (chapter 2) and function (chapter 3) in various β-cell models.

(This page is intentionally left blank)

Chapter 2: Cab45 in β-Cells

2.1 Introduction

Up until this point, Cab45 has only been investigated in the widely studied cervical carcinoma HeLa cell line where its mechanism of action has been thoroughly characterised. The data presented here in this thesis is the first investigation of Cab45 in models that have direct relevance to a specific physiological or pathological context. Proper analysis of Cab45 expression through the tissues of whole organisms has not yet been conducted aside from one study that performed crude Northern blotting analysis of Cab45 mRNA in mice, showing broad expression throughout a variety of tissues (Y. Zhu et al. 2008). Determination of Cab45 expression through mammalian tissues and, especially relevant to this study, islet cell types, is a critical first step in defining endogenous roles for Cab45. To this end, initial experiments were conducted to discover which tissues in whole organisms and which cell types in the pancreas express Cab45, before differences in islet Cab45 abundance during health and metabolic disease were measured. Cab45 has been characterised in HeLa cells as a protein that is dependent on Ca^{2+}-binding for its subcellular localisation and for the execution of its function as a protein sorter, and in doing so, simultaneously works as a luminal Ca^{2+} buffer (von Blume et al. 2012; Crevenna et al. 2016). Here, its subcellular localisation and the involvement of Ca^{2+} in its localisation and trafficking in β-cell models were examined from several angles using a combination of molecular techniques. In this chapter, a first take on the molecular behaviour of Cab45 in pancreatic β-cells is presented in the context of its potential relevance to T2D. These findings open a door to the presence of alternative Cab45 behaviour across mammalian cell types, with possible implications for the current understanding of protein trafficking in the β-cell.

2.2 Materials and Methods

2.2.1 *In-situ* hybridisation of Cab45 mRNA in mice

In-situ hybridisation of Cab45 mRNA was conducted as described previously (Seidah et al. 2003). Briefly, antisense and sense mRNA probes generated for Cab45 were labelled with 35^S-UTP and 35^S-CTP. Mice were sacrificed either at embryonic stages e10, e12 and e15, postnatal stages p1 and p5, or in adult mice. Hybridisation of probes was conducted overnight at 55 °C on 8-10 µm tissue cryostat sections that had been fixed with 4 % paraformaldehyde (PFA). For autoradiography, sections were dipped in photographic emulsion and exposed for 6-12 days, and also stained with cresyl violet for more imaging.

2.2.2 Preparation of human pancreas sections for immunocytochemistry

Human pancreas sections were provided by St. Vincent's Institute of Medical Research (Victoria, Australia) with informed consent from next of kin and human research ethics committees (HREC) approval. Approval for research use of human tissues was obtained from the University of Sydney HREC 2017/042. Pancreas tissue was harvested from the head and middle of the pancreas and fixed in 10% neutral-buffered formalin and embedded in paraffin.

2.2.3 Mice

B6.Cg-Lep*ob*/J mice were kindly provided by Prof. David James (University of Sydney). Age-matched male C57BL/6J mice were sourced from Australian BioResources (NSW, Australia) as controls. BKS.Cg-*Dock7*^{m} +/+ LepR^{db}/J mice and control C57BLKS/J mice were bred at Bosch Animal Facility, University of Sydney, Australia. Mice were housed on a 12 h light/dark cycle and given food and water ad libitum. All procedures performed followed the National Health and Medical Research Council (NHMRC) guidelines for animal research and approved by the University of Sydney Animal Ethics Committees.

2.2.4 Mouse islet isolation

For islet isolation, a 2 mL volume of 0.25 mg/mL Liberase (Roche Applied Science) in Hanks' buffered saline solution (Gibco™) with 20 mm HEPES was injected into the common bile duct. The inflated pancreas was extracted and incubated at 37 °C for 13 min, and washed twice before passing through a 1,000-mm mesh filter. The resulting tissue was centrifuged with no break at 1,000 x g in a Histopaque 1119 and 1077 (Sigma-Aldrich) gradient for 20 min before islets were hand-picked in Hanks' buffered saline solution (Gibco). Islets were lysed using RIPA buffer (Thermo Fisher Scientific™) supplemented with EDTA-free protease inhibitors (Roche), followed by sonication then

centrifugation at 12 000 x g for 15 min and supernatant transferred to a fresh tube. Protein concentrations were quantified using the Pierce™ BCA Protein Assay Kit (Thermo Fisher Scientific).

2.2.5 Insulinoma cell culture

Rat INS1 insulinoma cell lines were cultured at 37º C and 5% CO_2 in RPMI 1640 Medium (Gibco) containing 11 mM glucose, 2 mM L-Glutamine (Gibco), 10% foetal bovine serum (FBS) (Gibco), 10 mM HEPES, 1 mM Sodium Pyruvate, 0.05 mM 2-ß-mercaptoethanol and 1% penicillin-streptomycin (Gibco). Mouse MIN6 insulinoma cell lines were cultured at 37º C and 5% CO_2 in DMEM Medium (Gibco) containing 25 mM glucose, 2 mM L-Glutamine, 10% foetal bovine serum (FBS), 1 mM Sodium Pyruvate, and 1% penicillin-streptomycin (Gibco).

2.2.6 INS1 subcellular fractionation

INS1 cells were collected by scraping into a HEPES/EGTA buffer (5 mM HEPES, 1 mM EGTA, pH 7.4) with complete EDTA-free protease inhibitors (Roche), and sheared 20 times using a 22 G needle to break the cell membrane but preserve intracellular organelle membranes. The lysate was spun at 1000 x g for 5 minutes at 4° C to pellet nuclear protein and debris, and supernatant was transferred to a new tube and spun again under the same conditions. The pooled supernatant was layered atop a continuous 2.0 M to 0.45 M sucrose gradient and centrifuged at 30 000 rpm for 18 h at 4° C in a Sorvall™ LYNX 4000 superspeed centrifuge using an A22-24 x 15 Fixed Angle Rotor (Thermo Fisher Scientific). Equal volumes were removed into 13 fractions and analysed by SDS-PAGE.

2.2.7 INS1 calcium depletion

INS1 cells cultured on coverslips were subject to Ca^{2+}-free culture media (140 mM NaCl, 5 mM KCl, 1 mM $MgCl_2$, 5 mM $NaHCO_3$, 10 mM HEPES, pH 7.4) for 10 minutes before treatment. Cells were treated for 0, 2, 5, 10, 20, or 30 min with 5 µM ionomycin and 5 mM EGTA in Ca^{2+}-free culture media before immediate fixation with 4% paraformaldehyde and subsequent cell immunofluorescent staining procedures.

2.2.8 Stable transfection of INS1 cells

pLPCX retroviral expression vectors containing WT Cab45HA or 6EQ Cab45HA were gifts from A/Prof. Julia von Blume, generated as described previously (Crevenna et al. 2016). PlatE cells (Cell Biolabs, Inc) cultured in DMEM (Gibco) containing 25 mM glucose and 10% foetal bovine serum (FBS) were kept in 1 µg/mL puromycin, 10µg/mL penicillin-streptomycin and 10 µg/mL blasticidin (Cell Biolabs, Inc) for 3 days before splitting into new media not containing antibiotic, and

were transfected the next day using FugeneHD (Promega) with either WT or 6EQ Cab45HA pLPCX vectors. The next day, media was changed to DMEM and cultured for one day, then, this media was transferred to INS1 cells that had been split one day prior, in a 1:1 ratio with fresh RPMI medium and with 8 mg/mL polybrene. After 8 hours, the media was replaced with another lot of DMEM that had been collected from transfected PlatE cells, and 8 mg/mL polybrene. This was repeated again the next day, with PlatE medium being replaced in the morning and then 8 hours later in the afternoon, each time with 8 mg/mL polybrene. Two days later, INS1 cells were placed under 0.5 μg/mL puromycin and grown until confluence to select infected cells.

2.2.9 INS1 glucose-stimulated insulin secretion (GSIS) assay

INS1 cells stably transfected with WT Cab45HA or 6EQ Cab45HA were incubated in resting buffer for 2 h at 37 ºC (114 mM NaCl, 4.7 mM KCl, 1.2 mM KH_2PO_4, 1.16 mM $MgSO_4$, 20 mM HEPES, 2.5 mM $CaCl_2$, 25.5 mM $NaHCO_3$, 1 % bovine serum albumin (BSA), and 3 mM glucose, pH 7.2). Cells were washed twice with BSA-free resting buffer and incubated for 2 hours either with BSA-free resting buffer (containing 3 mM glucose) or BSA-free stimulating buffer containing 18 mM glucose. The supernatant was collected and spun down at 20,000 g for 10 min at 4 °C to remove cell debris. The supernatant was transferred into a new tube and precipitated with trichloroacetic acid (TCA) using 0.03% sodium deoxycholate as a carrier. Pellets were resuspended in SDS sample buffer. The cells were lysed on ice using 50 mM Tris-HCl, pH 8.0, 150 mM NaCl, 1% Triton X-100, 1 mM EDTA, and protease inhibitor cocktail (Pierce), clarified by centrifugation at 20,000 g for 10 min at 4 ºC, and then the supernatant was collected to a new tube. The protein concentration of cell lysates and precipitated media was measured using the BCA assay. Equal amounts of protein were resolved via SDS-PAGE and analysed by Western immunoblotting as described. Band intensity was quantified using ImageJ.

2.2.10 Immunofluorescent staining and microscopy

Paraffin-embedded human pancreas sections were deparaffinized and rehydrated through a xylene and ethanol series. Sections were washed in wash buffer (0.1% BSA in PBS with 0.01% sodium azide) before cell permeabilization in Dako® Target Retrieval Solution (Agilent).

INS1 or MIN6 insulinoma cells plated on coverslips were washed with PBS twice before fixing with 4% paraformaldehyde at RT for 20 min. Fixed cells were washed twice with PBS, twice with wash buffer (0.1% BSA in PBS with 0.01% sodium azide), then treated with 0.1% SDS for 5 min at RT to permeabilize cell membranes.

Non-specific binding was blocked for 1 h at room temperature (RT) using Dako Protein Block Serum-Free (Agilent) after washing, then cells/sections were incubated with primary antibodies in Dako Antibody Diluent (Agilent) overnight at 4° C. Cells/sections were washed then incubated with

appropriate Alexa Fluor® secondary antibodies (Thermo Fisher Scientific) in Dako Antibody Diluent for 1 h at RT. Coverslips were mounted onto glass slides using Prolong Diamond Antifade Mountant (Thermo Fisher Scientific) with/without DAPI.

Imaging was performed with either a Leica SP8 confocal or a Nikon A1 confocal microscope. Antibody sources and dilutions are as follows. Primary antibodies: Guinea Pig anti-Insulin pre-diluted (DAKO, A0564); mouse anti-glucagon (Sigma, G2654); rabbit anti-Cab45 (1:500, gifted by A/Prof. Julia von Blume); rabbit anti-SDF4 (1:200, Thermo Fisher PA5-52809); mouse anti-proinsulin (5 µg/mL, Developmental Studies Hybridoma Bank GS-9A8); mouse anti-GM130 (1:500, BD Biosciences 610822); mouse anti-TGN38 2F7.1 (1:500, Novus Biologicals NB300-575); mouse anti-TGN38A (1:50, R&D Systems MAB7944); rabbit anti-HA C29F4 (1:1000, Cell Signalling 3724). Secondary antibodies: all dilutions were at 1:1000. Thermo Fisher Scientific: goat anti-guinea Pig IgG Alexa Fluor 488; goat anti-rabbit IgG Alexa Fluor 594; goat anti-rabbit IgG Alexa Fluor 647; goat anti-mouse IgG Alexa Fluor 594. Jackson Immunoresearch: donkey anti-mouse Alexa Fluor 790 (1:20,000, 715-655-150).

2.2.11 Western immunoblotting

For experiments conducted in section 2.3.1.3, whole islets isolated from mice were washed once with PBS and then lysed in RIPA buffer (Thermo Fisher Scientific™) supplemented with EDTA-free protease inhibitors (Roche). Islets were lysed by sonication then centrifuged at 12 000 x g for 15 min, and lysate transferred to a fresh tube. Protein concentrations were quantified using the Pierce™ BCA Protein Assay Kit (Thermo Fisher Scientific) and were separated using Tris/glycine SDS-PAGE under denaturing conditions on a 10% polyacrylamide gel. For experiments conducted in 2.3.2.1, equal volumes from each fraction were separated using Tris/glycine-SDS-PAGE under denaturing conditions on 7.5%, 10%, or 12.5% polyacrylamide gels. For both sections 2.3.1.3 and 2.3.2.1, following SDS-PAGE, proteins were transferred to methanol-activated PVDF membranes which were then blocked in 5% skim milk for 1 h, washed with TBST (TBS + 0.1% Tween 20), and incubated overnight at 4 ºC with primary antibody diluted in TBST with 5% BSA and 0.1% sodium azide. Membranes were washed with TBST and incubated for 1 h at room temperature in secondary antibody diluted in 5% skim milk, then washed again and imaged using Immobilon Western Chemiluminescent HRP substrate (Merck) on a ChemiDoc MP system. To immunoblot for proinsulin, the modified Western blotting method recently described by Okita et al. (Okita et al. 2017) was used.

For experiments conducted in section 2.3.2.2, confluent cells were washed with PBS, gently scraped into tubes, and centrifuged at 1000 rpm for 3 min. The supernatant was aspirated and cells resuspended in RIPA buffer (Thermo Fisher Scientific™) supplemented with EDTA-free protease inhibitors (Roche). Cells were lysed by sonication then centrifuged at 12 000 x g for 15 min, and lysate transferred to a fresh tube. Protein concentrations were quantified using the Pierce™ BCA

Protein Assay Kit (Thermo Fisher Scientific). Proteins were separated using Tris/glycine-SDS-PAGE under denaturing conditions on a 10% polyacrylamide gel and transferred onto PVDF membranes. Membranes were blocked with Odyssey Blocking Buffer (Fisher Scientific), washed in PBST (PBS + 0.1% Tween 20), incubated overnight at 4 ºC with primary antibody diluted in Odyssey Blocking Buffer (PBS) supplemented with 0.2 % Tween 20. Membranes were washed with PBST and incubated for 1h at room temperature in secondary antibodies diluted in Odyssey Blocking Buffer (PBS) supplemented with 0.2 % Tween 20 and 0.01 % SDS. A LI-COR processor was used to image the membranes.

Antibody sources and dilutions are as follows. Primary antibodies: rabbit anti-Insulin (1:1000 Santa Cruz sc-9168); mouse IgM anti-SDF4 E-12 (1:100, Santa Cruz sc-393930); rabbit anti-VAMP8 (1:500, Abcam ab76021); rabbit anti-Lamp1 (1:1000, Abcam ab24170); rabbit anti-TGN38 (1:500, Sigma T9826); mouse anti-GM130 (1:1000, Cell Signalling 12480); mouse anti-β-actin (1:2000, Sigma A5441); rabbit anti-ERp72 (1:1000, Cell Signalling 5033); rabbit anti-SPCA1 (1:1000, Invitrogen PA534757); rabbit anti-HA C29F4 (1:1000, Cell Signalling 3724); mouse anti-β-Tubulin BT7R (1:1,000, Thermo Fisher MA5-16308). Aliquots of rabbit antibodies against PC2 were generously provided by Prof. Nabil Seidah and rabbit polyclonal anti-Rab7 provided by Prof. David James (University of Sydney). HRP-conjugated secondary antibodies: BioRad (1:5000 – 1:10,000): goat anti-rabbit IgG; donkey anti-rabbit IgG; rabbit anti-mouse IgG. Santa Cruz: goat anti-mouse IgM (1:500, sc-2064).

2.2.12 Statistical analysis

Statistical analyses were performed using GraphPad Prism 7 software. Statistical significance was determined by two-tailed Student's t-test, one-way ANOVA or two-way ANOVA with Tukey's multiple comparisons post-test corrected for multiple comparisons. A value of $p < 0.05$ was considered significant.

(This page is intentionally left blank)

2.3 Results

2.3.1 Cab45 expression in mouse and human islets during health and metabolic disease

At this point in time, there is very little known about the tissues in which Cab45 is expressed in mammalian organisms. This is essential for understanding its *in-vivo* function and will underline any involvement that Cab45 has in pathology. *In-situ* hybridisation of mRNA, immunofluorescent staining, and Western immunoblotting were performed to obtain a snapshot Cab45 expression in whole organisms and islets during health and metabolic disease.

2.3.1.1 Whole organism and islet expression of Cab45

In-situ hybridisation of Cab45 mRNA in mice. A collaborator (Prof. Nabil Seidah, McGill University) designed and applied complementary RNA probes for Cab45 mRNA to euthanised mice, to identify mammalian tissues where Cab45 is expressed (**Figure 10**). Cab45 mRNA is ubiquitously expressed during both embryonic development (**A-B**) and in adult mice (**C-D**), as indicated by the presence of bright signal during antisense mRNA hybridisation (**A/C**) that is not present with sense hybridisation (**B/D**). Clear variance in signal intensity indicate that expression is heterogeneous across tissues of adult mice (**C**), showing prominence in endocrine tissues (thymus, testis, thyroid, pituitary, adrenal, ovary, uterus, prostate), exocrine tissues (spleen, lung, kidney, submaxillary, epididymus, oviducts, intestines), as well as tissues of the nervous system (brain, spinal cord, dorsal root ganglion). Lower levels of Cab45 mRNA are observed in the heart, where muscular tissue dominates the organ's mass. Closer observation of the adrenal (**E-H**) and pituitary (**K-L**) glands reveal cell-specific expression of Cab45 mRNA in the adrenal medulla and in the intermediate and anterior lobes of the pituitary, suggesting that there may be a particular requirement of Cab45 to carry out its intracellular function in certain cell types. This is evidenced close-up by grainy silver Cab45 mRNA labelling in figures **G** and **K**, with cresyl violet stain to demarcate functional cell populations. Interestingly, Cab45 mRNA expression is low throughout the whole pancreas (**C-D**), which may be due to the abundance of pancreatic RNAses and/or due to the low relative abundance of the endocrine islets of Langerhans.

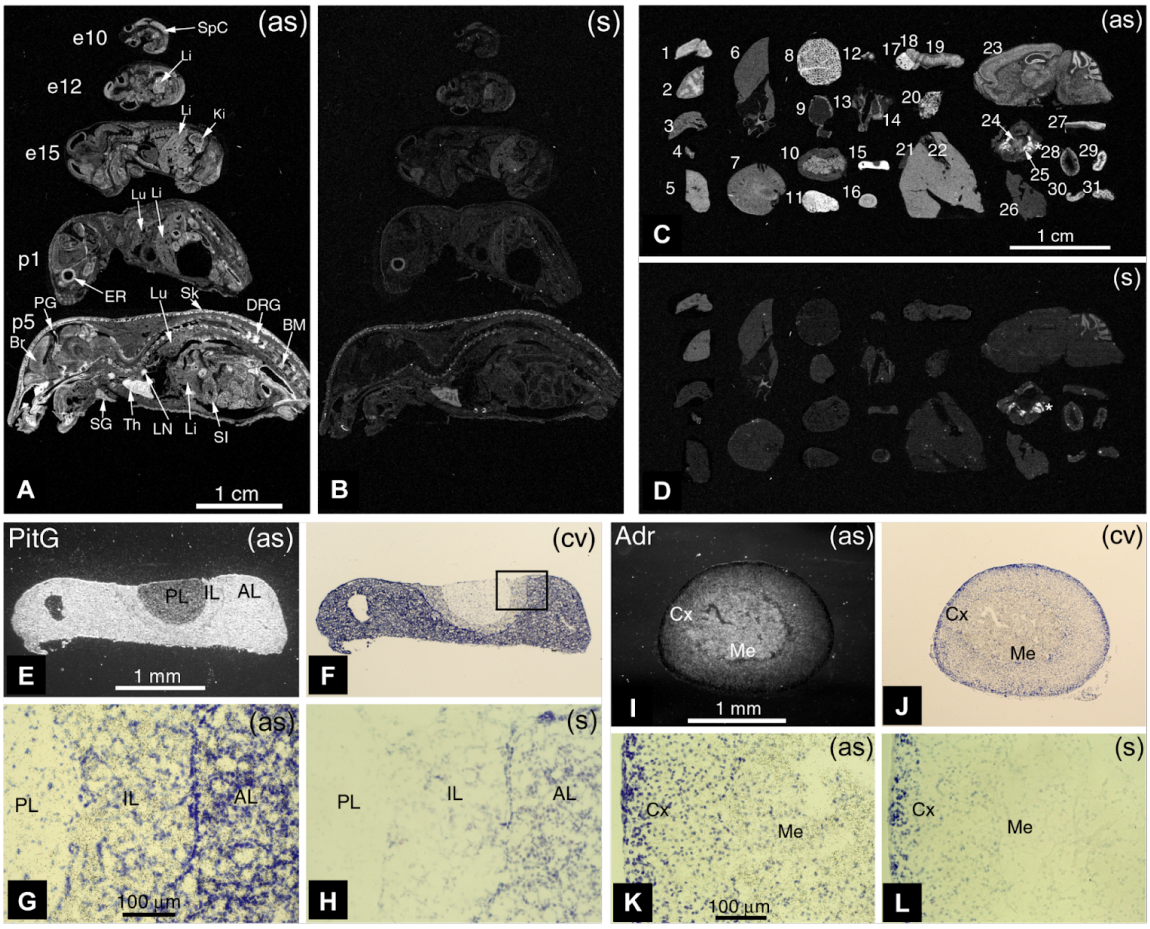

Figure 10. Heterogeneity of whole organism Cab45 expression in mice. *In-situ* hybridisation using antisense (as) and sense (s) (control) Cab45 mRNA probes in mice, scale bars as indicated. **(A-B)** Distribution of Cab45 mRNA in embryos (e10, e12 and e15) and postnatal (p1 and p5) mice visualised using x-ray autoradiography. **(C-D)** Ubiquitous distribution of Cab45 mRNA in a 31-tissue array of adult mice visualised using x-ray autoradiography. **(E-H)** Heterogeneous distribution of Cab45 mRNA in the adult mouse pituitary gland (PL - posterior lobe; IL - intermediate lobe; AL - anterior lobe) **(I-L)** or adrenal gland (Cx - cortex; Me - medulla) **(G-H)**: **(E/I)** emulsion autoradiography under dark-field illumination; **(F/J)** cresyl violet staining of **(E/I)**; **(G/K)** fragment of **(F/J)** at a higher magnification (dark silver grains indicate antisense hybridisation of probe); **(H/L)** adjacent section to **(G/K)** instead treated with sense probe. Abbreviations for **A-B**: BM - bone marrow; Br - brain; DRG - dorsal root ganglia; ER - eye retina; Li - liver; LN - lymph node; Lu - lung; PG - pineal gland; Th - thymus; SG - salivary gland; SI - small intestine; Sk - skin; SpC - spinal cord.

Tissues in **C-D**: 1 - thymus; 2 - spleen; 3 - lung; 4 - aorta; 5 - submaxillary gland; 6 - heart; 7 - kidney; 8 - testis; 9 - coagulating gland; 10 - urinary bladder; 11 - epididymis; 12 - oesophagus; 13 - trachea; 14 - thyroid gland; 15 - pituitary gland; 16 - adrenal gland; 17 - ovary; 18 - oviducts; 19 - uterus; 20 - prostate; 21 - liver; 22 - gallbladder; 23 - brain; 24 - spinal cord (* non-specific hybridisation in bone tissue); 25 - dorsal root ganglion; 26 - pancreas; 27 - stomach; 28 - duodenum; 29 - jejunum; 30 - ileum; 31 - colon.

Human pancreas Cab45 staining. Considering that islets of Langerhans make up just 1-2% of the total pancreatic area, pancreas sections from three separate human donors were immunostained with antibodies targeting all isoforms of Cab45 (total Cab45), as well as insulin and glucagon (**Figure 11A-C**). Donor information is provided in **Appendix Figure 1**. Across all individuals, the Cab45 signal is mostly undetectable in the exocrine portion of the pancreas but widely present throughout islets. Co-staining revealed that Cab45 is not expressed in the glucagon-expressing α-cells but is abundant within insulin-positive β-cells. There is variability between individuals; individual 3 displays many Cab45-positive cells that are not positive for either insulin or glucagon which does not occur in the other two individuals.

On a subcellular level, Cab45 staining reveals strong juxtanuclear Golgi 'ribbon' structures that are limited to the β-cells as well as punctate granular structures of a lower intensity throughout the cytoplasm that may be in both α- and β-cells. While the former confirms expression of the Cab45-G isoform, punctate staining could represent the presence of Cab45-G within post-Golgi secretory vesicles, or the expression of the cytosolic isoform Cab45-C or the ER isoform Cab45-S. Qualitatively, in individual 1 much of this punctate cytoplasmic staining does not co-localise with insulin, but in individual 3 there is strong overlap between signals and individual 2 has reasonable overlap. Ectopically expressed Cab45-C has been documented to participate in SG exocytosis from rodent β-cells (Zhang et al. 2009), but as mentioned previously, evidence for its endogenous expression and colocalisation with insulin SGs is questionable and therefore must be substantiated with more clarity. Nonetheless, individual differences in the pattern of Cab45 expression and localisation found here set a precedent for interpreting future findings.

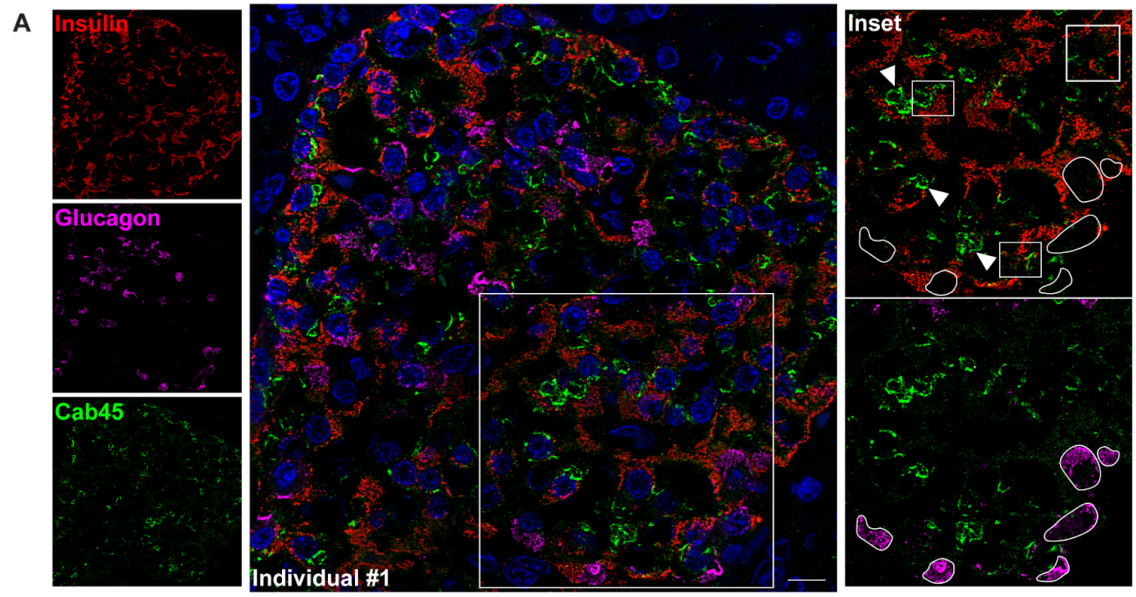

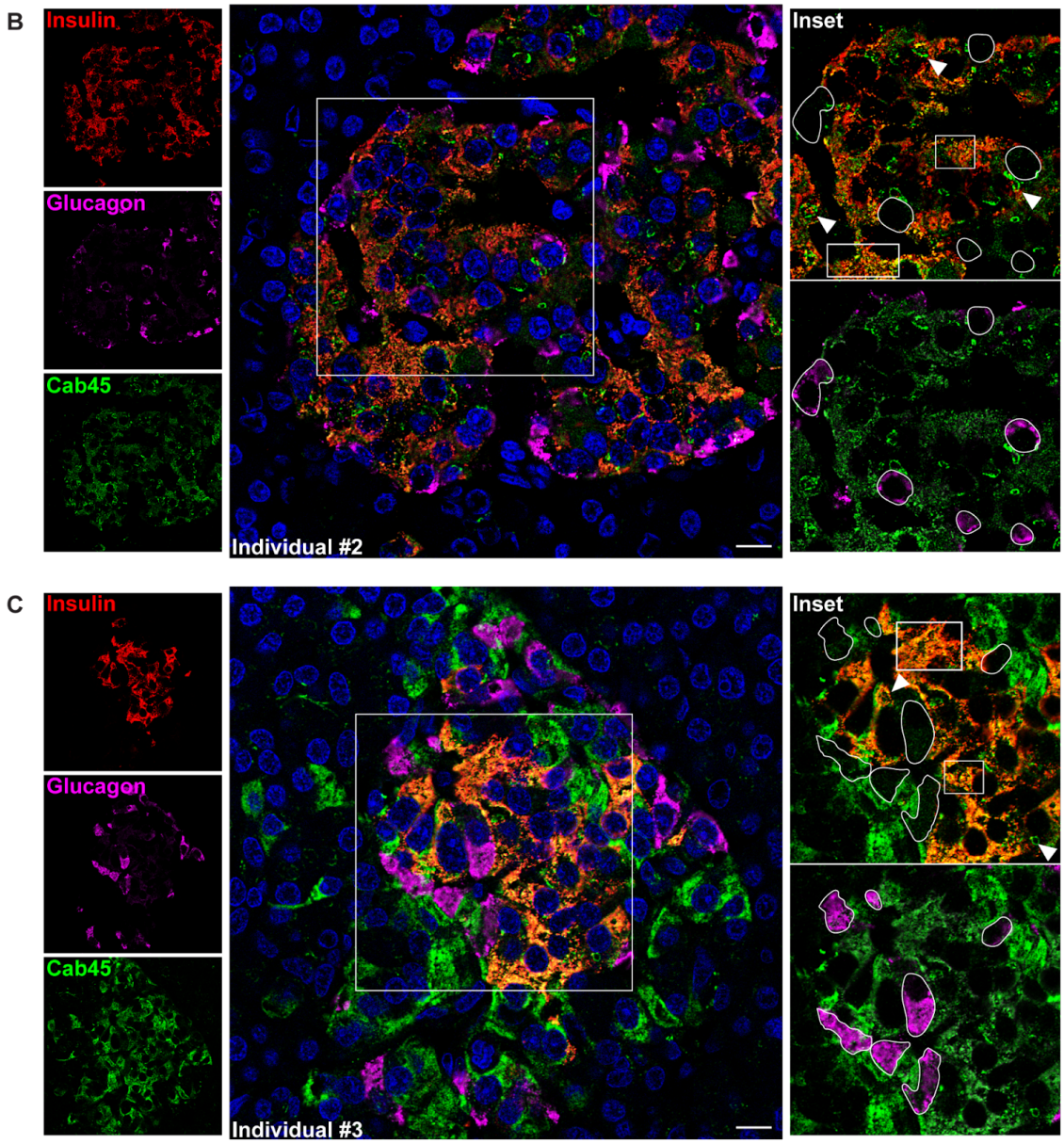

Figure 11. Specific expression of Cab45 in human islet β-cells. (**A-C**) Immunofluorescent staining of Cab45, insulin, and glucagon in the human pancreas from three individual donors. In the inset, white arrows point to juxtanuclear Cab45 illuminating Golgi 'ribbon' structures. White rectangles outline examples of regions in the cytosol where Cab45 and insulin have variable degrees of overlap between individuals. Irregular white outlines demarcate the border of glucagon-positive α-cells for visualisation of the absence of Cab45 expression. Scale bar = 10 μm.

2.3.1.2 Quantification of Cab45 abundance in non-diabetic and T2D human islets

To determine whether the abundance of Cab45 protein changes in β-cells of human type 2 diabetics, Cab45 and insulin were co-stained in pancreas sections from five non-diabetic and five type 2 diabetic human donors (**Figure 12A**). Donor information is provided in **Appendix Figure 1**. In contrast to **Figure 11**, human pancreas sections were stained with an antibody that was raised against the full-length Cab45-G isoform, delineating clear juxtanuclear Golgi ribbon structures (although, low-intensity cytosolic signal is evident) that are limited to the β-cell population (**Figure 12C**). Since Cab45 is restricted to the β-cells of human islets, the number of cells with positive immunostaining for Cab45 in the juxtanuclear region could be quantified as a ratio to the number of insulin-positive cells (**Figure 12B**). This was deduced by manually counting cells that contained a clear juxtanuclear Golgi Cab45 signal. This analysis revealed that non-diabetic humans possess Golgi-localised Cab45 in **84.5% ± 6.2%** of their β-cells compared to **48.1% ± 4.7%** in type 2 diabetic humans (mean ± SEM, $p < 0.0001$). Although a ratiometric quantification controls for factors such as β-cell de-differentiation and death that can occur in T2D, it does not consider potential differences in Cab45 abundance within single cells. Nonetheless, the binary presence/absence of Golgi-localised Cab45 within β-cells across the human islet correlates with its functional status; therefore, the distinct loss of Cab45 from this region in a considerable proportion of pancreatic β-cells may be clinically significant. Further lines of enquiry into the presence of peripheral/non-Golgi localised Cab45-G should be conducted to ascertain if either total expression is lost or if the protein becomes mis-localised toward the cell periphery in the diabetic state. This should be corroborated with existing single-cell transcriptomic datasets from islets in non-diabetic and type 2 diabetic humans.

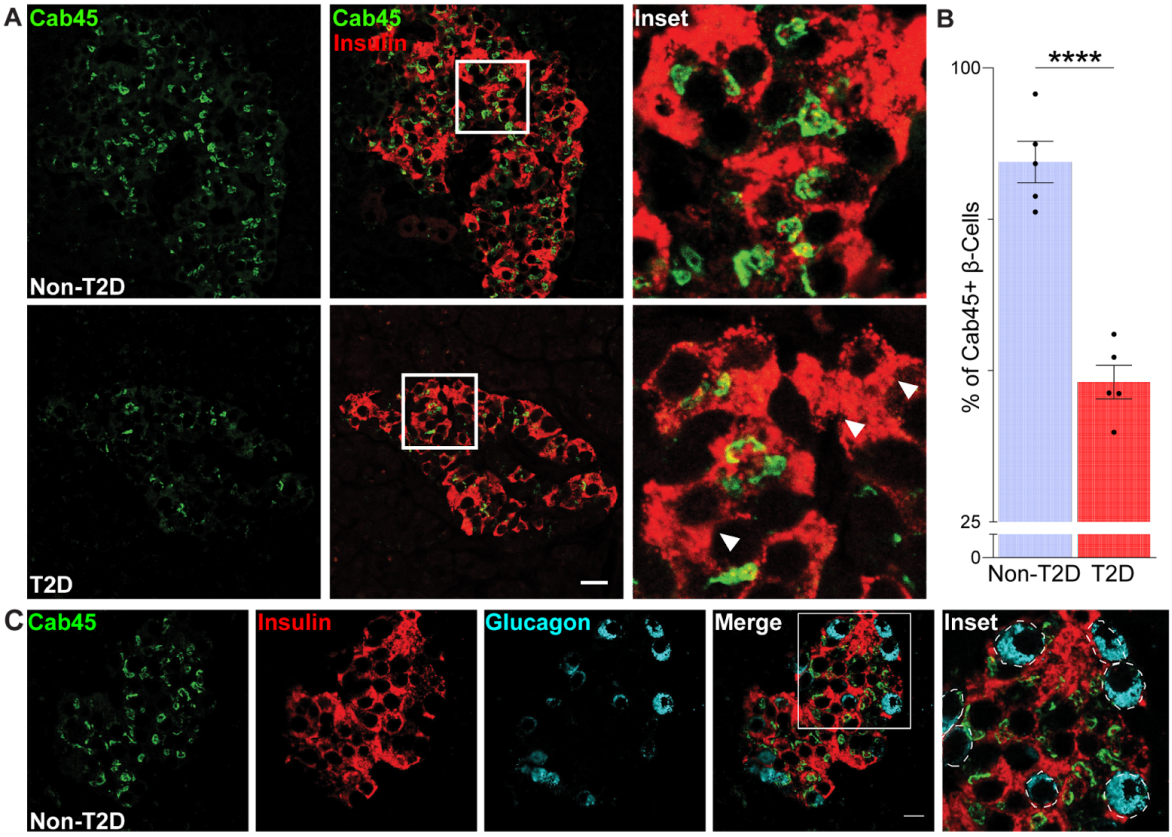

Figure 12. Cab45 is lost from a subset of β-cells in human T2D. (A) Pancreas sections from non-diabetic and type 2 diabetic human donors stained with antibodies targeting Cab45 and insulin. **(B)** Number of Cab45-positive cells expressed as a percentage of the total number of insulin-positive cells. Five islets each were quantified and averaged in 5 separate donors per condition. **(C)** Immunofluorescent staining of an antibody raised against full-length Cab45 with insulin and glucagon in a healthy subject. Scale bars = 10 μm Data presented as mean ± SEM; comparison made using an unpaired t-test.

2.3.1.3 Whole-islet Cab45 abundance in mouse models of insulin resistance and T2D

To further establish a link to metabolic disease, whole islet lysates from mouse models of T2D progression were subject to Western immunoblotting to quantify the abundance of Cab45 protein (**Figure 13**). Islets were isolated from three C57BL6/J (6/J) control and three C57BL6/J^{ob} (ob/ob) mice at 16 weeks of age, lysed, and total protein was immunoblotted with an antibody that recognises an epitope present in both Cab45-G and Cab45-S (total 45 kDa Cab45) as well as β-actin (**Figure 13A**, top). As mentioned previously, expression of Cab45-S in mice has not been documented. Ob/ob mice are spontaneous mutants derived from the 6/J strain. The mutation occurs in the gene encoding leptin, resulting in an inability to produce the appetite-suppressing hormone that leads to excessive food intake and the development of obesity. These mice display circulating hyperinsulinaemia and do not develop T2D due to the ability of β-cells from 6/J mice to successfully compensate in the setting of peripheral insulin resistance (Kennedy et al. 2010). 16-week old ob/ob mice showed a 2.5 fold increase in total Cab45 abundance compared to 6/J littermate controls (mean Cab45/β-actin band intensity relative to 6/J control ± SEM = [6/J: **1.00 ± 0.06**] *vs* [ob/ob: **2.62 ± 0.26**] ($p < 0.01$)) (**Figure 13B**).

Similarly, whole islets were isolated from three C57BLKS/J (KS/J) control and three C57BLKS^{db} (db/db) mice at 16 weeks of age, lysed, and total protein immunoblotted for total Cab45 and β-actin (**Figure 13A**). Db/db mice are also spontaneous mutants but instead are derived from the KS/J strain and do not synthesise the leptin receptor. This leads to the same behavioural phenotype leading to obesity and insulin resistance, but unlike ob/ob mice, db/db mice develop T2D by 16 weeks of age due to the inability of β-cells from KS/J mice to compensate in the setting of peripheral insulin resistance (Kennedy et al. 2010). 16-week old db/db mice showed a near five-fold decrease in total Cab45 abundance compared to KS/J littermate controls (mean Cab45/β-actin band intensity relative to KS/J control ± SEM = [KS/J: **1.00 ± 0.07**] *vs* [db/db: **0.20 ± 0.06**] ($p < 0.01$)) (**Figure 13B**). These results demonstrate that Cab45 abundance positively correlates with β-cell function in mice.

Notably, the extreme situations of obesity and T2D that are represented by these mouse models are potentially confounded by the occurrence of respective increases and decreases in β-cell mass. Furthermore, Cab45 expression in other islet cell types in mice has not yet been conducted. Therefore, normalisation of Cab45 abundance to β-actin across the whole islet may not be representative; instead, this line of enquiry would benefit from a similar analysis to what was conducted in **Figure 12**.

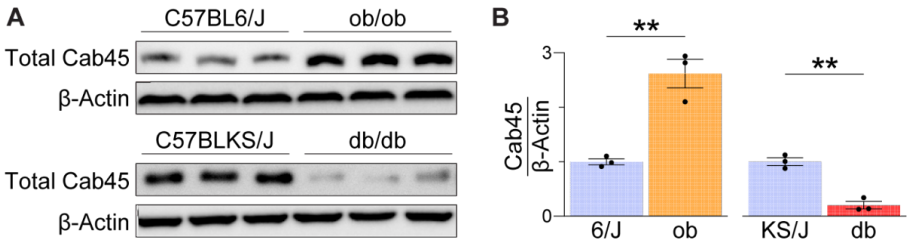

Figure 13. Islet Cab45 abundance correlates with the functional output of β-cells in mouse models of insulin resistance and T2D. (A) Western blot of islet lysates from three C57BL6/J control (6/J) and three C57BL6/J$^{ob/ob}$ (ob) (top), and three C57BLKS/J control (KS/J) and three C57BLKS/J$^{db/db}$ (db) (bottom) mouse littermates at 16 weeks of age for Cab45 and β-actin. **(B)** Cab45 abundance normalised to β-actin and expressed relative to respective control strain from **(A)**; comparisons made using unpaired t-test.

Unique donor identifier	Age	Sex	BMI	HbA_{1c}	T2D or ND	Diabetes duration (years)	Glucose-lowering therapy at time of death	Cause of death
SVI-007-17	22	F	21.2	n/a	ND	n/a	n/a	Hydrocephalus secondary to colloid cyst
SVI-012-17	64	F	26.1	n/a	ND	n/a	n/a	Intracranial haemorrhage
SVI-003-18	38	M	39.1	n/a	ND	n/a	n/a	Intracranial haemorrhage
SVI-008-15	55	F	31.2	8.1	T2D	10	Metformin	Cerebral hypoxia/ischaemia, cardiac arrest
SVI-020-15	58	M	32	8.1	T2D	14	Initially oral meds, then 10 years on insulin	Intracranial haemorrhage
SVI-028-15	64	M	31.2	6.4	T2D	2	Diet controlled	Cerebral infarction/posterior circulation stroke
SVI-030-16	53	F	27.6	n/a	ND	n/a	n/a	Cerebral hypoxia/ischemia
SVI-028-16	35	F	39.5	n/a	ND	n/a	n/a	Cerebral hypoxia/ischemia
SVI-035-16	48	F	33	5.5	ND	n/a	n/a	Intracranial haemorrhage
SVI-016-16	53	M	28.4	8	T2D	3	Diabex XR 100mg BD	Traumatic brain injury
SVI-034-15	68	M	28.6	7.5	T2D	10	Metformin for 10 years, then 5 years on insulin	Cerebral infarction
SVI-035-15	51	F	34.1	9.5	T2D	10-12	Diabex XR 1000mg extended release 1BD	Cerebral hypoxia/ischaemia

Appendix Figure 1. Human pancreas donor information.

(This page is intentionally left blank)

2.3.2 Cab45 localisation in β-cell lines INS1 and MIN6

Next, commonly used cell lines derived from rat (INS1) and mouse (MIN6) insulinomas were used to characterise the localisation of Cab45 in β-cells and enquire into its regulation by Ca^{2+}. In HeLa cells, it was established that Cab45 relies on Ca^{2+}-dependent oligomerisation to maintain localisation within the TGN despite being a soluble protein, and this mechanism is also crucial for its role as a secretory cargo sorter (von Blume et al. 2012; Crevenna et al. 2016).

2.3.2.1 Co-fractionation and colocalisation of Cab45 with β-cell components

INS1 cells were collected and sheared to disrupt the plasma membrane, and subject to ultracentrifugation through a continuous sucrose gradient to separate subcellular compartments by density. Thirteen fractions were isolated and resolved via SDS-PAGE, then immunoblotted for total 45 kDa Cab45 and compartmental markers (**Figure 14A**). Cab45 cofractionated strongly in fractions 7 to 9 with proinsulin, SPCA1, and the *cis*-Golgi marker GM130. Interestingly, the TGN marker TGN38 was enriched in fractions 5-6, suggesting that Cab45 may not localise to the TGN in β-cells as is the case in HeLa cells (von Blume et al. 2012).

Next, INS1 cells were immunostained for Cab45 (using antibody raised to full-length Cab45-G *in-vivo*) and either TGN38, GM130, insulin, or proinsulin (**Figure 14B**). Co-staining with markers for the Golgi apparatus and correlation analysis using Pearson's coefficient (r^2) confirmed results of subcellular fractionation, that Cab45 predominantly localises to the *cis*-Golgi of β-cells (mean $r^2 \pm$ SEM = [Cab45 x GM130: **0.84 ± 0.07**] *vs* [Cab45 x TGN38: **0.62 ± 0.03**] ($p < 0.05$)) (**Figure 14C**). Endogeneous Cab45-G is not prominent outside of the perinuclear Golgi region although some peripheral puncta are occasionally observed, and co-staining with an insulin antibody revealed colocalisation only at a perinuclear site but not with peripheral SGs. It should be noted that insulin antibodies used for all purposes described in this thesis are not specific to mature insulin, but will indiscriminately detect preproinsulin, proinsulin and processing intermediates. Therefore, colocalisation here is almost certainly with proinsulin since its conversion only occurs after entry into the SG. Indeed, co-staining Cab45 with an antibody specific for proinsulin reveals partial colocalisation occurring in distinct areas of the perinuclear region (**Figure 14C**) but not with the proinsulin that is present throughout the distal Golgi apparatus and within ISGs.

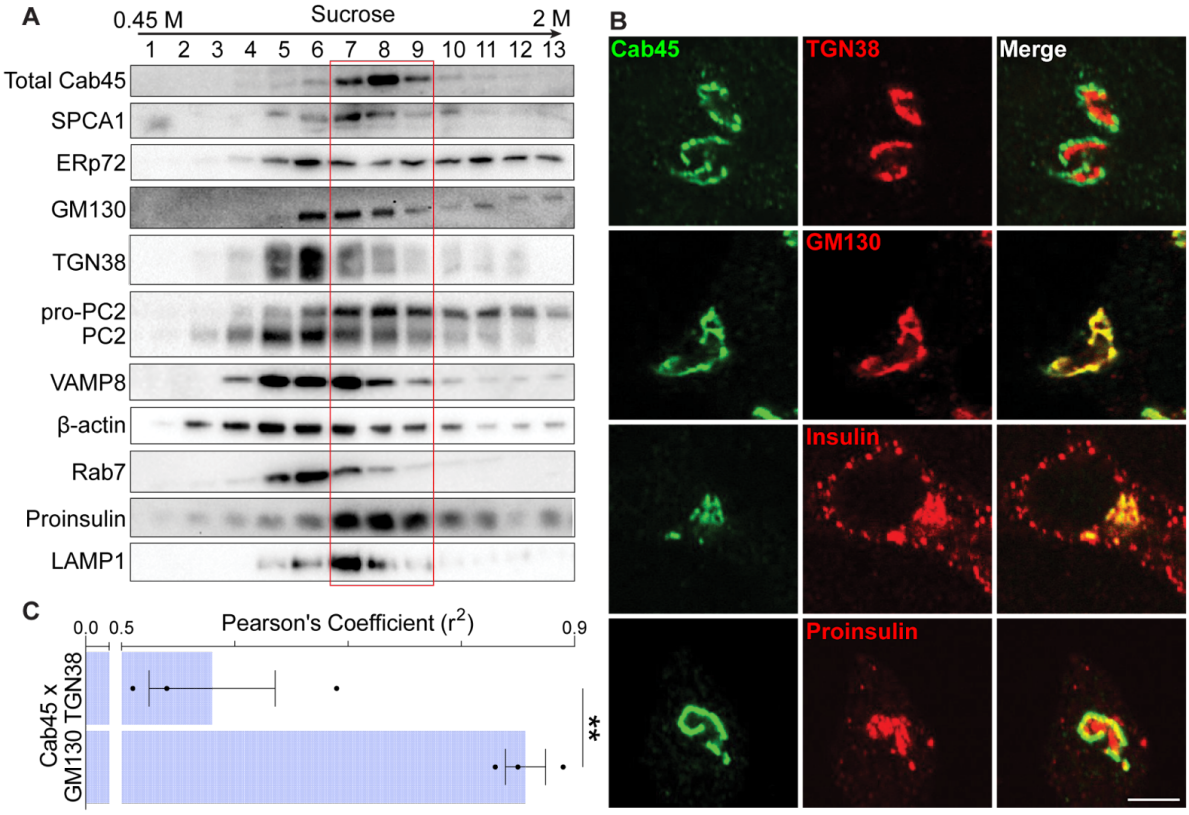

Figure 14. Cab45 localisation is concentrated in the *cis*-Golgi of INS1. (A) Western immunoblots of key compartmental markers following continuous subcellular fractionation of INS1 cells (n = 3). The red box shows the fractions enriched with Cab45. **(B)** Immunofluorescent staining of Cab45 with either TGN38, GM130, insulin or proinsulin in INS1 cells (n=3 from independent passages), scale bars = 10 μm; . **(C)** Pearson's coefficient of correlation between Cab45 and TGN38 versus Cab45 and GM130 from **(B)**. *, $p < 0.05$.

MIN6 cells were immunostained for the same combination of proteins (**Figure 15**), but this time with a Cab45 antibody targeting an epitope common to total Cab45. As was the case in human islets (**Figure 12**), this antibody reveals predominant expression of a Golgi-localised isoform although some peripheral punctae are occasionally observed, and near-identical results to the INS1 cells were found although more colocalisation with TGN38 is evident, and there may be slightly less overlap with the *cis*-Golgi marker GM130 (**Figure 15**). TGN38 is broadly distributed throughout the MIN6 cell as well as a perinuclear structure resembling the Golgi apparatus, therefore co-staining should be repeated with a bonafide MIN6 cell TGN marker. Like INS1 cells, there is partial colocalisation with proinsulin in the juxtanuclear region. Of course, colocalisation analysis should be conducted on this set of experiments to verify the situation.

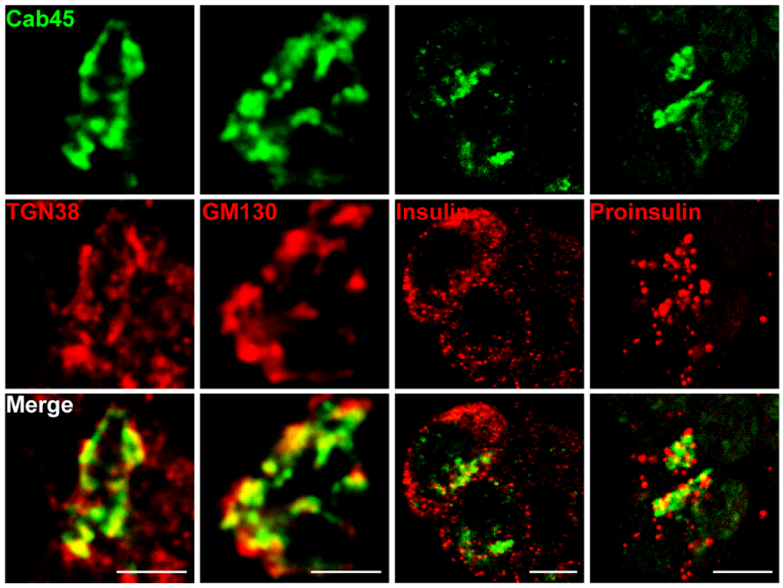

Figure 15. Cab45 localisation is concentrated in the *cis*-Golgi of MIN6 insulinoma cells. Immunofluorescent staining of Cab45 with either TGN38, GM130, insulin or proinsulin in MIN6 cells (n = 3 from independent passages), scale bars = 5 μm.

Taken together, it appears that Cab45 localisation in pancreatic β-cells is concentrated toward the *cis*-Golgi at steady state where it exists in close proximity to proinsulin. This is in contrast to HeLa cells where Cab45 occupies the TGN (von Blume et al. 2012). Consistent with the Uniprot database, it appears that only the Golgi isoform of Cab45 is expressed in rodent insulinoma cells. At this point, it is unclear whether endogenous Cab45 traffic flows through to the TGN and the immature secretory granule, but the presence of some overlap with TGN38 and the occasional observation of punctate Cab45 signal in the cell periphery indicates that it could do so. These data have obvious implications concerning the hypothesised role of Cab45 in sorting proinsulin from the TGN into ISGs, since this evidence suggests that Cab45 is not in the correct location to perform this function. It may be the case that a major pool of Cab45 resides within the early Golgi apparatus and that some Cab45 traffic flows distally, but this requires substantiation.

(Page intentionally left blank)

2.3.2.2 Calcium dependency of Cab45 localisation in INS1 cells

Cab45 extracted from purified HeLa cell Golgi membranes is present in both low and high molecular weight forms (Crevenna et al. 2016). It is well documented that Ca^{2+}-binding is required for the formation of high molecular weight Cab45 oligomers, the localisation of this soluble protein to the Golgi apparatus, and for specific Cab45-protein interactions (Crevenna et al. 2016; von Blume et al. 2012). Moreover, Fam20C kinase activity could mediate Cab45 phosphorylation to account for the presence of low molecular weight oligomeric Cab45 complexes (Hecht et al. 2020). Various experimental manipulations that interfere with Cab45 Ca^{2+}-binding disrupts oligomerisation, releases monomeric Cab45 from the cell, and impairs secretory cargo sorting in HeLa cells (Crevenna et al. 2016; von Blume et al. 2012).

Cab45 localisation after Ca^{2+}-depletion in INS1 cells. To study whether the localisation of Cab45 in β-cells is also dependent on Ca^{2+}, INS1 cells were treated with an ionophore, ionomycin, along with EGTA in a Ca^{2+}-free medium (**Figure 16**) - an established protocol for depleting cells and their intracellular compartments of Ca^{2+} (McCombs and Palmer 2008). Over the course of treatment, the localisation of Cab45 was monitored by co-staining with insulin and either GM130 (**Figure 16A**) or TGN38 (**Figure 16B**). Importantly, the pharmacological approach used here to deplete intracellular Ca^{2+} is sure to alter the behaviour of many other proteins within the cell.

Immediately following treatment, Cab45 exited the Golgi into vesicles as indicated by a reduction in the percentage of total cellular Cab45 that was localised in the perinuclear region (mean %perinuclear Cab45 ± SEM = [0 min: **78 ± 5**] *vs* [20 min: **43 ± 5**] ($p < 0.05$) *or* [30 min: **44 ± 3**] ($p < 0.05$)) (**Figure 16C**). While co-localisation analysis using the Mander's coefficient (R) (**Figure 16D**) revealed a reduction in both *cis*- and *trans*- Golgi localised Cab45 over the first 10 minutes, later time points demonstrated a rise in TGN localised Cab45 possibly because Cab45 exiting the *cis*-Golgi is moving through the TGN into vesicles (mean R Cab45 x GM130 ± SEM = [0 min: **0.776 ± 0.012**] *vs* [2 min **0.489 ± 0.009**] ($p < 0.0001$) *then vs* [10 min: **0.207 ± 0.007**] ($p < 0.01$) *then vs* [30 min: **0.204 ± 0.007**] ($p > 0.05$); mean R Cab45 x TGN38 ± SEM = [0 min: **0.459 ± 0.021**] *vs* [2 min **0.221 ± 0.008**] ($p < 0.0001$) *and* [5 min: **0.273 ± 0.008**] *vs* [10 min: **0.137 ± 0.019**] ($p < 0.01$) *then vs* [30 min: **0.242 ± 0.003**] ($p > 0.01$)). Interestingly, some Cab45 is retained within the Golgi apparatus, but notably, exiting Cab45 enters into vesicles that are not positive for insulin which appear to be retained within the cell. These findings demonstrate that monomeric Cab45 is released from the *cis*-Golgi into vesicles, but in contrast to the situation in HeLa cells (von Blume et al. 2012), monomeric Cab45 appears to be retained within the β-cell. The identity of these vesicles as of yet are unknown; it is possible that Cab45 moves retrograde into the ER-Golgi intermediate compartment (ERGIC) or to ER exit sites (ERES), however, transient increases in TGN-localised Cab45 would suggest that these are non-constitutive post-Golgi vesicles.

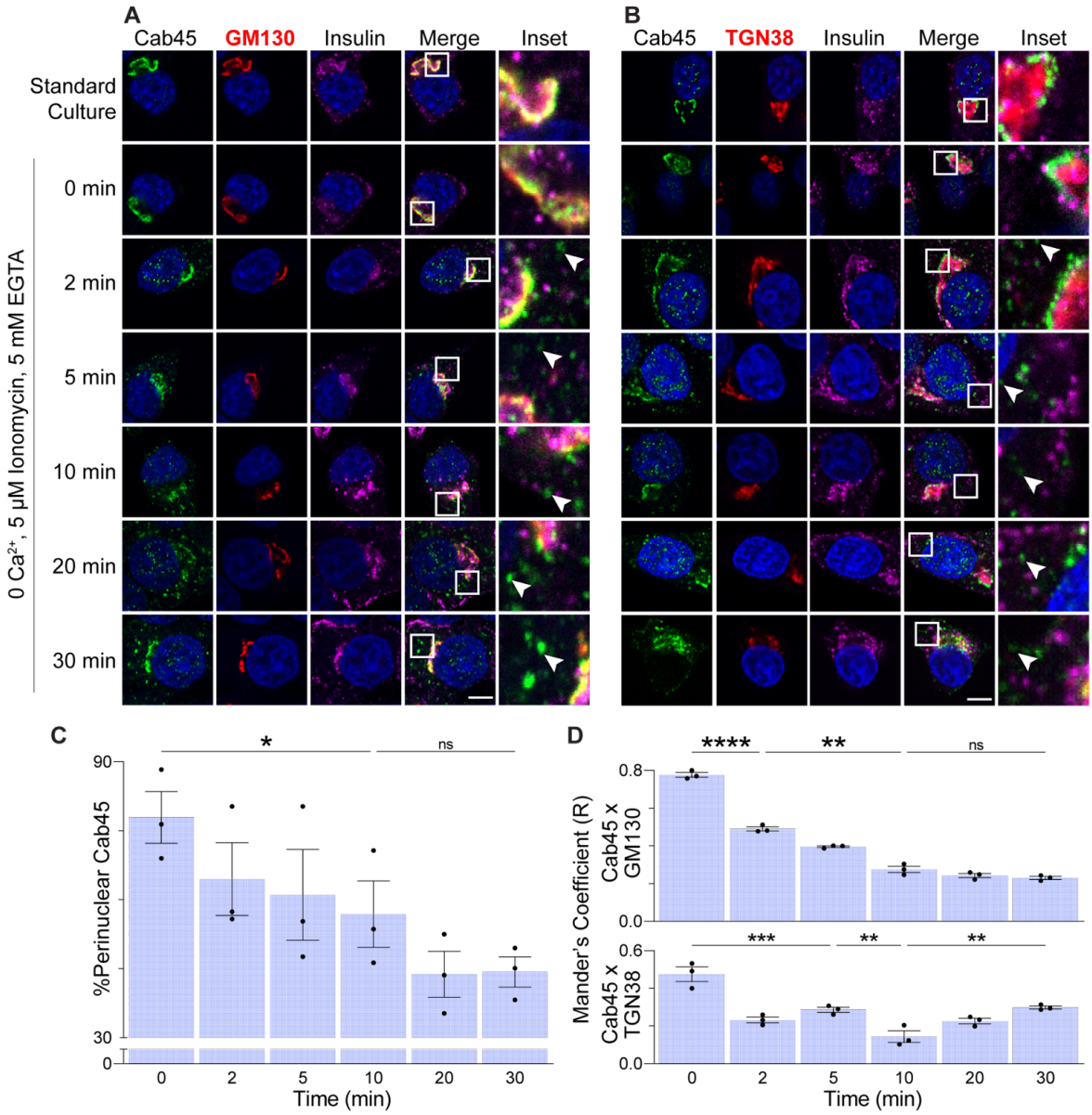

Figure 16. Cab45 exits into non-insulin-containing vesicles following Ca^{2+}-depletion of INS1 cells. INS1 cells were treated with ionomycin and EGTA in a Ca^{2+}-free medium over a time course of 30 minutes (n = 3). At various time points, cells were fixed and stained with antibodies targeting Cab45, insulin, and either GM130 **(A)** or TGN38 **(B)**, scale bars = 5 µm; white arrows indicate post-Golgi Cab45-positive vesicles. **(C)** The percentage of Cab45 in the perinuclear area (covering both the *cis* and the *trans*-Golgi) was quantified as a percentage of the total cellular Cab45. **(D)** Mander's coefficient of colocalisation was used to determine the presence of Cab45 in the *cis*-Golgi with GM130 (top) or the *trans*-Golgi with TGN38 (bottom). Data presented as mean ± SEM and comparisons made using one-way ANOVA. *, $p < 0.05$; ** $p < 0.01$; ***, ****, $p < 0.0001$.

Ca^{2+}-dependency of Cab45 localisation in INS1 cells. Finally, a collaborator (A/Prof. Michael Ailion and Dr. Jerome Cattin-Ortola, University of Washington) stably transfected INS1 cells with hemagglutinin (HA)-tagged wild-type Cab45 (WT Cab45HA) or a Ca^{2+}-binding mutant Cab45 (6EQ Cab45HA), where all six Ca^{2+}-binding EF hands have been rendered non-functional (**Figure 17**). Confidence that cells contained comparable amounts of ectopically expressed protein was provided by immunoblotting for the HA tag, which resolves a double band that is suggestive of an intracellular processing event (**Figure 17C**). In contrast to the method employed in **Figure 16**, this approach has more specificity to the Cab45 protein but it is not without its own pitfalls. Here, massive overexpression could violate the stoichiometric balance of endogenous secretory pathway proteins. Therefore, results should be interpreted with caution but can still provide interpretable insight into the nature of Cab45 behaviour considering the comparison of 6EQ Cab45HA to a WT Cab45HA control.

Immunofluorescent staining using antibodies directed against the HA tag revealed that overexpressed WT Cab45HA was widely localised throughout the cell secretory pathway and present within punctate structures in the cytosol (**Figure 17A**). Conversely, localisation of 6EQ Cab45HA was predominantly restricted to the TGN (**Figure 17A**) although some punctate signal in the periphery is evident. Pearson's coefficient of correlation between the HA and TGN38 signals confirmed the difference between WT and 6EQ Cab45HA distribution (mean $r^2 \pm$ SEM = [WT: **0.40 ± 0.02**] *vs* [6EQ: **0.79 ± 0.03**] ($p < 0.001$)) (**Figure 17B**).

Western immunoblotting of concentrated proteins from the extracellular medium revealed that a low level of WT Cab45HA was released from the cells during basal conditions of 2.8 mM glucose (low glucose - LG), but 6EQ Cab45HA was barely detectable (**Figure 17D**). Following 2 hours of stimulation with 16.7 mM glucose (high glucose - HG), WT Cab45HA was abundant in the culture medium whereas 6EQ Cab45 was less detectable (**Figure 17D**). These results indicate that overexpressed WT Cab45HA has a greater ability to occupy SGs of the regulated secretory pathway in β-cells than its Ca^{2+}-binding deficient counterpart. Interestingly, some induction of 6EQ Cab45HA secretion by glucose is evident thereby suggesting that it can in fact exit the TGN and occupy insulin SGs, albeit to a lesser degree (**Figure 17D**).

From these data it is clear that Ca^{2+}-binding alters the behaviour of Cab45 trafficking, and it is likely to do so by modifying the oligomeric state. 6EQ Cab45HA, which is presumably monomeric, could experience impaired exit from the TGN and/or it could enter the SG compartment only to be removed efficiently via the *sorting by exit* mechanism. On the contrary, sorting WT Cab45HA into ISGs from the TGN could be more efficient as a result of the enhanced Ca^{2+}-binding, and/or greater aggregation within the SG could limit WT Cab45HA excursion from the SG via *sorting by exit*. Nonetheless, both of the exogenously overexpressed proteins transit through the Golgi apparatus and exit into post-Golgi vesicles of INS1 insulinoma cells, demonstrating the molecular ability of both monomeric and oligomeric Cab45 to traffic into vesicles. Follow-up studies should be conducted to assess and compare any interference of the two Cab45 variants on insulin secretion.

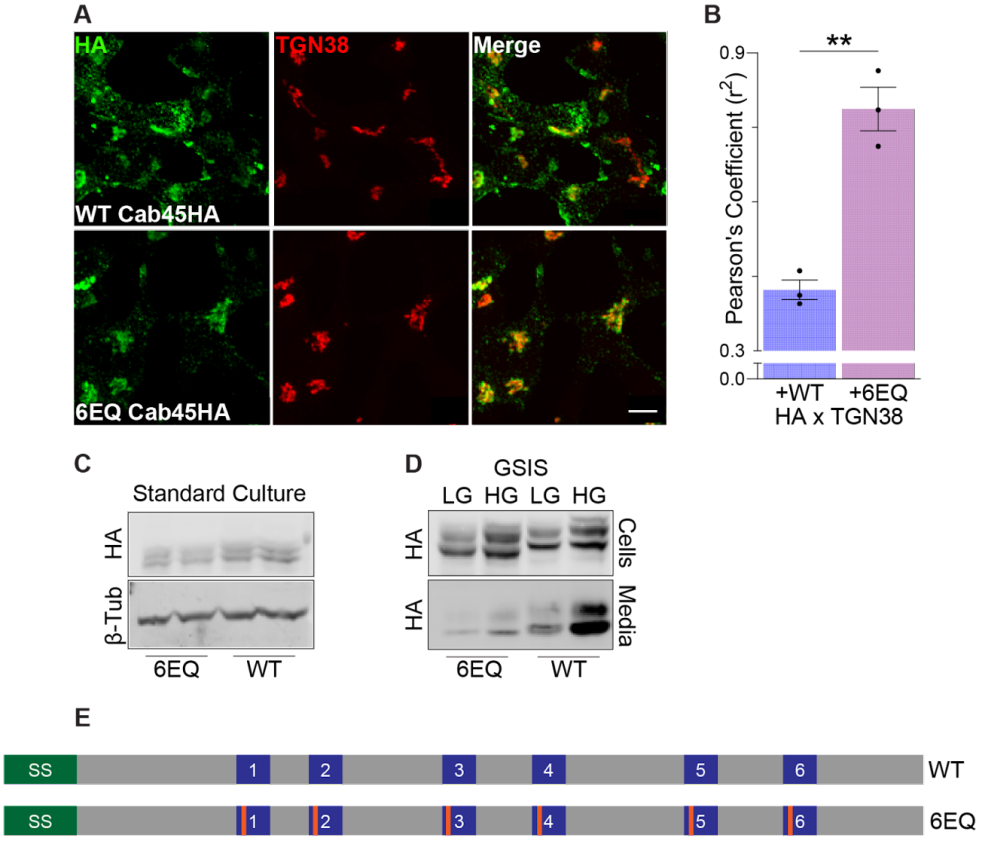

Figure 17. Ca^{2+} binding promotes the occupation of insulin SGs by overexpressed Cab45. (A) Immunofluorescent staining of HA and TGN38 in INS1 cells overexpressing WT or 6EQ Cab45HA at steady-state (n=3), scale bars = 5 µm. **(B)** Pearson's coefficient of correlation between HA and TGN38 signal presented as mean ± SEM and comparison made using paired t-test. **(C)** Western blots for HA and β-tubulin during standard culture conditions (n=3). **(D)** Western blots for HA in cells and extracellular medium during culture at two hours of 2.8 mM low glucose (LG) or 16.7 mM high glucose (HG) (n=3). ***, $p < 0.001$.

2.4 Discussion

Identification of proteins that are differentially expressed during the healthy state, β-cell compensation and β-cell failure can provide insight into dysfunctional processes that contribute to T2D. Cab45 is one such protein as its abundance appears to correlate with the functional output of pancreatic β-cells in settings of metabolic dysfunction, marking the first time that it has been implicated in disease pathology in both animal models and human subjects (**Figures 12 and 13**). Whether the loss of Cab45 expression contributes to or is a consequence of T2D remains a topic of curiosity.

Cab45 expression and localisation. *In-situ* mRNA hybridisation revealed broad expression of Cab45 mRNA throughout mouse tissues (**Figure 10**). Cab45 mRNA is almost ubiquitously expressed during embryonic development (**Figure 10: A-B**) and within the adult mouse (**Figure 10: C-D**), and is particularly prominent in tissues that have exocrine secretory functions and in the nervous system where neurotransmitter production relies on regulated secretory pathways. Cab45 mRNA is prominent in all tissues analysed that are responsible for hormone production aside from the pancreas (**Figure 10: C-D**). This could be due to the endocrine pancreas making up only 1-2% of total pancreatic area, or because of high RNAse abundance within the pancreas. Thus, antibodies that recognise all experimentally verified Cab45 isoforms were applied to human pancreas sections from three individuals to reveal that Cab45 protein is expressed in the human islet where it is restricted to the β-cell population (**Figure 11**). Juxtanuclear ribbon structures indicate the presence of Golgi-localised Cab45-G, and punctate staining of Cab45 throughout the cell periphery could represent either post-Golgi localised Cab45-G, the cytosolic isoform Cab45-C, or the ER isoform Cab45-S. Importantly, individuals display variability in Cab45 expression, with one subject harbouring many non-insulin-positive cells with abundant Cab45 signal through the entire cell (**Figure 11C**). It is unclear the identity of these cells, as they could be dedifferentiated β-cells or other islet cell types that are occupying a higher percentage of the islet cell population. Differential patterns of Cab45 expression between individuals should be characterised in more depth, first by using antibodies raised against only the full-length Cab45-G protein and followed with characterisation in the diabetic state, since the analysis in **Figure 12** did not take into account the peripheral Cab45 signal. Moreover, closer investigation of the adrenal and pituitary glands in mice revealed specific enrichment of Cab45 mRNA in the adrenal medulla and the intermediate and anterior lobes of the pituitary (**Figure 10: E-L**). Although several isoforms of Cab45 are verified in humans, UniProt lists only the canonical Golgi isoform Cab45-G expressed in mice. Therefore, specific expression of Cab45-G in these cell types indicate a potential involvement in functions that are required by specialised secretory cells, but due to its near ubiquity in expression and established role of protein sorting in HeLa cells, a role in constitutive secretory cells could co-exist.

Cab45 is expressed in insulinoma cell lines derived from mouse and rat where it partially colocalises with proinsulin, but this occurs predominantly in the *cis*-Golgi and not the TGN as expected (**Figure 14-15**). Therefore, the hypothesis that Cab45 directly regulates proinsulin entry into ISGs from the TGN is put into question, but the subcellular localisation of Cab45 remains to be confirmed in human cell lines or primary islets, and it is possible that low amounts of Cab45 traffic more distally. Occasionally, Cab45-positive puncta are observed, but whether these are secretory granules, extensions of the Golgi apparatus, or are staining artefacts have not been determined. Investigation of Cab45 localisation following treatment with cycloheximide, a biochemical agent used to inhibit the synthesis of new protein, could be useful in determining whether endogenous Cab45 normally traffics out of the *cis*-Golgi and is replenished by the synthesis of new Cab45 protein, co-staining with pre- and post-Golgi markers would also be helpful. A recent report using unbiased proteomics to identify the secretory repertoire of the human β-cell line EndoC-βH1 revealed that endogenous Cab45 is not secreted under basal conditions, but cell stress induced by non-targeted siRNAs over a range of 24 to 72 hours results in its extracellular release (Ryaboshapkina et al. 2022). The route of trafficking was not identified but secretion of SG-resident proteins (including insulin, VGF, CgA, and CgB) were also elevated during stress (Ryaboshapkina et al. 2022). Follow-up studies should be conducted to determine whether this can occur during alternate physiological states such as standard GSIS or prolonged nutrient excess. Localisation should also be assessed in islets from ob/ob mice where Cab45 protein (**Figure 12**) and mRNA (**Figure 9B**) expression increases during β-cell compensation.

Determinants of Cab45 localisation and trafficking. The data obtained from the INS1 line has gathered that Ca^{2+} is a key determinant of Cab45 localisation and trafficking, providing indirect confirmation that Cab45 interacts with Ca^{2+} in the β-cell (**Figures 16-17**). The experimental approaches utilised here each offer their own strengths and weaknesses, but when interpreted together provide a more well-rounded insight into the determinants of Cab45 localisation. In HeLa cells, Ca^{2+} maintains Cab45 in an oligomeric state which is its retention strategy within the Golgi, and interruption of this interaction through various manipulations releases Cab45 from the cell via the constitutive pathway (von Blume et al. 2012; Crevenna et al. 2016). However, comparable studies related to the Ca^{2+}-dependency of Cab45 localisation differ in some aspects between HeLa cells and INS1 cells. In both cases, crude pharmacological approaches that not only interfere with the interaction between endogenous Cab45 and Ca^{2+}, but are likely to alter the landscape of intracellular Ca^{2+}-binding proteins, results in the exit of Cab45 from the Golgi. However, Cab45 is observed to enter non-insulin-containing vesicles and is retained within the cell after 30 minutes treatment of INS1 cells (**Figure 16**), but is rapidly released into the medium from HeLa cells after 5 minutes of treatment (von Blume et al. 2012). Since this approach does not completely deplete Cab45 from the Golgi of INS1 cells, its retention within this compartment may not be entirely dependent on Ca^{2+}.

A more direct, less invasive approach is to assess the localisation of an overexpressed mutant Cab45 that is unable to bind Ca^{2+}. This approach has its own pitfalls, since overexpressed Cab45 could stoichiometrically overload the secretory pathway and return results that may not be physiologically relevant. Thus, although the overexpression system is more specific than broad pharmacologically-mediated Ca^{2+} manipulation, the latter provides a scenario where behaviour of the endogenous Cab45 protein can be assessed. Nonetheless, in HeLa cells, overexpressed 6EQ Cab45HA is more readily released into the culture medium during steady state conditions compared to WT Cab45HA (Crevenna et al. 2016). In INS1 cells, 6EQ Cab45HA is predominantly localised in the TGN and has minimal release from the cell during both resting and glucose-stimulated conditions, whereas WT Cab45HA is distributed in punctate vesicular structures throughout the cell periphery, is released to a greater extent at rest, and undergoes glucose-stimulated secretion (**Figure 17**). It is more likely that these cell lines are equipped with unique secretory compartmentalisation resulting from endowment of specific protein expression that accounts for the conflicting findings, rather than some difference in the Cab45-Ca^{2+} interaction between species and/or cell types. Here, in INS1 cells, a small amount of 6EQ Cab45HA secretion could be induced by glucose stimulation indicating that it does indeed enter into insulin containing SGs, but the near absence of release at basal glucose is evidence that monomeric Cab45 does not enter the constitutive pathway (**Figure 17D**). Perhaps, following entry into the regulated secretory pathway, the majority of 6EQ Cab45HA which fails to condense within the maturing SG is removed via the *sorting by exit* mechanism and targeted for degradation, explaining differences in localisation (**Figure 17B**).

In specialised secretory cells, the constitutive pathway is often thought of as the default route of trafficking taken by proteins that do not enter the regulated pathway, but whether this is actually the case has been a long-held topic of enquiry (Arvan and Halban 2004). An investigation published by Professor Peter Arvan's laboratory (*Lara-Lemus* et al.) established a marker for the constitutive pathway in β-cells by, conveniently, expressing a truncated Myc-tagged Cab45 mutant that was missing amino acids 309-361 (Cab_{308}Myc) into INS1 cells (Lara-Lemus et al. 2006). Authors used Cab_{308}Myc as a tool to reveal mechanisms of constitutive pathway targeting in the β-cell, but findings and interpretations related to Cab_{308}Myc were published prior to the knowledge of Cab45's intracellular behaviour and function as a soluble protein sorter. The data presented here in this thesis demonstrates that ectopically overexpressed Cab45 is not readily secreted during resting conditions but undergoes extensive glucose-stimulated release, reflecting its presence within insulin SGs (**Figure 17D**). Alternatively, ectopically overexpressed Cab_{308}Myc was found to distribute throughout non-insulin containing post-Golgi vesicular structures and was extensively secreted under non-stimulatory conditions (Lara-Lemus et al. 2006). Endogenous Cab45 colocalises with proinsulin in both insulinoma lines INS1 and MIN6 (**Figure 14B and Figure 15**), whereas this study found that Cab_{308}Myc is distinctly separated from proinsulin when expressed into INS1 cells (Lara-Lemus et al. 2006). Unlike full-length Cab45 which is a soluble protein, Cab_{308}Myc was associated with

intracellular membranes as early as the ER but became soluble at some point within the vesicle prior to its constitutive release from the cell (Lara-Lemus et al. 2006). Considering that a large proportion of translation and secretory pathway traffic are dedicated to proteins that comprise the insulin SG (Magro and Solimena 2013; Vasiljević et al. 2020), the authors postulated that entry into the insulin SG is the default pathway of traffic, and that membrane association in early secretory compartments is a general mechanism that proteins use to steer clear of the bulk flow of regulated cargo while seeking out the constitutive pathway (Lara-Lemus et al. 2006). This could account for the intracellular retention of soluble monomeric Cab45 either in the form of endogenous Cab45 unbound to Ca^{2+} (**Figure 16**) or 6EQ Cab45HA that cannot bind Ca^{2+} (**Figure 17D**) in INS1 cells, which are both readily secreted from HeLa cells (von Blume et al. 2012; Crevenna et al. 2016). Unaccounted for however, and of particular interest to this study, is why Cab_{308}Myc prefers to associate with the membrane.

Alongside the data presented in this thesis, findings by *Lara Lemus* et al. indicate that the C-terminus of Cab45 harbours information that may in fact be more crucial for its localisation than Ca^{2+} in β-cells. This region does not contain any Fam20C-targeted phosphosites, and while the 6th EF hand is located here, intracellular retention of 6EQ Cab45HA (**Figure 17**) argues against a defect in Ca^{2+}-binding as the cause of Cab_{308}Myc misdirection. Even when Cab45 exits the Golgi following Ca^{2+} depletion of INS1 cells and colocalisation with pro/insulin is lost, as is the case with Cab_{308}Myc, full length Cab45 is still retained within the cell (**Figure 16**). Barring any major conformational changes to Cab_{308}Myc at the monomeric or oligomeric level, observations are consistent with a possibility that the C-terminus of Cab45 is involved in interactions with other proteins that maintain its Golgi localisation and separation from the membrane, which occurs even when Cab45 is in the monomeric state. Interestingly, the C-terminus of human Cab45-S differs from that of Cab45-G only from amino acids 305 onward, and Cab45-S is localised to the ER despite not having a C-terminal KDEL sequence for ER retention. In HeLa cells, Cab45-S interacts with the sarco/endoplasmic reticulum Ca^{2+}-ATPase (SERCA2B) in the ER via a motif common to both Cab45-G and Cab45-S (L. Chen et al. 2016), yet, Cab45-G bypasses this interaction for trafficking beyond the ER. Thus contrary to current thought, Ca^{2+}-binding might not be a requirement for all Cab45-protein interactions, in turn suggesting that Ca^{2+} is not solely responsible for Cab45 localisation in the β-cell. All observations are consistent with the notion that the C-terminus of Cab45 is involved in protein-protein interactions.

In HeLa cells, findings are quite linear in that any method that disrupts Ca^{2+}-binding results in Cab45 release from the cell (von Blume et al. 2009, 2011, 2012; Crevenna et al. 2016). In INS1 cells, ionomycin and 6EQ Cab45HA expression experiments return alternate outcomes even though Cab45 is monomeric in both situations, but discrepancies provide speculative insight into the existence of Cab45-protein interactions that do not rely at all on Ca^{2+}-binding. When 6EQ Cab45HA is expressed into cells containing a stable population of potential interacting proteins, it is mostly distributed throughout the Golgi apparatus but can exit into insulin SGs (**Figure 17**). While such proteins could

be bound by Ca^{2+}-interactions themselves, their predictable localisation could assist that of 6EQ Cab45HA. Alternatively, when Ca^{2+} is extracted from the cell in what is a completely non-physiological circumstance (**Figure 16**), broad disruption of Ca^{2+}-dependent protein-protein interactions could disperse the population of Cab45-interacting proteins and explain the exit of monomeric Cab45 into non-insulin-containing but non-constitutive post-Golgi vesicles. Perhaps the fate of Cab45 in this instance is driven by the combination of proteins that are bound in a non-Ca^{2+}-dependent manner such that the monomeric Cab45 follows the trafficking of these proteins in the Ca^{2+}-depleted condition. If this is the case, closer examination using this experimental protocol might provide insight into a subset of Cab45-interacting proteins in the β-cell. In either case presented in **Figures 16 and 17**, the absence of Ca^{2+}-binding precludes that Cab45 is in the monomeric state yet the outcomes are vastly different. Common to both cases, however, is that Cab45 is retained in the cell when Ca^{2+}-binding is interrupted which is in direct contrast to Cab_{308}Myc as well as the same situations in HeLa cells. It follows that expression of unique β-cell-specific proteins could account for the differential localisation and patterns of Cab45 trafficking that are observed between HeLa cells and INS1 cells. On a broader level, the presence of unique proteins could dictate Cab45 behaviour and function in specialised versus non-specialised secretory cells throughout complex mammalian organisms (**Figure 10**).

In summary, the results indicate that Ca^{2+}-binding is involved in Cab45 localisation to the *cis*-Golgi where it exists in close proximity to proinsulin (**Figure 14-15**), but, that Ca^{2+} might not be entirely responsible for this (Lara-Lemus et al. 2006). When overexpressed, Ca^{2+}-binding enhances Cab45 retention within insulin-containing SGs (**Figure 17**). In the absence of Ca^{2+}-binding, predominant localisation of monomeric Cab45 in the TGN at steady-state, combined with a slight induction of glucose-stimulated release suggests that it enters the ISG only to be removed by post-Golgi sorting mechanisms (**Figure 17**). Evidence is not yet clear that endogenous Cab45 is present within the insulin SG either permanently or transiently during normal conditions. Therefore, the biological relevance of findings from overexpression systems are questionable, especially since the secretory pathway is overloaded with a protein that could alter its function. As mentioned, endogenous Cab45 is secreted when β-cells are under stress (Ryaboshapkina et al. 2022), so expression level does not necessarily need to be high for Cab45 to traffic out of the *cis*-Golgi. Moreover, immunostains of human pancreas sections (**Figure 11**) have indicated that Cab45 may occupy the insulin SG and that this could vary between individuals but this requires further clarification, and indeed, such variability could be clinically relevant. Physiologically, alterations in Ca^{2+} handling that occur during various stages of β-cell function (Sabatini, Speckmann, and Lynn 2019) could affect Cab45 behaviour, and on the other hand, changes to intracellular Cab45 expression that occurs during β-cell compensation and failure (**Figures 12 and 13**) could alter Ca^{2+} homeostasis. Now, the stage is set for functional studies interrogating the role of Cab45 in the pancreatic β-cell.

(This page is intentionally left blank)

(This page is intentionally left blank)

Chapter 3: Cab45 Knockout β-Cells

3.1 Introduction

To interrogate the function of Cab45 in pancreatic β-cells, Cab45 knockout (Cab45KO) INS1 and MIN6 insulinoma cell lines were generated using the CRISPR/Cas9 gene editing system and characterised. A β-cell-specific Cab45KO mouse was also generated using the Cre/Lox system and initial characterisation was performed at 8 weeks of age on standard chow diet followed by 8 weeks of high fat high sucrose diet (HFHSD) to investigate the systemic effect of Cab45 loss from pancreatic β-cells.

Cab45 has a definitive role in regulating the trafficking of secretory cargoes in the constitutively secreting HeLa cell line (Blank and von Blume 2017). Upon commencing this project, the central hypothesis was that Cab45 directly regulates the egress of proinsulin from the TGN into ISGs. Alternatively, Cab45 could be also responsible for trafficking other soluble or transmembrane cargoes of the regulated secretory pathway, or, could constitutively traffic soluble extracellular or transmembrane proteins that localise to the PM or other secretory pathway intermediaries. If Cab45 is not directly involved in protein trafficking in the β-cell, another possibility is that effects of its depletion could be mediated through altered secretory pathway Ca^{2+} homeostasis, which would place Cab45 one step removed from regulating SG biogenesis or other intracellular processes. These possibilities are of course not mutually exclusive.

3.2 Materials and Methods

3.2.1 CRISPR/Cas9 knockout of Cab45 in INS1 cells

INS1 cells were kindly provided by A/Prof. Cedric Asensio (University of Denver) transfected with lentiCRISPR v2 and a CRISPR/Cas9 pX330 vector containing gRNA (forward: 5' – CTGTGGTCTGGCTGCTCATG – 3'; reverse: 5' CATGAGCAGCCAGACCACAG – 3') that targets exon 2 of Cab45. 24 hours after transfection, cells were treated transiently with 2 µg/mL of puromycin (Goldbio) to select for transfected cells. A population of single clones following puromycin selection were plated in a round bottom 96-well plate and expanded.

3.2.2 Transient Cab45HA plasmid transfection of INS1 cells

pLPCX retroviral expression vectors containing WT Cab45HA, 2EQ Cab45HA, 1,3EQ Cab45HA or 6EQ Cab45HA were gifts from A/Prof. Julia von Blume, generated as described previously (Crevenna et al. 2016). 6-well plates of INS1 cells at around 60% confluency were incubated with 1.5 mL of OptiMEM (Gibco) for 25 minutes. Meanwhile, for each well, 0.5 βg plasmid DNA and 10 µL of Lipofectamine 2000 (Thermo Fisher) were added to separate tubes containing 250 µL OptiMEM (scaled per-well) for 5 minutes, then mixed together gently for 20 minutes to allow Lipofectamine to complex with plasmid DNA. Then, 500 µL of Lipofectamine/plasmid mix were added to each well and allowed to culture for 6 hours before media was changed to standard RPMI. Cells were cultured for 48 h prior to analysis to allow time for Cab45HA expression and phenotypic change.

3.2.3 siRNA-mediated Cab45 knockdown in INS1 cells

INS832/13 cells were seeded on a 12-well plate. siRNA to Cab45 (siCab45) was NM_130412.2_stealth_174: 5'-CCUUCUGAUGGAUGCAACUGCUAGA-3'from Invitrogen (a gift from Julia Von Blume) and non-targeting control (siCtrl) was Stealth RNAi™ siRNA Negative Control, Medium GC from Invitrogen (#12935300). When reaching 60% confluence, cells were transfected twice with either siCab45 or siCtrl on day 1 and 3 using Lipofectamine 2000 according to manufacturer's instructions. Cells were assayed on day 4 or 5. Efficiency of knockdown was over 50% as assessed by immunofluorescence using an anti-Cab45 antibody.

3.2.4 CRISPR/Cas9 knockout of Cab45 in MIN6 cells

MIN6 Cab45KO cells were generated by and purchased from GenScript. Cas9 endonuclease and gRNA sequence TCGGGAAAGAGCGGCTAACA was used to target the 2nd exon of Cab45.

Three individual clones were expanded, and insertions/deletions causing frameshift mutations were confirmed with genomic sequencing.

3.2.5 Transient adenoviral infection of MIN6 cells

Adenoviral vectors expressing either red fluorescent protein (RFP) or mouse Cab45 with green fluorescent protein (GFP) were purchased from Vector biolabs. RFP-expressing adenovirus was diluted 1:3000 and Cab45-expressing adenovirus diluted 1:10000 in DMEM, and MIN6 cells were cultured under infection for 48 hours before media changed to fresh DMEM for an additional 24 hours prior to experiment.

3.2.6 Generation of SDF4-floxed mice

C57BL6/N mice with the 3rd exon of Cab45 floxed were generated by Cyagen, and backcrossed onto the C57BL6/J strain for over 7 generations. To generate the floxed exon, first, bacterial artificial chromosomes were engineered to contain homology arms (HAs) specific to the genomic sequence surrounding the conditional KO (cKO) region, or the cKO region itself. These specific regions were amplified to create mouse genomic fragments that were then assembled into a targeting vector, by sequentially adding the first homology arm, then a loxP site, the cKO region, a second loxP site, and finally the second homology arm. Next, the targeting vector along with Cas9 endonuclease and guide RNAs which targeted genomic regions that flank the 3rd coding exon of the SDF4 gene were co-injected into fertilised eggs. Resultant pups were viable, but as they were initially on the C56BL6/N background, required at least 7 generations of backcrossing to the C57BL6/J background prior to experimentation.

3.2.7 Mouse housing, breeding and feeding

Mice were housed and bred at the Australian Bioresources (ABR) Facility in Moss Vale (Garvan Institute) on a 12 h light/dark cycle and given food and water ad libitum. To generate cKO mice, Cab45-floxed mice were bred with B6(Cg)-Ins1$^{tm1.1(cre)Thor}$/J (Jackson Laboratory, 026801). One-week prior to experimentation, mice were transported to the Charles Perkins Centre. All mice were fed ad-libitum on a standard chow diet up to 11 weeks of age and then subject to an ad libitum high fat high sucrose diet (HFHSD) (23% casein, 20.2% sucrose, 20.2% lard, 17% starch, 5.8% mineral mix, 5% bran, 3% safflower oil, 2% gelatin, 1.3% vitamin mix, 0.4% choline, 0.3% methionine). All procedures performed followed the National Health and Medical Research Council (NHMRC) guidelines for animal research and approved by the University of Sydney Animal Ethics Committees.

3.2.8 Label-free quantification mass spectrometry of INS1 cells

INS1 cells were cultured to 80% confluence, washed twice with PBS and lysed by collecting in 4% sodium deoxycholate (SDC) containing 100 mM Tris-HCl (pH 8.0), boiling for 10 minutes at 95 C and sonicated in a QSonica Q800R2 water bath for 10 minutes (3s on/off) at 20% magnitude. Following sonication, lysate was clarified by ultracentrifugation at 18,000 x g for 10 minutes, supernatant collected into a new tube and protein quantified using BCA. Trypsin digestion, LC-MS/MS and spectra analysis were performed as described previously (Harney et al. 2021).

3.2.9 Electron microscopy of INS1 cells

INS1 cells were cultured on Thermanox^{TM} coverslips, then fixed and prepared for sectioning as described previously (Shami et al. 2014). Silver-gold ultrathin sections (~70 nm) were generated using a Leica EM UC7 ultramicrotome (Leica, Heerbrugg, Switzerland), then mounted onto 200-mesh copper grids (G200-Cu, Electron Microscopy Sciences, Hatfield, PA, USA). Post-staining was performed using an aqueous solution of 2% uranyl acetate for 10 minutes, followed by Reynold's lead citrate for 10 minutes. Stained sections were viewed using a JEOL 1400 TEM (Tokyo, Japan) operating at 120 kV. Across three experiments, secretory granules were counted in 9 – 11 cell images per control and Cab45KO INS1 samples. Samples from EM data were processed and imaged blinded by the Australian Microscopy and Microanalysis Facility, University of Sydney.

3.2.10 GSIS and multiple challenge GSIS assays in INS1 cells

INS1 cells were subject to basal glucose conditions in Krebs buffer (20 mM HEPES, pH 7.4, 119 mM NaCl, 4.75 mM KCl, 2.54 mM $CaCl_2$, 1.2 mM $MgSO_4$, 1.18 mM KH2PO_4, 5 mM $NaHCO_3$, 0.5% BSA) containing 2.8 mM glucose for 1 h (basal). Following this, the media was replaced with either 2.8 mM glucose Krebs buffer or 16.7 mM glucose for 1 h. Media was collected to measure insulin secretion by HTRF assay (Cisbio) and proinsulin secretion by ELISA (Mercodia). Cells were collected in islet lysis buffer (100 mM Tris, 300 mM NaCl, 10 mM NaF, 2 mM Na_3VO_4, and protease inhibitors) and sonicated to measure insulin content by HTRF assay and DNA content with the Quant-iT PicoGreen dsDNA Assay kit (Thermo Fisher).

For overnight basal experiments, cells were starved in a low-glucose RPMI 1640 (Gibco) containing 2.8 mM glucose, 2.05 mM L-glutamine, 10 % FBS, 10 mM HEPES, 1 mM sodium pyruvate, 0.05 mM 2-ß-mercaptoethanol. The following day, assay procedure was conducted as above. Repeated challenge of insulin secretion was also performed using an overnight basal. Following 1 h stimulation at 16.7 mM glucose, cells were rested in basal glucose for 30 min and stimulated again for 1 hour. Post-assay measurements were conducted as above.

3.2.11 PC1/3 secretion in Cab45 knockdown INS1 cells

Cells treated with siCab45 or siCtrl were incubated in resting buffer for 2 h at 37 ºC (114 mM NaCl, 4.7 mM KCl, 1.2 mM KH_2PO_4, 1.16 mM $MgSO_4$, 20 mM HEPES, 2.5 mM $CaCl_2$, 25.5 mM $NaHCO_3$, 1 % bovine serum albumin (BSA), and 3 mM glucose, pH 7.2). Cells were washed twice with BSA-free resting buffer and incubated for 2 hours either with BSA-free resting buffer (containing 3 mM glucose) or BSA-free stimulating buffer (identical to resting buffer except that it contained 18 mM glucose). The supernatant was collected and spun down at 20,000 g for 10 min at 4 °C to remove cell debris. The supernatant was transferred into a new tube and precipitated with trichloroacetic acid (TCA) using 0.03 % sodium deoxycholate as a carrier. Pellets were resuspended in SDS sample buffer. The cells were lysed on ice using 50 mM Tris-HCl, pH 8.0, 150 mM NaCl, 1 % Triton X-100, 1 mM EDTA, and protease inhibitor cocktail (Pierce), clarified by centrifugation at 20,000 g for 10 min at 4 ºC, and then the supernatant was collected to a new tube. The protein concentration of cell lysates was measured using the BCA assay. The protein concentration of cell lysates and precipitated media was measured using the BCA assay. Equal amounts of protein were resolved via SDS-PAGE and analysed by western immunoblotting. Band intensity was quantified using ImageJ.

3.2.12 GSIS and KSIS assays in MIN6 cells

MIN6 cells were subject to basal conditions in Krebs buffer (20 mM HEPES, pH 7.4, 119 mM NaCl, 4.75 mM KCl, 2.54 mM $CaCl_2$, 1.2 mM $MgSO_4$, 1.18 mM KH2PO_4, 5 mM $NaHCO_3$, 0.5% BSA) containing 2.8 mM glucose for 1 h (basal). Following this, the media was replaced with 2.8 mM glucose in Krebs buffer for another hour and media collected. Then, either 16.7 mM glucose or 40 mM KCl Krebs buffer was applied to the same wells and media collected to measure insulin secretion by HTRF assay (Cisbio). Cells were collected in islet lysis buffer (100 mM Tris, 300 mM NaCl, 10 mM NaF, 2 mM Na_3VO_4, and protease inhibitors) and sonicated to measure insulin content by HTRF assay and protein content by the BCA assay (Pierce).

3.2.13 Immunofluorescent staining and microscopy

Immunofluorescent staining and imaging was performed the same as for section 2.2.6 describing the protocol used for insulinoma cell lines. Antibody sources and dilutions are as follows. Primary antibodies: Guinea Pig anti-Insulin pre-diluted (DAKO, A0564); rabbit anti-Cab45 (1:500, gifted by A/Prof. Julia von Blume); rabbit anti-SDF4 (1:200, Thermo Fisher PA5-52809); mouse anti-proinsulin (5 µg/mL, Developmental Studies Hybridoma Bank GS-9A8); mouse anti-GM130 (1:500, BD Biosciences 610822); mouse anti-TGN38 2F7.1 (1:500, Novus Biologicals NB300-575); rabbit anti-HA C29F4 (1:1000, Cell Signalling 3724). Secondary antibodies: all dilutions were at

1:1000. Thermo Fisher Scientific: goat anti-guinea Pig IgG Alexa Fluor 488; goat anti-rabbit IgG Alexa Fluor 594; goat anti-rabbit IgG Alexa Fluor 647; goat anti-mouse IgG Alexa Fluor 594. Jackson Immunoresearch: donkey anti-mouse Alexa Fluor 790 (1:20,000, 715-655-150).

3.2.14 Western immunoblotting

For Western immunoblots conducted in sections 3.1.1.1, confluent cells were washed with PBS, gently scraped into tubes, and centrifuged at 1000 rpm for 3 min. The supernatant was aspirated and cells resuspended in RIPA buffer (Thermo Fisher) supplemented with EDTA-free protease inhibitors (Roche). Cells were lysed by sonication then centrifuged at 12 000 x g for 15 min, and lysate transferred to a fresh tube. Protein concentrations were quantified using the Pierce™ BCA Protein Assay Kit (Thermo Fisher Scientific). Subsequent processing is as described in section 2.2.7, for immunoblots conducted in section 2.3.1.3 and 2.3.2.1 using a 10% polyacrylamide gel.

Western immunoblots conducted in section 3.3.1.5 are as described in section 2.2.7 for immunoblots conducted in section 2.3.2.2.

For Western immunoblots conducted in sections 3.3.2.1 and 3.3.2.3, confluent cells were washed with PBS then collected in SDS lysis buffer (75 mM Tris-HCl at pH 6.8, 1% SDS, 10% glycerol, 2.5% sucrose) without protease inhibitors by scraping. Next, cells were boiled at 95 degrees C and sonicated then centrifuged at 12 000 x g for 15 min, and lysate transferred to a fresh tube. Protein concentrations were quantified using the Pierce™ BCA Protein Assay Kit (Thermo Fisher Scientific). Proteins were separated using SDS-PAGE under denaturing conditions on a Bolt™ 4-12% Bis-Tris Plus gel, then transferred to methanol-activated PVDF membranes. Subsequent processing is as described in section 2.2.7 for immunoblots conducted in section 2.3.1.3 and 2.3.2.1.

3.2.15 Cellular insulin content measurement

INS1 and MIN6 cells were washed with PBS and lysed by collecting in islet lysis buffer (100 mM Tris, 300 mM NaCl, 10 mM NaF, 2 mM Na_3VO_4, and protease inhibitors) and sonicated to measure insulin content by HTRF assay (Cisbio) and DNA content with the Quant-iT PicoGreen dsDNA Assay kit (Thermo Fisher Scientific) or protein content with the BCA assay (Pierce).

For MIN6 insulin content measurements that were normalised to cell count, live cells were detached from the culture plate using TrypLE™ (Gibco), centrifuged at 300 x g to collect the cell pellet, and resuspended well in 10 mL of RPMI medium. From this, 1 mL of resuspension was removed to a separate tube, from which 10 µL of cells were mixed with 10 µL of trypan blue and counted using a Countess automated cell counter (Thermo Fisher). The remaining 990 mL was centrifuged to pellet cells, media was removed and cells washed with PBS twice. Cells were pelleted again for lysis using islet lysis buffer and sonication prior to insulin content measurement via HTRF assay (Cisbio).

3.2.16 Intracellular calcium measurement

The ratiometric calcium indicator Fura 2AM (Thermo Fisher) was utilised for intracellular calcium measurement. Cells were cultured in 3.5 cm glass-bottom dishes (Eppendorf) for 2 days prior to measurement. Protocol slightly varied for INS1 and MIN6 cells: INS1 cells were cultured at basal glucose in RPMI overnight whereas MIN6 cells were cultured at basal glucose for one hour in Krebs buffer (20 mM HEPES, pH 7.4, 119 mM NaCl, 4.75 mM KCl, 2.54 mM $CaCl_2$, 1.2 mM $MgSO_4$, 1.18 mM KH_2PO_4, 5 mM $NaHCO_3$, 0.5% BSA) containing 2.8 mM glucose prior to Fura-2AM loading. Cells were loaded with 4 μm Fura-2AM and 0.02% pluronic acid (Sigma Aldrich) in 2.8 mM glucose Krebs buffer and incubated (37° C, 95/5% air/CO_2) for 30 minutes. After labelling, cells were washed and incubated 2.8 mM glucose Krebs buffer for an additional 30 minutes. Then, dishes were transferred to a small volume chamber mounted on the stage of an inverted Nikon Eclipse Ti-E spinning disc confocal microscope with 10x objective. The chamber conditions were 37ºC and 5% CO_2. Cells were excited alternately with light at 340 and 380 nm every 50 ms using a Lambda DG-4 Xenon high-speed wavelength switcher (Sutter Instruments). Basal measurement was taken over a 3 minute time period before application of either 16.7 mM glucose or 40 mM KCl. Recordings were analysed using NIS-Elements software (Nikon) to draw regions of interest around cells and extract fluorescent traces. Fura-2 recordings were calibrated for intracellular [Ca^{2+}] using the Tsien formula (Grynkiewicz, Poenie, and Tsien 1985). Statistical analyses were performed using Microsoft Excel and Graphpad Prism 9.

3.2.17 Mouse oral glucose tolerance (OGTT) test

Mice were fasted 5 h and then analysed prior to oral glucose tolerance test by EchoMRI to calculate dose of 3 mg/kg glucose to lean mass. Mice were tail tipped for basal blood glucose and insulin measurement prior to ingestion of a 25% glucose solution in injectable water via oral gavage. Blood was collected at 0 and 15 min, and for some cohorts 30 min, for fed insulin measurement via ELISA (Crystal Chem) and at the following time points: 15, 30, 45, 60, 90, and 120 min for glucose measurements.

3.2.18 Mouse islet isolation and GSIS assay

For islet isolation, a 2 mL volume of 0.25 mg/mL Liberase (Roche Applied Science) in Hanks' buffered saline solution (Life Technologies) with 20 mm HEPES was injected into the common bile duct. The inflated pancreas was extracted and incubated at 37 °C for 13 min, and washed twice before passing through a 1,000-mm mesh filter. The resulting tissue was centrifuged with no break at 1,000 x g in a Histopaque 1119 and 1077 (Life Technologies) gradient for 20 min before islets were hand-picked in Hanks' buffered saline solution (Life Technologies).

Following overnight recovery in 11 mM glucose RPMI, islets were subject to basal conditions in Krebs buffer (20 mM HEPES, pH 7.4, 119 mM NaCl, 4.75 mM KCl, 2.54 mM $CaCl_2$, 1.2 mM $MgSO_4$, 1.18 mM KH2PO_4, 5 mM $NaHCO_3$, 0.5% BSA) containing 2.8 mM glucose for 1 h (basal). Then, 5 islets in three technical replicates were transferred to 96-well round-bottom plates containing either 2.8 or 16.7 mM glucose. Plates were centrifuged briefly at 300 x g to pellet islets and media was transferred into new wells. Islets were washed in PBS then islet lysis buffer (100 mM Tris, 300 mM NaCl, 10 mM NaF, 2 mM Na_3VO_4, and protease inhibitors) was applied before sonication to measure insulin content by HTRF assay and DNA content with the Quant-iT PicoGreen dsDNA Assay kit (Thermo Fisher Scientific).

3.2.19 Statistical analysis

Statistical analyses were performed using GraphPad Prism 7 software. Statistical significance was determined by two-tailed Student's t-test, one-way ANOVA or two-way ANOVA with Tukey's multiple comparisons post-test corrected for multiple comparisons. A value of $p < 0.05$ was considered significant.

(This page is intentionally left blank)

3.3 Results

3.3.1 Characterisation of rat INS1 cells with Cab45 depletion

3.3.1.1 INS1 Cab45 knockout generation and validation

To study the consequence of Cab45 loss in rat insulinoma cells, a collaborator (A/Prof. Cedric Asensio, University of Denver) designed CRISPR/Cas9 guide RNAs to insert premature stop codons into both alleles of exon 2, the first coding exon, of Cab45 in INS1 cells (**Figure 18A**). Western blotting and immunofluorescent staining using an antibody raised against the full Cab45-G protein confirmed knockout (KO) of the Cab45 protein (**Figure 18B-C**).

Label-free quantitative mass spectrometry (LFQ) showed the complete absence of Cab45 related peptides from KO INS1 cells (**Figure 18D**). This indicates that all other isoforms, if present, have also been deleted. Uniprot lists one 382 amino acid isoform present in rats that contains a 20 amino-acid extension on the N-terminus (Uniprot Consortium 2022) but the existence of this isoform has not yet been validated in publication. One study has reported that the cytosolic isoform, Cab45-C, is expressed in β-cells of rat islets (Zhang et al. 2009), although evidence is questionable due to aforementioned issues surrounding potential antibody cross-reactivity, and its existence in rat remains to be validated by other studies. Since the start codon of Cab45-C is located on exon 5, its translation should not be affected by the frameshift at exon 2 and thus would be detected in KO cells if expressed normally in the INS1 cell line. Therefore, there is some level of confidence that only the Cab45-G protein has been deleted, and that Cab45-C is not normally expressed in the rat β-cell. Immunofluorescent staining should be repeated with the aforementioned antibody used in **Figures 11** and **15** that targets an epitope common to all Cab45 isoforms to completely verify the situation.

Finally, LFQ mass spectrometry also revealed that the abundance of only a small proportion of INS1 proteins are significantly altered in KO INS1 cells (**Figure 18E**). Moreover, off-target effects of the CRISPR/Cas9 editing based on the gRNA sequences were not evident in the proteome as revealed by basic local alignment search tool (BLAST) and checking the data for potential off-target proteins. This provides confidence that phenotypes observed in KO INS1 cells are specifically driven by the loss of Cab45-G, but since insulinoma cells are known to be functionally heterogeneous (Lilla et al. 2003; R. Zhao et al. 2021) phenotypic differences could also arise from the expansion of KO cells from subclonal populations. Indeed, a host of proteins that may contribute to a range of cellular processes are differentially regulated in between WT and KO INS1 cells (**Figure 18G**).

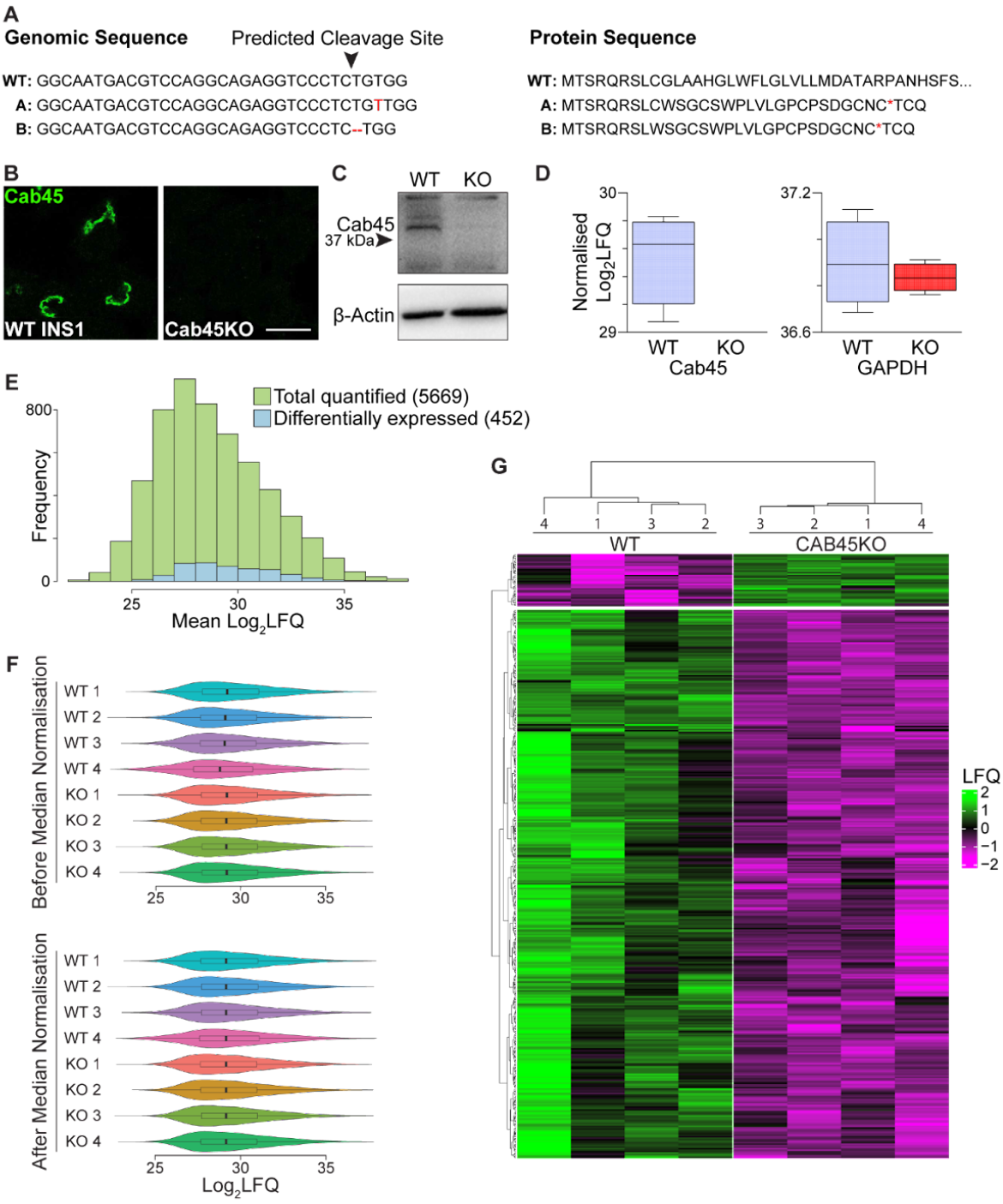

Figure 18. Validation of Cab45 deletion from INS1 insulinoma cells. (A) Schematic representation of targeted deletion strategy, showing genomic insertions and deletions (red) and conversion to a premature stop codon (red) in the Cab45 protein. **(B)** Immunofluorescent staining of Cab45 in WT and Cab45KO INS1 cells, scale bar = 5 µm. **(C)** Western blot of Cab45 and β-actin in WT and KO cells. **(D)** Label-free quantification of Cab45 protein in WT and KO cells presented as the mean ± 95% CI, n = 4 per condition. **(E)** Frequency histogram of proteomic analysis quantifying the relative abundance of differentially regulated proteins to the total abundance of proteins in KO cells. **(F)** Violin plots before and after Log_2 median normalisation of protein LFQ intensities. **(G)** Heat map of significantly regulated proteins between WT and KO INS1 cells.

3.3.1.2 Insulin and secretory granule content deficits in Cab45KO INS1 cells

Cab45 has been demonstrated to regulate the sorting of secretory cargo from the TGN into vesicles of the constitutive secretory pathway in HeLa cells (von Blume et al. 2012; Hecht et al. 2020). To assess the regulation of intracellular insulin content by Cab45, immunofluorescent staining, electron microscopy (EM), and label free quantification (LFQ) proteomic analysis were employed (**Figure 19-21**).

Immunofluorescent staining. First, co-staining insulin with TGN38 showed that in WT cells, insulin was broadly distributed throughout the cytoplasm and cell periphery within SGs (**Figure 19A**). In contrast, there was a clear redistribution of the insulin signal from the cell periphery to the TGN in KO cells (**Figure 19A**). Pearson's coefficient of correlation between insulin and TGN38 fluorescence confirmed the redistribution of insulin, likely proinsulin, into the TGN38-positive compartment of KO cells (mean r^2 ± SEM = [WT: **0.16 ± 0.02**] *vs* [KO: **0.26 ± 0.01**] ($p < 0.05$)) (**Figure 19B**).

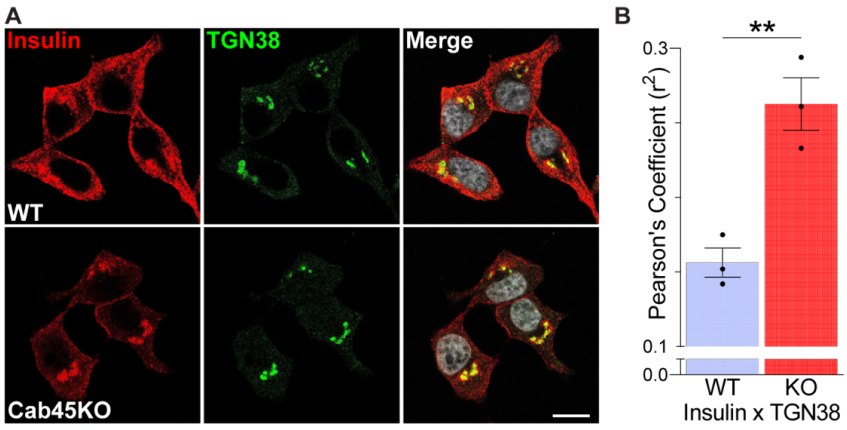

Figure 19. Peripheral insulin SG content is depleted in Cab45KO INS1 cells. (A) Immunofluorescent staining of WT and Cab45KO INS1 cells for insulin and TGN38, scale bars = 5 µm. **(B)** Pearson's coefficient of correlation between insulin and TGN38 signal from **(A)**. Data presented as mean ± SEM and comparison made using paired t-test: **, $p < 0.01$.

Electron microscopy. Using EM, it was confirmed that KO cells had a near 3-fold reduction in the number of SGs compared to WT (mean granules/5µm ± SEM = [WT: **18.0 ± 2.2**] *vs* [KO: **6.1 ± 2.1**] ($p < 0.001$)) (**Figure 20A**). Moreover, the area of SGs in KO cells were significantly lower compared to WT cells (mean nm^2 ± SEM = [WT: **14678 ± 738**] *vs* [KO: **10781 ± 1401**] ($p < 0.05$)) (**Figure 20B**). Qualitatively, SGs in KO cells are darker within the dense core area and lack the typical halo that is clearly evident in WT cells. Thus, not only are Cab45KO INS1 cells severely depleted of insulin SGs, but existing granules have morphological differences that reflect fundamental changes in composition which, in turn, could impact intracellular SG function and secretory output.

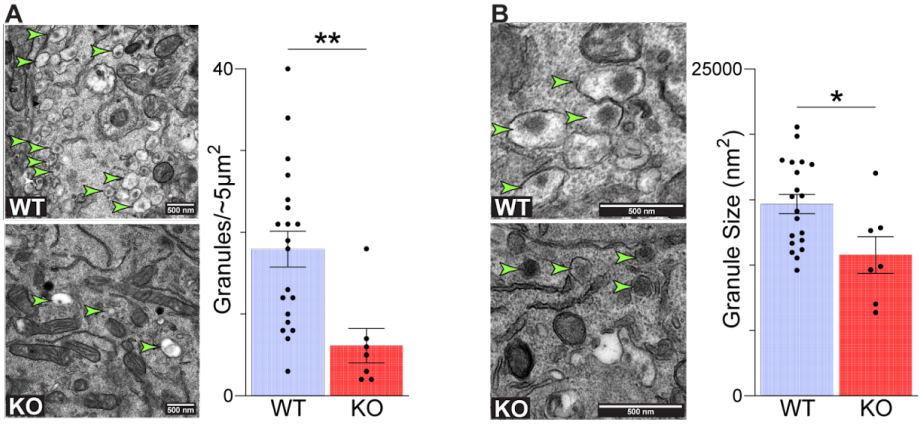

Figure 20. Both insulin SG abundance and size is reduced in Cab45KO INS1 cells. (A) EM of WT and Cab45KO INS1 cells using immunogold labelling of insulin with SGs indicated by bright green arrows, and quantification of granule abundance per 5 µm; scale bar = 500 nm. **(B)** Close-up images of SGs in WT and Cab45KO INS1 cells with quantification of SG area; scale bar = 500 nm. Data presented as mean ± SEM with individual points representing separate cells, and comparisons made using unpaired t-tests: *, $p < 0.05$; **, $p < 0.01$.

LFQ proteomic analysis. In line with the reduction in SG abundance, LFQ mass spectrometry (**Figure 21**) revealed a decrease in the abundance of SG resident proteins PC1/3, CgA and CgB in KO cells, with PC2 showing a downward trend (normalised log_2LFQ intensity (95% CI) = [WT PC1/3: **32.6 ± (32.4, 33.9)**] *vs* [KO PC1/3: **31.5 (31.4, 31.6)**]; [WT PC2: **33.1 ± (32.7, 33.6)**] *vs* [KO PC2: **32.8 (32.7, 32.9)**]; [WT CgA: **33.4 (32.5, 33.8)**] *vs* [KO CgA: **31.7 (31.6, 31.8)**]; [WT CgB: **33.9 (33.3, 34.2)**] *vs* [KO CgB: **32.7 (32.5, 32.8)**]) (**Figure 21**). Follow-up quantification of mRNA levels should complete the picture to ascertain how these proteins are being lost.

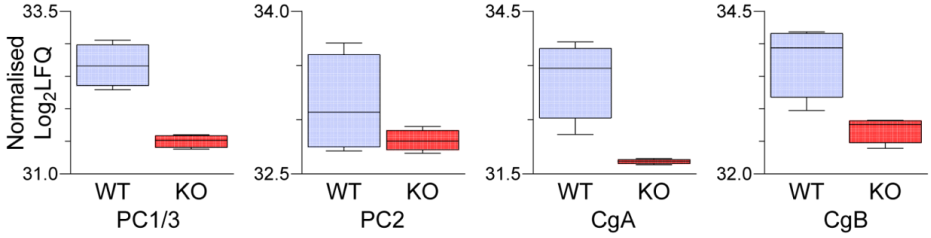

Figure 21. Peripheral insulin SG content is depleted in Cab45KO INS1 cells. Label free quantification of PC1/3, PC2, CgA, and CgB in WT and Cab45KO INS1 cells. Data presented as mean ± 95% CI.

3.3.1.3 Rescuing insulin and SG content in Cab45KO INS1 cells by rest or re-expression of Cab45

Assay-based quantification of insulin content rescue. Relatively high glucose concentrations are required for insulinoma culture medium to optimise cell growth, which could compromise the maintenance of insulin stores if SG production is impaired. During standard INS1 cell culture at 11 mM glucose, KO cells showed a reduced insulin content compared to WT cells as revealed using an insulin homogeneous time resolved fluorescence (HTRF) assay (mean ng insulin/µg DNA ± SEM = [WT: **35 ± 10**] *vs* [KO: **20 ± 10**] ($p < 0.05$)) (**Figure 22A**). Overnight rest at basal (2.8 mM) glucose brought the insulin content of KO cells within a statistically insignificant range of WT cells (mean ng insulin/µg DNA ± SEM = [WT: **56 ± 7**] *vs* [KO: **45 ± 5**] ($p > 0.05$)) and reinstated an abundance of insulin SGs in the cell periphery (**Figure 22B**), in line with reports describing the adaptive plasticity of rested β-cells (Alarcon et al. 2016). Finally, re-expression of Cab45HA raised the relative insulin content of KO cells compared to non-transfected KO controls (mean ng insulin/µg DNA ± SEM = [WT: **1 ± 0.02**] *vs* [KO: **1.25 ± 0.04**] ($p < 0.001$)) (**Figure 22C**). Importantly, low transfection efficiency visualised in **Figure 22D** suggests that insulin content rescue by re-expressed Cab45HA may be under-represented. Taken together, these results show that in the absence of Cab45, SG insulin stores become depleted from INS1 insulinoma cells when they are cultured under moderately high glucose.

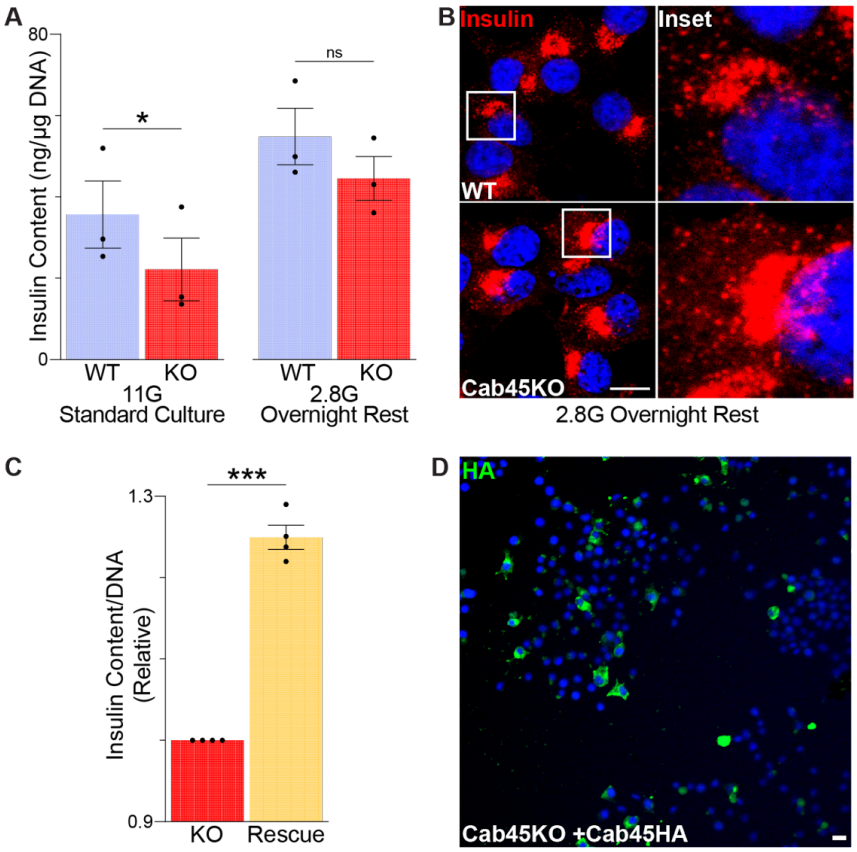

Figure 22. Overnight rest or Cab45 re-expression raises the insulin content of Cab45KO INS1 cells. (A) Quantification of insulin content in WT and Cab45KO INS1 cells during standard 11 mM (left) or 2.8 mM (right) glucose culture conditions. **(B)** Immunofluorescent staining of insulin in WT and Cab45KO INS1 cells cultured at 2.8 mM glucose. **(C)** Quantification of insulin content in Cab45KO INS1 cells with or without re-expressed Cab45HA (Rescue), expressed relative to the KO control per-experiment. **(D)** Visualisation of transfection efficiency of Cab45HA in KO cells. Data presented as mean ± SEM and comparisons made using paired t-tests: *, $p < 0.05$; ***, $p < 0.001$. Scale bars = 10 µm.

Immunofluorescence quantification of insulin content rescue. WT Cab45HA and several Ca^{2+}-binding mutants were re-expressed into KO INS1 cells and the distribution of insulin at 72 hours post-transfection was observed during standard culture conditions (**Figure 23**). In addition to the 6EQ Cab45HA previously described in which all three EF hand pairs are rendered non-functional, this experiment also included mutants with one (2EQ) or two (1,3EQ) non-functional EF hand pairs (**Figure 23D**). In doing so, the degree of Ca^{2+}-binding required for phenotypic rescue could be assessed. Notably, the transfection protocol utilised here results in overflow of expressed Cab45HA through the TGN and SG compartments, and unlike the experiment described in **Figure 17**, Ca^{2+}-binding mutants are being re-expressed into KO cells. It follows from the latter that if Cab45 regulates Ca^{2+} homeostasis and/or protein trafficking, re-expressed protein into KO cells could be subject to an altered landscape of ionic balance and protein distribution compared to WT cells.

Nonetheless, re-expression of WT Cab45 and all Ca^{2+}-binding variants rescued the distribution of insulin from the perinuclear area to the cell periphery (mean %perinuclear insulin ± SEM = [KO: **52.2** ± **6.4**] *vs* [KO + WT Cab45HA: **32.3** ± **5.8**] ($p < 0.05$) *or* [KO + 2EQ Cab45HA: **27.1 ± 6.1**] ($p < 0.05$) *or* [KO + 1,3EQ Cab45HA: **24.8 ± 8.9**] ($p < 0.05$) *or* [6EQ Cab45HA: **20.4 ± 5.7**] ($p < 0.05$)) (**Figure 23B**). These results indicate that Cab45 may have an involvement in the process of SG biogenesis when localised to more distal secretory compartments of the β-cell, but that Ca^{2+}-binding does not appear to be a requirement.

It is important to point out here that ectopic Cab45HA expression using the lipofectamine-based system here results in massive overspill of Cab45 out from the Golgi apparatus into secretory vesicles. This phenomenon is essentially uncontrollable and is an inherent limitation to the study, but molecular insight can certainly still be drawn by comparison to the WT condition. Quantification of post-Golgi Cab45HA localisation revealed that a greater proportion of WT Cab45HA resides within peripheral insulin SGs compared to the Ca^{2+}-binding mutants (**Figure 23C**) (mean r^2 ± SEM = [KO + WT Cab45HA: **0.57 ± 0.19**] *vs* [KO + 2EQ Cab45HA: **0.40 ± 0.21**] ($p < 0.05$) *or* [KO + 1,3EQ Cab45HA: **0.24 ± 0.58**] ($p < 0.05$) *or* [6EQ Cab45HA: **0.41 ± 0.01**] ($p < 0.05$)). This emphasises the control that Ca^{2+} has over Cab45 localisation within the β-cell, but positive coefficients show that in the absence of Ca^{2+}-binding, considerable occupation of SGs by Cab45 still exists.

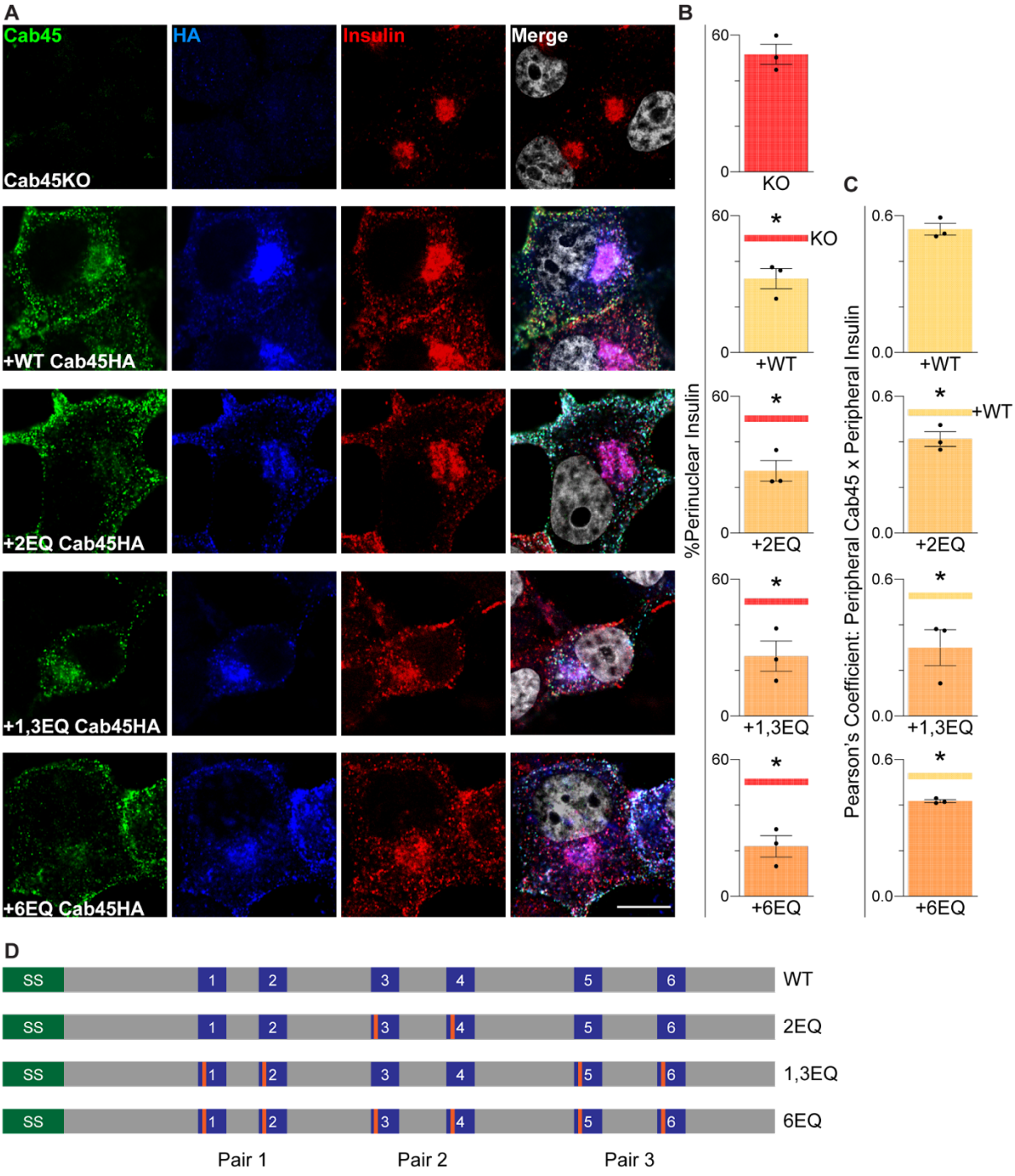

Figure 23. Re-expression of Cab45 rescues peripheral insulin SG distribution through a Ca^{2+}-independent mechanism. (A) Immunofluorescent staining of Cab45, HA, and insulin in Cab45KO INS1 cells re-expressing WT, 2EQ, 1,3 EQ or 6EQ Cab45HA, scale bars = 10 µm. **(B)** Percentage of total insulin residing in the perinuclear Golgi area quantified in at least 10 cells per replicate. **(C)** Pearson's coefficient of correlation between overlaid Cab45/HA signal with the insulin signal (perinuclear signal removed). **(D)** Schematic representation of Cab45 Ca^{2+}-binding-deficient mutants. Data presented as mean ± SEM and comparisons made using paired t-tests: *, $p < 0.05$.

3.3.1.4 Insulin secretion in Cab45KO INS1 cells

Next, functional studies were performed to assess whether GSIS is affected by the loss of Cab45 (**Figure 24-25**). This assay involves resting the cells at basal before exposing cells to either basal (2.8 mM) or stimulatory (16.7 mM) glucose levels for one hour.

In the first set of experiments, cells were rested for one hour prior to stimulation (**Figure 24**). Surprisingly, KO cells had an elevated secretory response to 16.7 mM glucose due to the release of almost twice the amount of insulin during stimulation (mean ng insulin/µg DNA ± SEM = [WT 2.8 mM: **5.4 ± 1.8** to 16.7 mM: **18.3 ± 5.7**] ($p > 0.05$) *vs* [KO 2.8 mM: **6.1 ± 2.3** to 16.7 mM: **31 ± 10.8**] ($p < 0.01$)) (**Figure 24A**). These were not due to increased release of proinsulin; in fact, secreted proinsulin was lower in KO cells during both conditions (mean pg proinsulin/µg DNA ± SEM = [WT 2.8 mM: **0.142 ± 0.024**] *vs* [KO 2.8 mM: **0.097 ± 0.041**] ($p < 0.05$); [WT 16.7 mM: **0.173 ± 0.030**] *vs* [KO 16.7 mM: **0.104 ± 0.036**] ($p < 0.01$)) (**Figure 24B**). Lower proinsulin release at basal therefore argues against a proinsulin sorting defect into the constitutive pathway. When considered as a proportion of secreted proinsulin to total insulin, KO cells returned statistically significant reductions that indicate enhanced intracellular proinsulin processing in the absence of Cab45 (pg proinsulin/ng insulin/µg DNA = [WT 2.8 mM: **0.022 ± 0.041**] *vs* [KO 2.8 mM: **0.011 ± 0.019**] ($p < 0.01$); [WT 16.7 mM: **0.022 ± 0.041**] *vs* [KO 16.7 mM: **0.011 ± 0.019**] ($p < 0.01$)) (**Figure 24C**). Thus, not only do Cab45KO INS1 cells secrete more total insulin, but they also have a greater proportional release of mature insulin compared to WT INS1 cells. This could be related to the reduced size of SGs in Cab45KO INS1 cells (**Figure 20B**), where elevated prohormone conversion facilitates enhanced protein packing and volumetric shrinkage of the SG. Moreover, augmented exocytotic output could explain the depletion of SG stores observed in Cab45KO cells (**Figure 19 and 20A**) under culture at the moderately-high level of 11 mM glucose.

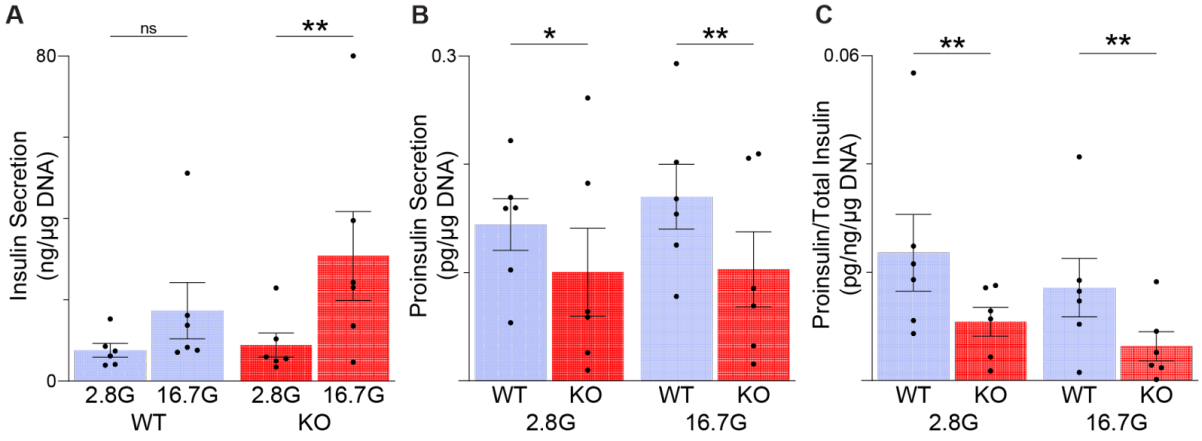

Figure 24. Cab45KO INS1 cells hypersecrete and release a greater proportion of mature insulin. (A-C) WT and Cab45KO INS1 cells were rested in basal glucose for 1 hour prior to incubation with either 2.8 or 16.7 mM glucose for one hour. Secreted insulin **(A)** and proinsulin **(B)** were normalised to cellular DNA, and expressed as a ratio of proinsulin to insulin **(C)**. Data presented as mean ± SEM and comparisons made using two-way ANOVA: *, $p < 0.05$; ** $p < 0.01$.

(This page is intentionally left blank)

In the second set of experiments, cells were rested overnight at basal prior to stimulation to provide time for SG replenishment in KO cells and evoke greater secretory responses from WT cells (**Figure 25**), and a condition was included where WT Cab45HA was re-expressed in KO cells (Rescue) (**Figure 25A-C**). Here, KO cells secreted over three times the amount of insulin compared to WT cells and re-expression of Cab45 into KO cells restored secretion to the normal WT level (mean ng secreted insulin/ng insulin content/μg DNA ± SEM = [WT 16.7 mM: **1.252 ± 0.458**] *vs* [KO 16.7 mM: **3.986 ± 1.213**] ($p < 0.01$) *or* [KO + WT Cab45HA 16.7 mM: **1.719 ± 0.416**] ($p > 0.05$)) (**Figure 25A-C**). Basal insulin secretion was unaffected by the absence of Cab45 (**Figure 25B**), whereas cellular insulin content following stimulation was consistent across cell lines (**Figure 25C**) confirming that overnight rest prior to stimulation allows for insulin content replenishment regardless of the presence or absence of Cab45. Importantly, considering the low transfection efficiency achieved by the lipofectamine-based system in INS1 cells (**Figure 22D**), restored GSIS in the rescue condition is likely to be achieved by a drastic undersecretion of insulin from cells that are overloaded with the WT Cab45HA protein.

Repeated challenge. Since KO cells are initially depleted of peripheral insulin SGs and secrete significantly higher amounts during stimulation, experiments were performed to ask whether these cells could reproduce a hypersecretory response when exposed to consecutive stimulatory challenges (**Figure 25D-E**). Following overnight basal, cells were subject to two separate one-hour glucose challenges spaced thirty minutes apart, and KO cells were shown to have a reduced response on the second challenge (mean fold change ± SEM = [WT: **7.5 ± 0.5**] vs [KO: **3.3 ± 0.3**] ($p < 0.01$)) (**Figure 25D-E**). Thus, it appears that Cab45 depletion from the INS1 cell line results in an insulin secretory defect during situations of continual metabolic demand. This could be clinically relevant in human T2D where Cab45 is lost from a significant population of pancreatic β-cells (**Figure 12**).

Cytosolic Ca^{2+} is the final messenger during GSIS that activates exocytotic machinery to mobilise and fuse SGs with the PM, therefore altered cytosolic Ca^{2+} handling could explain the hypersecretory response of Cab45KO INS1 cells. The loss of Cab45 could directly affect the buffering capacity of the Golgi apparatus or impair the trafficking of PM-localised ion transporters. Cytosolic Ca^{2+} was measured with the widely used cell-permeant Fura-2 ratiometric Ca^{2+}-binding dye (**Figure 26**) in basal and glucose-stimulated conditions (**Figure 26A**). KO cells displayed an increase in the resting and glucose-stimulated Ca^{2+} concentration as quantified by the area under the curve (AUC), correlating nicely with the observed hypersecretory response (mean nM x seconds ± SEM = [WT basal: **10909 ± 942**] *vs* [KO basal: **14873 ± 876**] ($p < 0.01$); [WT total: **48910 ± 6182**] *vs* [KO total: **126238 ± 14718**] ($p < 0.001$)) (**Figure 26B-C**).

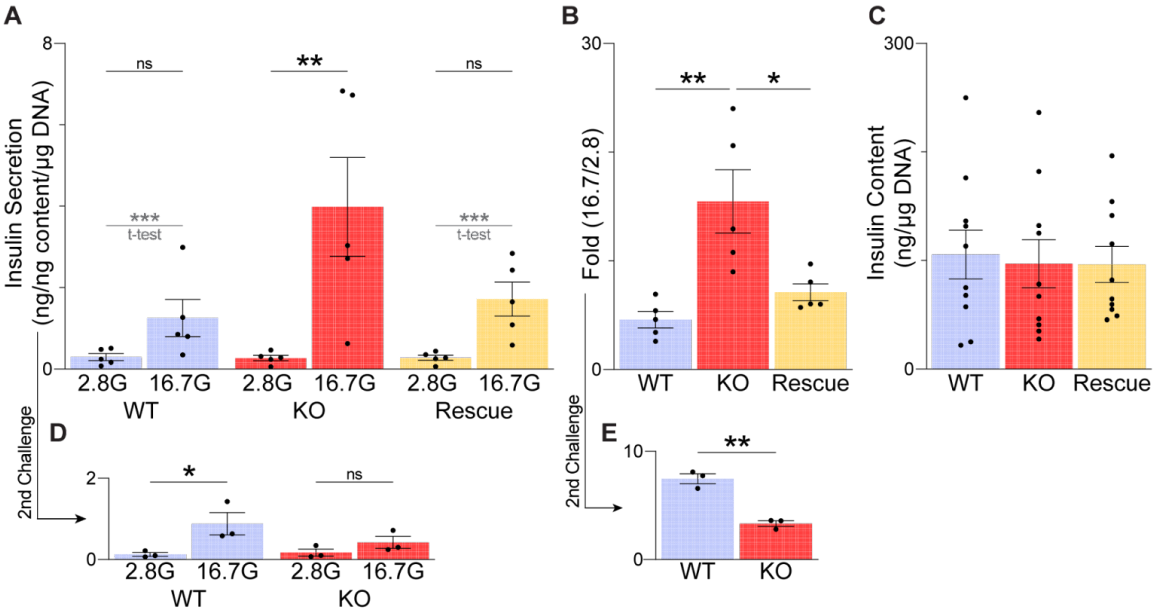

Figure 25. Re-expression of Cab45HA into Cab45KO INS1 cells rescues the hypersecretory response, but KO cells have a secretory defect in an experimental situation of chronic metabolic demand. (A-C) WT and Cab45KO INS1 cells with or without re-expressed Cab45HA (rescue) were rested in basal glucose overnight before incubation with either 2.8 or 16.7 mM glucose for one hour. Secreted insulin **(A)** was normalised to cellular insulin content and DNA **(shown in C)**, and expressed as the fold change from 2.8 to 16.7 mM glucose **(B)**. In a separate experiment **(D-E)**, WT and Cab45KO INS1 cells were subjected to two consecutive 1 hour glucose-challenges spaced 30 minutes apart. **(D)** Secreted insulin normalised to cellular insulin content and DNA and **(E)** fold change from 2.8 to 16.7 mM glucose **(E)** of the second challenge in WT and Cab45KO cells. Data presented as mean ± SEM and comparisons made using two-way ANOVA **(A and D)**, one-way ANOVA **(B-C),** or paired t-test **(E)**. Individual t-tests were performed on WT and rescue cells in **(A)** to demonstrate competent stimulus-secretion coupling in these cells: *, $p < 0.05$; ** $p < 0.01$; ** $p < 0.001$.

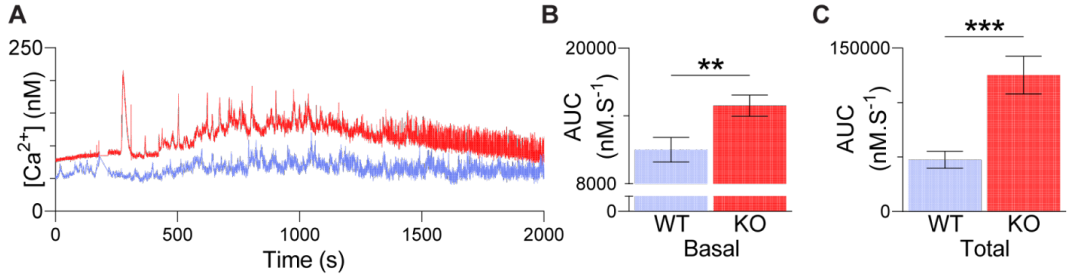

Figure 26. Cab45KO INS1 cells have elevated cytosolic Ca^{2+} concentration at rest and during glucose-stimulation. WT and Cab45KO INS1 cells loaded with Fura-2AM dye were stimulated with 16.7 mM glucose for 45 minutes following overnight rest at 2.8 mM glucose. **(A)** Representative traces of cytosolic Ca^{2+} concentration. **(B)** Area under the curve (AUC) during the three-minute basal time course. **(C)** Total AUC including both the basal and glucose-stimulated periods. Data presented as mean ± SEM and comparisons made using paired t-tests: ** $p < 0.01$; ***, $p < 0.001$.

3.3.1.5 Effect of acute Cab45 depletion on PC1/3 content and secretion

Characterisation of INS1 cells subject to chronic Cab45 deletion is limited by the establishment of long-term adaptations, and the possible caveats surrounding the expansion of KO cells from clonal subpopulations (Lilla et al. 2003; R. Zhao et al. 2021). A collaborator (A/Prof. Michael Ailion, University of Washington; Dr. Jerome Cattin, University of Washington) performed siRNA-mediated depletion of Cab45 in INS1 cells to study the acute effect of its loss, also working to circumvent some of these limitations and caveats (**Figure 27**). Following siRNA treatment, Western immunoblots of the SG-resident enzyme PC1/3 were used to assess SG exocytosis during 2 hour rest at 3 mM glucose or 2 hour stimulation with 18 mM glucose (**Figure 27A**). PC1/3 is a viable protein to measure since mature PC1/3 is soluble within the SG and is therefore secreted alongside insulin under glucose stimulation, and like insulin, was also depleted in the chronic KO INS1 line (**Figure 21**).

Firstly, basal release of PC1/3 was slightly elevated when Cab45 was depleted (**Figure 27B**). Consistent with the chronic situation, acute Cab45 depletion was shown to enhance secretion during two hours of glucose stimulation compared to non-targeting siRNA controls (mean raw band intensity ± SEM = [siCtrl: **24.3 ± 8.7**] *vs* [siCab45: **44.8 ± 11.7**] ($p < 0.05$)) (**Figure 27B**). However, unlike the chronic situation (**Figure 21**), intracellular PC1/3 content was elevated (**Figure 27B**). Therefore, expressing the amount of secreted PC1/3 secreted relative to intracellular content normalised and almost resulted in a significant reduction in the glucose-stimulated secretory response of siCab45 treated cells (**Figure 27C**) (mean PC1/3 raw band intensity ± SEM = [siCtrl PC1/3 content: **31.3 ± 7.8**] *vs* [siCab45 PC1/3 content: **82.4 ± 12.3**] ($p < 0.05$); mean secreted/cellular band intensity ± SEM = [siCtrl: **0.78 ± 0.26**] *vs* [siCab45: **0.56 ± 0.19**] ($p = 0.0859$)). This indicates that acute Cab45 depletion increases intracellular PC1/3 content which drives the observed hypersecretory phenotype, rather than some augmentation to the exocytotic response. This is in stark contrast to the chronic situation where intracellular insulin content is depleted during normal culture conditions but normalised prior to experimental stimulation, indicating that hypersecretory phenotypes are achieved through different mechanisms in these separate models.

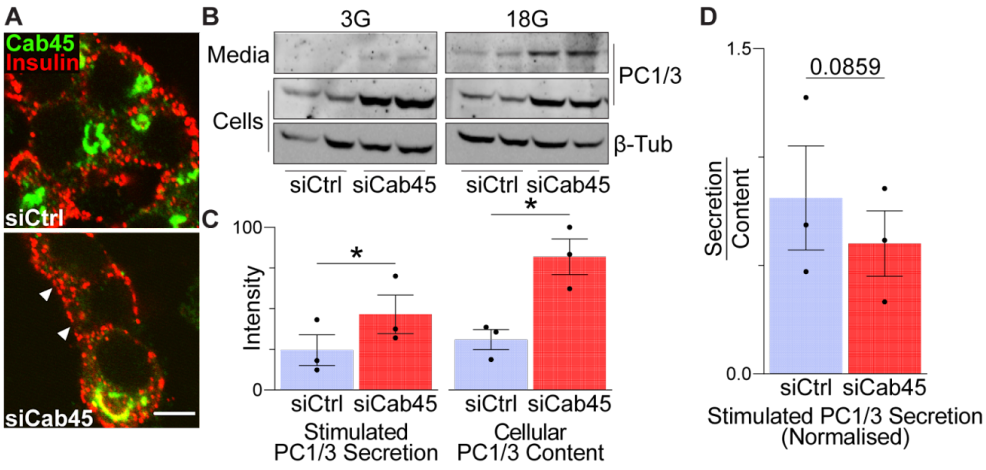

Figure 27. Cab45 depletion acutely elevates intracellular PC1/3 content and secretion. INS1 cells were treated with non-targeting (siCtrl) and Cab45-specific (siCab45) siRNAs, scale bars = 5 µm. **(A)** Immunofluorescent staining of Cab45 and insulin in siRNA-treated INS1 cells. **(B)** Western immunoblots of PC1/3 and β-tubulin in cells or media of siRNA-treated INS1 cells resting at 3 mM glucose or stimulated with 18 mM glucose for two hours (top), with quantification of the raw PC1/3 band intensity in the cells and media during stimulation (bottom). **(C)** Stimulated PC1/3 secretion normalised to the cellular PC1/3 level of siRNA-treated cells. Data presented as mean ± SEM and comparisons made using paired t-tests. *, $p < 0.05$.

3.3.1.6 Summary

In summary, Cab45KO INS1 cells exhibit elevated cytosolic Ca^{2+} flux that functions to produce an enhanced secretory response to glucose. This is likely to explain the pronounced loss of insulin SGs when KO cells are consistently cultured at moderately high (11 mM) glucose, which in turn, accounts for their inability to maintain secretion when they are exposed to consecutive glucose challenges. This could be directly due to the loss of Cab45, but also could result from alterations in expression of other proteins that occur in these cells. Re-expression of WT Cab45HA rescues the hypersecretory response, which is achieved by a minority of cells that massively overexpress the protein and minimally secrete. Surprisingly, both WT Cab45HA and Ca^{2+}-binding deficient Cab45HA mutants rescue insulin SG abundance in the cell periphery. If Cab45 does not exert direct control over stimulus-secretion coupling or SG exocytosis, these findings suggest that re-expressed Cab45HA rescues normal GSIS by an alternative mechanism. Interestingly, acute depletion of Cab45 from INS1 cells actually enhances the cellular content of SG resident protein PC1/3, which drives an increase in its release during basal and stimulatory conditions. This may parallel the situation in Cab45KO INS1 cells, as indications suggest that these cells exhibit enhanced proinsulin conversion to insulin that could be linked to their possession of smaller insulin SGs, possibly due to enhanced condensation of mature resident proteins.

(This page is intentionally left blank)

3.3.2 Characterisation of mouse MIN6 cells with Cab45 depletion

3.3.2.1 MIN6 Cab45 knockout validation

In order to validate findings from the rat INS1 insulinoma cell line in a separate model, and to study the function of Cab45 in a mouse insulinoma line so that the data can be better compared to mouse models, Cab45 was deleted from mouse MIN6 insulinoma cells. CRISPR/Cas9 was used to generate frameshift mutations in exon 2 of Cab45 in MIN6 cells, resulting in premature stop codons within the Cab45 transcript (**Figure 28A**). One clonal WT control and three separate clonal KO cell lines (denoted KO-1, KO-2, KO-3) were expanded from a common pool of cells treated with the same guide RNA, and an antibody raised against the full Cab45-G protein confirmed KO at the protein level with Western immunoblotting (**Figure 28B**). For immunofluorescence validation of KO (**Figure 28C**), the antibody used was raised against an epitope common to total Cab45 (Cab45-G, Cab45-S, and Cab45-C) yet only a Golgi-localised isoform is detectable in WT cells, as seen in **Figure 14**. Although punctate signal is reproducibly observed in all cell lines when using this antibody, it is uniformly present throughout the entire cell and cellular nucleus (**Figure 28D**) thereby suggesting that much of the signal is a staining artefact in MIN6 cells. Staining should be repeated using the antibody raised against full-length Cab45-G to ascertain whether signal in the periphery is depleted in KO conditions.

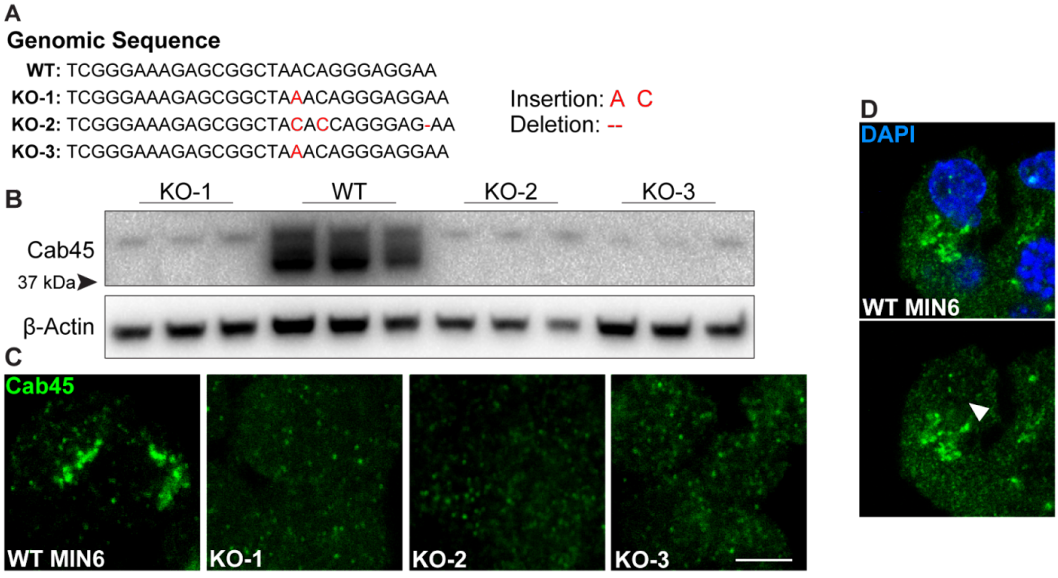

Figure 28. Validation of Cab45 deletion from three separate clonal MIN6 insulinoma lines. (A) Schematic representation of targeted deletion strategy, showing sequencing validation of genomic insertions and deletions **(B)** Western immunoblot of Cab45 and β-actin in three separate passages of WT and Cab45KO MIN6 lines. **(C)** Immunofluorescent staining of Cab45 in WT and three separate Cab45KO MIN6 cell lines (designated as KO-1, KO-2 and KO-3) generated with CRISPR using the same targeting guide RNA. **(D)** Immunofluorescent staining of Cab45 with DAPI in WT MIN6 cells, with an arrow pointing to the Cab45 signal present in the cell nucleus. Scale bar = 5 μm.

3.3.2.2 Insulin and proinsulin content of Cab45KO MIN6 cells

Insulin content. To ascertain whether insulin content deficits that were observed in Cab45KO INS1 cells are reproducibly observed in MIN6 cells, assessment of intracellular insulin content and distribution were undertaken (**Figure 29**). Immunofluorescent staining revealed no obvious alterations in the cellular insulin distribution of KO lines despite standard culture at supra-stimulatory (25 mM) glucose levels (**Figure 29A**). Likewise, no differences in insulin content were revealed via insulin HTRF assay aside from a trend towards increase in the KO-2 line (**Figure 29B**).

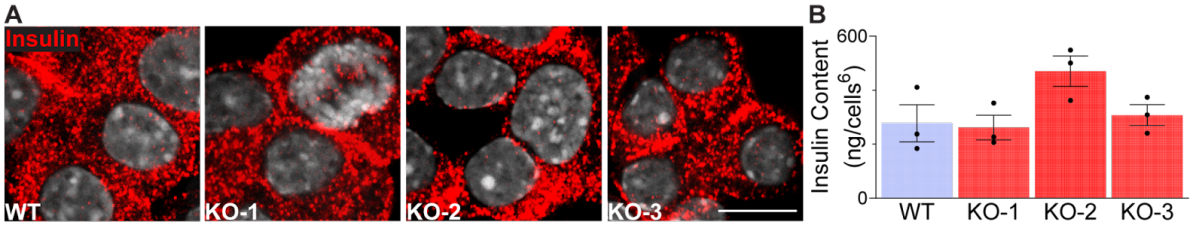

Figure 29. Total insulin content is maintained in Cab45KO MIN6 cells. (A) Immunofluorescent staining of insulin in WT and Cab45KO MIN6 lines, scale bar = 10 µm. **(B)** Insulin content normalised to cell number of WT and KO lines. Data presented as mean ± SEM and comparisons made using one-way ANOVA.

Proinsulin content. Antibodies targeted to both proinsulin and total insulin (**Figure 30**) however revealed a reduction in the level of intracellular proinsulin content in KO-1 cells, as assessed by the ratio of proinsulin to total insulin (mean proinsulin:insulin intensity ± SEM = [WT: **0.48 ± 0.09**] *vs* [KO-1: **0.30 ± 0.07**] ($p < 0.05$)) (**Figure 30B**). This could indicate impaired proinsulin trafficking leading to constitutive proinsulin secretion in Cab45KO MIN6 cells, or enhanced conversion of proinsulin as is also indicated in the INS1 model.

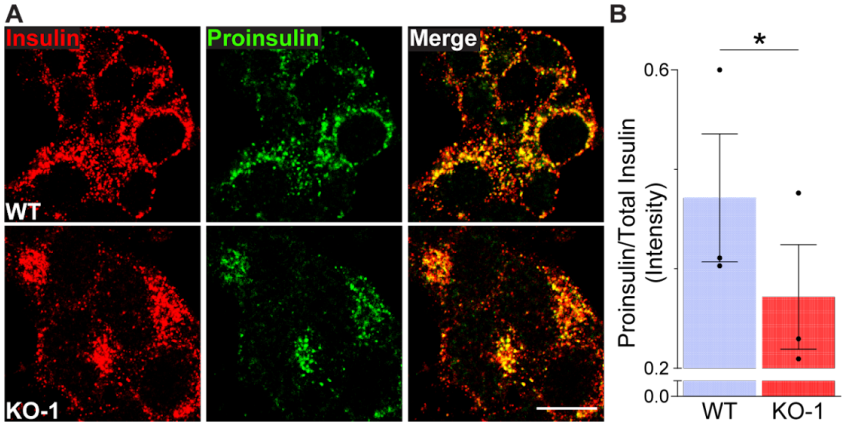

Figure 30. Proinsulin content is reduced in Cab45KO-1 MIN6 cells. (A) Immunofluorescent staining of insulin and proinsulin in WT and Cab45KO-1 MIN6 cells, scale bar = 10 µm. **(B)** Quantification of the proinsulin to insulin signal intensity from **(A)**, measured as the average of at least 10 cells per experiment (n=3). Data presented as mean ± SEM and comparisons made using paired t-test: *, $p < 0.05$.

3.3.2.3 Insulin secretion in Cab45KO MIN6 cells

GSIS. Next GSIS assays (**Figure 31**) found that all three MIN6 Cab45KO lines had reduced fold-change secretory responses compared to WT (mean fold change ± SEM = [WT: **3.64 ± 0.90**] *vs* [KO-1: **1.00 ± 0.08**] ($p < 0.01$) *or* [KO-2: **2.81 ± 0.78**] ($p < 0.05$) *or* [KO-3: **1.26 ± 0.17**] ($p < 0.01$)) (**Figure 31B**). Notably, KO-1 and KO-3 cells had a complete lack of response to 16.7 mM glucose whereas KO-2 cells responded to stimulus and secreted a comparable amount of insulin to WT cells, although reduced fold change appears to result from an increased basal secretion (**Figure 31A**). Therefore, in contrast to the INS1 model, MIN6 Cab45KO cells have no change in total insulin content but have secretory defects upon exposure to a single glucose challenge.

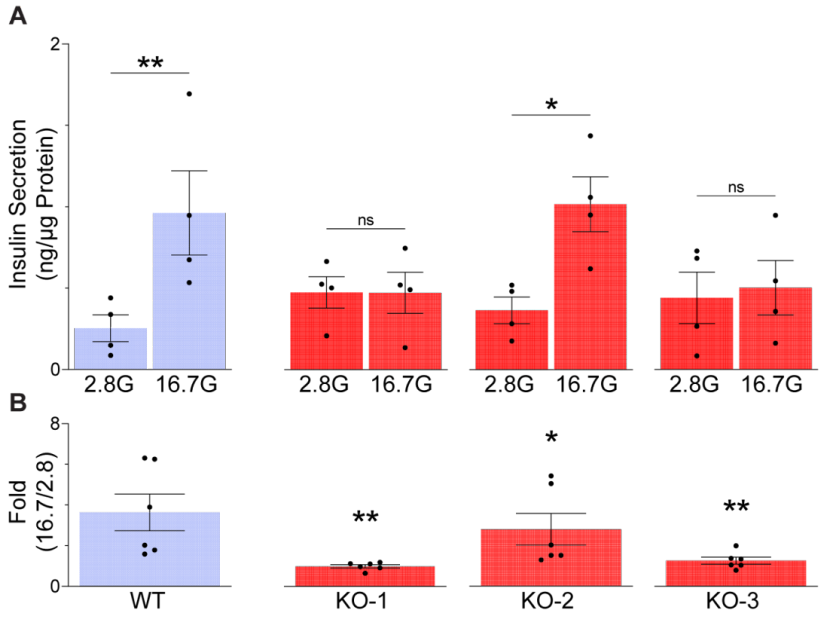

Figure 31. Glucose-stimulated insulin secretion is impaired in Cab45KO MIN6 cells. GSIS in WT vs Cab45KO MIN6 cell lines following two-hour rest at low glucose. Insulin secretion is normalised to cellular protein **(A)** and also presented as the fold change from basal levels **(B)**. Data presented as mean ± SEM and comparisons made using paired t-tests: *, $p < 0.05$; ** $p < 0.01$.

KSIS. To assess secretory responses independent of glucose metabolism, cells were subject to potassium chloride (KCl)-stimulated insulin secretion (KSIS) assays (**Figure 32**). KCl depolarises the β-cell membrane, which works to open voltage-gated Ca^{2+} channels and permit the influx of Ca^{2+} to trigger SG exocytosis. In doing so this bypasses several intracellular steps required to elicit the secretory response to glucose. All KO cell lines show stimulus-secretion coupling in response to 40 mM KCl, but KO-1 and KO-3 demonstrate a reduced fold change compared to WT cells (mean fold change ± SEM = [WT: **4.26 ± 0.92**] *or* [KO-1: **2.13 ± 0.31**] ($p < 0.001$) *or* [KO-2: **3.28 ± 0.72**] ($p > 0.05$) *or* [KO-3: **2.60 ± 0.54**] ($p < 0.0001$)) (**Figure 32**).

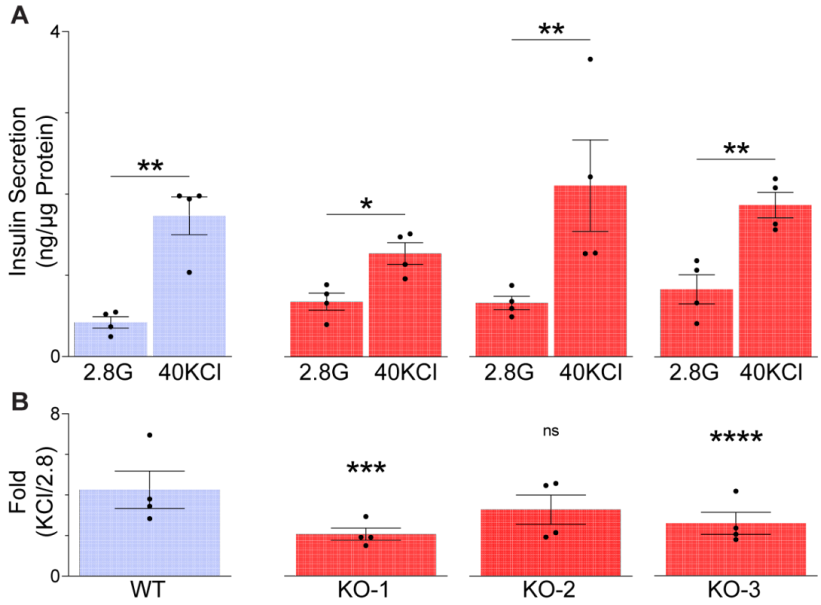

Figure 32. Stimulation with KCl triggers partial secretory responses from Cab45KO MIN6 cells. KSIS in WT vs Cab45KO MIN6 cell lines following two-hour rest at low glucose. Insulin secretion is normalised to cellular protein **(A)** and also presented as the fold change from basal levels **(B)**. Data presented as mean ± SEM and comparisons made using paired t-tests: *, $p < 0.05$; ** $p < 0.01$; ***, $p < 0.001$; ***, $p < 0.0001$.

Cytosolic Ca.$^{2+}$ during stimulation. To investigate the underlying cause of the secretory defect in one Cab45KO MIN6 line, Fura-2 measurement of cytosolic Ca^{2+} (**Figure 33**) revealed a reduced basal Ca^{2+} concentration and a direct loss of the initial influx of Ca^{2+} into KO-1 cells following glucose stimulation (**Figure 33A-B**), consistent with the complete loss of GSIS seen in this line in **Figure 31** (mean AUC ± SEM = [WT basal: **8828 ± 982**] *vs* [KO-1 basal: **5389 ± 436**] ($p < 0.05$); [WT peak: **19517 ± 3120**] *vs* [KO-1 peak: **7441 ± 963**] ($p < 0.05$)). This is in direct contrast to the INS1 KO line which showed elevated basal and enhanced glucose stimulated Ca^{2+} responses (**Figure 26**). In response to 40 mM KCl stimulation (**Figure 33C-D**), KO-1 cells displayed a reduced and slightly delayed Ca^{2+} influx which is consistent with the partial secretory response seen in this line in **Figure 32** (mean AUC ± SEM = [WT basal: **6652 ± 561**] *vs* [KO-1 basal: **5349 ± 402**] ($p < 0.05$); [WT peak: **30645 ± 2209**] vs [KO-1 peak: **21215 ± 74**] ($p < 0.05$).

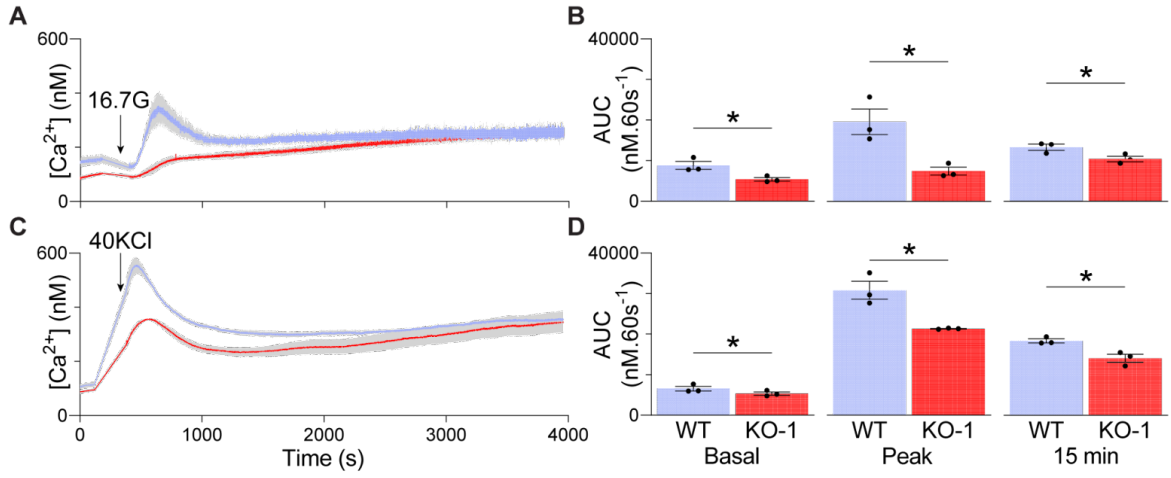

Figure 33. Cab45KO-1 MIN6 cells have reduced Ca^{2+} responses to both glucose and KCl. WT and Cab45KO-1 MIN6 cells loaded with Fura-2AM dye were stimulated with 16.7 mM glucose **(A)** or 40 mM KCl **(C)** (arrowhead) for 1 hour following a two hour rest at 2.8 mM glucose. **(B/D)** Area under the curve (AUC) during 60 second periods at time points that had significant differences throughout the course of the experiment. Data presented as mean ± SEM and comparisons made using paired t-tests. *, $p < 0.05$.

Basal insulin secretion. Next, basal insulin secretion measurements from GSIS and KSIS secretion assays were pooled together for a separate analysis (**Figure 34**). This is viable as protocols are identical up until this point in each experiment. Despite the KO-1 cell line harbouring a lower resting cytosolic Ca^{2+} concentration, all KO cell lines had significant elevations in the basal release of insulin compared to WT controls (mean ng insulin/µg protein ± SEM = [WT: **0.34 ± 0.06**] *vs* [KO-1: **0.58 ± 0.08**] ($p < 0.001$) *vs* [KO-2: **0.51 ± 0.07**] ($p > 0.001$) *vs* [KO-3: **0.64 ± 0.13**] ($p < 0.01$)). These results either indicate that proinsulin is released constitutively from MIN6 Cab45KO cells or that the basal release of proinsulin or mature insulin directly from the regulated secretory pathway is elevated.

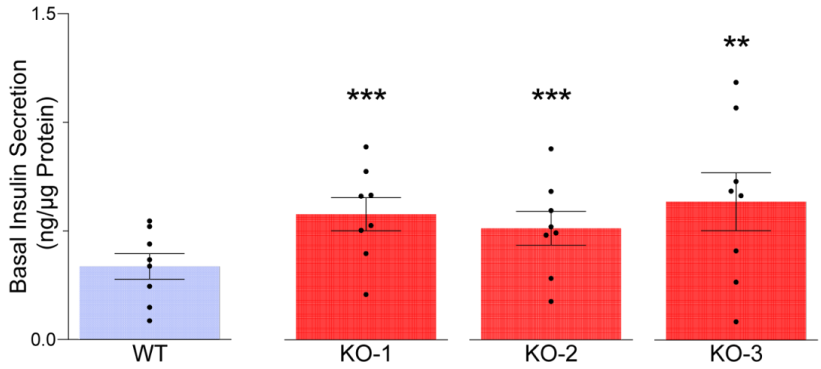

Figure 34. Cab45KO MIN6 cells exhibit elevated basal insulin secretion. Basal measurements of insulin secretion were pooled from GSIS and KSIS shown in **Figure 32** and **Figure 33**. Data presented as mean ± SEM and comparisons made using paired t-tests: **, $p < 0.01$; ***, $p < 0.001$.

Rescue attempt. Finally, mouse Cab45 and green fluorescent protein (GFP) or red fluorescent protein (RFP) alone used as a control were expressed into WT and KO-1 MIN6 cells using an adenovirus, and GSIS was assessed for phenotypic rescue (**Figure 35**). Both WT and KO-1 cells expressed comparable amounts of ectopically expressed Cab45 protein as assessed by Western immunoblotting, but notably, this is in excess to endogenous levels (**Figure 35A**). In contrast to **Figure 23** where lipofectamine-based transfection of plasmid DNA into INS1 KO cells resulted in massive overspill of Cab45 into insulin SGs, the adenoviral system resulted in normal Cab45 localisation to the Golgi apparatus (**Figure 35C**). Moreover, transfection efficiency appears to be superior using the adenoviral system (**Figure 35B**) compared to the lipofectamine system used in INS1 KO cells (**Figure 22D**).

Cab45 re-expression into KO-1 cells did not restore the glucose-stimulated secretory response; in fact, in both WT and KO-1 cells, Cab45 re-expression appears to reduce the stimulated secretory response (**Figure 35D**). Importantly, direct comparison between RFP and Cab45 expression conditions in either line do not reach significance and may require more experimental power for a more confident conclusion to be made. Indeed, here, results appear to be confounded by one KO-1 biological replicate with abnormally high KO-1 readings. Nonetheless, when basal measurements are directly compared, Cab45 re-expression into KO-1 cells reduces insulin secretion during resting conditions compared to the RFP control (**Figure 35E**) (mean ng insulin/μg protein ± SEM = [KO-1 +RFP: **2.05 ± 0.71**] *vs* [KO-1 +Cab45: **1.56 ± 0.54**] ($p < 0.05$)). These results demonstrate that Cab45 expression does not correlate with regulated insulin secretion in response to stimulation. Cab45KO-1 cells have impaired GSIS, but this appears to worsen upon re-expression of Cab45. On the contrary, Cab45 expression correlates with basal secretory output, which is elevated in its absence and reduced in its presence.

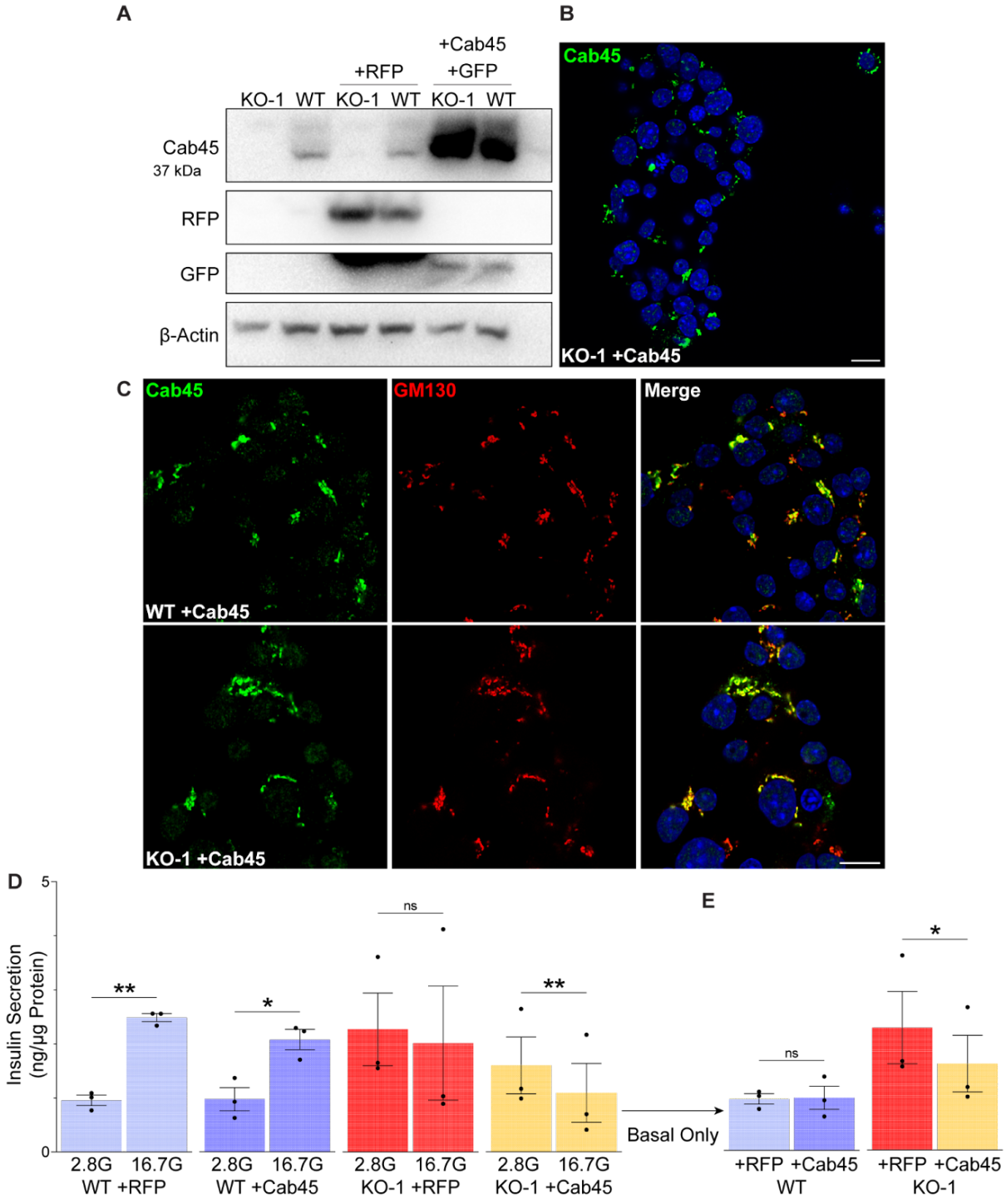

Figure 35. Re-expressed Cab45 lowers secretory output from Cab45KO-1 MIN6 cells during basal and glucose-stimulated conditions. (A) Western immunoblot of WT and KO-1 MIN6 cells infected for 72 hours with adenovirus expressing either RFP alone or co-expressing mouse Cab45 and GFP. **(B)** Immunofluorescent staining of Cab45 in KO-1 cells expressing Cab45, displaying transfection efficiency. **(C)** Immunofluorescent staining of Cab45 and GM130 in WT and KO-1 cells. Notably, the GFP signal is not detectable via immunofluorescence. **(D)** GSIS from WT or KO-1 cells infected with adenoviral vectors expressing either Cab45 or RFP. **(E)** Comparison of basal measurements only from **(D)**. Data presented as mean ± SEM and comparisons made using paired t-tests: *, $p < 0.05$; **, $p < 0.01$.

3.3.2.4 Summary

In contrast to what is seen in Cab45KO INS1 cells, all three clonal Cab45KO MIN6 cell lines have impaired secretory responses to glucose, although the extent of which does vary. In KO-2 cells the secretory defect is minimal, and predominantly driven by an elevated basal release rather than a difference in absolute release at 16.7 mM glucose. In the KO-1 line, blunted GSIS is associated with impaired cytosolic Ca^{2+} signals that underlie the secretory response. Stimulation using KCl to assess SG exocytosis independent of upstream glucose metabolism reveals a limited secretory response in the KO-1 and KO-3 line but not the KO-2 line, and this is also associated with a restricted cytosolic Ca^{2+} response in the KO-1 line. Initially, these findings indicated that Cab45 directly regulates stimulus-secretion coupling, but this is unlikely since re-expressed Cab45 does not rescue GSIS. Cab45 re-expression does however rescue basal secretory output in the KO-1 line, a phenotype that is consistent across all MIN6 KO lines and even occurs despite KO-1 cells having a lowered basal Ca^{2+} concentration. Together, results suggest that some inherent quality of the insulin SG is affected by the loss of Cab45 that contributes downstream to basal secretory output. Indeed, while there are no differences in insulin content between WT and KO lines, KO-1 cells display a reduction in the intracellular ratio of proinsulin to insulin content that indicates enhanced conversion of prohormones within the SG. This finding provides an early indication that SG form or function is altered in Cab45KO MIN6 cells, which could underlie the elevated secretion of insulin during basal conditions. Importantly, these observations track nicely with the discovery of altered SG size and the indication of enhanced proinsulin processing in the Cab45KO INS1 cell line, and Cab45 re-expression into both INS1 KO and MIN6 KO-1 cells also consistently lowers secretory output despite these models having opposite secretory behaviours.

(This page is intentionally left blank)

3.3.3 Characterisation of mice with β-cell specific Cab45 deletion

3.3.3.1 β-cell specific Cab45 knockout mouse generation

To investigate the functional consequence of Cab45 deletion *in-vivo* in the context of whole-body glucose homeostasis, and to obtain a source of primary islets for *ex-vivo* functional experimentation, a β-cell specific Cab45KO (βCab45KO) C57BL6/J mouse model was generated using the Cre/Lox system. This model exploits the insulin-1 (Ins1) promoter (commonly known as the mouse insulin promoter, MIP) to drive expression of the Cre protein only in pancreatic β-cells, which is superior to the insulin-2 (Ins2) promoter (commonly known as the rat insulin promoter, RIP) that also has activity in the brain (J. D. Johnson 2014; Wicksteed et al. 2010) where Cab45 is strongly expressed (**Figure 10**). Importantly, current models of the Ins1-Cre mouse (i.e Ins1-Cre^{Thor} (Thorens et al. 2015)) have been engineered without expression of the second cistron of the human growth hormone (hGH) minigene (Estall and Screaton 2020); a genomic element used in earlier models (i.e. MIP-Cre/ERT (Wicksteed et al. 2010)) which, unbeknownst to researchers at the time, is sufficient to generate active hGH that signals via the prolactin receptor to produce off-target phenotypes (Brouwers et al. 2014). The current models make use of a knock-in system that displaces the coding region for Ins-1, but two intact Ins-2 alleles (plus one Ins-1 allele, if the Cre allele is heterozygous) maintain the generation of mature insulin. These new models still have several issues, such as the potential for poor target deletion efficiency with certain floxed alleles, and have interlaboratory variability when the same genes are floxed (Mosleh et al. 2020). Even so, expression of the Cre protein itself driven by the Ins-1 promotor (and/or the loss of insulin-1 gene expression) in non-obese diabetic (NOD) mice has been shown to protect against T1D (Skovsø et al. 2022), so Ins1-Cre models could have altered β-cell function. Therefore, in this study, Ins1-Cre (CRE) control lines have been analysed separately to SDF4-floxed (FLOX) control lines unless otherwise indicated. Importantly, the dosage of the Cre allele have not been taken into account in the following analyses. Mice containing the floxed SDF4 gene, generated by gRNA-directed Cas9-mediated knock-in of loxP sites, were crossed with Ins1-Cre mice to develop heterozygotes (HET) and homozygotes (KO) of the deleted SDF4 gene/Cab45 protein. Collectively, mice in this lineage are referred to as βCab45 mice.

3.3.3.2 *In-vivo* metabolic characterisation of βCab45 mice

Body composition. At 8 weeks of age, *in-vivo* metabolic characterisation was performed on mice fed a standard chow diet **(Figures 36 to 40)**. No major differences in body weight or composition were found, aside from a slight increase in percentage body fat in HET and KO females compared to CRE controls **(Figure 36)** (mean fat mass/lean mass (%) ± SEM = [CRE: **8.2 ± 0.9**] *vs* [HET: **10.4 ± 0.8**] ($p < 0.05$) *or* [KO: **11.3 ± 1.6**] ($p < 0.05$)).

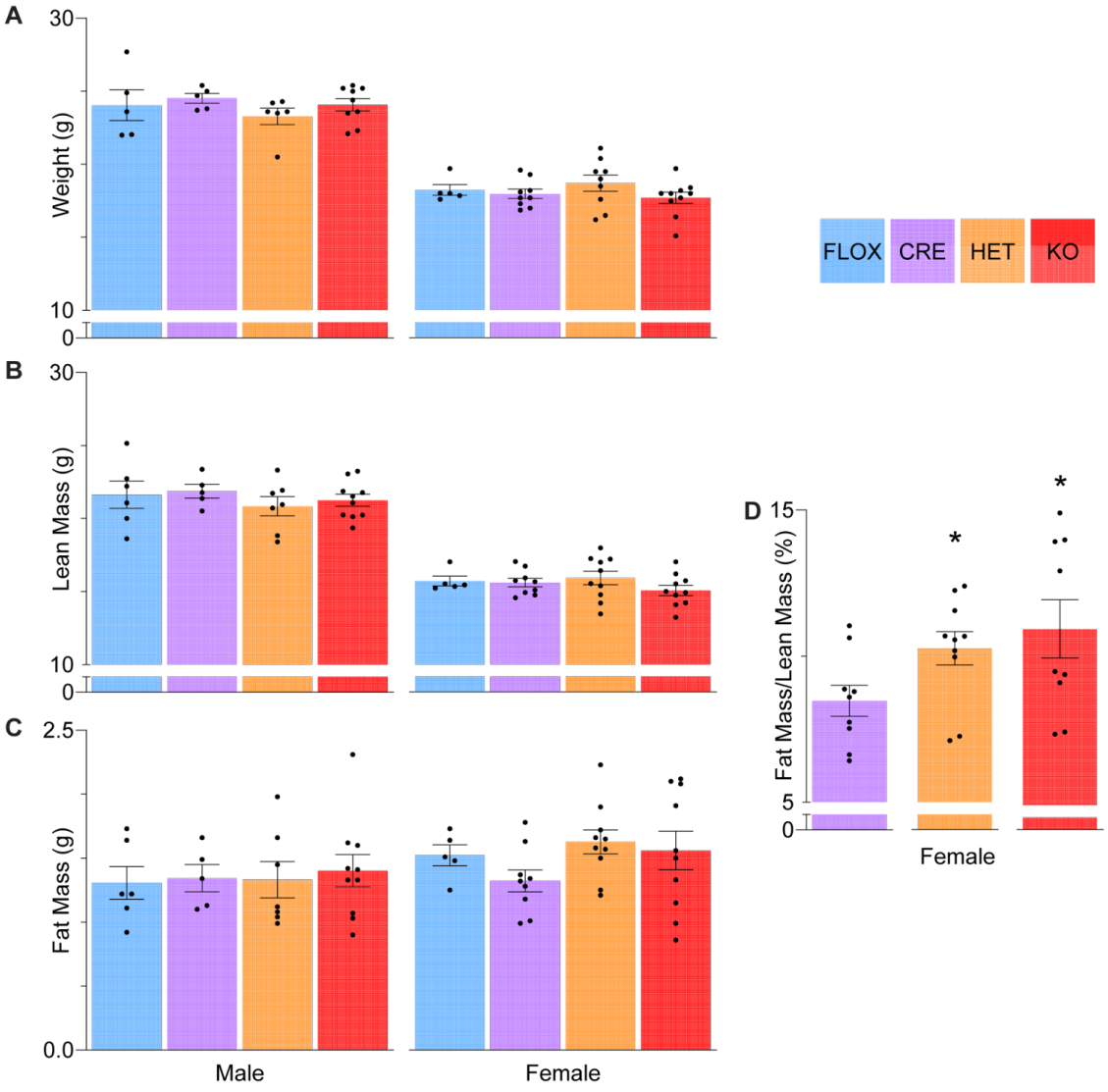

Figure 36. Body composition of 8-week old βCab45 mice. (A-C) Males displayed on the right and females displayed on the left. **(A)** Body weight, **(B)** Lean mass, and **(C)** Fat mass of βCab45 mice. **(D)** Fat mass as a percentage of lean mass. Data presented as mean ± SEM and comparisons made using unpaired t-tests. *, $p < 0.05$.

OGTT. 8-week old βCab45 mice were subject to an oral glucose tolerance test (OGTT), which involves fasting mice for 5 hours before oral administration of 3 mg glucose per gram of lean body mass using a gavage directly into the gastrointestinal tract. Circulating glucose (**Figure 37**) and insulin (**Figure 38**) were measured by drawing blood from the tail prior to injection and at regular intervals over the course of the experiment.

Blood glucose during OGTT. Notably, CRE controls appear to have superior glucose tolerance compared to FLOX controls (**Figure 37B**), which could be due to enhanced islet function due to the expression of Cre protein in β-cells as recognised by a recent study in the context of T1D (Skovsø et al. 2022). Therefore, most comparisons made from here on in are made in relation to CRE controls. Qualitative assessment of the circulating glucose concentration curve reveals possible defects in glucose tolerance in HET and KO mice compared to CRE controls, particularly between 15 and 60 minutes (**Figure 37C-D**).

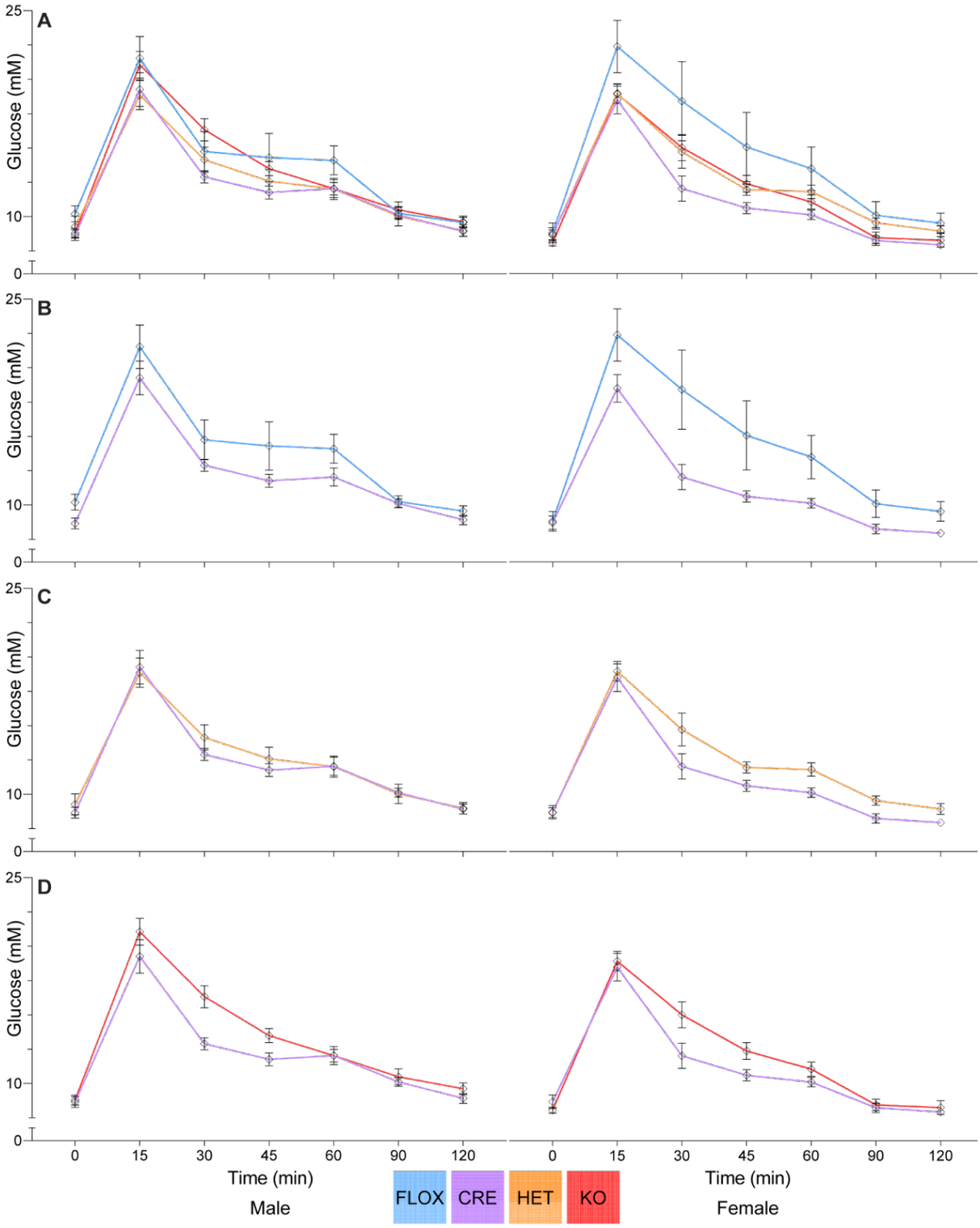

Figure 37. Measurement of blood glucose concentration during OGTT of 8-week old βCab45 mice. Males displayed on the right and females displayed on the left. **(A)** Comparison of all genotypes **(B)** CRE vs FLOX comparison. **(C)** CRE vs HET comparison. **(D)** CRE vs KO comparison. Male mice: n = 5 FLOX, n= 5 CRE, n = 7 HET, n = 10 KO. Female mice: n = 5 FLOX, n = 9 CRE, n = 10 HET, n= 10 KO.

Blood insulin during OGTT. No major differences were found in fasting insulin or at 15 minutes post-administration (**Figure 38A-B**), but HET mice appear to have reduced circulating insulin at 30 minutes (**Figure 38C**). This requires substantiation with more mice and of course with KOs. Importantly, all of the phenotypes presented in **Figures 37** and **38** appear to be consistent in both male and female βCab45 mice. Considering potential alterations to SG morphology and intracellular proinsulin conversion in Cab45KO cells as indicated by **Figures 20 and 24**, circulating proinsulin and the proinsulin to insulin ratio should be measured in these mice.

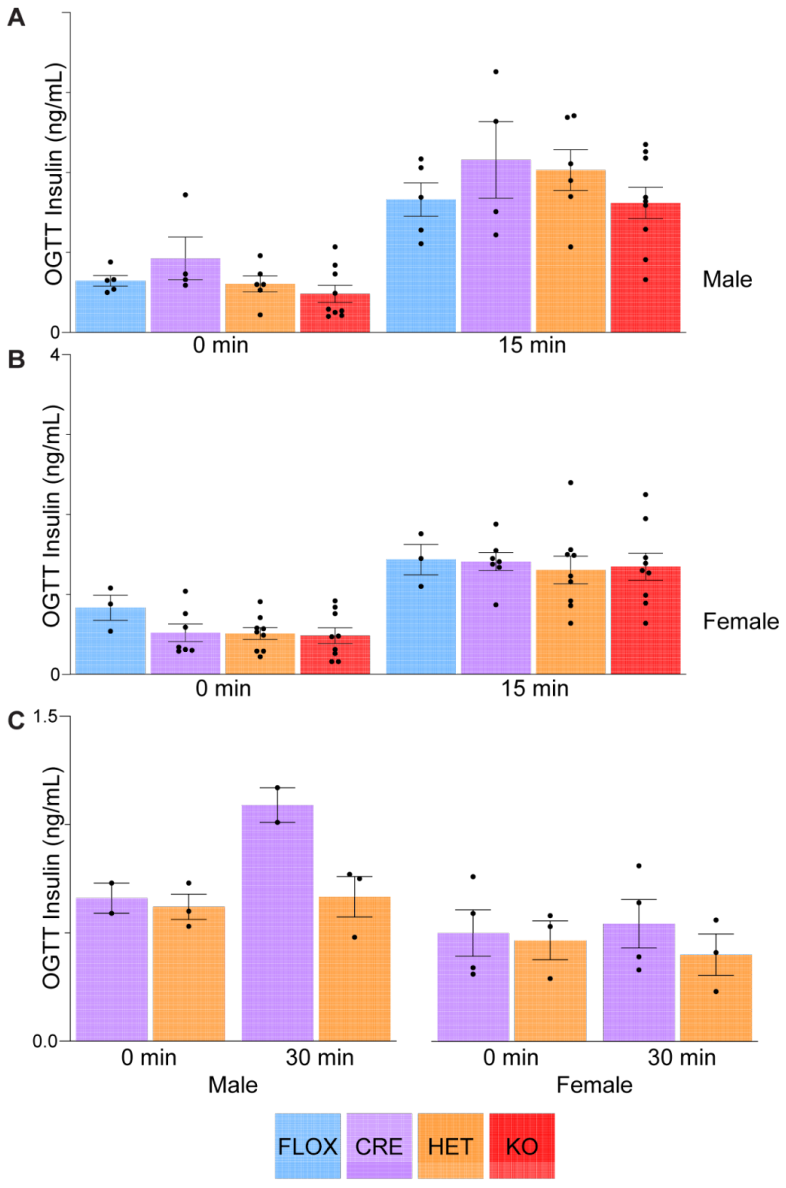

Figure 38. Measurement of blood insulin concentration during OGTT of 8-week old βCab45 mice. (A) Circulating insulin concentration at 0 and 15 minutes during OGTT in male mice. **(B)** Circulating insulin concentration at 0 and 15 minutes during OGTT in female mice. **(C)** Circulating insulin concentration at 0, 15 and 30 minutes during OGTT in female mice.

Blood glucose at specific time points during OGTT. To extract more information from this experiment, glucose concentrations at specific time points during the OGTT were quantified (**Figure 39**). In both male and female βCab45 mice, circulating glucose at 30 and 45 minutes post-administration was elevated in KO mice compared to CRE controls (**Figure 39**) (mean glucose concentration (mM) ± SEM = [30 min male CRE: **12.8 ± 0.8**] *vs* [30 min male KO: **17.5 ± 1.4**] ($p < 0.05$); [30 min female CRE: **11.9 ± 1.0**] *vs* [30 min female KO: **14.4 ± 1.4**] ($p < 0.05$); [45 min male CRE: **10.8 ± 0.6**] *vs* [45 min male KO: **12.8 ± 0.9**] ($p < 0.05$); [45 min female CRE: **10.2 ± 0.4**] *vs* [45 min female KO: **11.9 ± 1.2**] ($p < 0.05$)). At 30 and 45 minutes both male and female HET mice trended towards a significant elevated circulating glucose concentration, but only female HET mice were significantly elevated compared to CRE controls at 45 minutes (**Figure 39**) (mean glucose concentration (mM) ± SEM = [45 min female CRE: **10.2 ± 0.4**] *vs* [45 min female HET: **11.6 ± 0.5**] ($p < 0.05$)). At 60 minutes, male mice had normal circulating glucose but female HET mice remained elevated, and female KO mice appeared to normalise their glucose concentration (**Figure 39B**) (mean glucose concentration (mM) ± SEM = [60 min female CRE: **10.0 ± 0.4**] *vs* [60 min female HET: **11.3 ± 0.7**] ($p < 0.05$)).

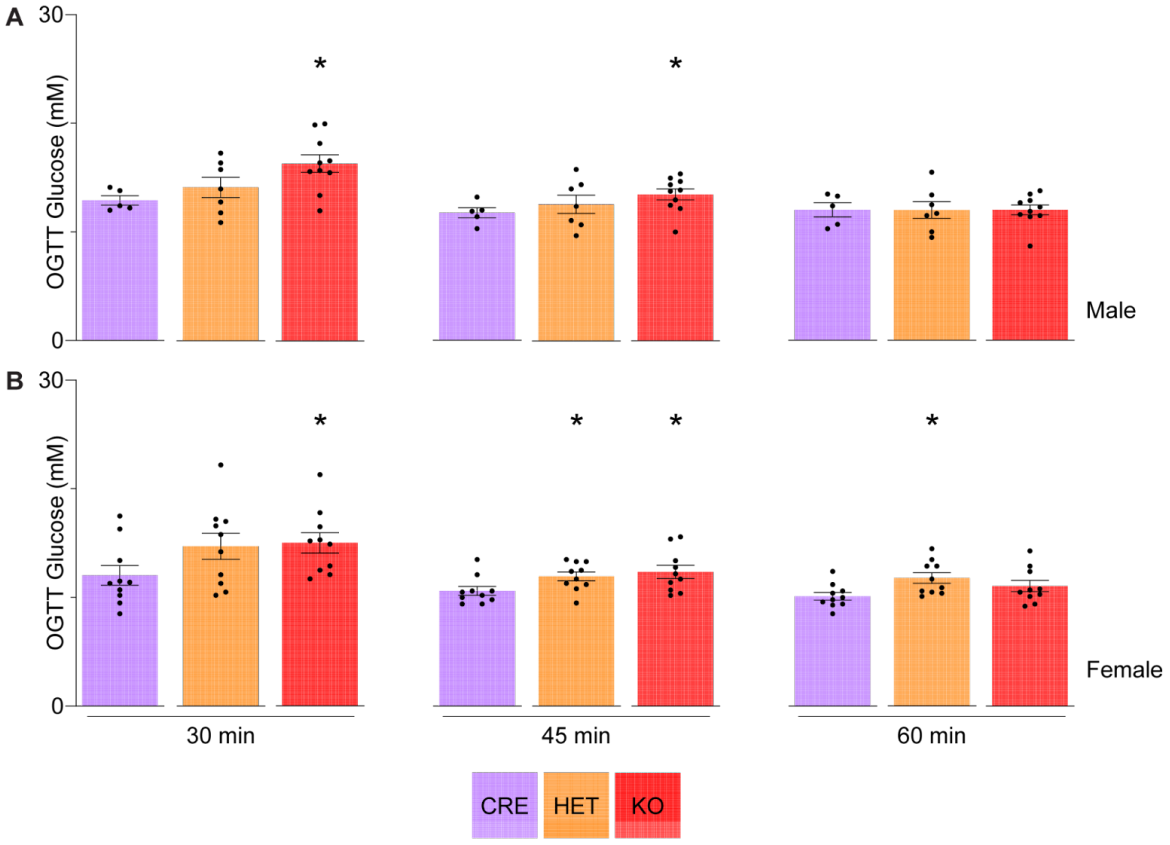

Figure 39. Blood glucose concentration at specific time points during OGTT of 8-week old βCab45 mice. **(A)** Circulating glucose concentration at 30, 45, and 60 minutes during OGTT in male mice. **(B)** Circulating glucose concentration at 30, 45, and 60 minutes during OGTT in female mice. Data presented as mean ± SEM and comparisons made using unpaired t-tests: *, $p < 0.05$.

Glucose tolerance during specific time periods of OGTT. The incremental area under the curve (iAUC) provides a normalised measure of glucose tolerance across individual mice, and is computed by measuring the fold change response in circulating glucose concentration at all time points relative to the basal concentration, and then quantifying an AUC. Here, the iAUC over specific periods of time (**Figure 40**) were quantified. Glucose tolerance as measured via the iAUC revealed that males were not different to CRE controls, but almost reached significance during the 30-45 minute time period which may be due to a lack of statistical power (**Figure 40D**) (mean iAUC ± SEM = [30-45 min male CRE: **621 ± 68**] *vs* [30-45 min male KO: **917 ± 108**] ($p = 0.09$). Female KO mice however had impaired glucose tolerance through all time periods assessed **(Figure 40B-D**) (mean iAUC ± SEM = [15-60 min female CRE: **4088 ± 829**] *vs* [15-60 min female KO: **6024 ± 449**] ($p < 0.05$); [30-60 min female CRE: **2278 ± 512**] *vs* [30-60 min female KO: **4459 ± 237**] ($p < 0.05$); [30-45 min female CRE: **1553 ± 256**] *vs* [30-45 min female KO: **2022 ± 187**] ($p < 0.05$)), with HET mice showing stepwise but insignificant differences compared to CRE controls.

Taken together, these findings could indicate that the second phase of GSIS is affected by the depletion of Cab45 in βCab45 mice, as indicated in **Figure 38C**. Notably, a major proportion of the first phase of GSIS originates from SGs that are pre-docked on the PM and primed to be ready for fusion and release (Yau et al. 2021). The second phase of GSIS however is thought to rely on insulin SGs originating from deeper within the cell (Yau et al. 2021). Newly synthesised SGs are thought to be more motile than older SGs and thus are preferentially secreted, contributing to both phases of GSIS (Yau et al. 2021). Since the second phase relies more so on SGs localised in the cell interior, limited production of new SGs might have a tendency to compromise second-phase GSIS. Importantly, these claims must be substantiated with more direct experiments since multiple factors can influence the temporal regulation of circulating glucose and insulin secretion. One potential strategy is to perform dynamic perifusion experiments on isolated islets to interrogate the phasic nature of insulin release. Alternatively, if mature insulin is indeed secreted in excess compared to biologically inactive proinsulin in cells that are lacking Cab45 expression, as suggested by **Figures 20 and 24**, this could lead to slight insulin resistance in peripheral tissues that explains the mild glucose-intolerance phenotype. Insulin tolerance tests as well as measurement of circulating proinsulin levels during OGTTs would prove useful in advancing this theory.

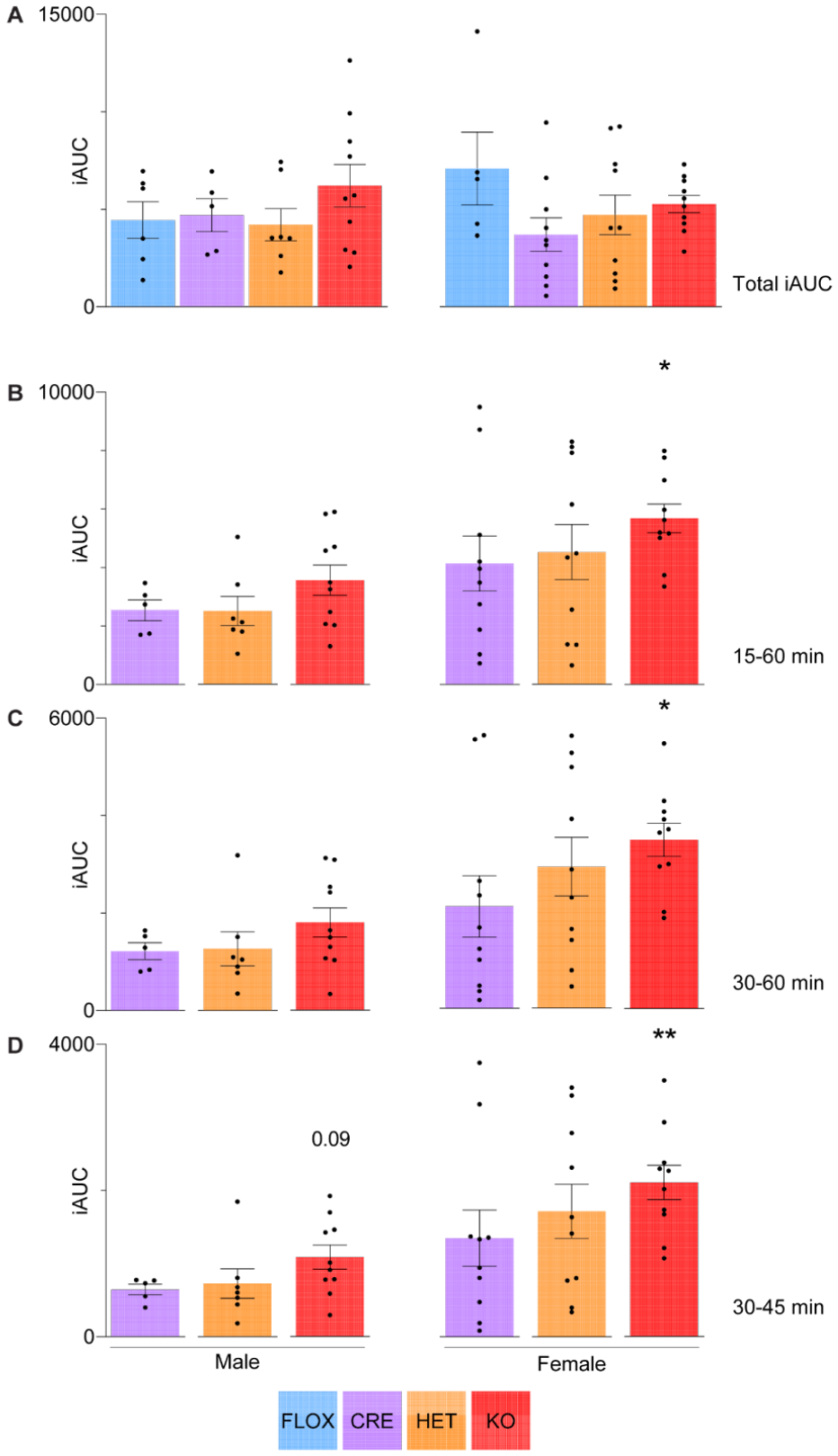

Figure 40. iAUC between specific time points during OGTT of 8-week old βCab45 mice. Males displayed on the right and females displayed on the left. iAUC of glucose concentration during the entire OGTT **(A)**, between 15-60 minutes **(B)**, 30-60 minutes **(C)**, and 30-45 minutes **(D)**. Data presented as mean ± SEM and comparisons made using unpaired t-tests: *, $p < 0.05$; ** $p < 0.01$.

3.3.3.3 *Ex-vivo* functional characterisation of βCab45 mouse islets

At 8 weeks of age, *ex-vivo* functional characterisation was performed on islets isolated from βCab45 mice fed a standard chow diet **(Figure 41**). At this stage, there were not enough male CRE mice to include for analysis. Islets were harvested through standard procedures described in the materials and methods section, and recovered overnight in media containing 11 mM glucose. Then, islets were allowed to rest for 1 hour at 2.8 mM glucose before transfer to either 2.8 or 16.7 mM glucose, after which medium and islet lysates were collected for insulin quantification. Islets from all genotypes could respond to glucose by secreting insulin (**Figure 41A**) and displayed comparable intracellular insulin content (**Figure 41B**).

Subtle differences however were apparent and extracted for further analysis (**Figures 41C-E**). Islets from female KO mice had an elevated secretion of insulin during rest at basal glucose (**Figure 41C**), which could account for a decrease in the fold change of secreted insulin from 2.8 to 16.7 mM glucose that almost reaches significance (**Figure 41D**) when compared to pooled FLOX/CRE controls (mean ng insulin/μg DNA ± SEM = [female FLOX/CRE: **3.82 ± 0.85**] *vs* [female KO: **12.02 ± 2.10**] ($p < 0.01$); mean fold change ± SEM = [female FLOX/CRE: **4.71 ± 0.93**] *vs* [female KO: **1.95 ± 0.48**] ($p = 0.065$)). While this was not observed *in-vivo* after a 5 hour fast (**Figure 38B**), here, islets were left to recover overnight at the moderately high level of 11 mM glucose prior to just 2 hours of the basal condition. Moreover, irrespective of gender, it was observed that out of 10 KO mice, 8 showed a reduction in islet insulin content following stimulation at 16.7 mM glucose compared to those kept at 2.8 mM glucose, whereas this only occurred in 5 out of 13 pooled FLOX/CRE controls (**Figure 41E**). Upon exclusion of one clear outlier KO mouse from statistical analysis, this reduction in islet insulin content following stimulation was found to be significant (**Figure 41E**) (mean ng insulin/μg DNA ± SEM = [CTRL 2.8 mM: **1008 ± 119**] *vs* [CTRL 16.7 mM: **998 ± 117**] ($p > 0.05$); [KO 2.8 mM: **1077 ± 128**] *vs* [KO 16.7 mM: **822 ± 75**] ($p < 0.05$)). This suggests an inability of β-cells from βCab45KO mice to fully replenish insulin SG stores following GSIS, similar to the depletion of SG stores that could underlie the inability of INS1 Cab45KO cells to reproduce a secretory response if subject to consecutive glucose challenges (**Figure 25D-E**). This may be linked to the mild difference in glucose tolerance observed between 15-60 minutes of the OGTT *in-vivo* (**Figures 37-40**) which could underlie the aforementioned discussion on second-phase GSIS.

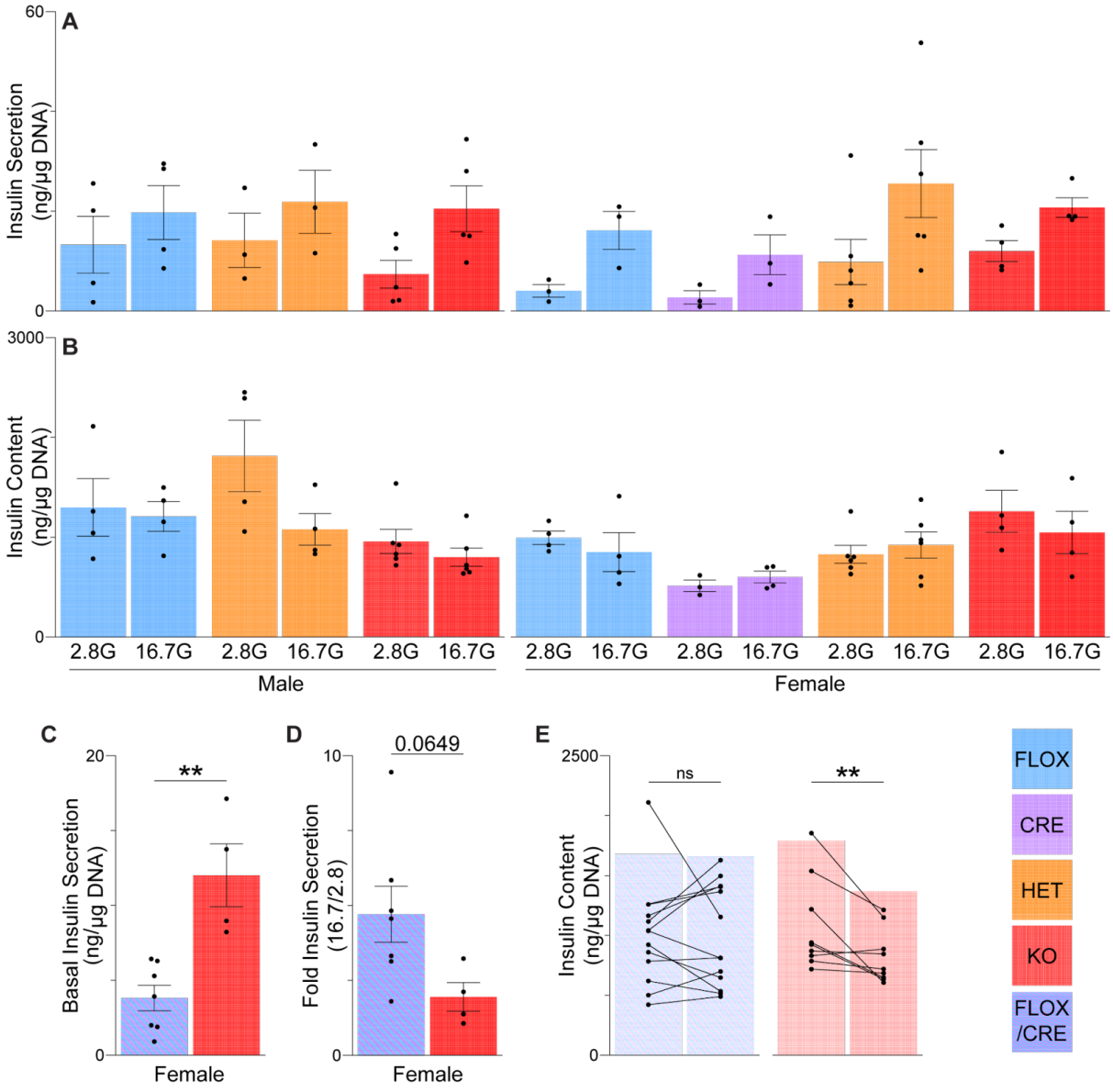

Figure 41. GSIS in islets isolated from βCab45 mice at 8-weeks of age. (A) GSIS following overnight recovery at 11 mM glucose and rest for one-hour at low glucose, prior to one-hour of 2.8 mM glucose basal or 16.7 mM glucose stimulation. Insulin secretion is normalised to DNA. **(B)** Insulin content following GSIS protocol normalised to DNA. **(C)** Separated comparison of basal insulin secretion in islets from pooled female FLOX and CRE controls compared to female KOs. **(D)** Separated comparison of the fold change of insulin secretion from 2.8 to 16.7 mM glucose in islets from pooled female FLOX and CRE controls vs female KOs. **(E)** Separated comparison of insulin content following rest at 2.8 mM glucose vs stimulation at 16.7 mM glucose, in either pooled FLOX and CRE controls or in KOs from both sexes. Data presented as mean ± SEM and comparisons made using unpaired t-tests: *, $p < 0.05$; ** $p < 0.01$.

3.3.3.4 *In-vivo* metabolic characterisation of βCab45 mice on high-fat high-sucrose diet

β-cell dysfunction is often precipitated by a sub-optimal lifestyle, superimposed onto genetically susceptible individuals. Early observations at 8 weeks of age on a standard chow diet indicate that βCab45 KO mice mildly recapitulate some of the phenotypes that are observed in Cab45KO insulinoma cell lines. To assess whether metabolic challenge exacerbates the impact that the loss of Cab45 has on glucose tolerance and β-cell function, βCab45 mice were subject to 8 weeks of HFHSD feeding from 11 to 19 weeks of age and were then characterised *in-vivo* (**Figures 42-45**). At this stage, only two cohorts of mice have been tested and presented here are results for CRE and KO mice. Since there are not enough mice to conduct statistical comparison, a rudimentary qualitative assessment of the data will be presented.

Body composition on HFHSD. At 19 weeks of age after 8 weeks of HFHSD, female KO mice appeared to have gained a higher percentage of body fat than CRE controls when compared to pre-diet measures (**Figure 42D**).

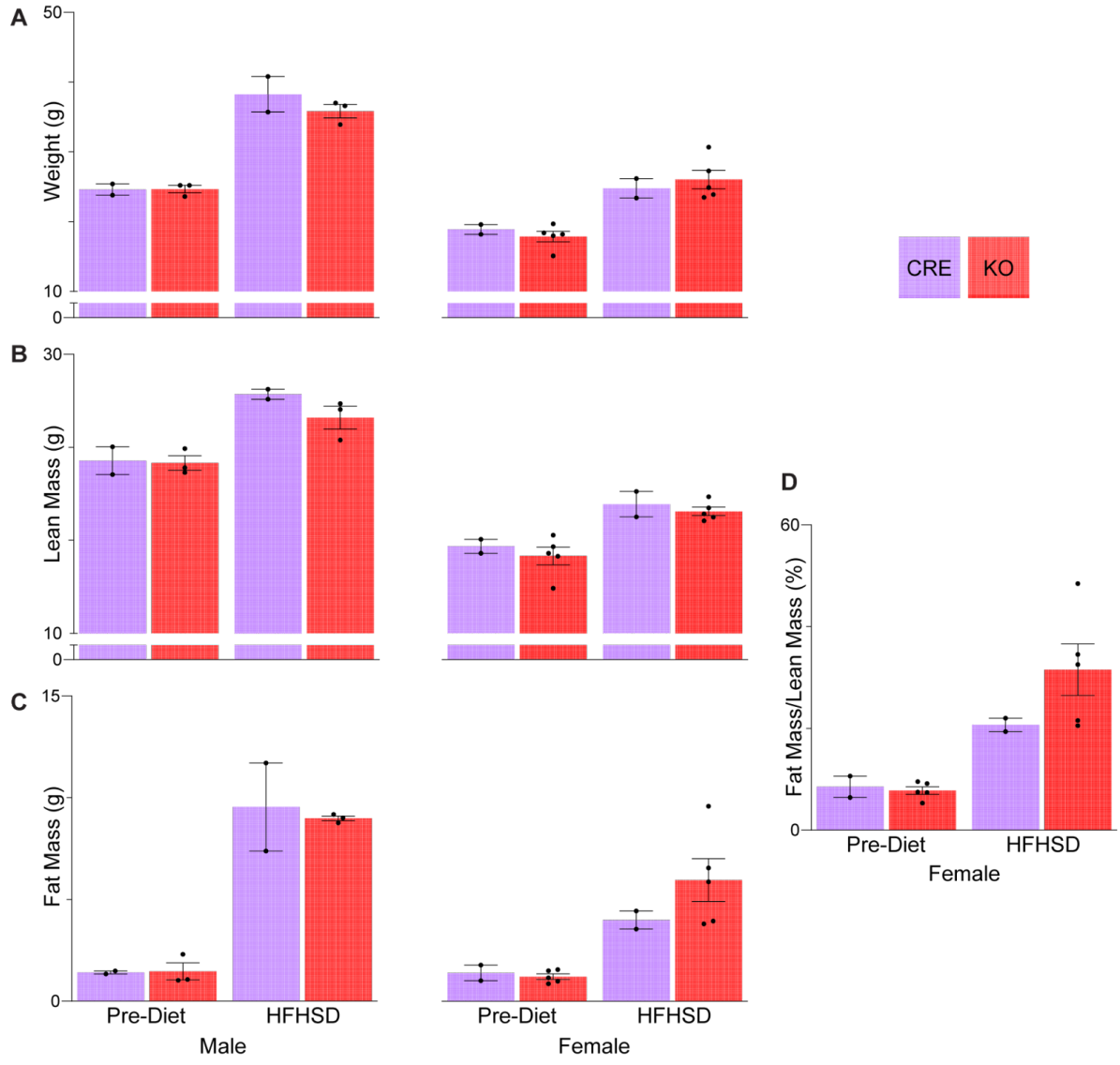

Figure 42. Body composition of 19-week old CRE and KO βCab45 mice subject to 8 weeks of HFHSD. **(A-C)** Males displayed on the right and females displayed on the left. **(A)** Body weight, **(B)** Lean mass, and **(C)** Fat mass of βCab45 mice. **(D)** Fat mass as a percentage of lean mass.

Blood glucose and insulin during OGTT on HFHSD. At 11 weeks of age prior to HFHSD, both male and female KO mice had minor elevations in glucose tolerance compared to CRE controls, and this separation increased following the dietary intervention (**Figure 43**). Both KO and CRE control mice had elevated fasting insulin following HFHSD (**Figure 44**). Prior to diet, males appeared to have lower fasting insulin than CRE controls but this appears to have switched after HFHSD (**Figure 44A**).

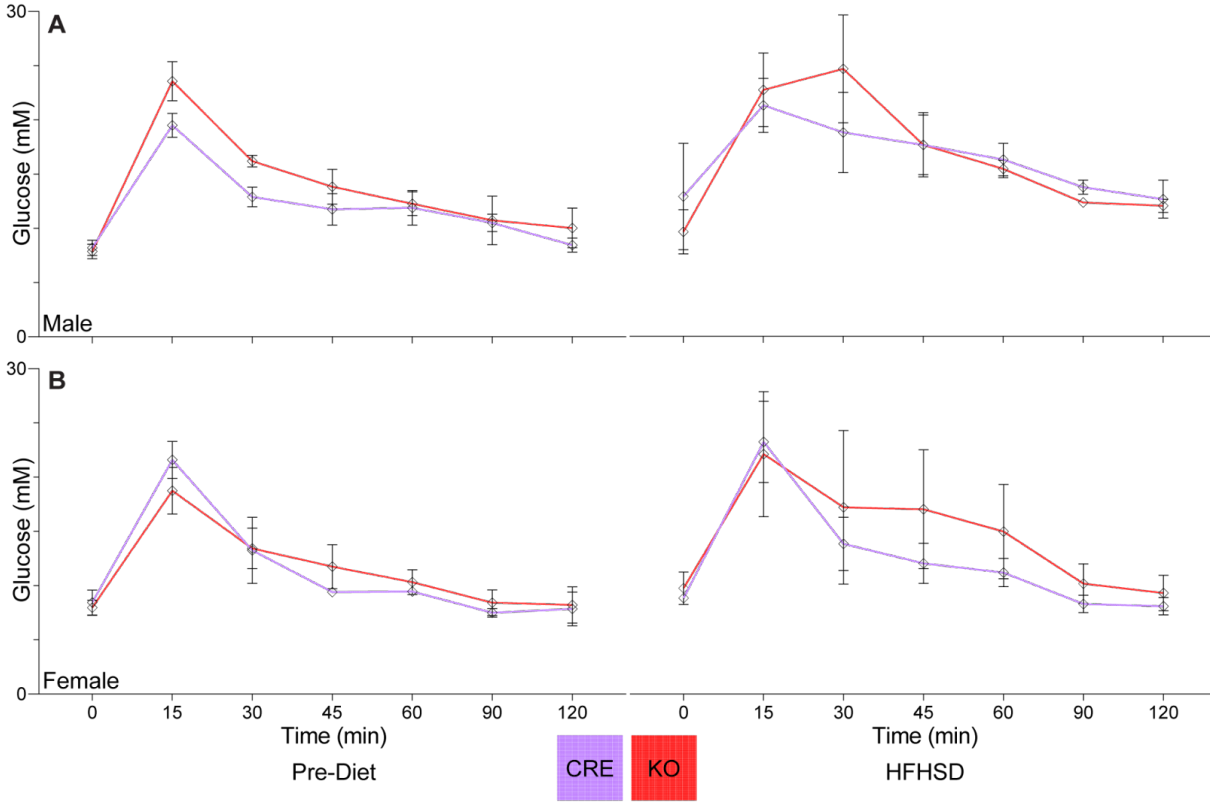

Figure 43. Measurement of blood glucose concentration during OGTT of 19-week old CRE and KO βCab45 mice subject to 8 weeks of HFHSD. Pre-diet measurements taken at 8 weeks of age on a chow diet displayed on the right, and post-diet measurements displayed on the left. **(A)** Male mice: n=2 CRE, n=3 KO. **(B)** Female mice: n=3 CRE, n=5 KO.

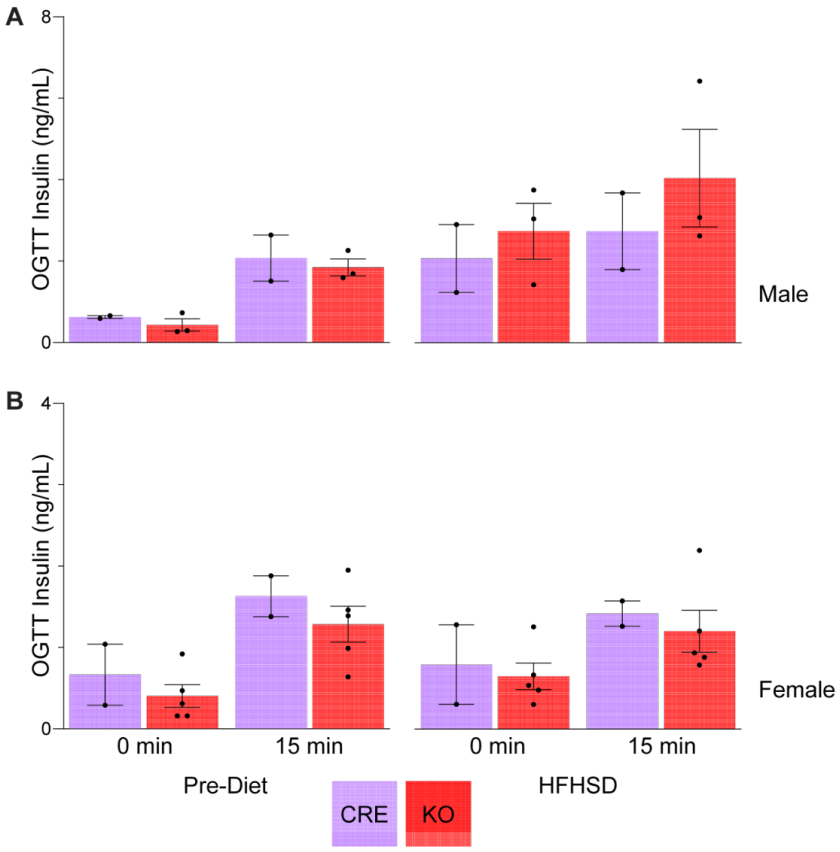

Figure 44. Measurement of blood insulin concentration during OGTT of 19-week old CRE and KO βCab45 mice subject to 8 weeks of HFHSD. Pre-diet measurements taken at 8 weeks of age on a chow diet displayed on the right, and post-diet measurements displayed on the left. Circulating insulin concentration at 0 and 15 minutes during OGTT in male mice **(A)** and female mice **(B)**.

Blood glucose concentration and glucose tolerance at/between specific time periods during OGTT on HFHSD. As performed in **Figures 39** and **40**, notable comparisons of glucose concentration and iAUC at/between specific time points in βCab45 mice are presented (**Figure 45**). At 30 minutes during the OGTT, pre-diet male KO mice have an elevated circulating glucose concentration as reported in **Figure 39**, but after HFHSD these mice appear to pull away from CRE controls (**Figure 45A**). This pattern of elevated circulating glucose also appears to be the case in female mice but from 30 through to 60 minutes (**Figure 45B**), and is reflected in the iAUC measurement during both the 30-60 and the 60-90 minute time periods (**Figure 45C**).

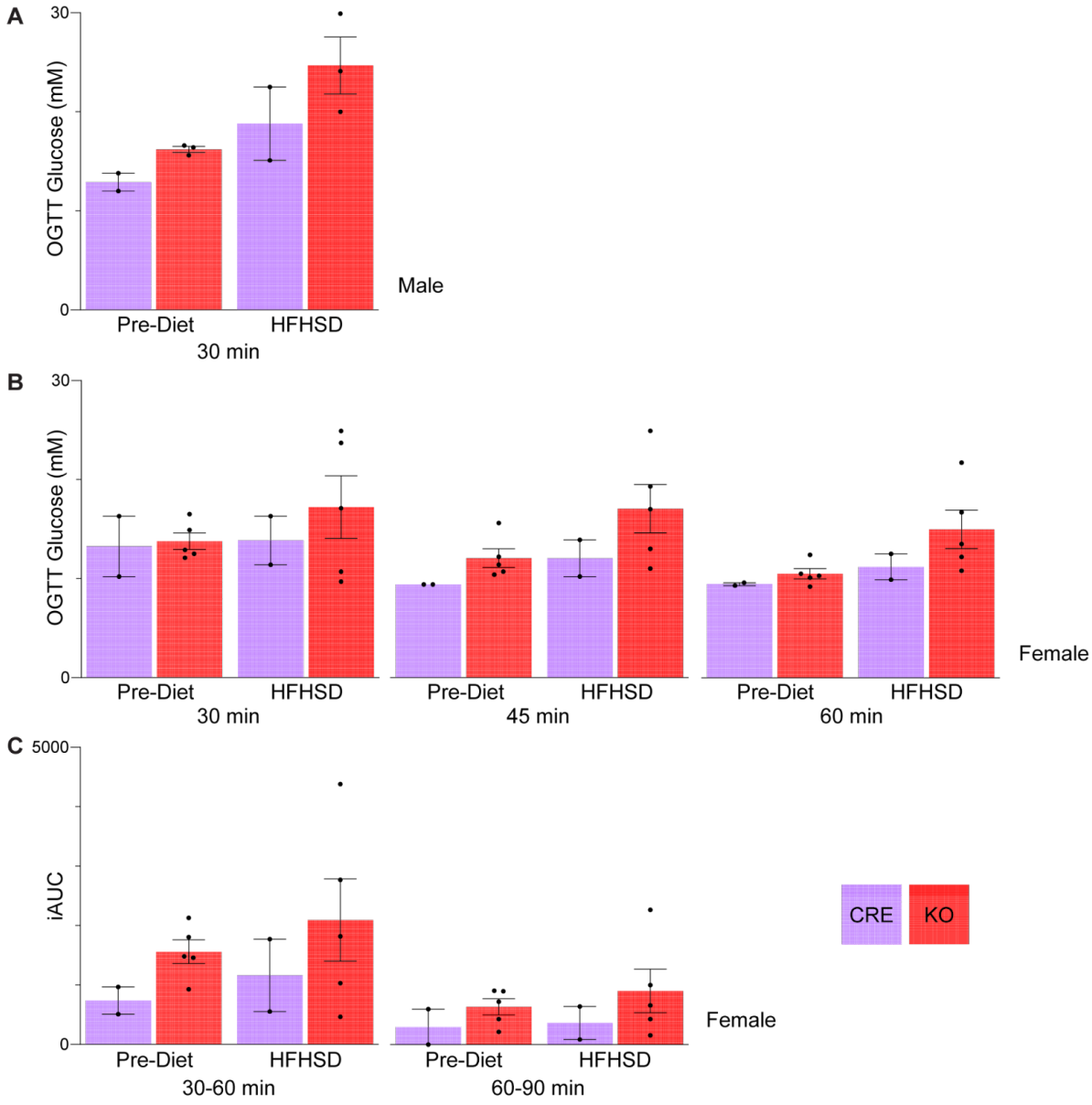

Figure 45. Blood glucose concentration and iAUC at/between specific time points during OGTT of 19-week old CRE and KO βCab45 mice subject to 8 weeks of HFHSD. (A) Circulating glucose concentration at 30 minutes during OGTT in male mice. **(B)** Circulating glucose concentration at 30, 45, and 60 minutes during OGTT in female mice. **(C)** iAUC between 30-60 minutes and 60-90 minutes in female mice.

OGTT at 12 weeks on HFHSD. At this stage, one cohort of mice has been assessed after 12 weeks of HFHSD and the OGTT is presented in **Figure 46**. In comparison to the single CRE mouse, the control of circulating glucose is becoming progressively lost in female KO littermates, with two out of three mice displaying clear glucose intolerance. Undoubtedly, there is eagerness in what the data will show with more biological replicates and with longer diet intervention.

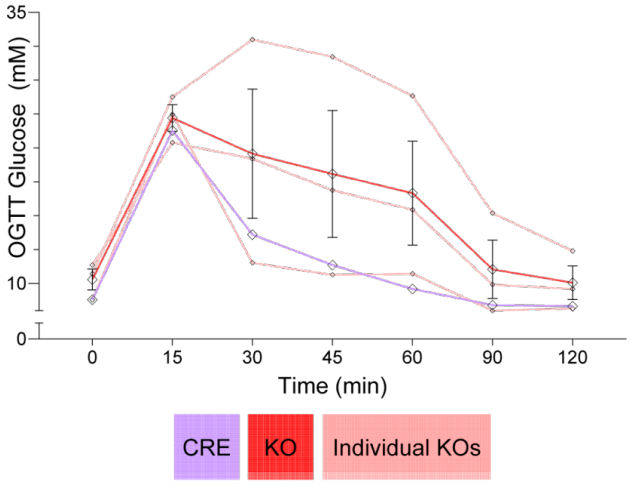

Figure 46. Measurement of blood glucose concentration during OGTT of 23-week old female CRE and KO βCab45 mice (all littermates) subject to 12 weeks of HFHSD. Individual KO mice are presented here in addition to a grouped line with error bars displayed.

3.3.3.5 Summary

Taken together, the data obtained from βCab45 mice suggest a role for Cab45 in replenishing the pool of newly synthesised insulin SGs during GSIS. Although insulin secretion at the 15 minute time point during an OGTT is not affected by β-cell Cab45 depletion, the preliminary data indicates that HET mice secrete less insulin 30 minutes after oral administration of glucose. This corresponds with slightly impaired glucose tolerance through the 30-60 minute time period in HET and KO mice from both sexes which appears to be exacerbated when mice are subject to 8 weeks of HFHSD. When islets are isolated from βCab45 mice for *ex-vivo* functional assessment of GSIS, there are no clear differences in the total amount of insulin secreted over the course of 1 hour stimulation. This is in stark contrast to Cab45KO insulinoma cell lines which display major (but opposing) secretory phenotypes. Notably, following glucose-stimulation, isolated islets from KO mice have reduced insulin content when compared to pooled controls, suggesting some defect in SG replenishment that could underlie an impaired second-phase secretory response. Finally, insulin secretion during basal conditions in isolated islets from female KOs is elevated controls, which tracks nicely with that in MIN6 Cab45KO cells and could be related to possible compositional changes in insulin SGs that are observed in both INS1 and MIN6 Cab45KO cells. Since insulin is also a potent anabolic hormone, perhaps this slight dysregulation in secretory function drives initial changes to body composition that are observed in female HET and KO mice.

(Page intentionally left blank)

3.4 Discussion

Two rodent insulinoma cell-line Cab45KO models were developed and characterised to provide an understanding of the consequence of its loss from β-cells. This was followed up by deleting Cab45 from the β-cells of mice and performing initial characterisation at 8 weeks of age followed by the subjugation of 8 weeks of HFHSD.

Major functional phenotypes of Cab45KO cell line models. While the main findings in each cell line appear to be conflicting, they may in fact lead to common ground. In the INS1 line, KO cells have a severe degranulation of SGs (**Figure 19, 20A**) which is associated with reduced abundance of several common SG resident proteins (**Figure 21**). KO INS1 cells can normalise their peripheral insulin SG content following rest in low glucose (**Figure 22A-B**), after which they can secrete triple the amount of insulin compared to WT cells when stimulated with high glucose (**Figure 25A-B**). If subject to a second consecutive glucose challenge to mimic a metabolically stressful situation such as insulin resistance or T2D, KO INS1 cells have impaired secretion (**Figure 25D-E**), probably due to the release of available SGs during the first challenge. Moreover, the initial hypersecretory response can be explained by an elevated cytosolic Ca^{2+} concentration that would work to enhance exocytosis (**Figure 26**). Thus, KO INS1 cells can still generate and secrete SGs, but when cultured at the moderately high level of 11 mM glucose these appear to be secreted at a rate that exceeds synthesis, accounting for the reduction in insulin content.

In contrast, Cab45KO MIN6 cells do not have any change in SG content compared to WT (**Figure 29**), but two out of three KO lines (KO-1 and KO-3) have marked secretory defects in response to both glucose and KCl (**Figure 31** and **32**). KO-2 MIN6 cells secrete well in either situation, but still lack in comparison to WT when stimulated with glucose (**Figure 31** and **32**). As is the case in the INS1 model, secretory responses to both stimuli are correlated to the cytosolic Ca^{2+} concentration. Impaired Ca^{2+} responses during stimulation by glucose or KCl (**Figure 33**) explains the reduced secretory response of the KO-1 cell line, which accounts for the maintenance of insulin content even though MIN6 cells are cultured at the supra-stimulatory level of 25 mM glucose. Taken together, the lack of a degranulation phenotype in MIN6 KO cells is evidence supporting the notion that reduced insulin content in the INS1 KO line is driven by enhanced SG release rather than major impediments to SG biogenesis.

From these data, it appears that Cab45, which is situated predominantly in the *cis*-Golgi, is involved in regulating distal aspects of the β-cell insulin secretory pathway. However, the reason why INS1 and MIN6 cell line models have opposing Ca^{2+} responses remains to be elucidated. One possibility is that there is species or cell-line variability in the expression of proteins that Cab45 could regulate and/or interact with Cab45 isoform expression could also vary, as there could be unverified isoforms present in both mouse and rat. If true, mass spectrometry analysis has revealed that the INS1 model could be a complete KO of all Cab45 isoforms (**Figure 18E**), but this has not yet been verified

in the MIN6 model. Immunostaining with an antibody that targets an epitope common to all known Cab45 isoforms revealed expression of only Golgi-localised Cab45 in MIN6 cells (**Figure 13, 28C**), but the same antibody has not yet been applied to INS1 cells.

Alternatively, since insulinoma lines are composed of functionally heterogeneous cells (Lilla et al. 2003; R. Zhao et al. 2021), variable phenotypes may be a result of the clonal expansion of KOs from single cells. Evidence for this is that all three MIN6 KO lines were expanded from cells edited with the same guide RNA sequence to drive similar polymorphisms in the genomic Cab45 sequence (**Figure 28A**), yet, the KO-2 line is a competent secretor whereas KO-1 and KO-3 lines are poor secretors (**Figure 27**). The INS1 Cab45KO line was derived from a small pool of clonal KO cells, but these could collectively exhibit superior GSIS (**Figure 19**). Moreover, the lack of a clear secretory phenotype observed both *in-vivo* (**Figure 38**) and *ex-vivo* (**Figure 41A**) from islets of βCab45 mice, which contain a heterogeneous population of β-cells, suggests that strong secretory phenotypes observed in cell lines are not directly due to the loss of Cab45. This could explain why re-expression of Cab45 rescues the secretory phenotype in INS1 cells (**Figure 25A-B**) but not MIN6 cells (**Figure 365B**), via a singular mechanism that functions to reduce secretory output. If this is the case, differential responses in insulinoma cell lines may provide several contexts from which to assess phenotypes that could be occurring more proximal to the site of Cab45 localisation, but further characterisation is required to confirm the situation. Indeed, differential effects of gene knockout have been widely documented to result in alternate effects in cell lines compared to rodents due to the unique biological nature and circumstances that exist between such models.

Now, while disparities in SG abundance and insulin content (**Figures 19, 20 and 29**) between cell-line models are explained by the variability in secretory phenotypes (**Figures 24, 25 and 31**), there is no evidence yet to suggest that SG biogenesis is unaffected by the loss of Cab45. SG biogenesis is a collaborative process involving many proteins, and the removal of contributing factors can affect parameters related to SG function, such as rate of formation and composition, without limiting generation and steady-state abundance. From the current data it appears that all KO models can generate a substantial population of SGs provided that downstream insulin secretion is not overwhelming, but whether certain parameters of SG biogenesis are altered remains a subject of investigation.

Evidence for altered SG composition in Cab45KO cells. Several independent observations indicate that Cab45 depletion alters the composition of granules. In INS1 cells, acute Cab45 silencing results in increased intracellular PC1/3 content up to levels that are capable of driving an increase in its basal and glucose-stimulated secretion (**Figure 27**). As mentioned previously, PC1/3 is a resident member of the SG and is the principal enzyme required for processing proinsulin to insulin. Although this remains to be confirmed, INS1 cells with acute Cab45 loss do not appear to have elevated SG abundance via immunofluorescence (**Figure 29**), and MIN6 cells with chronic Cab45 loss do not display elevated peripheral SG abundance despite having exocytotic defects (**Figures 29 and 31**).

Moreover, the average size of mature insulin SGs in KO INS1 cells are smaller and visually appear to be more dense under EM (**Figure 20B**), and validation of this in MIN6 KO cell lines is underway. Taken together, it is possible that the packaging of PC1/3 and other cargo proteins into individual granules are enhanced in the absence of Cab45, resulting in greater protein condensation during SG maturation and accounting for increased cargo release during basal conditions and glucose-stimulation if cells are competent secretors.

In KO INS1 cells, overall PC1/3 abundance is reduced however this is in line with the depletion of insulin SGs that occurs in this model (**Figure 20A, 21**). Nonetheless, in these cells there is a reduction in the released proinsulin to insulin ratio during basal and glucose stimulation (**Figure 24B-C**), indicating that proinsulin conversion is actually enhanced in the absence of Cab45. In the MIN6 model, cellular proinsulin content was measured in the KO-1 line and shown to be reduced (**Figure 30**), and across all lines, there is enhanced basal release of total insulin (**Figure 34**) which is reversed in the KO-1 line upon re-expression of Cab45 (**Figure 35E**). Interestingly, isolated islets from female βCab45KO mice following overnight in media containing 11 mM glucose also display elevated basal insulin secretion, but this is not observed *in-vivo* when fasting glucose levels appear normal (**Figure 37**). While these phenotypes could indicate proinsulin leakage into the constitutive pathway due to defective sorting at the TGN in Cab45KO β-cell models, it could also result from enhanced proinsulin conversion and the basal release of mature SGs that contain more cargo than those in WT cells. Measurement of secreted proinsulin under basal and glucose stimulation from the MIN6 model and islets from βCab45KO mice will help to solidify the conclusions made from these data.

Thus, it seems that the limited supply of SGs contained within KO INS1 cells may in fact be bolstered with extra cargo. Following rest at low glucose and replenishment of SG stores, this could contribute to hypersecretion (**Figure 25A-B**) in addition to the already enhanced cytosolic Ca^{2+} response (**Figure 26**). Since two out of three KO MIN6 lines harbour downstream defects in the stimulus-secretion coupling pathway (**Figure 31 and 32**), SGs with greater density may not have the opportunity to augment the stimulated secretory response. In the KO-2 line which has seemingly retained a decent level of secretory abilities (**Figure 31 and 32**), this implies that secretory functions are in fact more restricted than initially thought, either due to Cab45 loss or an effect of clonal expansion. In the INS1 KO model, elevated basal release is probably not observed because of the extensive peripheral SG depletion (**Figure 19 and 20A**), but the difference between INS1 WT and KO lines in SG abundance could mean that this is an inappropriately controlled model. The acute setting can serve as a substitute here, since INS1 cells depleted of Cab45 maintain normal SG abundance but show an elevated PC1/3 release at basal (**Figure 27**). Therefore, elevated basal secretion appears to be a common phenotype observed across all β-cell models without Cab45, suggesting that the composition of granules could be fundamentally altered when Cab45 is absent. Indeed, as mentioned, granule size is reduced in Cab45KO INS1 cells (**Figure 20B**) Importantly,

excessive basal secretion of mature insulin that occurs in *ex-vivo* islets subject to overnight recovery at moderately high 11 mM glucose (**Figure 41C**) could drive the change in body composition that is observed in female βCab45KO mice when fed *ad-libitum* (**Figure 36D**), which does not occur in male βCab45KO mice where basal insulin release is not affected **(Figure 38A and 41A**). These observations are also suggestive of enhanced mature insulin release in βCab45KO *in-vivo*, which could drive slight insulin resistance to explain the mild glucose-interolerant phenotype in these mice.

Mechanistically, these phenotypes could be mediated through the Cab45-Ca^{2+} interaction. Cab45 depletion has been shown to affect the free Golgi Ca^{2+} concentration in HeLa cells (von Blume et al. 2012), and in the β-cell secretory pathway, Ca^{2+} assists protein condensation in the TGN to facilitate sorting of many SG resident proteins into ISGs (Chanat and Huttner 1991; Yoo and Albanesi 1991) and is also a co-factor for prohormone convertase enzyme activity within the SG (Y. Zhou and Lindberg 1993, 1994; Davidson, Rhodes, and Hutton 1988). Perhaps when β-cells are devoid of Cab45, there is more Ca^{2+} available to bind cargo proteins to enhance packaging and enzymatic activation. Proximally, this could lead to a greater density of cargo proteins per-granule and greater ratio of mature to immature proteins. Distally, this could elevate the total amount of cargo released into the medium at basal if cells contain peripheral SGs, and potentially during stimulation if cells are competent secretors. Of course, more direct evidence will be required to substantiate these claims.

Evidence for a role of Cab45 in SG function. Although endogenous Cab45 localisation is concentrated within the *cis*-Golgi, some overlap with the TGN marker in both INS1 and in MIN6 cells indicates that it may traffic distally (**Figures 14 and 15**). Here, Cab45 could be hard to detect due to the overwhelming *cis*-Golgi fluorescence signal, therefore, a direct role for Cab45 in SG biogenesis or function cannot yet be ruled out unless it is verified that endogenous Cab45 does not traffic to the TGN. Indeed, staining of human pancreas sections suggest that Cab45-G could occupy insulin SGs or non-insulin-containing post-Golgi vesicles (**Figure 11**). The transient transfection protocol utilised in KO INS1 cells results in overexpression and overflow of Cab45HA throughout the TGN and into ISGs (**Figure 23**), allowing the study of Cab45 function when it is localised to these compartments. Here, expression of WT Cab45HA into KO INS1 cells restored the abundance of SGs in the cell periphery (**Figure 23B**), raised the intracellular insulin content (**Figure 22C**), and also rescued the hypersecretory phenotype of KO INS1 cells (**Figure 25A-B**).

At this point, there is no direct evidence to explain how rescue is achieved. Considerable colocalisation of overexpressed WT Cab45HA with insulin inside SGs (**Figure 25C**) indicates that Cab45 could interact with SG components to play a role in cargo sorting and granule biogenesis. Alternatively, Cab45 could indirectly rescue by lowering exocytosis to enable SG replenishment, and its entry into SGs could be an unrelated event. This could be achieved by restoring either the trafficking of PM-localised ion transporters or the Ca^{2+}-buffering capacity of the Golgi which, in turn, might rectify the cytosolic Ca^{2+} concentration during basal and stimulatory conditions.

Earlier, the observed lack of secretion in KO MIN6 cells was used to rationalise the maintenance of their SG stores, and to reason that granule depletion in INS1 cells was due to their hypersecretory behaviour. By similar logic, failed attempts to rescue the secretory defect in KO-1 MIN6 cells (**Figure 35A**) indicate that the rescue of SG abundance and secretion in KO INS1 cells (**Figure 23B and 25A-B**) is not achieved by restoring normal stimulus-secretion coupling. Therefore it is unlikely that Cab45HA re-expression into KO INS1 cells restores PM-localised ion transporter trafficking/abundance to rescue the WT level of secretion. Moreover, the surprising observation that Ca^{2+}-binding deficient Cab45HA mutants also rescue peripheral SG abundance to the same level as WT Cab45HA (**Figure 23B**) provides evidence against the restoration of Golgi Ca^{2+} homeostasis as a mechanism of rescue. By process of elimination, it appears that overexpressed Cab45 directly exerts influence on the SG independent of Ca^{2+}-binding to rescue SG abundance. This is exemplified by isolated islets from βCab45KO mice, where a reduction in insulin content following competent GSIS *ex-vivo* suggests that granule replenishment lags in the absence of Cab45 (**Figure 41E**). Moreover, this could contribute to the mild difference in glucose tolerance observed in βCab45KO during time points corresponding to the second phase of GSIS (**Figures 37-40**). This phase relies less on SGs that are pre-docked to the PM and more so on those that are newly synthesised and originating from deeper within the cell. Fine experimental techniques will be employed to dissect the relative contribution of first and second phase GSIS on total insulin secretion in islets from βCab45KO mice.

From here, the data now indicates that Cab45 could directly promote SG biogenesis, but several caveats remain that paint a more complicated picture. Transfection efficiency is relatively low in the INS1 model (**Figure 22D**), but the cells that have Cab45 are massively overexpressing the protein probably to levels far greater than what is seen physiologically (**Figure 23A**). These cells must be very poor secretors, working against a majority of non-transfected cells that are hypersecreting in order to revert the total secretory load back to WT level. If the absence of Cab45 enhances the amount of cargo per granule, perhaps drastic overexpression and overflow of Cab45 into SGs does the opposite and drives the formation of a greater number of SGs, albeit with reduced insulin content per-SG. Thus when stimulated, these cells secrete much less total insulin but retain more granules. SGs overloaded with Cab45 could also have restricted mobility and exocytotic capacity due to altered composition, providing an alternative route by which SG abundance is restored through a functionally undesirable mechanism. Although in regards to the latter, competent secretion of WT Cab45HA from WT INS1 cells (**Figure 17D**) argues against this being the case. Therefore, provided that exocytotic function is indeed unaffected by ectopic Cab45 overexpression, evidence indicates that overexpressed Cab45 promotes SG biogenesis.

Physiologically, the data obtained from both male and female βCab45 mice indicates that altered SG composition, function, or delayed SG biogenesis due to the loss of Cab45 can impair glucose-stimulated insulinaemic output from pancreatic β-cells (**Figures 38-40**). Importantly, islet cell populations are functionally heterogeneous and thus do not offer the pitfalls associated with the

expansion of KO insulinoma cells from clonal subpopulations. In mice, although *in-vivo* insulin secretion is maintained 15 minutes after oral administration of glucose, βCab45HET mice display reduced circulating insulin at the 30 minute time point (**Figure 38C**). Assessment of 30 minute insulin during the OGTT in βCab45KO mice is underway. This is concomitant with mildly elevated circulating glucose concentrations through the intermediate stages of the OGTT in βCab45HET and βCab45KO mice (30-60 minutes) (**Figure 39**), and is reflected by significant differences in the iAUC measurement during these intermediate time periods (**Figure 40**). βCab45KO islets *ex-vivo* have reduced insulin content post-stimulation (**Figure 41E**) that could reflect a delayed replenishment of insulin stores and contribute to the inability to control circulating glucose during these intermediate stages. Clearly, the loss of Cab45 does not affect stimulus-secretion coupling both *in-vivo* and *ex-vivo*, although there may be a reduction in the fold change of insulin secretion in female βCab45KO islets *ex-vivo* (**Figure 41D**) that cannot be quickly discounted simply due to higher basal insulin secretion (**Figure 41C**). Therefore, evidence points to the existence of proximal alterations in SG biogenesis that contribute to a reduced secretory output during the second phase of GSIS, which appears to be progressively exacerbated over the duration of HFHS dietary intervention (**Figures 43-46**).

T2D is a progressive disease caused predominantly from sub-optimal lifestyle factors but is underlined by pre-existing genetic susceptibility. Several mutations in the SDF4 gene encoding Cab45 are associated with undesirable markers of metabolism such as elevated fasting glucose (HuGeAMP 2022), and the Cab45 protein is lost from a significant proportion of β-cells in human T2D (**Figure 12**). It is likely the case that alteration in SG function due to individual genomic variation is bearable during good health but problematic when health is poor. Considering that SG formation precedes exocytosis, proximal defects could underscore issues with distal output to contribute to the progression from β-cell compensation into β-cell failure. The data presented here proposes a possibility that Cab45 abundance determines where balance is struck between SG abundance and composition, ultimately influencing insulin output upon granule fusion. This could be utilised in physiologically relevant situations such as β-cell compensation where Cab45 abundance is elevated, probably to a reasonable degree on a per-cell basis, to help generate more SGs in unison with a complete β-cell response to an increased demand for insulin. Studies to assess Cab45 localisation in islets of ob/ob mice undergoing β-cell compensation are a pertinent next step to forward this theory. On the contrary, Cab45 absence from β-cells could delay the formation of nascent SGs which could be a critical limitation during times of metabolic stress. SGs that are formed without Cab45 might have bolstered content and augmented conversion of proinsulin, but could contribute to basal hyperinsulinaemia during prediabetes or even hyperproinsulinaemia during T2D when ISGs are secreted prematurely.

(Page intentionally left blank)

Chapter 4: Final Discussion

4.1 Introduction

The mechanisms underlying secretory protein trafficking through the distal Golgi apparatus and early ISG in pancreatic β-cells are poorly defined. The current consensus, which has not been updated for almost two decades, is that ionic forces drive the fairly non-selective condensation of proteins destined for the ISG first in the TGN, and that subsequent ISG-based sorting mechanisms refine the composition of the maturing granule (Arvan and Halban 2004). It is likely, however, that there are uncharacterised luminal proteins specifically responsible for trafficking SG-resident proteins in the β-cell, and that their dysregulation underlies aspects of β-cell dysfunction and failure that occurs in T2D. The data presented in this thesis provides evidence for the involvement of one such protein, Cab45, in this process.

Cab45 expression and function has not yet been studied in whole organisms. Considering its well-defined role in regulating protein sorting in the constitutively secreting human HeLa cell line (Blank and von Blume 2017), identifying its involvement in the context of human disease is important. Initial characterisation revealed that Cab45 is broadly expressed throughout pancreatic β-cells in the human islet but is absent in the glucagon-producing α-cells and the exocrine pancreas (**Figure 11**). Islet Cab45 abundance also positively correlates with insulinaemic output during situations of heightened or dampened activity in both humans and animal models of metabolic disease (**Figures 12-13**). Cab45 mRNA is expressed throughout other tissues in mice including those that participate in both constitutive and regulated secretory activities, but like the islet, demonstrates cell-type specific expression upon closer inspection of the adrenal and pituitary glands (**Figure 10**). These insights position Cab45 as an exciting prospect that could regulate whole-body communication through its involvement in the secretory pathway. It follows that mutations in Cab45 or loss of expression could underlie various systemic dysfunctions.

Endogenous Cab45 is localised predominantly in the *cis*-Golgi of insulinoma cell lines (**Figures 14-15**), therefore its hypothesised involvement in sorting proteins into ISGs was, at first, questionable. Initial findings in the Cab45KO INS1 model provided the surprising observation that insulin is hypersecreted in the absence of Cab45 (**Figures 24-25**), pointing to a role for Cab45 in stimulus-secretion coupling. However, later observation of blunted insulin secretion from Cab45KO MIN6 lines put this into question by asking how Cab45 depletion could cause such opposing phenotypes, and why the degree of secretory defect is inconsistently affected across different MIN6 KO lines (**Figures 31-32**) that were created through precisely the same method (**Figure 28**). More discrepancies between models were uncovered during attempts to rescue, where re-introduced Cab45 reversed hypersecretion in the INS1 KO model (**Figure 25**) but failed to restore normal secretion in

the MIN6 KO-1 model and instead appeared to reduce secretory output (**Figure 25**). Taken together, a plausible theory is that secretory phenotypes are mostly explained by the expansion of KO lines from single cells that were derived from a functionally heterogeneous population of cells - a documented phenomenon (Lilla et al. 2003; R. Zhao et al. 2021). This could mean that phenotypic rescue in INS1 KO cells is not due to restored stimulus-secretion coupling (**Figure 25**); after all, Cab45 localisation is quite far removed from SG exocytosis to have such robust control over secretory output. Of course, this is something that requires experimental confirmation since it cannot be ruled out that changes through the early secretory pathway contribute to secretory defects. Indeed, slightly impaired secretory responses in isolated islets from female βCab45KO mice suggest that Cab45 depletion could contribute in some way to secretory impairment (**Figure 41**). This is reflected by βCab45KO mice displaying mildly impaired glucose tolerance (**Figure 37-40**) that is exacerbated following HFHSD (**Figure 43-46**). Of course, since islets from βCab45HET and KO mice display competent GSIS both *in-vivo* (**Figure 38**) and *ex-vivo* (**Figure 41**), it is unlikely that Cab45 directly controls stimulus-secretion coupling. Nonetheless, from this point of view, Cab45KO models provide several contexts from which to observe phenotypes that are occurring more proximal to the site of Cab45 localisation. If changes to Cab45 expression in humans occurs prior to the development of disease or if acquired genetic variants impair Cab45 protein function, these contexts could provide basic insight into the outcomes of Cab45 deficiency through various stages of β-cell function or in functionally distinct populations of islet β-cells.

(Page intentionally left blank)

4.2 Cab45 Trafficking and SG Biogenesis

Ascertaining whether endogenous Cab45 traffics through to the TGN even in small amounts, or if it is held within the *cis*-Golgi, is paramount to uncovering its involvement in SG biogenesis. Cab45 has the molecular potential to traffic distally through the TGN and into insulin SGs when overexpressed (**Figures 17 and 23**), which could occur during β-cell compensation when Cab45 protein abundance increases (**Figure 13**). Recent reports show that Cab45 can be secreted from human EndoC-βH1 β-cells experiencing non-targeted siRNA-induced stress (Ryaboshapkina et al. 2022), demonstrating that endogenous Cab45 traffics beyond the Golgi apparatus during altered cell states. Cycloheximide treatment to prevent synthesis of nascent protein could prove useful in determining whether endogenous Cab45 traffics distally or maintains its localisation in the *cis*-Golgi during non-stressful conditions or variable physiological states. In HeLa cells, Fam20C-mediated phosphorylation enables Cab45 trafficking into secretory vesicles by reducing the size of Cab45 oligomers (Hecht et al. 2020), and Fam20C is expressed in the β-cell where it is a master regulator of adaptive secretory pathway homeostasis (Kang et al. 2019). Interestingly, the 6EQ Cab45HA Ca^{2+}-binding deficient mutant that is presumably monomeric has the ability to traffic beyond the TGN (**Figures 17 and 23**) and is not routed to the constitutive pathway (**Figure 17**), but enters and occupies insulin SGs before it is sorted out of the maturing granule (**Figure 17 and 23**). The default route of Cab45 trafficking is therefore into the insulin SG, even when monomeric. This is in stark contrast to C-terminally truncated Cab45 described by *Lara Lemus* et al., designated Cab_{308}Myc which associates with early secretory pathway membranes for direct targeting into the constitutive pathway (Lara-Lemus et al. 2006), demonstrating that the C-terminus is critical for its localisation and trafficking.

Common to all models studied, secretable SGs can be generated without Cab45 arguing against its absolute requirement for SG biogenesis (**Figures 22, 27, 29, 31, 32, 34, 35**), in line with the redundancy of luminal proteins such as granins that are known contributors to SG formation (Wollam et al. 2017). Reduced insulin SG content in INS1 KO cells (**Figures 19, 20, and 22**) that exhibit hypersecretion and the reduced insulin content of βCab45KO islets post-stimulation (**Figure 41**) however indicates that granule biogenesis could be slowed in the absence of Cab45. Still, the ability of KO cells to generate releasable SGs at any rate suggests that resident proteins do not require Cab45 for direction into ISGs. Nonetheless, SG production is enhanced when Cab45 is present in TGN (**Figure 23**). Moreover, successful rescue of the SG population in INS1 Cab45KO cells by 6EQ Cab45HA and other Ca^{2+}-binding deficient mutants (**Figure 23**) combined with non-impeded exit of 6EQ Cab45HA from the TGN (**Figure 17 and 23**) provides additional insight, by suggesting that this process is driven by Ca^{2+}-independent interactions of Cab45 with potential bound cargoes prior to ISG-based sorting mechanisms taking effect. It is plausible however to hypothesise that Ca^{2+}-binding could help to accelerate the trafficking and/or aggregation and sorting of potential bound cargo. Of

course, identification of such cargoes are absolutely vital for substantiating these claims, and current efforts to immunoprecipitate endogenous Cab45 with a knock-in HA tag from MIN6 insulinoma cells are underway. Distinct separation of Cab_{308}Myc from proinsulin (Lara-Lemus et al. 2006) opens doors to the possibility that the C-terminus of Cab45 mediates such interactions, but loss of colocalisation between insulin and Cab45 following disruption to Ca^{2+}-mediated protein-protein interactions indicates that the C-terminus does not mediate direct or indirect interactions with proinsulin (**Figure 16**). Colocalisation studies in the Ca^{2+}-depleted state are therefore pertinent for identifying proteins involved in Ca^{2+}-independent Cab45 interactions. Taken together, it is likely the case that the C-terminus brings Cab45 in proximity with SG resident proteins, where conformational changes induced by Ca^{2+} drive the collective association of cargo with proinsulin and accelerate transit through the secretory pathway. Physiologically, these interactions could underlie the mildly impaired glucose tolerance that is observed during time periods that correspond to the second phase of GSIS in βCab45HET and KO mice (**Figures 37-40**), which is exacerbated with feeding on a HFHSD (**Figures 43-46**). Second phase GSIS relies on newly synthesised SGs originating from deeper within the cell more so than the first phase (Yau et al. 2021), therefore delayed cargo transit through the secretory pathway could underlie impaired insulin output from the β-cell as evidenced by reduced circulating insulin levels in βCab45HET mice 30 minutes post-oral glucose administration (**Figure 38**).

4.3 Molecular Interactions of Cab45 in the β-cell

A collage of separate observations sheds light on the molecular interactions of Cab45, and in doing so, provides insight into the nature of secretory pathway trafficking in the β-cell. Cab45 colocalises with proinsulin in the *cis*-Golgi of both insulinoma lines INS1 and MIN6 (**Figure 14-15**), but intracellular Ca^{2+} depletion using ionomycin releases Cab45 from its oligomeric retention strategy and sends it anterograde through the Golgi apparatus (**Figure 16**). In contrast to Cab_{308}Myc, in this instance monomeric Cab45 enters non-insulin-containing, non-constitutive post-Golgi vesicles (**Figure 16**). When both WT and 6EQ Cab45HA are ectopically overexpressed into INS1 cells containing a stable population of potential interacting proteins, they each have comparable distribution in the juxtanuclear region overlapping with proinsulin (**Figures 17 and 23**). This suggests that the Cab45-Ca^{2+} interaction does not drive its proximity with proinsulin but that theorised Ca^{2+}-independent protein-protein interactions play a more important role. Cab45 exit from the Golgi apparatus following ionomycin treatment could therefore reflect the broad dispersion of cargoes into various post-Golgi carriers, where those bound to Cab45 via Ca^{2+}-independent interactions end up in the same carrier. However, Ca^{2+} is a determinant of Cab45 trafficking since the presence of overexpressed Cab45HA within insulin SGs is reduced in the absence of Ca^{2+}-binding (**Figures 17 and 23**), seemingly due to its exit from the maturing SG (**Figure 23**). But, as this does not impair the rescue of SG abundance in KO INS1 cells (**Figure 23**), evidence argues against a requirement of oligomeric Cab45 for associated entry with SG-resident proteins from the TGN into the ISG.

Collectively, results speak to the existence of intracellular Cab45 regulation whereby the oligomeric state controls its localisation and trafficking, but not its function. Considering the documented activity of Fam20C in β-cells and its role in Cab45-dependent sorting in HeLa cells (Hecht et al. 2020), phosphorylation could reduce Cab45 to smaller oligomers as a release mechanism from its *cis*-Golgi retention strategy, while also predisposing Cab45 for exit from the maturing SG. Such a mechanism could explain the lack of observed Cab45-related peptides in published studies enquiring into the proteomic composition of the insulin SG (Norris, Yau, and Kebede 2021), while maintaining its hypothesised function in SG biogenesis. Importantly, in the overexpression system used for study, Fam20C could be stoichiometrically overwhelmed such that WT Cab45HA is predominantly oligomeric, accounting for its inhibited exit from the maturing SG (**Figure 23**). Since 6EQ Cab45HA is already monomeric, it readily exits the SG without a phosphorylative signal. This experimental context thus indicates that entry into the ISG is not discriminative for monomeric or oligomeric Cab45. Intriguingly, individual variation in Cab45 occupation of insulin SGs in humans is observed (**Figure 11**), which could reflect differences in the efficiency of Cab45 exit either due to inherent variation in Cab45 itself or the *sorting by exit* mechanism. This could be predisposing for β-cell dysfunction in metabolically stressful situations such as peripheral insulin resistance.

Conveniently, *Lara Lemus* et al. originally used Cab_{308}Myc to discern a targeting mechanism for constitutive secretory proteins within the INS1 cell (Lara-Lemus et al. 2006), by showing that Cab_{308}Myc was separated from the bulk-flow of regulated secretory cargo via association with early secretory pathway membranes prior to its constitutive release from the cell. Although monomeric, 6EQ Cab45HA avoids the constitutive secretory pathway and is retained within the INS1 cell (**Figure 17**) but is readily secreted from the HeLa cell (Crevenna et al. 2016). This pattern of localisation is consistent with the argument by *Lara Lemus* et al. that default routing to the constitutive pathway may not be an occurrence in specialised secretory cells, but instead, that constitutive secretion requires dedicated targeting (Lara-Lemus et al. 2006). Cab_{308}Myc possesses five intact Ca^{2+}-binding EF hands and all phosphosites, implicating the C-terminus as a mediator of Cab45 solubility/separation from the membrane. Notably, human Cab45-S is retained within the ER where interactions with SERCA2B are mediated by a motif common to both Cab45-G and Cab45-S (L. Chen et al. 2016), yet, Cab45-G (which differs to Cab45-S from amino acids 305 onwards, **Figure 9A**) bypasses this interaction and traffics to the Golgi. Routing to the constitutive pathway could occur when interactions with soluble proteins are prevented due to the loss of the C-terminal region, accounting for the differential behaviour of Cab45 between insulinoma cells and HeLa cells and the differential localisation of Cab45-G and Cab45-S. Indeed, many SG-resident proteins of the β-cell are also expressed in other (neuro)endocrine cell types where Cab45 could also be expressed, and are critical for the formation and function of SGs in general (Bartolomucci et al. 2011; Seidah et al. 2013). It follows that expression of proteins unique to specialised secretory cells, such as the granins and subtilisin-related proprotein convertases as well as principle prohormones like proinsulin and pro-IAPP, could determine the endogenous behaviour of Cab45. This could govern differential Cab45 function in cells that participate in constitutive and regulated secretion.

4.4 Cab45 Controls Insulin SG Composition in the β-cell

Several measures indicate that SG composition is altered in the absence of Cab45. Acute siRNA-mediated depletion Cab45 depletion from INS1 cells drives an elevation in intracellular PC1/3 content (**Figure 27**), and in chronic Cab45KO conditions, SG size is reduced (**Figure 20**) and proinsulin conversion is augmented (**Figures 24 and 30**). This could enhance total secretory output only if cells have competent stimulus-secretion coupling and appears to consistently elevate basal secretion in all appropriate β-cell Cab45-deficient models (**Figures 27, 34 and 41**). Differences in prohormone conversion and basal and stimulated release of proinsulin should be directly assessed in all models to solidify these phenotypes, since dysregulated proinsulin exit via the constitutive pathway has not yet been ruled out. Moreover, excess proportional release of mature insulin in the absence of a difference in total insulin secretion could contribute to the development of mild insulin resistance, accounting for slightly impaired glucose intolerance in βCab45KO mice (**Figures 37-40**).

Depletion of Cab45 could alter the ionic properties of the secretory pathway to drive the changes in SG composition and protein processing. In Cab45KO cells, the absence of secretory pathway Ca^{2+} quenching by endogenous Cab45 could allow the provision of more Ca^{2+} to drive dense packaging of secretory cargoes into individual granules and enhance endoprotease activation, reducing SG size during the maturation process and contributing to an elevated basal secretion. Measuring unbound and total Ca^{2+} throughout the Golgi apparatus and within insulin SG should advance this theory. The converse is that the presence of Cab45 could function to reduce insulin secretory output (**Figures 25 and 35**). In the MIN6 KO model, Cab45 overexpression and appropriate localisation to the Golgi apparatus has a mild effect on reducing secretory output (**Figure 35**), but the robust occupation of insulin SGs in the INS1 KO model appears to exacerbate the phenotype by achieving complete secretory rescue despite low transfection efficiency (**Figures 22, 23 and 25**). This does not appear to occur via preventing granule fusion with the PM since overexpressed Cab45 is readily released from the WT INS1 cells during glucose stimulation (**Figure 17**). To speculate, Cab45 overexpression could drive the generation of more granules but reduce insulin content on a per-granule basis, simultaneously reducing secretory output and rescuing SG abundance (**Figures 23, 25 and 35**). Live-cell imaging of extracellular dye uptake coupled with fluorescently labelled insulin (Low et al. 2014) could be used to assess parameters of SG-PM fusion, which would provide insight into the effect that altered granule composition has on cargo release. Again, individual human variation in SG occupation by Cab45 (**Figure 11**) could have positive or negative effects based on the systemic metabolic context that is being experienced by the islet β-cells.

Further evidence that SG composition is altered in the absence of endogenous Cab45 is provided by comparing two separate experiments conducted in independent laboratories that used precisely the same condition of control. In WT (**Figure 17**) versus KO (**Figure 23**) INS1 cells, 6EQ Cab45HA is differentially localised. Specifically, 6EQ Cab45HA is mostly retained within the Golgi

apparatus of WT INS1 cells (**Figure 17**) but is broadly distributed throughout the cell periphery in KO INS1 cells (**Figure 23**). As stated, these observations were found in separate experimental settings conducted in different laboratories, but in either case, WT Cab45HA served as a neat control by reproducibly occupying insulin SGs. In contrast to ionomycin-induced Ca^{2+}-depletion (**Figure 16**), both of these cell lines contain a stable, uninterrupted population of interacting proteins, but the presence or absence of endogeneous Cab45 could be the differentiating factor here. 6EQ Cab45HA should not be able to rectify changes to secretory pathway Ca^{2+} concentration and/or distribution that may result from endogenous Cab45 depletion; thus, if the composition of SGs in Cab45KO cell lines are in fact altered, this could determine the landscape of endogenous Cab45 interacting proteins to explain differential 6EQ Cab45HA localisation. Further experiments to compare the concentration of bound and unbound Ca^{2+} through various sites along the secretory pathway in WT versus Cab45KO cells will be critical for substantiating this theory. This would lend a deep sense of insight and appreciation into the molecular processes that fine-tune the composition of the insulin SG. Considering the power of insulin within the broad context of metabolic health and disease, the identification of factors that control the intragranular environment and the detail of how they do so could inspire novel therapeutics and strategies to combat T2D. This would be especially helpful if such alterations are found to be a common occurrence amongst the plethora of humans experiencing this disease.

4.5 Proposed Mechanism of Cab45-Dependent Trafficking in β-cells

The mechanism by which Cab45 regulates SG biogenesis could expand models of protein trafficking in specialised secretory cells. At this stage, the proposed model has been pieced together by separate observations and therefore requires rigorous experimental substantiation (**Figure 47**). *Cis*-Golgi localisation of Cab45 would necessitate that the process begins with protein-protein interactions occurring prior to the TGN. Indeed, TGN-based sorting of SG-resident proteins in the β-cell are poorly defined, but events that occur in the early Golgi apparatus are even less so. SG biogenesis could originate in the *cis*-Golgi where a built up population of Cab45 protein meets a steady influx of SG-destined proteins arriving from the ER. Upon arrival, specific interacting proteins could bind to and, in combination with Fam20C-mediated phosphorylation, mobilise a small proportion of Cab45 from its high-molecular weight oligomeric retention strategy. En route to the TGN cargoes will naturally aggregate, but the presence of Cab45 and its interaction with Ca^{2+} accelerates their collective transit toward the TGN. At the TGN, the SG-destined proteins are sorted by entry through the various mechanisms reviewed earlier, and ISG-based sorting mechanisms remove monomeric or low-molecular weight oligomeric Cab45 from the maturing granule. In this way, a protein that resides in the *cis*-Golgi could venture out to drive cargo trafficking into ISGs, fitting a refined model of protein trafficking by bulk-flow.

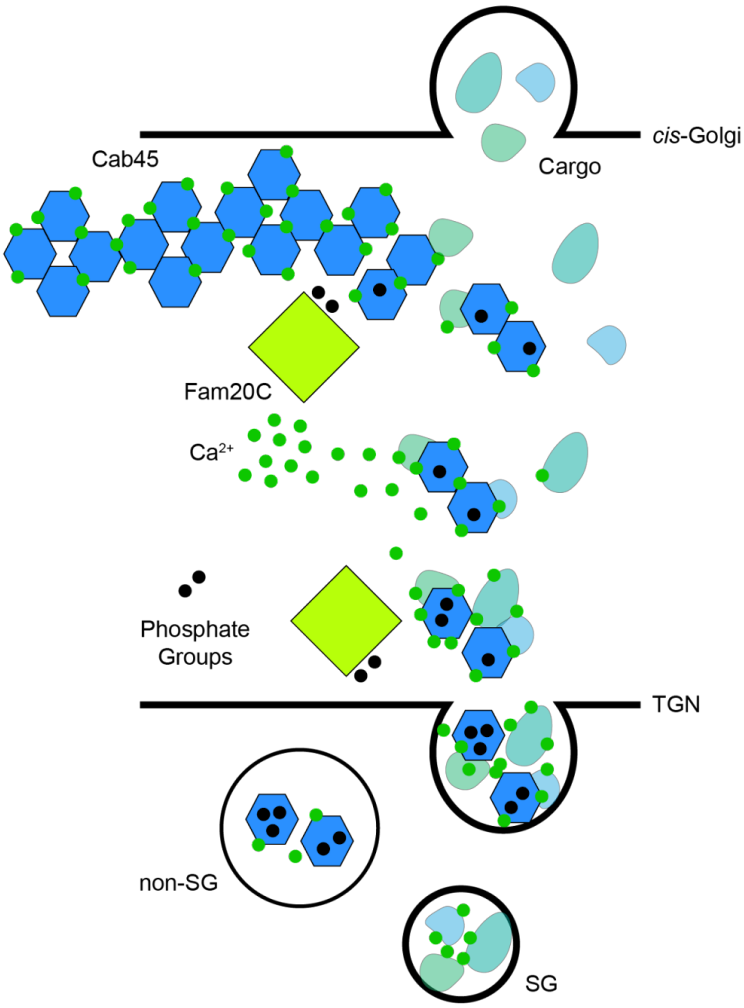

Figure 47. Proposed mechanism of Cab45-dependent secretory cargo trafficking in β-cells.

4.5 Conclusion

When there is heightened demand for insulin, Cab45 protein is elevated in the β-cell. Functionally, this appears to drive cargo transit for the synthesis of more insulin. On the other side of the coin, the inability of overwhelmed β-cells to secrete enough insulin during T2D is invariably connected to changes in Cab45 abundance and/or distribution. The evidence presented in this thesis moves the field one step forward in defining mechanisms of SG biogenesis in both β-cells and specialised secretory cells in general, and implicates Cab45 as a protein that has an important role in the context of metabolic health and disease via its control over insulin biogenesis and secretion.

(Page intentionally left blank)

References

Alarcon, C., B. Boland, Y. Uchizono, P. Moore, B. Peterson, S. Rajan, O. Rhodes, et al. 2016. "Pancreatic β-Cell Adaptive Plasticity in Obesity Increases Insulin Production but Adversely Affects Secretory Function." *Diabetes* 65 (2): 438–50.

Alarcón, C., J. L. Leahy, G. T. Schuppin, and C. J. Rhodes. 1995. "Increased Secretory Demand rather than a Defect in the Proinsulin Conversion Mechanism Causes Hyperproinsulinemia in a Glucose-Infusion Rat Model of Non-Insulin-Dependent Diabetes Mellitus." *The Journal of Clinical Investigation* 95 (3): 1032–39.

Arias, A., C. Vélez-Granell, G. Mayer, and M. Bendayan. 2000. "Colocalization of Chaperone Cpn60, Proinsulin and Convertase PC1 within Immature Secretory Granules of Insulin-Secreting Cells Suggests a Role for Cpn60 in Insulin Processing." *Journal of Cell Science* 113 (Pt 11) (June): 2075–83.

Arvan, P., and D. Castle. 1998. "Sorting and Storage during Secretory Granule Biogenesis: Looking Backward and Looking Forward." *Biochemical Journal* 332 (Pt 3) (June): 593–610.

Arvan, P., and P. Halban. 2004. "Sorting Ourselves out: Seeking Consensus on Trafficking in the Beta-Cell." *Traffic* 5 (1): 53–61.

Arvan, P., R. Kuliawat, D. Prabakaran, A. Zavacki, D. Elahi, S. Wang, and D. Pilkey. 1991. "Protein Discharge from Immature Secretory Granules Displays Both Regulated and Constitutive Characteristics." *The Journal of Biological Chemistry* 266 (22): 14171–74.

Bafaro, E., Y. Liu, Y. Xu, and R. Dempski. 2017. "The Emerging Role of Zinc Transporters in Cellular Homeostasis and Cancer." *Signal Transduction and Targeted Therapy* 2 (July). https://doi.org/10.1038/sigtrans.2017.29.

Bailyes, E., D. Bennett, and J. Hutton. 1991. "Proprotein-Processing Endopeptidases of the Insulin Secretory Granule." *Enzyme* 45 (5-6): 301–13.

Baker, Edward N., Thomas Leon Blundell, John F. Cutfield, Eleanor Joy Dodson, George Guy Dodson, Dorothy Mary Crowfoot Hodgkin, Roderick E. Hubbard, et al. 1988. "The Structure of 2Zn Pig Insulin Crystals at 1.5 Å Resolution." *Philosophical Transactions of the Royal Society of London. Series B, Biological Sciences* 319 (1195): 369–456.

Banaszak, M., I. Górna, and J. Przysławski. 2021. "Zinc and the Innovative Zinc-α2-Glycoprotein Adipokine Play an Important Role in Lipid Metabolism: A Critical Review." *Nutrients* 13 (6). https://doi.org/10.3390/nu13062023.

Banerjee, S., and P. Kane. 2020. "Regulation of V-ATPase Activity and Organelle pH by Phosphatidylinositol Phosphate Lipids." *Frontiers in Cell and Developmental Biology* 8 (June): 510.

Barbero, P., and P. Kitabgi. 1999. "Protein 7B2 Is Essential for the Targeting and Activation of PC2 into the Regulated Secretory Pathway of rMTC 6-23 Cells." *Biochemical and Biophysical Research Communications* 257 (2): 473–79.

Barg, S., P. Huang, L. Eliasson, D. Nelson, S. Obermüller, P. Rorsman, F. Thévenod, and E. Renström. 2001. "Priming of Insulin Granules for Exocytosis by Granular Cl(-) Uptake and Acidification." *Journal of Cell Science* 114 (Pt 11): 2145–54.

Barragán-Álvarez, C., E. Padilla-Camberos, N. Díaz, A. Cota-Coronado, C. Hernández-Jiménez, C. Bravo-Reyna, and N. Díaz-Martínez. 2021. "Loss of Znt8 Function in Diabetes Mellitus: Risk or Benefit?" *Molecular and Cellular Biochemistry*, March. https://doi.org/10.1007/s11010-021-04114-4.

Bartolomucci, A., R. Possenti, S. Mahata, R. Fischer-Colbrie, P. Loh, and S. Salton. 2011. "The Extended Granin Family: Structure, Function, and Biomedical Implications." *Endocrine Reviews* 32 (6): 755–97.

Bearrows, S., C. Bauchle, M. Becker, J. Haldeman, S. Swaminathan, and S. Stephens. 2019. "Chromogranin B Regulates Early-Stage Insulin Granule Trafficking from the Golgi in Pancreatic Islet β-Cells." *Journal of Cell Science* 132 (13). https://doi.org/10.1242/jcs.231373.

Bellomo, E., G. Meur, and G. Rutter. 2011. “Glucose Regulates Free Cytosolic Zn^{2+} Concentration, Slc39 (ZiP), and Metallothionein Gene Expression in Primary Pancreatic Islet β-Cells.” *The Journal of Biological Chemistry* 286 (29): 25778–89.

Benjannet, S., A. M. Mamarbachi, J. Hamelin, D. Savaria, J. S. Munzer, M. Chrétien, and N. G. Seidah. 1998. “Residues Unique to the pro-Hormone Convertase PC2 Modulate Its Autoactivation, Binding to 7B2 and Enzymatic Activity.” *FEBS Letters* 428 (1-2): 37–42.

Benjannet, S., N. Rondeau, R. Day, M. Chrétien, and N. G. Seidah. 1991. “PC1 and PC2 Are Proprotein Convertases Capable of Cleaving Proopiomelanocortin at Distinct Pairs of Basic Residues.” *Proceedings of the National Academy of Sciences of the United States of America* 88 (9): 3564–68.

Benjannet, S., N. Rondeau, L. Paquet, A. Boudreault, C. Lazure, M. Chrétien, and N. G. Seidah. 1993. “Comparative Biosynthesis, Covalent Post-Translational Modifications and Efficiency of Prosegment Cleavage of the Prohormone Convertases PC1 and PC2: Glycosylation, Sulphation and Identification of the Intracellular Site of Prosegment Cleavage of PC1 and PC2.” *Biochemical Journal* 294 (Pt 3) (September): 735–43.

Benjannet, S., D. Savaria, M. Chrétien, and N. G. Seidah. 1995. “7B2 Is a Specific Intracellular Binding Protein of the Prohormone Convertase PC2.” *Journal of Neurochemistry* 64 (5): 2303–11.

Billings, Liana K., and Jose C. Florez. 2010. “The Genetics of Type 2 Diabetes: What Have We Learned from GWAS?” *Annals of the New York Academy of Sciences* 1212 (November): 59–77.

Binger, Katrina J., Martin Neukam, Sudhir Gopal Tattikota, Fatimunnisa Qadri, Dmytro Puchkov, Diana M. Willmes, Sabrina Wurmsee, et al. 2019. “Atp6ap2 Deletion Causes Extensive Vacuolation That Consumes the Insulin Content of Pancreatic β Cells.” *Proceedings of the National Academy of Sciences of the United States of America* 116 (40): 19983–88.

Blackmore, C. G., A. Varro, R. Dimaline, L. Bishop, D. V. Gallacher, and G. J. Dockray. 2001. “Measurement of Secretory Vesicle pH Reveals Intravesicular Alkalinization by Vesicular Monoamine Transporter Type 2 Resulting in Inhibition of Prohormone Cleavage.” *The Journal of Physiology* 531 (Pt 3): 605–17.

Blank, Birgit, and Julia von Blume. 2017. “Cab45-Unraveling Key Features of a Novel Secretory Cargo Sorter at the Trans-Golgi Network.” *European Journal of Cell Biology* 96 (5): 383–90.

Blázquez, M., K. Docherty, and K. I. Shennan. 2001. “Association of Prohormone Convertase 3 with Membrane Lipid Rafts.” *Journal of Molecular Endocrinology* 27 (1): 107–16.

Blázquez, M., C. Thiele, W. B. Huttner, K. Docherty, and K. I. Shennan. 2000. “Involvement of the Membrane Lipid Bilayer in Sorting Prohormone Convertase 2 into the Regulated Secretory Pathway.” *Biochemical Journal* 349 Pt 3 (August): 843–52.

Blondel, O., M. M. Moody, A. M. Depaoli, A. H. Sharp, C. A. Ross, H. Swift, and G. I. Bell. 1994. “Localization of Inositol Trisphosphate Receptor Subtype 3 to Insulin and Somatostatin Secretory Granules and Regulation of Expression in Islets and Insulinoma Cells.” *Proceedings of the National Academy of Sciences of the United States of America* 91 (16): 7777–81.

Blume, Julia von, Anne-Marie Alleaume, Gerard Cantero-Recasens, Amy Curwin, Amado Carreras-Sureda, Timo Zimmermann, Josse van Galen, Yuichi Wakana, Miguel Angel Valverde, and Vivek Malhotra. 2011. “ADF/cofilin Regulates Secretory Cargo Sorting at the TGN via the Ca2+ ATPase SPCA1.” *Developmental Cell* 20 (5): 652–62.

Blume, Julia von, Anne-Marie Alleaume, Christine Kienzle, Amado Carreras-Sureda, Miguel Valverde, and Vivek Malhotra. 2012. “Cab45 Is Required for Ca(2+)-Dependent Secretory Cargo Sorting at the Trans-Golgi Network.” *The Journal of Cell Biology* 199 (7): 1057–66.

Blume, Julia von, Juan M. Duran, Elena Forlanelli, Anne-Marie Alleaume, Mikhail Egorov, Roman Polishchuk, Henrik Molina, and Vivek Malhotra. 2009. “Actin Remodeling by ADF/cofilin Is Required for Cargo Sorting at the Trans-Golgi Network.” *The Journal of Cell Biology* 187 (7): 1055–69.

Blume, Julia von, and Angelika Hausser. 2019. “Lipid-Dependent Coupling of Secretory Cargo Sorting and Trafficking at the Trans-Golgi Network.” *FEBS Letters* 593 (17): 2412–27.

Bogan, Jonathan S., Yingke Xu, and Mingming Hao. 2012. “Cholesterol Accumulation Increases Insulin Granule Size and Impairs Membrane Trafficking.” *Traffic* 13 (11): 1466–80.

Boland, Brandon B., Charles Brown Jr, Cristina Alarcon, Damien Demozay, Joseph S. Grimsby, and Christopher J. Rhodes. 2018. “β-Cell Control of Insulin Production During Starvation-Refeeding in Male Rats.” *Endocrinology* 159 (2): 895–906.

Boudreault, Alain, Dany Gauthier, and Claude Lazure. 1998. “Proprotein Convertase PC1/3-Related Peptides Are Potent Slow Tight-Binding Inhibitors of Murine PC1/3 and Hfurin*.” *The Journal of Biological Chemistry* 273 (47): 31574–80.

Bousquet-Moore, Danielle, Richard E. Mains, and Betty A. Eipper. 2010. “Peptidylglycine α-Amidating Monooxygenase and Copper: A Gene-Nutrient Interaction Critical to Nervous System Function.” *Journal of Neuroscience Research* 88 (12): 2535–45.

Bradbury, A. F., M. D. Finnie, and D. G. Smyth. 1982. “Mechanism of C-Terminal Amide Formation by Pituitary Enzymes.” *Nature* 298 (5875): 686–88.

Braks, J. A., A. M. Van Horssen, and G. J. Martens. 1996. “Dissociation of the Complex between the Neuroendocrine Chaperone 7B2 and Prohormone Convertase PC2 Is Not Associated with proPC2 Maturation.” *European Journal of Biochemistry / FEBS* 238 (2): 505–10.

Brender, Jeffrey R., Kevin Hartman, Ravi Prakash Reddy Nanga, Nataliya Popovych, Roberto de la Salud Bea, Subramanian Vivekanandan, E. Neil G. Marsh, and Ayyalusamy Ramamoorthy. 2010. “Role of Zinc in Human Islet Amyloid Polypeptide Aggregation.” *Journal of the American Chemical Society* 132 (26): 8973–83.

Brender, Jeffrey R., Edgar L. Lee, Marchello A. Cavitt, Ari Gafni, Duncan G. Steel, and Ayyalusamy Ramamoorthy. 2008. “Amyloid Fiber Formation and Membrane Disruption Are Separate Processes Localized in Two Distinct Regions of IAPP, the Type-2-Diabetes-Related Peptide.” *Journal of the American Chemical Society* 130 (20): 6424–29.

Brender, Jeffrey R., Samer Salamekh, and Ayyalusamy Ramamoorthy. 2012. “Membrane Disruption and Early Events in the Aggregation of the Diabetes Related Peptide IAPP from a Molecular Perspective.” *Accounts of Chemical Research* 45 (3): 454–62.

Brouwers, Bas, Ilaria Coppola, Katlijn Vints, Bastian Dislich, Nathalie Jouvet, Leentje Van Lommel, Charlotte Segers, et al. 2021. “Loss of Furin in β-Cells Induces an mTORC1-ATF4 Anabolic Pathway That Leads to β-Cell Dysfunction.” *Diabetes* 70 (2): 492–503.

Brouwers, Bas, Geoffroy de Faudeur, Anna B. Osipovich, Lotte Goyvaerts, Katleen Lemaire, Leen Boesmans, Elisa J. G. Cauwelier, et al. 2014. “Impaired Islet Function in Commonly Used Transgenic Mouse Lines due to Human Growth Hormone Minigene Expression.” *Cell Metabolism* 20 (6): 979–90.

Bundgaard, Hans, and Anne H. Kahns. 1991. “Chemical Stability and Plasma-Catalyzed Dealkylation of Peptidyl-α-Hydroxyglycine derivatives—Intermediates in Peptide α-Amidation.” *Peptides* 12 (4): 745–48.

Carmon, Ophélie, Fanny Laguerre, Lina Riachy, Charlène Delestre-Delacour, Qili Wang, Emeline Tanguy, Lydie Jeandel, et al. 2020. “Chromogranin A Preferential Interaction with Golgi Phosphatidic Acid Induces Membrane Deformation and Contributes to Secretory Granule Biogenesis.” *FASEB Journal: Official Publication of the Federation of American Societies for Experimental Biology*, March. https://doi.org/10.1096/fj.202000074R.

Carroll, R. J., R. E. Hammer, S. J. Chan, H. H. Swift, A. H. Rubenstein, and D. F. Steiner. 1988. “A Mutant Human Proinsulin Is Secreted from Islets of Langerhans in Increased Amounts via an Unregulated Pathway.” *Proceedings of the National Academy of Sciences of the United States of America* 85 (23): 8943–47.

Cauchi, Stéphane, Kevin T. Nead, Hélène Choquet, Fritz Horber, Natascha Potoczna, Beverley Balkau, Michel Marre, Guillaume Charpentier, Philippe Froguel, and David Meyre. 2008. “The Genetic Susceptibility to Type 2 Diabetes May Be Modulated by Obesity Status: Implications for Association Studies.” *BMC Medical Genetics* 9 (May): 45.

Chanat, E., and W. B. Huttner. 1991. “Milieu-Induced, Selective Aggregation of Regulated Secretory Proteins in the Trans-Golgi Network.” *The Journal of Cell Biology* 115 (6): 1505–19.

Chang, Guoying, Rui Yang, Yanan Cao, Aifang Nie, Xuefan Gu, and Huiwen Zhang. 2016. “SIDT2 Is Involved in the NAADP-Mediated Release of Calcium from Insulin Secretory Granules.” *Journal of Molecular Endocrinology* 56 (3): 249–59.

Chan, S. J., S. Seino, P. A. Gruppuso, R. Schwartz, and D. F. Steiner. 1987. “A Mutation in the B Chain Coding Region Is Associated with Impaired Proinsulin Conversion in a Family with Hyperproinsulinemia.” *Proceedings of the National Academy of Sciences of the United States of America* 84 (8): 2194–97.

Chen, L., S. Xu, L. Liu, X. Wen, Y. Xu, J. Chen, and J. Teng. 2014. “Cab45S Inhibits the ER Stress-Induced IRE1-JNK Pathway and Apoptosis via GRP78/BiP.” *Cell Death & Disease* 5 (May): e1219.

Chen, L., S. Xu, Y. Xu, W. Lu, L. Liu, D. Yue, J. Teng, and J. Chen. 2016. “Cab45S Promotes Cell Proliferation through SERCA2b Inhibition and Ca2+ Signaling.” *Oncogene* 35 (1): 35–46.

Chen, Yi-Chun, Richard E. Mains, Betty A. Eipper, Brad G. Hoffman, Traci A. Czyzyk, John E. Pintar, and C. Bruce Verchere. 2020. “PAM Haploinsufficiency Does Not Accelerate the Development of Diet- and Human IAPP-Induced Diabetes in Mice.” *Diabetologia* 63 (3): 561–76.

Chen, Yi-Chun, Austin J. Taylor, and C. Bruce Verchere. 2018. “Islet Prohormone Processing in Health and Disease.” *Diabetes, Obesity & Metabolism* 20 Suppl 2 (September): 64–76.

Chufán, Eduardo E., Mithu De, Betty A. Eipper, Richard E. Mains, and L. Mario Amzel. 2009. “Amidation of Bioactive Peptides: The Structure of the Lyase Domain of the Amidating Enzyme.” *Structure* 17 (7): 965–73.

Chu, Kwan Yi, Meredith J. L. Briggs, Tobias Albrecht, Peter F. Drain, and James D. Johnson. 2011. “Differential Regulation and Localization of Carboxypeptidase D and Carboxypeptidase E in Human and Mouse β-Cells.” *Islets* 3 (4): 155–65.

Chung, Ji-Hyun, Robert L. Lester, and Robert C. Dickson. 2003. “Sphingolipid Requirement for Generation of a Functional V1 Component of the Vacuolar ATPase*.” *The Journal of Biological Chemistry* 278 (31): 28872–81.

Clark, P. M., J. C. Levy, L. Cox, M. Burnett, R. C. Turner, and C. N. Hales. 1992. “Immunoradiometric Assay of Insulin, Intact Proinsulin and 32-33 Split Proinsulin and Radioimmunoassay of Insulin in Diet-Treated Type 2 (non-Insulin-Dependent) Diabetic Subjects.” *Diabetologia* 35 (5): 469–74.

Cool, D. R., E. Normant, F. Shen, H. C. Chen, L. Pannell, Y. Zhang, and Y. P. Loh. 1997. “Carboxypeptidase E Is a Regulated Secretory Pathway Sorting Receptor: Genetic Obliteration Leads to Endocrine Disorders in Cpe(fat) Mice.” *Cell* 88 (1): 73–83.

Cooper-Capetini, Vinícius, Diogo Antonio Alves de Vasconcelos, Amanda Roque Martins, Sandro Massao Hirabara, José Donato Jr, Angelo Rafael Carpinelli, and Fernando Abdulkader. 2017. “Zinc Supplementation Improves Glucose Homeostasis in High Fat-Fed Mice by Enhancing Pancreatic β-Cell Function.” *Nutrients* 9 (10). https://doi.org/10.3390/nu9101150.

Courel, Maïté, Alex Soler-Jover, Juan L. Rodriguez-Flores, Sushil K. Mahata, Salah Elias, Maïté Montero-Hadjadje, Youssef Anouar, Richard J. Giuly, Daniel T. O’Connor, and Laurent Taupenot. 2010. “Pro-Hormone Secretogranin II Regulates Dense Core Secretory Granule Biogenesis in Catecholaminergic Cells.” *The Journal of Biological Chemistry* 285 (13): 10030–43.

Courel, Maïté, Michael S. Vasquez, Vivian Y. Hook, Sushil K. Mahata, and Laurent Taupenot. 2008. “Sorting of the Neuroendocrine Secretory Protein Secretogranin II into the Regulated Secretory Pathway: Role of N- and C-Terminal Alpha-Helical Domains.” *The Journal of Biological Chemistry* 283 (17): 11807–22.

Courtade, Jaques A., Evan Y. Wang, Paul Yen, Derek L. Dai, Galina Soukhatcheva, Paul C. Orban, and C. Bruce Verchere. 2017. “Loss of Prohormone Convertase 2 Promotes Beta Cell Dysfunction in a Rodent Transplant Model Expressing Human pro-Islet Amyloid Polypeptide.” *Diabetologia* 60 (3): 453–63.

Crevenna, Alvaro H., Birgit Blank, Andreas Maiser, Derya Emin, Jens Prescher, Gisela Beck, Christine Kienzle, et al. 2016. “Secretory Cargo Sorting by Ca2+-Dependent Cab45 Oligomerization at the Trans-Golgi Network.” *The Journal of Cell Biology* 213 (3): 305–14.

Cross, Richard L., and Volker Müller. 2004. “The Evolution of A-, F-, and V-Type ATP Synthases and ATPases: Reversals in Function and Changes in the H+/ATP Coupling Ratio.” *FEBS Letters* 576 (1-2): 1–4.

Curry, D. L., L. L. Bennett, and G. M. Grodsky. 1968. “Dynamics of Insulin Secretion by the Perfused Rat Pancreas.” *Endocrinology* 83 (3): 572–84.
Dai, Feihan F., Alpana Bhattacharjee, Ying Liu, Battsetseg Batchuluun, Ming Zhang, Xinye Serena Wang, Xinyi Huang, et al. 2015. “A Novel GLP1 Receptor Interacting Protein ATP6ap2 Regulates Insulin Secretion in Pancreatic Beta Cells.” *The Journal of Biological Chemistry* 290 (41): 25045–61.
Daniels, Mark J., Maciej Jagielnicki, and Mark Yeager. 2020. “Structure/Function Analysis of Human ZnT8 (SLC30A8): A Diabetes Risk Factor and Zinc Transporter.” *Current Research in Structural Biology* 2 (June): 144–55.
Da Silva Xavier, Gabriela. 2018. “The Cells of the Islets of Langerhans.” *Journal of Clinical Medicine Research* 7 (3). https://doi.org/10.3390/jcm7030054.
Davidson, H. W., and J. C. Hutton. 1987. “The Insulin-Secretory-Granule Carboxypeptidase H. Purification and Demonstration of Involvement in Proinsulin Processing.” *Biochemical Journal* 245 (2): 575–82.
Davidson, H. W., C. J. Rhodes, and J. C. Hutton. 1988. “Intraorganellar Calcium and pH Control Proinsulin Cleavage in the Pancreatic Beta Cell via Two Distinct Site-Specific Endopeptidases.” *Nature* 333 (6168): 93–96.
Davidson, H. W., Janet M. Wenzlau, and Richard M. O’Brien. 2014. “Zinc Transporter 8 (ZnT8) and β Cell Function.” *Trends in Endocrinology and Metabolism: TEM* 25 (8): 415–24.
Demaurex, N., W. Furuya, S. D’Souza, J. S. Bonifacino, and S. Grinstein. 1998. “Mechanism of Acidification of the Trans-Golgi Network (TGN). In Situ Measurements of pH Using Retrieval of TGN38 and Furin from the Cell Surface.” *The Journal of Biological Chemistry* 273 (4): 2044–51.
Deng, Yongqiang, Mehrshad Pakdel, Birgit Blank, Emma L. Sundberg, Christopher G. Burd, and Julia von Blume. 2018. “Activity of the SPCA1 Calcium Pump Couples Sphingomyelin Synthesis to Sorting of Secretory Proteins in the Trans-Golgi Network.” *Developmental Cell* 47 (4): 464–78.e8.
Deriy, Ludmila V., Erwin A. Gomez, David A. Jacobson, Xueqing Wang, Jessika A. Hopson, Xiang Y. Liu, Guangping Zhang, Vytautas P. Bindokas, Louis H. Philipson, and Deborah J. Nelson. 2009. “The Granular Chloride Channel ClC-3 Is Permissive for Insulin Secretion.” *Cell Metabolism* 10 (4): 316–23.
Dhanvantari, Savita, Irina Arnaoutova, Chris R. Snell, Peter J. Steinbach, Kelli Hammond, Gregory A. Caputo, Erwin London, and Y. Peng Loh. 2002. “Carboxypeptidase E, a Prohormone Sorting Receptor, Is Anchored to Secretory Granules via a C-Terminal Transmembrane Insertion.” *Biochemistry* 41 (1): 52–60.
Diabetes Wisconsin. 2022. “Attie Lab Diabetes Database.” 2022. http://diabetes.wisc.edu/.
Dittié, A. S., J. Klumperman, and S. A. Tooze. 1999. “Differential Distribution of Mannose-6-Phosphate Receptors and Furin in Immature Secretory Granules.” *Journal of Cell Science* 112 (Pt 22) (November): 3955–66.
Dittié, A. S., L. Thomas, G. Thomas, and S. A. Tooze. 1997. “Interaction of Furin in Immature Secretory Granules from Neuroendocrine Cells with the AP-1 Adaptor Complex Is Modulated by Casein Kinase II Phosphorylation.” *The EMBO Journal* 16 (16): 4859–70.
Docherty, K., and J. C. Hutton. 1983. “Carboxypeptidase Activity in the Insulin Secretory Granule.” *FEBS Letters* 162 (1): 137–41.
Dwivedi, Om Prakash, Mikko Lehtovirta, Benoit Hastoy, Vikash Chandra, Nicole A. J. Krentz, Sandra Kleiner, Deepak Jain, et al. 2019. “Loss of ZnT8 Function Protects against Diabetes by Enhanced Insulin Secretion.” *Nature Genetics* 51 (11): 1596–1606.
Eipper, B. A., S. N. Perkins, E. J. Husten, R. C. Johnson, H. T. Keutmann, and R. E. Mains. 1991. “Peptidyl-Alpha-Hydroxyglycine Alpha-Amidating Lyase. Purification, Characterization, and Expression.” *The Journal of Biological Chemistry* 266 (12): 7827–33.
Ekholm, R., L. E. Ericson, and I. Lundquist. 1971. “Monoamines in the Pancreatic Islets of the Mouse. Subcellular Localization of 5-Hydroxytryptamine by Electron Microscopic Autoradiography.” *Diabetologia* 7 (5): 339–48.

Elias, Salah, Charlène Delestre, Stéphane Ory, Sébastien Marais, Maïté Courel, Rafael Vazquez-Martinez, Sophie Bernard, et al. 2012. “Chromogranin A Induces the Biogenesis of Granules with Calcium- and Actin-Dependent Dynamics and Exocytosis in Constitutively Secreting Cells.” *Endocrinology* 153 (9): 4444–56.

El Meskini, R., G. J. Galano, R. Marx, R. E. Mains, and B. A. Eipper. 2001. “Targeting of Membrane Proteins to the Regulated Secretory Pathway in Anterior Pituitary Endocrine Cells.” *The Journal of Biological Chemistry* 276 (5): 3384–93.

Ericson, L. E., R. Håkanson, and I. Lundquist. 1977. “Accumulation of Dopamine in Mouse Pancreatic B-Cells Following Injection of L-DOPA. Localization to Secretory Granules and Inhibition of Insulin Secretion.” *Diabetologia* 13 (2): 117–24.

Estall, Jennifer L., and Robert A. Screaton. 2020. “Of Mice and Men, Redux: Modern Challenges in β Cell Gene Targeting.” *Endocrinology*. https://doi.org/10.1210/endocr/bqaa078.

Fricker, L. D., B. Das, and R. H. Angeletti. 1990. “Identification of the pH-Dependent Membrane Anchor of Carboxypeptidase E (EC 3.4.17.10).” *The Journal of Biological Chemistry* 265 (5): 2476–82.

Furuta, M., R. Carroll, S. Martin, H. H. Swift, M. Ravazzola, L. Orci, and D. F. Steiner. 1998. “Incomplete Processing of Proinsulin to Insulin Accompanied by Elevation of Des-31,32 Proinsulin Intermediates in Islets of Mice Lacking Active PC2.” *The Journal of Biological Chemistry* 273 (6): 3431–37.

Gao, Jialin, Xuefan Gu, Don J. Mahuran, Zhugang Wang, and Huiwen Zhang. 2013. “Impaired Glucose Tolerance in a Mouse Model of sidt2 Deficiency.” *PloS One* 8 (6): e66139.

Garcia, Angelo L., Shan-Kuo Han, William G. Janssen, Zin Z. Khaing, Timothy Ito, Marc J. Glucksman, Deanna L. Benson, and Stephen R. J. Salton. 2005. “A Prohormone Convertase Cleavage Site within a Predicted α-Helix Mediates Sorting of the Neuronal and Endocrine Polypeptide VGF into the Regulated Secretory Pathway *.” *The Journal of Biological Chemistry* 280 (50): 41595–608.

Geisler, Jessica C., Kathryn L. Corbin, Qin Li, Andrew P. Feranchak, Craig S. Nunemaker, and Chien Li. 2013. “Vesicular Nucleotide Transporter-Mediated ATP Release Regulates Insulin Secretion.” *Endocrinology* 154 (2): 675–84.

Gerdes, H. H., P. Rosa, E. Phillips, P. A. Baeuerle, R. Frank, P. Argos, and W. B. Huttner. 1989. “The Primary Structure of Human Secretogranin II, a Widespread Tyrosine-Sulfated Secretory Granule Protein That Exhibits Low pH- and Calcium-Induced Aggregation.” *The Journal of Biological Chemistry* 264 (20): 12009–15.

Germanos, Mark, Andy Gao, Matthew Taper, Belinda Yau, and Melkam A. Kebede. 2021. “Inside the Insulin Secretory Granule.” *Metabolites* 11 (8). https://doi.org/10.3390/metabo11080515.

Gharanei, Seley, Malgorzata Zatyka, Dewi Astuti, Janine Fenton, Attila Sik, Zsuzsanna Nagy, and Timothy G. Barrett. 2013. “Vacuolar-Type H+-ATPase V1A Subunit Is a Molecular Partner of Wolfram Syndrome 1 (WFS1) Protein, Which Regulates Its Expression and Stability.” *Human Molecular Genetics* 22 (2): 203–17.

Giordano, T., C. Brigatti, P. Podini, E. Bonifacio, J. Meldolesi, and M. L. Malosio. 2008. “Beta Cell Chromogranin B Is Partially Segregated in Distinct Granules and Can Be Released Separately from Insulin in Response to Stimulation.” *Diabetologia* 51 (6): 997–1007.

Glombik, M. M., A. Krömer, T. Salm, W. B. Huttner, and H. H. Gerdes. 1999. “The Disulfide-Bonded Loop of Chromogranin B Mediates Membrane Binding and Directs Sorting from the Trans-Golgi Network to Secretory Granules.” *The EMBO Journal* 18 (4): 1059–70.

Gold, G., and G. M. Grodsky. 1984. “Kinetic Aspects of Compartmental Storage and Secretion of Insulin and Zinc.” *Experientia* 40 (10): 1105–14.

Greene, D., B. Das, and L. D. Fricker. 1992. “Regulation of Carboxypeptidase E. Effect of pH, Temperature and Co2+ on Kinetic Parameters of Substrate Hydrolysis.” *Biochemical Journal* 285 (Pt 2) (July): 613–18.

Grynkiewicz, G., M. Poenie, and R. Y. Tsien. 1985. “A New Generation of Ca2+ Indicators with Greatly Improved Fluorescence Properties.” *The Journal of Biological Chemistry* 260 (6): 3440–50.

Guest, P. C., S. D. Arden, N. G. Rutherford, and J. C. Hutton. 1995. “The Post-Translational Processing and Intracellular Sorting of Carboxypeptidase H in the Islets of Langerhans.” *Molecular and Cellular Endocrinology* 113 (1): 99–108.

Gurlo, Tatyana, Sergey Ryazantsev, Chang-Jiang Huang, Michael W. Yeh, Howard A. Reber, O. Joe Hines, Timothy D. O’Brien, Charles G. Glabe, and Peter C. Butler. 2010. “Evidence for Proteotoxicity in Beta Cells in Type 2 Diabetes: Toxic Islet Amyloid Polypeptide Oligomers Form Intracellularly in the Secretory Pathway.” *The American Journal of Pathology* 176 (2): 861–69.

Haataja, Leena, Tatyana Gurlo, Chang J. Huang, and Peter C. Butler. 2008. “Islet Amyloid in Type 2 Diabetes, and the Toxic Oligomer Hypothesis.” *Endocrine Reviews* 29 (3): 303–16.

Haataja, Leena, Erik Snapp, Jordan Wright, Ming Liu, Alexandre B. Hardy, Michael B. Wheeler, Michele L. Markwardt, Mark Rizzo, and Peter Arvan. 2013. “Proinsulin Intermolecular Interactions during Secretory Trafficking in Pancreatic β Cells.” *The Journal of Biological Chemistry* 288 (3): 1896–1906.

Halban, P. A. 1982. “Inhibition of Proinsulin to Insulin Conversion in Rat Islets Using Arginine and Lysine Analogs. Lack of Effect on Rate of Release of Modified Products.” *The Journal of Biological Chemistry* 257 (22): 13177–80.

Halban, P A. 1994. “Proinsulin Processing in the Regulated and the Constitutive Secretory Pathway.” *Diabetologia* 37 Suppl 2 (September): S65–72.

Halban, P. A., and Jean-Claude Irminger. 2003. “Mutant Proinsulin That Cannot Be Converted Is Secreted Efficiently from Primary Rat Beta-Cells via the Regulated Pathway.” *Molecular Biology of the Cell* 14 (3): 1195–1203.

Han, Lu, Masayuki Suda, Keisuke Tsuzuki, Rong Wang, Yoshihide Ohe, Hirokazu Hirai, Tsuyoshi Watanabe, Toshiyuki Takeuchi, and Masahiro Hosaka. 2008. “A Large Form of Secretogranin III Functions as a Sorting Receptor for Chromogranin A Aggregates in PC12 Cells.” *Molecular Endocrinology* 22 (8): 1935–49.

Harding, Jessica L., Meda E. Pavkov, Dianna J. Magliano, Jonathan E. Shaw, and Edward W. Gregg. 2019. “Global Trends in Diabetes Complications: A Review of Current Evidence.” *Diabetologia* 62 (1): 3–16.

Hardy, A. B., A. S. Serino, N. Wijesekara, F. Chimienti, and M. B. Wheeler. 2011. “Regulation of Glucagon Secretion by Zinc: Lessons from the β Cell-Specific Znt8 Knockout Mouse Model.” *Diabetes, Obesity & Metabolism* 13 Suppl 1 (October): 112–17.

Harney, Dylan J., Michelle Cielesh, Renee Chu, Kristen C. Cooke, David E. James, Jacqueline Stöckli, and Mark Larance. 2021. “Proteomics Analysis of Adipose Depots after Intermittent Fasting Reveals Visceral Fat Preservation Mechanisms.” *Cell Reports* 34 (9): 108804.

Hatanaka, Masayuki, Katsuya Tanabe, Akie Yanai, Yasuharu Ohta, Manabu Kondo, Masaru Akiyama, Koh Shinoda, Yoshitomo Oka, and Yukio Tanizawa. 2011. “Wolfram Syndrome 1 Gene (WFS1) Product Localizes to Secretory Granules and Determines Granule Acidification in Pancreatic Beta-Cells.” *Human Molecular Genetics* 20 (7): 1274–84.

Hecht, Tobias Karl-Heinz, Birgit Blank, Martin Steger, Victor Lopez, Gisela Beck, Bulat Ramazanov, Matthias Mann, Vincent Tagliabracci, and Julia von Blume. 2020. “Fam20C Regulates Protein Secretion by Cab45 Phosphorylation.” *The Journal of Cell Biology* 219 (6). https://doi.org/10.1083/jcb.201910089.

Henquin, Jean-Claude. 2021. “Paracrine and Autocrine Control of Insulin Secretion in Human Islets: Evidence and Pending Questions.” *American Journal of Physiology. Endocrinology and Metabolism* 320 (1): E78–86.

Henquin, Jean-Claude, Myriam Nenquin, Patrick Stiernet, and Bo Ahren. 2006. “In Vivo and in Vitro Glucose-Induced Biphasic Insulin Secretion in the Mouse: Pattern and Role of Cytoplasmic Ca2+ and Amplification Signals in Beta-Cells.” *Diabetes* 55 (2): 441–51.

Holliday, L. Shannon. 2014. “Vacuolar H+-ATPase: An Essential Multitasking Enzyme in Physiology and Pathophysiology.” *New Journal of Science* 2014 (January). https://doi.org/10.1155/2014/675430.

Honoré, Bent. 2009. “The Rapidly Expanding CREC Protein Family: Members, Localization, Function, and Role in Disease.” *BioEssays: News and Reviews in Molecular, Cellular and Developmental Biology* 31 (3): 262–77.

Honore, Bent, and Henrik Vorum. 2000. “The CREC Family, a Novel Family of Multiple EF-Hand, Low-A, Nity Ca-Binding Proteins Localised to the Secretory Pathway of Mammalian Cells.” *FEBS Letters* 466: 11–18.

Hosaka, Masahiro, Masayuki Suda, Yuko Sakai, Tetsuro Izumi, Tsuyoshi Watanabe, and Toshiyuki Takeuchi. 2004. “Secretogranin III Binds to Cholesterol in the Secretory Granule Membrane as an Adapter for Chromogranin A.” *The Journal of Biological Chemistry* 279 (5): 3627–34.

Hosaka, Masahiro, Tsuyoshi Watanabe, Yuko Sakai, Takeshi Kato, and Toshiyuki Takeuchi. 2005. “Interaction between Secretogranin III and Carboxypeptidase E Facilitates Prohormone Sorting within Secretory Granules.” *Journal of Cell Science* 118 (Pt 20): 4785–95.

Hosaka, Masahiro, Tsuyoshi Watanabe, Yuko Sakai, Yasuo Uchiyama, and Toshiyuki Takeuchi. 2002. “Identification of a Chromogranin A Domain That Mediates Binding to Secretogranin III and Targeting to Secretory Granules in Pituitary Cells and Pancreatic Beta-Cells.” *Molecular Biology of the Cell* 13 (10): 3388–99.

Hotta, Kikuko, Masahiro Hosaka, Atsushi Tanabe, and Toshiyuki Takeuchi. 2009. “Secretogranin II Binds to Secretogranin III and Forms Secretory Granules with Orexin, Neuropeptide Y, and POMC.” *The Journal of Endocrinology* 202 (1): 111–21.

Huang, X. F., and P. Arvan. 1995. “Intracellular Transport of Proinsulin in Pancreatic Beta-Cells. Structural Maturation Probed by Disulfide Accessibility.” *The Journal of Biological Chemistry* 270 (35): 20417–23.

HuGeAMP. 2022. “T2D Knowledge Portal.” 2022. https://t2d.hugeamp.org/gene.html?gene=SDF4.

Huh, Yang Hoon, Soung Hoo Jeon, and Seung Hyun Yoo. 2003. “Chromogranin B-Induced Secretory Granule Biogenesis: Comparison with the Similar Role of Chromogranin A.” *The Journal of Biological Chemistry* 278 (42): 40581–89.

Huh, Yang Hoon, Ki Deok Kim, and Seung Hyun Yoo. 2007. “Comparison of and Chromogranin Effect on Inositol 1,4,5-Trisphosphate Sensitivity of Cytoplasmic and Nucleoplasmic Inositol 1,4,5-Trisphosphate receptor/Ca2+ Channels.” *Biochemistry* 46 (49): 14032–43.

Hull, Rebecca L., Gunilla T. Westermark, Per Westermark, and Steven E. Kahn. 2004. “Islet Amyloid: A Critical Entity in the Pathogenesis of Type 2 Diabetes.” *The Journal of Clinical Endocrinology and Metabolism* 89 (8): 3629–43.

Hummer, Blake H., Drew Maslar, Margarita Soltero-Gutierrez, Noah F. de Leeuw, and Cedric S. Asensio. 2020. “Differential Sorting Behavior for Soluble and Transmembrane Cargoes at the Trans-Golgi Network in Endocrine Cells.” *Molecular Biology of the Cell* 31 (3): 157–66.

Hur, Yong Suk, and Seung Hyun Yoo. 2015. “Distribution Profile of Inositol 1,4,5-Trisphosphate Receptor/Ca2+ Channels in α and β Cells of Pancreas: Dominant Localization in Secretory Granules and Common Error in Identification of Secretory Granule Membranes.” *Pancreas* 44 (1): 158–65.

Hussain, Syed Saad, Megan T. Harris, Alex J. B. Kreutzberger, Candice M. Inouye, Catherine A. Doyle, Anna M. Castle, Peter Arvan, and J. David Castle. 2018. “Control of Insulin Granule Formation and Function by the ABC Transporters ABCG1 and ABCA1 and by Oxysterol Binding Protein OSBP.” *Molecular Biology of the Cell* 29 (10): 1238–57.

Husten, E. J., and B. A. Eipper. 1994. “Purification and Characterization of PAM-1, an Integral Membrane Protein Involved in Peptide Processing.” *Archives of Biochemistry and Biophysics* 312 (2): 487–92.

Hutton, J. C. 1982. “The Internal pH and Membrane Potential of the Insulin-Secretory Granule.” *Biochemical Journal* 204 (1): 171–78.

Hutton, J. C., E. J. Penn, and M. Peshavaria. 1983. “Low-Molecular-Weight Constituents of Isolated Insulin-Secretory Granules. Bivalent Cations, Adenine Nucleotides and Inorganic Phosphate.” *Biochemical Journal* 210 (2): 297–305.

Hutton, J. C., and M. Peshavaria. 1982. “Proton-Translocating Mg2+-Dependent ATPase Activity in Insulin-Secretory Granules.” *Biochemical Journal* 204 (1): 161–70.

Hwang, J. R., and I. Lindberg. 2001. “Inactivation of the 7B2 Inhibitory CT Peptide Depends on a Functional Furin Cleavage Site.” *Journal of Neurochemistry* 79 (2): 437–44.

Inomoto, Chie, Shinobu Umemura, Noboru Egashira, Takeo Minematsu, Susumu Takekoshi, Yoshiko Itoh, Johbu Itoh, Laurent Taupenot, Daniel T. O'Connor, and R. Yoshiyuki Osamura. 2007. "Granulogenesis in Non-Neuroendocrine COS-7 Cells Induced by EGFP-Tagged Chromogranin A Gene Transfection: Identical and Distinct Distribution of CgA and EGFP." *The Journal of Histochemistry and Cytochemistry: Official Journal of the Histochemistry Society* 55 (5): 487–93.

Irminger, J. C., K. Meyer, and P. Halban. 1996. "Proinsulin Processing in the Rat Insulinoma Cell Line INS after Overexpression of the Endoproteases PC2 or PC3 by Recombinant Adenovirus." *Biochemical Journal* 320 (Pt 1) (November): 11–15.

Irminger, J. C., C. B. Verchere, K. Meyer, and P. A. Halban. 1997. "Proinsulin Targeting to the Regulated Pathway Is Not Impaired in Carboxypeptidase E-Deficient Cpefat/Cpefat Mice." *The Journal of Biological Chemistry* 272 (44): 27532–34.

Irminger, J. C., F. M. Vollenweider, M. Neerman-Arbez, and P. A. Halban. 1994. "Human Proinsulin Conversion in the Regulated and the Constitutive Pathways of Transfected AtT20 Cells." *The Journal of Biological Chemistry* 269 (3): 1756–62.

Jaikaran, Emma T. A. S., Melanie R. Nilsson, and Anne Clark. 2004. "Pancreatic Beta-Cell Granule Peptides Form Heteromolecular Complexes Which Inhibit Islet Amyloid Polypeptide Fibril Formation." *Biochemical Journal* 377 (Pt 3): 709–16.

James, David E., Jacqueline Stöckli, and Morris J. Birnbaum. 2021. "The Aetiology and Molecular Landscape of Insulin Resistance." *Nature Reviews. Molecular Cell Biology* 22 (11): 751–71.

Janciauskiene, S., S. Eriksson, E. Carlemalm, and B. Ahrén. 1997. "B Cell Granule Peptides Affect Human Islet Amyloid Polypeptide (IAPP) Fibril Formation in Vitro." *Biochemical and Biophysical Research Communications* 236 (3): 580–85.

Janson, J., R. H. Ashley, D. Harrison, S. McIntyre, and P. C. Butler. 1999. "The Mechanism of Islet Amyloid Polypeptide Toxicity Is Membrane Disruption by Intermediate-Sized Toxic Amyloid Particles." *Diabetes* 48 (3): 491–98.

Jentsch, Thomas J., Tanja Maritzen, Damien J. Keating, Anselm A. Zdebik, and Frank Thévenod. 2010. "ClC-3--a Granular Anion Transporter Involved in Insulin Secretion?" *Cell Metabolism*.

Johnson, James D. 2014. "A Practical Guide to Genetic Engineering of Pancreatic β-Cells in Vivo: Getting a Grip on RIP and MIP." *Islets* 6 (3): e944439.

Johnson, K. H., T. D. O'Brien, K. Jordan, and P. Westermark. 1989. "Impaired Glucose Tolerance Is Associated with Increased Islet Amyloid Polypeptide (IAPP) Immunoreactivity in Pancreatic Beta Cells." *The American Journal of Pathology* 135 (2): 245–50.

Jutras, I., N. G. Seidah, and T. L. Reudelhuber. 2000. "A Predicted Alpha -Helix Mediates Targeting of the Proprotein Convertase PC1 to the Regulated Secretory Pathway." *The Journal of Biological Chemistry* 275 (51): 40337–43.

Jutras, I., N. G. Seidah, T. L. Reudelhuber, and V. Brechler. 1997. "Two Activation States of the Prohormone Convertase PC1 in the Secretory Pathway." *The Journal of Biological Chemistry* 272 (24): 15184–88.

Kahn, S. E., and P. A. Halban. 1997. "Release of Incompletely Processed Proinsulin Is the Cause of the Disproportionate Proinsulinemia of NIDDM." *Diabetes* 46 (11): 1725–32.

Kane, P. M. 1995. "Disassembly and Reassembly of the Yeast Vacuolar H(+)-ATPase in Vivo." *The Journal of Biological Chemistry* 270 (28): 17025–32.

Kang, Taewook, Brandon B. Boland, Cristina Alarcon, Joseph S. Grimsby, Christopher J. Rhodes, and Martin R. Larsen. 2019. "Proteomic Analysis of Restored Insulin Production and Trafficking in Obese Diabetic Mouse Pancreatic Islets Following Euglycemia." *Journal of Proteome Research* 18 (9): 3245–58.

Kaufmann, J. E., J. C. Irminger, and P. A. Halban. 1995. "Sequence Requirements for Proinsulin Processing at the B-chain/C-Peptide Junction." *Biochemical Journal* 310 (Pt 3) (September): 869–74.

Kaufmann, J. E., J. C. Irminger, J. Mungall, and P. A. Halban. 1997. "Proinsulin Conversion in GH3 Cells after Coexpression of Human Proinsulin with the Endoproteases PC2 And/or PC3." *Diabetes* 46 (6): 978–82.

Kawasaki-Nishi, Shoko, Katherine Bowers, Tsuyoshi Nishi, Michael Forgac, and Tom H. Stevens. 2001. “The Amino-Terminal Domain of the Vacuolar Proton-Translocating ATPase a Subunit Controls Targeting and in Vivo Dissociation, and the Carboxyl-Terminal Domain Affects Coupling of Proton Transport and ATP Hydrolysis*.” *The Journal of Biological Chemistry* 276 (50): 47411–20.

Kennedy, Arion J., Kate L. J. Ellacott, Victoria L. King, and Alyssa H. Hasty. 2010. “Mouse Models of the Metabolic Syndrome.” *Disease Models & Mechanisms* 3 (3-4): 156–66.

Kettner, Carsten, Adam Bertl, Gerhard Obermeyer, Clifford Slayman, and Hermann Bihler. 2003. “Electrophysiological Analysis of the Yeast V-Type Proton Pump: Variable Coupling Ratio and Proton Shunt.” *Biophysical Journal* 85 (6): 3730–38.

Khemtémourian, Lucie, Elena Doménech, Jacques P. F. Doux, Martijn C. Koorengevel, and J. Antoinette Killian. 2011. “Low pH Acts as Inhibitor of Membrane Damage Induced by Human Islet Amyloid Polypeptide.” *Journal of the American Chemical Society* 133 (39): 15598–604.

Kienzle, Christine, Nirakar Basnet, Alvaro H. Crevenna, Gisela Beck, Bianca Habermann, Naoko Mizuno, and Julia von Blume. 2014. “Cofilin Recruits F-Actin to SPCA1 and Promotes Ca2+-Mediated Secretory Cargo Sorting.” *The Journal of Cell Biology* 206 (5): 635–54.

Kienzle, Christine, and Julia von Blume. 2014. “Secretory Cargo Sorting at the Trans-Golgi Network.” *Trends in Cell Biology* 24 (10): 584–93.

Kim, I., E. S. Kang, Y. S. Yim, S. J. Ko, S-H Jeong, J. H. Rim, Y. S. Kim, et al. 2011. “A Low-Risk ZnT-8 Allele (W325) for Post-Transplantation Diabetes Mellitus Is Protective against Cyclosporin A-Induced Impairment of Insulin Secretion.” *The Pharmacogenomics Journal* 11 (3): 191–98.

Kirchhoff, K., F. Machicao, A. Haupt, S. A. Schäfer, O. Tschritter, H. Staiger, N. Stefan, H-U Häring, and A. Fritsche. 2008. “Polymorphisms in the TCF7L2, CDKAL1 and SLC30A8 Genes Are Associated with Impaired Proinsulin Conversion.” *Diabetologia* 51 (4): 597–601.

Kiselar, Janna G., Manish Datt, Mark R. Chance, and Michael A. Weiss. 2011. “Structural Analysis of Proinsulin Hexamer Assembly by Hydroxyl Radical Footprinting and Computational Modeling.” *The Journal of Biological Chemistry* 286 (51): 43710–16.

Klemm, Robin W., Christer S. Ejsing, Michal A. Surma, Hermann-Josef Kaiser, Mathias J. Gerl, Julio L. Sampaio, Quentin de Robillard, et al. 2009. “Segregation of Sphingolipids and Sterols during Formation of Secretory Vesicles at the Trans-Golgi Network.” *The Journal of Cell Biology* 185 (4): 601–12.

Klumperman, J., A. Hille, T. Veenendaal, V. Oorschot, W. Stoorvogel, K. von Figura, and H. J. Geuze. 1993. “Differences in the Endosomal Distributions of the Two Mannose 6-Phosphate Receptors.” *The Journal of Cell Biology* 121 (5): 997–1010.

Klumperman, J., R. Kuliawat, J. M. Griffith, H. J. Geuze, and P. Arvan. 1998. “Mannose 6-Phosphate Receptors Are Sorted from Immature Secretory Granules via Adaptor Protein AP-1, Clathrin, and Syntaxin 6-Positive Vesicles.” *The Journal of Cell Biology* 141 (2): 359–71.

Kreutzberger, Alex J. B., Volker Kiessling, Catherine A. Doyle, Noah Schenk, Clint M. Upchurch, Margaret Elmer-Dixon, Amanda E. Ward, et al. 2020. “Distinct Insulin Granule Subpopulations Implicated in the Secretory Pathology of Diabetes Types 1 and 2.” *eLife* 9 (November). https://doi.org/10.7554/eLife.62506.

Kudva, Y. C., C. Mueske, P. C. Butler, and N. L. Eberhardt. 1998. “A Novel Assay in Vitro of Human Islet Amyloid Polypeptide Amyloidogenesis and Effects of Insulin Secretory Vesicle Peptides on Amyloid Formation.” *Biochemical Journal* 331 (Pt 3) (May): 809–13.

Kulathila, R., A. P. Consalvo, P. F. Fitzpatrick, J. C. Freeman, L. M. Snyder, J. J. Villafranca, and D. J. Merkler. 1994. “Bifunctional Peptidylglcine Alpha-Amidating Enzyme Requires Two Copper Atoms for Maximum Activity.” *Archives of Biochemistry and Biophysics* 311 (1): 191–95.

Kuliawat, R., and P. Arvan. 1992. “Protein Targeting via the ‘Constitutive-like’ Secretory Pathway in Isolated Pancreatic Islets: Passive Sorting in the Immature Granule Compartment.” *The Journal of Cell Biology* 118 (3): 521–29.

Kuliawat, R., and P. Arvan. 1994. “Distinct Molecular Mechanisms for Protein Sorting within Immature Secretory Granules of Pancreatic Beta-Cells.” *The Journal of Cell Biology* 126 (1): 77–86.

Kuliawat, R., J. Klumperman, T. Ludwig, and P. Arvan. 1997. “Differential Sorting of Lysosomal Enzymes out of the Regulated Secretory Pathway in Pancreatic Beta-Cells.” *The Journal of Cell Biology* 137 (3): 595–608.

Kumar, Dhivya, Richard E. Mains, and Betty A. Eipper. 2016. “60 YEARS OF POMC: From POMC and α-MSH to PAM, Molecular Oxygen, Copper, and Vitamin C.” *Journal of Molecular Endocrinology* 56 (4): T63–76.

Kyun-Hwan, Kim, and Seong Baik L. 2001. “Peptide Amidation: Production of Peptide Hormonesin Vivo Andin Vitro.” *Biotechnology and Bioprocess Engineering: BBE* 6 (4): 244–51.

Lafourcade, Céline, Komla Sobo, Sylvie Kieffer-Jaquinod, Jérome Garin, and F. Gisou van der Goot. 2008. “Regulation of the V-ATPase along the Endocytic Pathway Occurs through Reversible Subunit Association and Membrane Localization.” *PloS One* 3 (7): e2758.

Lamango, N. S., E. Apletalina, J. Liu, and I. Lindberg. 1999. “The Proteolytic Maturation of Prohormone Convertase 2 (PC2) Is a pH-Driven Process.” *Archives of Biochemistry and Biophysics* 362 (2): 275–82.

Lam, Patrick P. L., Kati Hyva Rinen, Maria Kauppi, Laura Cosen-Binker, Saara Laitinen, Sirkka Kera Nen, Herbert Y. Gaisano, and Vesa M. Olkkonen. 2007. “A Cytosolic Splice Variant of Cab45 Interacts with Munc18b and Impacts on Amylase Secretion by Pancreatic Acini.” https://doi.org/10.1091/mbc.E06.

Landreh, Michael, Gunvor Alvelius, Hanna Willander, Jan-Bernd Stukenborg, Olle Söder, Jan Johansson, and Hans Jörnvall. 2012. “Insulin Solubility Transitions by pH-Dependent Interactions with Proinsulin C-Peptide.” *The FEBS Journal* 279 (24): 4589–97.

Lara-Lemus, Roberto, Ming Liu, Mark D. Turner, Philipp Scherer, Gudrun Stenbeck, Puneeth Iyengar, and Peter Arvan. 2006. “Lumenal Protein Sorting to the Constitutive Secretory Pathway of a Regulated Secretory Cell.” *Journal of Cell Science* 119 (Pt 9): 1833–42.

Lee, Sang-Nam, and Iris Lindberg. 2008. “7B2 Prevents Unfolding and Aggregation of Prohormone Convertase 2.” *Endocrinology* 149 (8): 4116–27.

Lemaire, K., Fabrice Chimienti, and Frans Schuit. 2012. “Zinc Transporters and Their Role in the Pancreatic β-Cell.” *Journal of Diabetes Investigation* 3 (3): 202–11.

Lemaire, K., M. A. Ravier, A. Schraenen, J. W. M. Creemers, R. Van de Plas, M. Granvik, L. Van Lommel, et al. 2009. “Insulin Crystallization Depends on Zinc Transporter ZnT8 Expression, but Is Not Required for Normal Glucose Homeostasis in Mice.” *Proceedings of the National Academy of Sciences of the United States of America* 106 (35): 14872–77.

Li, Dai-Qing, Xingjun Jing, Albert Salehi, Stephan C. Collins, Michael B. Hoppa, Anders H. Rosengren, Enming Zhang, et al. 2009. “Suppression of Sulfonylurea- and Glucose-Induced Insulin Secretion in Vitro and in Vivo in Mice Lacking the Chloride Transport Protein ClC-3.” *Cell Metabolism* 10 (4): 309–15.

Lilla, Valérie, Gene Webb, Katharina Rickenbach, Andres Maturana, Donald F. Steiner, Philippe A. Halban, and Jean-Claude Irminger. 2003. “Differential Gene Expression in Well-Regulated and Dysregulated Pancreatic Beta-Cell (MIN6) Sublines.” *Endocrinology* 144 (4): 1368–79.

Linard, C. G., H. Tadros, F. Sirois, and M. Mbikay. 1995. “Calcium-Induced Aggregation of Neuroendocrine Protein 7B2 in Vitro and Its Modulation by ATP.” *Molecular and Cellular Biochemistry* 151 (1): 39–47.

Lin, Chia-Yu, Tatyana Gurlo, Rakez Kayed, Alexandra E. Butler, Leena Haataja, Charles G. Glabe, and Peter C. Butler. 2007. “Toxic Human Islet Amyloid Polypeptide (h-IAPP) Oligomers Are Intracellular, and Vaccination to Induce Anti-Toxic Oligomer Antibodies Does Not Prevent H-IAPP-Induced Beta-Cell Apoptosis in H-IAPP Transgenic Mice.” *Diabetes* 56 (5): 1324–32.

Liu, Ming, Roberto Lara-Lemus, Shu-Ou Shan, Jordan Wright, Leena Haataja, Fabrizio Barbetti, Huan Guo, Dennis Larkin, and Peter Arvan. 2012. “Impaired Cleavage of Preproinsulin Signal Peptide Linked to Autosomal-Dominant Diabetes.” *Diabetes* 61 (4): 828–37.

Louagie, Els, Neil A. Taylor, Daisy Flamez, Anton J. M. Roebroek, Nicholas A. Bright, Sandra Meulemans, Roel Quintens, et al. 2008. “Role of Furin in Granular Acidification in the Endocrine Pancreas: Identification of the V-ATPase Subunit Ac45 as a Candidate Substrate.” *Proceedings of the National Academy of Sciences of the United States of America* 105 (34): 12319–24.

Low, Jiun T., Michael Zavortink, Justin M. Mitchell, Wan J. Gan, Oanh Hoang Do, Christof J. Schwiening, Herbert Y. Gaisano, and Peter Thorn. 2014. “Insulin Secretion from Beta Cells in Intact Mouse Islets Is Targeted towards the Vasculature.” *Diabetologia* 57 (8): 1655–63.

Lubag, Angelo J. M., Luis M. De Leon-Rodriguez, Shawn C. Burgess, and A. Dean Sherry. 2011. “Noninvasive MRI of β-Cell Function Using a Zn2+-Responsive Contrast Agent.” *Proceedings of the National Academy of Sciences of the United States of America* 108 (45): 18400–405.

Lukinius, A., E. Wilander, G. T. Westermark, U. Engström, and P. Westermark. 1989. “Co-Localization of Islet Amyloid Polypeptide and Insulin in the B Cell Secretory Granules of the Human Pancreatic Islets.” *Diabetologia* 32 (4): 240–44.

Lundquist, I., R. Ekholm, and L. E. Ericson. 1971. “Monoamines in the Pancreatic Islets of the Mouse. 5-Hydroxytryptamine as an Intracellular Modifier of Insulin Secretion, and the Hypoglycaemic Action of Monoamine Oxidase Inhibitors.” *Diabetologia* 7 (6): 414–22.

Maeda, Yoshinori, Saki Kudo, Ken Tsushima, Eri Sato, Chisato Kubota, Aika Kayamori, Hiroki Bochimoto, et al. 2018. “Impaired Processing of Prohormones in Secretogranin III-Null Mice Causes Maladaptation to an Inadequate Diet and Stress.” *Endocrinology* 159 (2): 1213–27.

Magro, Maria Grazia, and Michele Solimena. 2013. “Regulation of β-Cell Function by RNA-Binding Proteins.” *Molecular Metabolism* 2 (4): 348–55.

Manialawy, Yousef, Saifur R. Khan, Alpana Bhattacharjee, and Michael B. Wheeler. 2020. “The Magnesium Transporter NIPAL1 Is a Pancreatic Islet-Expressed Protein That Conditionally Impacts Insulin Secretion.” *The Journal of Biological Chemistry*, May. https://doi.org/10.1074/jbc.RA120.013277.

Maritzen, Tanja, Damien J. Keating, Ioana Neagoe, Anselm A. Zdebik, and Thomas J. Jentsch. 2008. “Role of the Vesicular Chloride Transporter ClC-3 in Neuroendocrine Tissue.” *The Journal of Neuroscience: The Official Journal of the Society for Neuroscience* 28 (42): 10587–98.

Marshall, I. C., and C. W. Taylor. 1993. “Biphasic Effects of Cytosolic Ca2+ on Ins(1,4,5)P3-Stimulated Ca2+ Mobilization in Hepatocytes.” *The Journal of Biological Chemistry* 268 (18): 13214–20.

Marx, Ruth, and Richard E. Mains. 2002. “Routing of Membrane Proteins to Large Dense Core Vesicles in PC12 Cells.” *Journal of Molecular Neuroscience: MN* 18 (1-2): 113–27.

Marzban, Lucy, Galina Soukhatcheva, and C. Bruce Verchere. 2005. “Role of Carboxypeptidase E in Processing of Pro-Islet Amyloid Polypeptide in β-Cells.” *Endocrinology* 146 (4): 1808–17.

Marzban, Lucy, Genny Trigo-Gonzalez, and C. Bruce Verchere. 2005. “Processing of pro-Islet Amyloid Polypeptide in the Constitutive and Regulated Secretory Pathways of Beta Cells.” *Molecular Endocrinology* 19 (8): 2154–63.

Marzban, Lucy, Genny Trigo-Gonzalez, Xiaorong Zhu, Christopher J. Rhodes, Philippe A. Halban, Donald F. Steiner, and C. Bruce Verchere. 2004. “Role of Beta-Cell Prohormone Convertase (PC)1/3 in Processing of pro-Islet Amyloid Polypeptide.” *Diabetes* 53 (1): 141–48.

Masgrau, Roser, Grant C. Churchill, Anthony J. Morgan, Stephen J. H. Ashcroft, and Antony Galione. 2003. “NAADP: A New Second Messenger for Glucose-Induced Ca2+ Responses in Clonal Pancreatic Beta Cells.” *Current Biology: CB* 13 (3): 247–51.

Maxson, Michelle E., and Sergio Grinstein. 2014. “The Vacuolar-Type H^+-ATPase at a Glance - More than a Proton Pump.” *Journal of Cell Science* 127 (Pt 23): 4987–93.

McCombs, Janet E., and Amy E. Palmer. 2008. “Measuring Calcium Dynamics in Living Cells with Genetically Encodable Calcium Indicators.” *Methods* 46 (3): 152–59.

Merkler, D. J. 1994. “C-Terminal Amidated Peptides: Production by the in Vitro Enzymatic Amidation of Glycine-Extended Peptides and the Importance of the Amide to Bioactivity.” *Enzyme and Microbial Technology* 16 (6): 450–56.

Merriman, Chengfeng, Qiong Huang, Guy A. Rutter, and Dax Fu. 2016. “Lipid-Tuned Zinc Transport Activity of Human ZnT8 Protein Correlates with Risk for Type-2 Diabetes.” *The Journal of Biological Chemistry* 291 (53): 26950–57.

Mezza, Teresa, Pietro M. Ferraro, Vinsin A. Sun, Simona Moffa, Chiara M. A. Cefalo, Giuseppe Quero, Francesca Cinti, et al. 2018. “Increased β-Cell Workload Modulates Proinsulin-to-Insulin Ratio in Humans.” *Diabetes* 67 (11): 2389–96.

Michael, J., R. Carroll, H. H. Swift, and D. F. Steiner. 1987. “Studies on the Molecular Organization of Rat Insulin Secretory Granules.” *The Journal of Biological Chemistry* 262 (34): 16531–35.
Milgram, S. L., B. A. Eipper, and R. E. Mains. 1994. “Differential Trafficking of Soluble and Integral Membrane Secretory Granule-Associated Proteins.” *The Journal of Cell Biology* 124 (1-2): 33–41.
Milgram, S. L., R. C. Johnson, and R. E. Mains. 1992. “Expression of Individual Forms of Peptidylglycine Alpha-Amidating Monooxygenase in AtT-20 Cells: Endoproteolytic Processing and Routing to Secretory Granules.” *The Journal of Cell Biology* 117 (4): 717–28.
Milgram, S. L., R. E. Mains, and B. A. Eipper. 1993. “COOH-Terminal Signals Mediate the Trafficking of a Peptide Processing Enzyme in Endocrine Cells.” *The Journal of Cell Biology* 121 (1): 23–36.
Milgram, S. L., R. E. Mains, and B. A. Eipper. 1996. “Identification of Routing Determinants in the Cytosolic Domain of a Secretory Granule-Associated Integral Membrane Protein.” *The Journal of Biological Chemistry* 271 (29): 17526–35.
Mitchell, Kathryn J., F. Anthony Lai, and Guy A. Rutter. 2003. “Ryanodine Receptor Type I and Nicotinic Acid Adenine Dinucleotide Phosphate Receptors Mediate Ca2+ Release from Insulin-Containing Vesicles in Living Pancreatic Beta-Cells (MIN6).” *The Journal of Biological Chemistry* 278 (13): 11057–64.
Mitchell, Kathryn J., P. Pinton, A. Varadi, C. Tacchetti, E. K. Ainscow, T. Pozzan, R. Rizzuto, and G. A. Rutter. 2001. “Dense Core Secretory Vesicles Revealed as a Dynamic Ca(2+) Store in Neuroendocrine Cells with a Vesicle-Associated Membrane Protein Aequorin Chimaera.” *The Journal of Cell Biology* 155 (1): 41–51.
Mitchell, Kathryn J., Takashi Tsuboi, and Guy A. Rutter. 2004. “Role for Plasma Membrane-Related Ca2+-ATPase-1 (ATP2C1) in Pancreatic Beta-Cell Ca2+ Homeostasis Revealed by RNA Silencing.” *Diabetes* 53 (2): 393–400.
Mizuno, Kensaku. 2013. “Signaling Mechanisms and Functional Roles of Cofilin Phosphorylation and Dephosphorylation.” *Cellular Signalling* 25 (2): 457–69.
Molinete, M., J. C. Irminger, S. A. Tooze, and P. A. Halban. 2000. “Trafficking/sorting and Granule Biogenesis in the Beta-Cell.” *Seminars in Cell & Developmental Biology* 11 (4): 243–51.
Montero-Hadjadje, Maité, Salah Elias, Laurence Chevalier, Magalie Benard, Yannick Tanguy, Valérie Turquier, Ludovic Galas, et al. 2009. “Chromogranin A Promotes Peptide Hormone Sorting to Mobile Granules in Constitutively and Regulated Secreting Cells: Role of Conserved N- and C-Terminal Peptides.” *The Journal of Biological Chemistry* 284 (18): 12420–31.
Mosleh, Elham, Kristy Ou, Matthew W. Haemmerle, Teguru Tembo, Andrew Yuhas, Bethany A. Carboneau, Shannon E. Townsend, et al. 2020. “Ins1-Cre and Ins1-CreER Gene Replacement Alleles Are Susceptible To Silencing By DNA Hypermethylation.” *Endocrinology* 161 (8). https://doi.org/10.1210/endocr/bqaa054.
Moulin, Pierre, Yves Guiot, Jean-Christophe Jonas, Jacques Rahier, Olivier Devuyst, and Jean-Claude Henquin. 2007. “Identification and Subcellular Localization of the Na+/H+ Exchanger and a Novel Related Protein in the Endocrine Pancreas and Adrenal Medulla.” *Journal of Molecular Endocrinology* 38 (3): 409–22.
Muller, L., Angus Cameron, Yolanda Fortenberry, Ekaterina V. Apletalina, and Iris Lindberg. 2000. “Processing and Sorting of the Prohormone Convertase 2 Propeptide *.” *The Journal of Biological Chemistry* 275 (50): 39213–22.
Muller, L., X. Zhu, and I. Lindberg. 1997. “Mechanism of the Facilitation of PC2 Maturation by 7B2: Involvement in ProPC2 Transport and Activation but Not Folding.” *The Journal of Cell Biology* 139 (3): 625–38.
Nagao, Mototsugu, Jonathan L. S. Esguerra, Akira Asai, Jones K. Ofori, Anna Edlund, Anna Wendt, Hitoshi Sugihara, Claes B. Wollheim, Shinichi Oikawa, and Lena Eliasson. 2020. “Potential Protection Against Type 2 Diabetes in Obesity Through Lower CD36 Expression and Improved Exocytosis in β-Cells.” *Diabetes* 69 (6): 1193–1205.
Nakazato, M., M. Miyazato, J. Asai, T. Mitsukawa, K. Kangawa, H. Matsuo, and S. Matsukura. 1990. “Islet Amyloid Polypeptide, a Novel Pancreatic Peptide, Is a Circulating Hormone Secreted under Glucose Stimulation.” *Biochemical and Biophysical Research Communications* 169 (2): 713–18.

National Center for Biotechnology Information. 2022. “SDF4.” 2022. https://www.ncbi.nlm.nih.gov/gene/51150.
Natori, S., and W. B. Huttner. 1996. “Chromogranin B (secretogranin I) Promotes Sorting to the Regulated Secretory Pathway of Processing Intermediates Derived from a Peptide Hormone Precursor.” *Proceedings of the National Academy of Sciences of the United States of America* 93 (9): 4431–36.
Nedumpully-Govindan, Praveen, and Feng Ding. 2015. “Inhibition of IAPP Aggregation by Insulin Depends on the Insulin Oligomeric State Regulated by Zinc Ion Concentration.” *Scientific Reports* 5 (February): 8240.
Neerman-Arbez, M., V. Cirulli, and P. A. Halban. 1994. “Levels of the Conversion Endoproteases PC1 (PC3) and PC2 Distinguish between Insulin-Producing Pancreatic Islet Beta Cells and Non-Beta Cells.” *Biochemical Journal* 300 (Pt 1) (May): 57–61.
Neerman-Arbez, M., S. Sizonenko, and P. A. Halban. 1993. “Slow Cleavage at the Proinsulin B-Chain/connecting Peptide Junction Associated with Low Levels of Endoprotease PC1/3 in Transformed Beta Cells.” *The Journal of Biological Chemistry* 268 (22): 16098–100.
Nijpels, G., C. Popp-Snijders, P. J. Kostense, L. M. Bouter, and R. J. Heine. 1996. “Fasting Proinsulin and 2-H Post-Load Glucose Levels Predict the Conversion to NIDDM in Subjects with Impaired Glucose Tolerance: The Hoorn Study.” *Diabetologia* 39 (1): 113–18.
Normant, E., and Y. P. Loh. 1998. “Depletion of Carboxypeptidase E, a Regulated Secretory Pathway Sorting Receptor, Causes Misrouting and Constitutive Secretion of Proinsulin and Proenkephalin, but Not Chromogranin A.” *Endocrinology* 139 (4): 2137–45.
Norris, Nicholas, Belinda Yau, and Melkam Alamerew Kebede. 2021. “Isolation and Proteomics of the Insulin Secretory Granule.” *Metabolites* 11 (5). https://doi.org/10.3390/metabo11050288.
Norrman, Mathias, and Gerd Schluckebier. 2007. “Crystallographic Characterization of Two Novel Crystal Forms of Human Insulin Induced by Chaotropic Agents and a Shift in pH.” *BMC Structural Biology* 7 (December): 83.
Noushmehr, Houtan, Eugenio D’Amico, Loredana Farilla, Hongxiang Hui, Kolja A. Wawrowsky, Wojciech Mlynarski, Alessandro Doria, Nada A. Abumrad, and Riccardo Perfetti. 2005. “Fatty Acid Translocase (FAT/CD36) Is Localized on Insulin-Containing Granules in Human Pancreatic Beta-Cells and Mediates Fatty Acid Effects on Insulin Secretion.” *Diabetes* 54 (2): 472–81.
Obermüller, Stefanie, Federico Calegari, Angus King, Anders Lindqvist, Ingmar Lundquist, Albert Salehi, Maura Francolini, et al. 2010. “Defective Secretion of Islet Hormones in Chromogranin-B Deficient Mice.” *PloS One* 5 (1): e8936.
O’Halloran, Thomas V., Melkam Kebede, Steven J. Philips, and Alan D. Attie. 2013. “Zinc, Insulin, and the Liver: A Ménage à Trois.” *The Journal of Clinical Investigation*.
Ohsawa, H., A. Kanatsuka, T. Yamaguchi, H. Makino, and S. Yoshida. 1989. “Islet Amyloid Polypeptide Inhibits Glucose-Stimulated Insulin Secretion from Isolated Rat Pancreatic Islets.” *Biochemical and Biophysical Research Communications* 160 (2): 961–67.
Okita, Naoyuki, Yoshikazu Higami, Fumio Fukai, Masaki Kobayashi, Miku Mitarai, Takao Sekiya, and Takashi Sasaki. 2017. “Modified Western Blotting for Insulin and Other Diabetes-Associated Peptide Hormones.” *Scientific Reports* 7 (1): 6949.
Omar-Hmeadi, Muhmmad, and Olof Idevall-Hagren. 2020. “Insulin Granule Biogenesis and Exocytosis.” *Cellular and Molecular Life Sciences: CMLS*, November. https://doi.org/10.1007/s00018-020-03688-4.
Orci, L., P. Halban, M. Amherdt, M. Ravazzola, J. D. Vassalli, and A. Perrelet. 1984. “Nonconverted, Amino Acid Analog-Modified Proinsulin Stays in a Golgi-Derived Clathrin-Coated Membrane Compartment.” *The Journal of Cell Biology* 99 (6): 2187–92.
Orci, L., R. Montesano, P. Meda, F. Malaisse-Lagae, D. Brown, A. Perrelet, and P. Vassalli. 1981. “Heterogeneous Distribution of Filipin--Cholesterol Complexes across the Cisternae of the Golgi Apparatus.” *Proceedings of the National Academy of Sciences of the United States of America* 78 (1): 293–97.
Orci, L., M. Ravazzola, and A. Perrelet. 1984. “(Pro)insulin Associates with Golgi Membranes of Pancreatic B Cells.” *Proceedings of the National Academy of Sciences of the United States of America* 81 (21): 6743–46.

Orci, L., M. Ravazzola, M. J. Storch, R. G. Anderson, J. D. Vassalli, and A. Perrelet. 1987. "Proteolytic Maturation of Insulin Is a Post-Golgi Event Which Occurs in Acidifying Clathrin-Coated Secretory Vesicles." *Cell* 49 (6): 865–68.
Ostrega, D., K. Polonsky, D. Nagi, J. Yudkin, L. J. Cox, P. M. Clark, and C. N. Hales. 1995. "Measurement of Proinsulin and Intermediates. Validation of Immunoassay Methods by High-Performance Liquid Chromatography." *Diabetes* 44 (4): 437–40.
Oyarce, A. M., and B. A. Eipper. 1993. "Neurosecretory Vesicles Contain Soluble and Membrane-Associated Monofunctional and Bifunctional Peptidylglycine Alpha-Amidating Monooxygenase Proteins." *Journal of Neurochemistry* 60 (3): 1105–14.
Pakdel, Mehrshad, and Julia von Blume. 2018. "Exploring New Routes for Secretory Protein Export from the Trans-Golgi Network." *Molecular Biology of the Cell* 29 (3): 235–40.
Paquet, L., F. Bergeron, A. Boudreault, N. G. Seidah, M. Chrétien, M. Mbikay, and C. Lazure. 1994. "The Neuroendocrine Precursor 7B2 Is a Sulfated Protein Proteolytically Processed by a Ubiquitous Furin-like Convertase." *The Journal of Biological Chemistry* 269 (30): 19279–85.
Payet, Laurie-Anne, Ludovic Pineau, Ellen C. R. Snyder, Jenny Colas, Ahmed Moussa, Brigitte Vannier, Joelle Bigay, et al. 2013. "Saturated Fatty Acids Alter the Late Secretory Pathway by Modulating Membrane Properties." *Traffic* 14 (12): 1228–41.
Perkins, S. N., E. J. Husten, and B. A. Eipper. 1990. "The 108-kDA Peptidylglycine Alpha-Amidating Monooxygenase Precursor Contains Two Separable Enzymatic Activities Involved in Peptide Amidation." *Biochemical and Biophysical Research Communications* 171 (3): 926–32.
Pfützner, Andreas, Eberhard Standl, Cloth Hohberg, Thomas Konrad, Hermann-Josef Strotmann, Georg Lübben, Matthias R. Langenfeld, Jan Schulze, and Thomas Forst. 2005. "IRIS II Study: Intact Proinsulin Is Confirmed as a Highly Specific Indicator for Insulin Resistance in a Large Cross-Sectional Study Design." *Diabetes Technology & Therapeutics* 7 (3): 478–86.
Pimplikar, S. W., and W. B. Huttner. 1992. "Chromogranin B (secretogranin I), a Secretory Protein of the Regulated Pathway, Is Also Present in a Tightly Membrane-Associated Form in PC12 Cells." *The Journal of Biological Chemistry* 267 (6): 4110–18.
Porte, D., Jr, and S. E. Kahn. 1989. "Hyperproinsulinemia and Amyloid in NIDDM. Clues to Etiology of Islet Beta-Cell Dysfunction?" *Diabetes* 38 (11): 1333–36.
Pradhan, Aruna D., Joann E. Manson, James B. Meigs, Nader Rifai, Julie E. Buring, Simin Liu, and Paul M. Ridker. 2003. "Insulin, Proinsulin, Proinsulin:insulin Ratio, and the Risk of Developing Type 2 Diabetes Mellitus in Women." *The American Journal of Medicine* 114 (6): 438–44.
Prentki, Marc, and Christopher J. Nolan. 2006. "Islet Beta Cell Failure in Type 2 Diabetes." *The Journal of Clinical Investigation* 116 (7): 1802–12.
Puertollano, R., R. C. Aguilar, I. Gorshkova, R. J. Crouch, and J. S. Bonifacino. 2001. "Sorting of Mannose 6-Phosphate Receptors Mediated by the GGAs." *Science* 292 (5522): 1712–16.
Rabah, Nadia, Dany Gauthier, Jimmy D. Dikeakos, Timothy L. Reudelhuber, and Claude Lazure. 2007. "The C-Terminal Region of the Proprotein Convertase 1/3 (PC1/3) Exerts a Bimodal Regulation of the Enzyme Activity in Vitro." *The FEBS Journal* 274 (13): 3482–91.
Raleigh, Daniel, Xiaoxue Zhang, Benoît Hastoy, and Anne Clark. 2017. "The β-Cell Assassin: IAPP Cytotoxicity." *Journal of Molecular Endocrinology* 59 (3): R121–40.
Ramzy, Adam, Ali Asadi, and Timothy J. Kieffer. 2020. "Revisiting Proinsulin Processing: Evidence That Human β-Cells Process Proinsulin With Prohormone Convertase (PC) 1/3 but Not PC2." *Diabetes* 69 (7): 1451–62.
Ravazzola, M., P. A. Halban, and L. Orci. 1996. "Inositol 1,4,5-Trisphosphate Receptor Subtype 3 in Pancreatic Islet Cell Secretory Granules Revisited." *Proceedings of the National Academy of Sciences of the United States of America* 93 (7): 2745–48.
Rhodes, C. J., and C. Alarcón. 1994. "What Beta-Cell Defect Could Lead to Hyperproinsulinemia in NIDDM? Some Clues from Recent Advances Made in Understanding the Proinsulin-Processing Mechanism." *Diabetes* 43 (4): 511–17.
Rhodes, C. J., and P. A. Halban. 1987. "Newly Synthesized Proinsulin/insulin and Stored Insulin Are Released from Pancreatic B Cells Predominantly via a Regulated, rather than a Constitutive, Pathway." *The Journal of Cell Biology* 105 (1): 145–53.

Rhodes, C. J., B. Lincoln, and S. E. Shoelson. 1992. “Preferential Cleavage of Des-31,32-Proinsulin over Intact Proinsulin by the Insulin Secretory Granule Type II Endopeptidase. Implication of a Favored Route for Prohormone Processing.” *The Journal of Biological Chemistry* 267 (32): 22719–27.

Rindler, M. J. 1998. “Carboxypeptidase E, a Peripheral Membrane Protein Implicated in the Targeting of Hormones to Secretory Granules, Co-Aggregates with Granule Content Proteins at Acidic pH.” *The Journal of Biological Chemistry* 273 (47): 31180–85.

Rovère, C., J. S. Mort, M. Chrétien, and N. G. Seidah. 2000. “Cathepsin-B Fusion Proteins Misroute Secretory Protein Partners such as the Proprotein Convertase PC2-7B2 Complex toward the Lysosomal Degradation Pathways.” *Biochemical and Biophysical Research Communications* 276 (2): 594–99.

Rulifson, Ingrid C., Ping Cao, Li Miao, David Kopecky, Linda Huang, Ryan D. White, Kim Samayoa, et al. 2016. “Identification of Human Islet Amyloid Polypeptide as a BACE2 Substrate.” *PloS One* 11 (2): e0147254.

Rutter, Guy, Pauline Chabosseau, Elisa A. Bellomo, Wolfgang Maret, Ryan K. Mitchell, David J. Hodson, Antonia Solomou, and Ming Hu. 2016. “Intracellular Zinc in Insulin Secretion and Action: A Determinant of Diabetes Risk?” *The Proceedings of the Nutrition Society* 75 (1): 61–72.

Rutter, Guy, and Fabrice Chimienti. 2014. “SLC30A8 Mutations in Type 2 Diabetes.” *Diabetologia* 58 (1). https://link.springer.com/article/10.1007%2Fs00125-014-3405-7.

Ryaboshapkina, Maria, Kevin Saitoski, Ghaith M. Hamza, Andrew F. Jarnuczak, Séverine Pechberty, Claire Berthault, Kaushik Sengupta, Christina Rye Underwood, Shalini Andersson, and Raphael Scharfmann. 2022. “Characterization of the Secretome, Transcriptome, and Proteome of Human β Cell Line EndoC-βH1.” *Molecular & Cellular Proteomics: MCP* 21 (5): 100229.

Sabatini, Paul V., Thilo Speckmann, and Francis C. Lynn. 2019. “Friend and Foe: β-Cell Ca2+ Signaling and the Development of Diabetes.” *Molecular Metabolism* 21 (March): 1–12.

Sakamoto, Shohei, Takaaki Miyaji, Miki Hiasa, Reiko Ichikawa, Akira Uematsu, Ken Iwatsuki, Atsushi Shibata, et al. 2014. “Impairment of Vesicular ATP Release Affects Glucose Metabolism and Increases Insulin Sensitivity.” *Scientific Reports* 4 (October): 6689.

Schechter, I., and A. Berger. 1967. “On the Size of the Active Site in Proteases. I. Papain.” *Biochemical and Biophysical Research Communications* 27 (2): 157–62.

Scheenen, W. J., C. B. Wollheim, T. Pozzan, and C. Fasolato. 1998. “Ca2+ Depletion from Granules Inhibits Exocytosis. A Study with Insulin-Secreting Cells.” *The Journal of Biological Chemistry* 273 (30): 19002–8.

Schoonderwoert, V. T., J. C. Holthuis, S. Tanaka, S. A. Tooze, and G. J. Martens. 2000. “Inhibition of the Vacuolar H+-ATPase Perturbs the Transport, Sorting, Processing and Release of Regulated Secretory Proteins.” *European Journal of Biochemistry / FEBS* 267 (17): 5646–54.

Seaquist, E. R., S. E. Kahn, P. M. Clark, C. N. Hales, D. Porte Jr, and R. P. Robertson. 1996. “Hyperproinsulinemia Is Associated with Increased Beta Cell Demand after Hemipancreatectomy in Humans.” *The Journal of Clinical Investigation* 97 (2): 455–60.

Seidah, Nabil G., Suzanne Benjannet, Louise Wickham, Jadwiga Marcinkiewicz, Stephanie Belanger Jasmin, Stefano Stifani, Ajoy Basak, Annik Prat, and Michel Chretien. 2003. “The Secretory Proprotein Convertase Neural Apoptosis-Regulated Convertase 1 (NARC-1): Liver Regeneration and Neuronal Differentiation.” *Proceedings of the National Academy of Sciences of the United States of America* 100 (3): 928–33.

Seidah, Nabil G., Mohamad S. Sadr, Michel Chrétien, and Majambu Mbikay. 2013. “The Multifaceted Proprotein Convertases: Their Unique, Redundant, Complementary, and Opposite Functions.” *The Journal of Biological Chemistry* 288 (30): 21473–81.

Shami, Gerald, Delfine Cheng, Jeffrey Henriquez, and Filip Braet. 2014. “Assessment of Different Fixation Protocols on the Presence of Membrane-Bound Vesicles in Caco-2 Cells: A Multidimensional View by Means of Correlative Light and 3-D Transmission Electron Microscopy.” *Micron* 67 (December): 20–29.

Shennan, K. I., N. A. Taylor, and K. Docherty. 1994. “Calcium- and pH-Dependent Aggregation and Membrane Association of the Precursor of the Prohormone Convertase PC2.” *The Journal of Biological Chemistry* 269 (28): 18646–50.

Shennan, K. I., N. A. Taylor, J. L. Jermany, G. Matthews, and K. Docherty. 1995. “Differences in pH Optima and Calcium Requirements for Maturation of the Prohormone Convertases PC2 and PC3 Indicates Different Intracellular Locations for These Events.” *The Journal of Biological Chemistry* 270 (3): 1402–7.

Sizonenko, S., and P. A. Halban. 1991. “Differential Rates of Conversion of Rat Proinsulins I and II. Evidence for Slow Cleavage at the B-chain/C-Peptide Junction of Proinsulin II.” *Biochemical Journal* 278 (Pt 3) (September): 621–25.

Sizonenko, S., J. C. Irminger, L. Buhler, S. Deng, P. Morel, and P. A. Halban. 1993. “Kinetics of Proinsulin Conversion in Human Islets.” *Diabetes* 42 (6): 933–36.

Skovsø, Søs, Peter Overby, Jasmine Memar-Zadeh, Jason Lee, Iryna Shanina, Vaibhav Sidarala, Elena Levi-D’Ancona, et al. 2022. “Beta-Cell Cre Expression and Reduced Ins1 Gene Dosage Protect Mice from Type 1 Diabetes.” *bioRxiv*. https://doi.org/10.1101/2022.02.03.479027.

Slepchenko, Kira G., Nigel A. Daniels, Aili Guo, and Yang V. Li. 2015. “Autocrine Effect of Zn^{2+} on the Glucose-Stimulated Insulin Secretion.” *Endocrine* 50 (1): 110–22.

Slepchenko, Kira G., Calvin B. L. James, and Yang V. Li. 2013. “Inhibitory Effect of Zinc on Glucose-Stimulated Zinc/insulin Secretion in an Insulin-Secreting β-Cell Line.” *Experimental Physiology* 98 (8): 1301–11.

Smeekens, S. P., A. G. Montag, G. Thomas, C. Albiges-Rizo, R. Carroll, M. Benig, L. A. Phillips, S. Martin, S. Ohagi, and P. Gardner. 1992. “Proinsulin Processing by the Subtilisin-Related Proprotein Convertases Furin, PC2, and PC3.” *Proceedings of the National Academy of Sciences of the United States of America* 89 (18): 8822–26.

Smidt, Kamille, Agnete Larsen, Andreas Brønden, Karen S. Sørensen, Julie V. Nielsen, Jeppe Praetorius, Pia M. Martensen, and Jørgen Rungby. 2016. “The Zinc Transporter ZNT3 Co-Localizes with Insulin in INS-1E Pancreatic Beta Cells and Influences Cell Survival, Insulin Secretion Capacity, and ZNT8 Expression.” *Biometals: An International Journal on the Role of Metal Ions in Biology, Biochemistry, and Medicine* 29 (2): 287–98.

Song, L., and L. D. Fricker. 1995. “Calcium- and pH-Dependent Aggregation of Carboxypeptidase E.” *The Journal of Biological Chemistry* 270 (14): 7963–67.

Steiner, D. F. 1973. “Cocrystallization of Proinsulin and Insulin.” *Nature* 243 (June): 528–30.

Stephens, Samuel B., Robert J. Edwards, Masato Sadahiro, Wei-Jye Lin, Cheng Jiang, Stephen R. Salton, and Christopher B. Newgard. 2017. “The Prohormone VGF Regulates β Cell Function via Insulin Secretory Granule Biogenesis.” *Cell Reports* 20 (10): 2480–89.

Stiernet, Patrick, Yves Guiot, Patrick Gilon, and Jean-Claude Henquin. 2006. “Glucose Acutely Decreases pH of Secretory Granules in Mouse Pancreatic Islets. Mechanisms and Influence on Insulin Secretion.” *The Journal of Biological Chemistry* 281 (31): 22142–51.

Storto, Marianna, Loredana Capobianco, Giuseppe Battaglia, Gemma Molinaro, Roberto Gradini, Barbara Riozzi, Alessandra Di Mambro, et al. 2006. “Insulin Secretion Is Controlled by mGlu5 Metabotropic Glutamate Receptors.” *Molecular Pharmacology* 69 (4): 1234–41.

Stridsberg, M., S. Sandler, and E. Wilander. 1993. “Cosecretion of Islet Amyloid Polypeptide (IAPP) and Insulin from Isolated Rat Pancreatic Islets Following Stimulation or Inhibition of Beta-Cell Function.” *Regulatory Peptides* 45 (3): 363–70.

Sun, Meng, Tsuyoshi Watanabe, Hiroki Bochimoto, Yuko Sakai, Seiji Torii, Toshiyuki Takeuchi, and Masahiro Hosaka. 2013. “Multiple Sorting Systems for Secretory Granules Ensure the Regulated Secretion of Peptide Hormones.” *Traffic* 14 (2): 205–18.

Sun-Wada, Ge-Hong, Takao Toyomura, Yoshiko Murata, Akitsugu Yamamoto, Masamitsu Futai, and Yoh Wada. 2006. “The a3 Isoform of V-ATPase Regulates Insulin Secretion from Pancreatic Beta-Cells.” *Journal of Cell Science* 119 (Pt 21): 4531–40.

Su, Xiong, and Nada A. Abumrad. 2009. “Cellular Fatty Acid Uptake: A Pathway under Construction.” *Trends in Endocrinology and Metabolism: TEM* 20 (2): 72–77.

Su, Ya, Aiwu Zhou, Rafia S. Al-Lamki, and Fiona E. Karet. 2003. “The a-Subunit of the V-Type H+-ATPase Interacts with Phosphofructokinase-1 in Humans.” *The Journal of Biological Chemistry* 278 (22): 20013–18.

Syring, Kristen E., Kayla A. Boortz, James K. Oeser, Alessandro Ustione, Kenneth A. Platt, Melanie K. Shadoan, Owen P. McGuinness, David W. Piston, David R. Powell, and Richard M. O'Brien. 2016. "Combined Deletion of Slc30a7 and Slc30a8 Unmasks a Critical Role for ZnT8 in Glucose-Stimulated Insulin Secretion." *Endocrinology* 157 (12): 4534–41.

Syring, Kristen E., Karin J. Bosma, Slavina B. Goleva, Kritika Singh, James K. Oeser, Christopher A. Lopez, Eric P. Skaar, et al. 2020. "Potential Positive and Negative Consequences of ZnT8 Inhibition." *The Journal of Endocrinology* 246 (2): 189–205.

Takahashi, Harumi, Norihide Yokoi, and Susumu Seino. 2019. "Glutamate as Intracellular and Extracellular Signals in Pancreatic Islet Functions." *Proceedings of the Japan Academy. Series B, Physical and Biological Sciences* 95 (6): 246–60.

Tamaki, Motoyuki, Yoshio Fujitani, Akemi Hara, Toyoyoshi Uchida, Yoshifumi Tamura, Kageumi Takeno, Minako Kawaguchi, et al. 2013. "The Diabetes-Susceptible Gene SLC30A8/ZnT8 Regulates Hepatic Insulin Clearance." *The Journal of Clinical Investigation* 123 (10): 4513–24.

Taupenot, Laurent, Kimberly L. Harper, and Daniel T. O'Connor. 2005. "Role of H+-ATPase-Mediated Acidification in Sorting and Release of the Regulated Secretory Protein Chromogranin A: Evidence for a Vesiculogenic Function." *The Journal of Biological Chemistry* 280 (5): 3885–97.

Taylor, Colin W., and Vera Konieczny. 2016. "IP3 Receptors: Take Four IP3 to Open." *Science Signaling* 9 (422): e1.

Taylor, Colin W., and Stephen C. Tovey. 2010. "IP(3) Receptors: Toward Understanding Their Activation." *Cold Spring Harbor Perspectives in Biology* 2 (12): a004010.

Thomas, L., R. Leduc, B. A. Thorne, S. P. Smeekens, D. F. Steiner, and G. Thomas. 1991. "Kex2-like Endoproteases PC2 and PC3 Accurately Cleave a Model Prohormone in Mammalian Cells: Evidence for a Common Core of Neuroendocrine Processing Enzymes." *Proceedings of the National Academy of Sciences of the United States of America* 88 (12): 5297–5301.

Thomsen, Soren K., Anne Raimondo, Benoit Hastoy, Shahana Sengupta, Xiao-Qing Dai, Austin Bautista, Jenny Censin, et al. 2018. "Type 2 Diabetes Risk Alleles in PAM Impact Insulin Release from Human Pancreatic β-Cells." *Nature Genetics* 50 (8): 1122–31.

Thorens, Bernard, David Tarussio, Miguel Angel Maestro, Meritxell Rovira, Eija Heikkilä, and Jorge Ferrer. 2015. "Ins1(Cre) Knock-in Mice for Beta Cell-Specific Gene Recombination." *Diabetologia* 58 (3): 558–65.

Thurmond, Debbie C., and Herbert Y. Gaisano. 2020. "Recent Insights into Beta-Cell Exocytosis in Type 2 Diabetes." *Journal of Molecular Biology* 432 (5): 1310–25.

Tumarada, Nirmala, Li Li, Shi Bai, and Christian T. Sheline. 2017. "hZnT8 (Slc30a8) Transgenic Mice That Overexpress the R325W Polymorph Have Reduced Islet Zn2+ and Proinsulin Levels, Increased Glucose Tolerance After a High-Fat Diet, and Altered Levels of Pancreatic Zinc Binding Proteins." *Diabetes* 66 (2): 551–59.

Uenishi, Eita, Tadao Shibasaki, Harumi Takahashi, Chihiro Seki, Hitomi Hamaguchi, Takao Yasuda, Masao Tatebe, Yutaka Oiso, Tadaomi Takenawa, and Susumu Seino. 2013. "Actin Dynamics Regulated by the Balance of Neuronal Wiskott-Aldrich Syndrome Protein (N-WASP) and Cofilin Activities Determines the Biphasic Response of Glucose-Induced Insulin Secretion." *The Journal of Biological Chemistry* 288 (36): 25851–64.

Uniprot Consortium. 2022. "Cab45 (Q9BRK5)." 2022. https://www.uniprot.org/uniprotkb/Q9BRK5/entry.

Vangipurapu, Jagadish, Alena Stančáková, Teemu Kuulasmaa, Johanna Kuusisto, and Markku Laakso. 2015. "Both Fasting and Glucose-Stimulated Proinsulin Levels Predict Hyperglycemia and Incident Type 2 Diabetes: A Population-Based Study of 9,396 Finnish Men." *PloS One* 10 (4): e0124028.

Vasiljević, Jovana, Juha M. Torkko, Klaus-Peter Knoch, and Michele Solimena. 2020. "The Making of Insulin in Health and Disease." *Diabetologia* 63 (10): 1981–89.

Verchere, C. B., M. Paoletta, M. Neerman-Arbez, K. Rose, J. C. Irminger, R. L. Gingerich, S. E. Kahn, and P. A. Halban. 1996. "Des-(27-31)C-Peptide. A Novel Secretory Product of the Rat Pancreatic Beta Cell Produced by Truncation of Proinsulin Connecting Peptide in Secretory Granules." *The Journal of Biological Chemistry* 271 (44): 27475–81.

Vinkenborg, Jan L., Tamara J. Nicolson, Elisa A. Bellomo, Melissa S. Koay, Guy A. Rutter, and Maarten Merkx. 2009. “Genetically Encoded FRET Sensors to Monitor Intracellular Zn2+ Homeostasis.” *Nature Methods* 6 (10): 737–40.

Wang, Hui, and Daniel P. Raleigh. 2014. “The Ability of Insulin to Inhibit the Formation of Amyloid by pro-Islet Amyloid Polypeptide Processing Intermediates Is Significantly Reduced in the Presence of Sulfated Glycosaminoglycans.” *Biochemistry* 53 (16): 2605–14.

Wang, J., J. Xu, J. Finnerty, M. Furuta, D. F. Steiner, and C. B. Verchere. 2001. “The Prohormone Convertase Enzyme 2 (PC2) Is Essential for Processing pro-Islet Amyloid Polypeptide at the NH2-Terminal Cleavage Site.” *Diabetes* 50 (3): 534–39.

Wang, T. Y., and J. R. Silvius. 2000. “Different Sphingolipids Show Differential Partitioning into Sphingolipid/cholesterol-Rich Domains in Lipid Bilayers.” *Biophysical Journal* 79 (3): 1478–89.

Wang, Y., C. Thiele, and W. B. Huttner. 2000. “Cholesterol Is Required for the Formation of Regulated and Constitutive Secretory Vesicles from the Trans-Golgi Network.” *Traffic* 1 (12): 952–62.

Wang, Z, Eunjin Oh, D Wade Clapp, Jonathan Chernoff, Debbie C Thurmond. 2011. “Inhibition or Ablation of p21-Activated Kinase (PAK1)Disrupts Glucose Homeostatic Mechanismsin Vivo.” *J. Biol. Chem.*, December. https://www.ncbi.nlm.nih.gov/pmc/articles/PMC3308848/.

Wang, Z., and Debbie C. Thurmond. 2009. “Mechanisms of Biphasic Insulin-Granule Exocytosis - Roles of the Cytoskeleton, Small GTPases and SNARE Proteins.” *Journal of Cell Science* 122 (Pt 7): 893–903.

Ward, W. K., E. C. LaCava, T. L. Paquette, J. C. Beard, B. J. Wallum, and D. Porte Jr. 1987. “Disproportionate Elevation of Immunoreactive Proinsulin in Type 2 (non-Insulin-Dependent) Diabetes Mellitus and in Experimental Insulin Resistance.” *Diabetologia* 30 (9): 698–702.

Weir, Gordon C., and Susan Bonner-Weir. 2004. “Five Stages of Evolving Beta-Cell Dysfunction during Progression to Diabetes.” *Diabetes* 53 Suppl 3 (December): S16–21.

Weiss, Michael, Donald F. Steiner, and Louis H. Philipson. 2014. “Insulin Biosynthesis, Secretion, Structure, and Structure-Activity Relationships.” In *Endotext*, edited by Kenneth R. Feingold, Bradley Anawalt, Alison Boyce, George Chrousos, Kathleen Dungan, Ashley Grossman, Jerome M. Hershman, et al. South Dartmouth (MA): MDText.com, Inc.

Westermark, G. T., D. F. Steiner, S. Gebre-Medhin, U. Engström, and P. Westermark. 2000. “Pro Islet Amyloid Polypeptide (ProIAPP) Immunoreactivity in the Islets of Langerhans.” *Upsala Journal of Medical Sciences* 105 (2): 97–106.

Westermark, P., U. Engström, K. H. Johnson, G. T. Westermark, and C. Betsholtz. 1990. “Islet Amyloid Polypeptide: Pinpointing Amino Acid Residues Linked to Amyloid Fibril Formation.” *Proceedings of the National Academy of Sciences of the United States of America* 87 (13): 5036–40.

Westermark, P., U. Engström, G. T. Westermark, K. H. Johnson, J. Permerth, and C. Betsholtz. 1989. “Islet Amyloid Polypeptide (IAPP) and pro-IAPP Immunoreactivity in Human Islets of Langerhans.” *Diabetes Research and Clinical Practice* 7 (3): 219–26.

Westermark, Per, Arne Andersson, and Gunilla T. Westermark. 2011. “Islet Amyloid Polypeptide, Islet Amyloid, and Diabetes Mellitus.” *Physiological Reviews* 91 (3): 795–826.

Westermark, P., and L. Grimelius. 1973. “The Pancreatic Islet Cells in Insular Amyloidosis in Human Diabetic and Non-Diabetic Adults.” *Acta Pathologica et Microbiologica Scandinavica. Section A, Pathology* 81 (3): 291–300.

Westermark, P., Z. C. Li, G. T. Westermark, A. Leckström, and D. F. Steiner. 1996. “Effects of Beta Cell Granule Components on Human Islet Amyloid Polypeptide Fibril Formation.” *FEBS Letters* 379 (3): 203–6.

Westermark, P., and E. Wilander. 1978. “The Influence of Amyloid Deposits on the Islet Volume in Maturity Onset Diabetes Mellitus.” *Diabetologia* 15 (5): 417–21.

Wicksteed, Barton, Marcela Brissova, Wenbo Yan, Darren M. Opland, Jennifer L. Plank, Rachel B. Reinert, Lorna M. Dickson, et al. 2010. “Conditional Gene Targeting in Mouse Pancreatic ß-Cells: Analysis of Ectopic Cre Transgene Expression in the Brain.” *Diabetes* 59 (12): 3090–98.

Wollam, Joshua, Sumana Mahata, Matthew Riopel, Angelina Hernandez-Carretero, Angshuman Biswas, Gautam K. Bandyopadhyay, Nai-Wen Chi, et al. 2017. “Chromogranin A Regulates Vesicle Storage and Mitochondrial Dynamics to Influence Insulin Secretion.” *Cell and Tissue Research* 368 (3): 487–501.

Xu, Jie, Nadeeja Wijesekara, Romario Regeenes, Dana Al Rijjal, Anthony L. Piro, Youchen Song, Anne Wu, et al. 2021. “Pancreatic β Cell-Selective Zinc Transporter 8 Insufficiency Accelerates Diabetes Associated with Islet Amyloidosis.” *JCI Insight* 6 (10). https://doi.org/10.1172/jci.insight.143037.

Yagui, K., T. Yamaguchi, A. Kanatsuka, F. Shimada, C. I. Huang, Y. Tokuyama, H. Ohsawa, K. Yamamura, J. Miyazaki, and A. Mikata. 1995. “Formation of Islet Amyloid Fibrils in Beta-Secretory Granules of Transgenic Mice Expressing Human Islet Amyloid Polypeptide/amylin.” *European Journal of Endocrinology / European Federation of Endocrine Societies* 132 (4): 487–96.

Yang, Ying, Min Wang, Jingzhi Tong, Zuoliang Dong, Min Deng, Xiaojun Ren, Hui Li, et al. 2019. “Impaired Glucose-Stimulated Proinsulin Secretion Is an Early Marker of β-Cell Impairment Before Prediabetes Stage.” *The Journal of Clinical Endocrinology and Metabolism* 104 (10): 4341–46.

Yau, Belinda, Samantha Hocking, Sofianos Andrikopoulos, and Melkam A. Kebede. 2021. “Targeting the Insulin Granule for Modulation of Insulin Exocytosis.” *Biochemical Pharmacology* 194 (December): 114821.

Yonemoto, Isaac T., Gerard J. A. Kroon, H. Jane Dyson, William E. Balch, and Jeffery W. Kelly. 2008. “Amylin Proprotein Processing Generates Progressively More Amyloidogenic Peptides That Initially Sample the Helical State.” *Biochemistry* 47 (37): 9900–9910.

Yoo, S. H. 2000. “Coupling of the IP3 receptor/Ca2+ Channel with Ca2+ Storage Proteins Chromogranins A and B in Secretory Granules.” *Trends in Neurosciences* 23 (9): 424–28.

Yoo, S. H. 2010. “Secretory Granules in Inositol 1,4,5-Trisphosphate-Dependent Ca2+ Signaling in the Cytoplasm of Neuroendocrine Cells.” *FASEB Journal: Official Publication of the Federation of American Societies for Experimental Biology* 24 (3): 653–64.

Yoo, S. H., and J. P. Albanesi. 1991. “High Capacity, Low Affinity Ca2+ Binding of Chromogranin A. Relationship between the pH-Induced Conformational Change and Ca2+ Binding Property.” *The Journal of Biological Chemistry* 266 (12): 7740–45.

Yoo, S. H., Sei Yoon Chu, Ki Deok Kim, and Yang Hoon Huh. 2007. “Presence of Secretogranin II and High-Capacity, Low-Affinity Ca2+ Storage Role in Nucleoplasmic Ca2+ Store Vesicles.” *Biochemistry* 46 (50): 14663–71.

Yoo, S. H., and C. J. Jeon. 2000. “Inositol 1,4,5-Trisphosphate receptor/Ca2+ Channel Modulatory Role of Chromogranin A, a Ca2+ Storage Protein of Secretory Granules.” *The Journal of Biological Chemistry* 275 (20): 15067–73.

Yoo, S. H., and M. S. Lewis. 1995. “Thermodynamic Study of the pH-Dependent Interaction of Chromogranin A with an Intraluminal Loop Peptide of the Inositol 1,4,5-Trisphosphate Receptor.” *Biochemistry* 34 (2): 632–38.

Yoo, S. H., and M. S. Lewis. 1996. “Effects of pH and Ca2+ on Heterodimer and Heterotetramer Formation by Chromogranin A and Chromogranin B.” *The Journal of Biological Chemistry* 271 (29): 17041–46.

Yoo, S. H., and M. S. Lewis. 2000. “Interaction of Chromogranin B and the near N-Terminal Region of Chromogranin B with an Intraluminal Loop Peptide of the Inositol 1,4, 5-Trisphosphate Receptor.” *The Journal of Biological Chemistry* 275 (39): 30293–300.

Yoo, S. H., Young Soo Oh, Moon Kyung Kang, Yang Hoon Huh, Seung Ho So, Hyung Seon Park, and Hee Yun Park. 2001. “Localization of Three Types of the Inositol 1,4,5-Trisphosphate Receptor/Ca2+ Channel in the Secretory Granules and Coupling with the Ca2+ Storage Proteins Chromogranins A and B*.” *The Journal of Biological Chemistry* 276 (49): 45806–12.

Yoo, S. H., S. H. So, H. S. Kweon, J. S. Lee, M. K. Kang, and C. J. Jeon. 2000. “Coupling of the Inositol 1,4,5-Trisphosphate Receptor and Chromogranins A and B in Secretory Granules.” *The Journal of Biological Chemistry* 275 (17): 12553–59.

Yoshino, Hiroshi, Kyoko Kawakami, Gen Yoshino, and Takahisa Hirose. 2018. “Age-Related Changes of Proinsulin Processing in Diabetic and Non-Diabetic Japanese Individuals.” *Geriatrics & Gerontology International* 18 (7): 1046–50.

Zhang, Yi, You-Hou Kang, Nathan Chang, Patrick P. L. Lam, Yunfeng Liu, Vesa M. Olkkonen, and Herbert Y. Gaisano. 2009. “Cab45b, a Munc18b-Interacting Partner, Regulates Exocytosis in Pancreatic Beta-Cells.” *The Journal of Biological Chemistry* 284 (31): 20840–47.

Zhao, Hai-Lu, Fernand M. M. Lai, Peter C. Y. Tong, Ding-Rong Zhong, Di Yang, Brian Tomlinson, and Juliana C. N. Chan. 2003. “Prevalence and Clinicopathological Characteristics of Islet Amyloid in Chinese Patients with Type 2 Diabetes.” *Diabetes* 52 (11): 2759–66.

Zhao, Ruxuan, Jing Lu, Qi Li, Fengran Xiong, Yingchao Zhang, Juanjuan Zhu, Gongxin Peng, and Jinkui Yang. 2021. “Single-Cell Heterogeneity Analysis and CRISPR Screens in MIN6 Cell Line Reveal Transcriptional Regulators of Insulin.” *Cell Cycle* 20 (19): 2053–65.

Zheng, Xiaoya, Wei Ren, Suhua Zhang, Jingjing Liu, Sufang Li, Jinchao Li, Ping Yang, Jun He, Shaochu Su, and Ping Li. 2010. “Serum Levels of Proamylin and Amylin in Normal Subjects and Patients with Impaired Glucose Regulation and Type 2 Diabetes Mellitus.” *Acta Diabetologica* 47 (3): 265–70.

Zhou, A., and R. E. Mains. 1994. “Endoproteolytic Processing of Proopiomelanocortin and Prohormone Convertases 1 and 2 in Neuroendocrine Cells Overexpressing Prohormone Convertases 1 or 2.” *The Journal of Biological Chemistry* 269 (26): 17440–47.

Zhou, Huarong, Tao Zhang, Jamie S. Harmon, Joseph Bryan, and R. Paul Robertson. 2007. “Zinc, Not Insulin, Regulates the Rat Alpha-Cell Response to Hypoglycemia in Vivo.” *Diabetes* 56 (4): 1107–12.

Zhou, Y., and I. Lindberg. 1993. “Purification and Characterization of the Prohormone Convertase PC1(PC3).” *The Journal of Biological Chemistry* 268 (8): 5615–23.

Zhou, Y., and I. Lindberg. 1994. “Enzymatic Properties of Carboxyl-Terminally Truncated Prohormone Convertase 1 (PC1/SPC3) and Evidence for Autocatalytic Conversion.” *The Journal of Biological Chemistry* 269 (28): 18408–13.

Zhu, X, Lelio Orci, Raymond Carroll, Christina Norrbom, Mariella Ravazzola, and Donald F. Steiner. 2002. “Severe Block in Processing of Proinsulin to Insulin Accompanied by Elevation of Des-64,65 Proinsulin Intermediates in Islets of Mice Lacking Prohormone Convertase 1/3.” *Proceedings of the National Academy of Sciences of the United States of America* 99 (16): 10299–304.

Zhu, X., Y. Rouille, N. S. Lamango, D. F. Steiner, and I. Lindberg. 1996. “Internal Cleavage of the Inhibitory 7B2 Carboxyl-Terminal Peptide by PC2: A Potential Mechanism for Its Inactivation.” *Proceedings of the National Academy of Sciences of the United States of America* 93 (10): 4919–24.

Zhu, Yunfeng, Quanli Wang, Wangru Xu, and Sha Li. 2008. “The Ethanol Response Gene Cab45 Can Modulate the Impairment Elicited by Ethanol and Ultraviolet in PC12 Cells.” *Journal of Genetics and Genomics = Yi Chuan Xue Bao* 35 (3): 153–61.

Zimmerman, A. E., D. I. Kells, and C. C. Yip. 1972. “Physical and Biological Properties of Guinea Pig Insulin.” *Biochemical and Biophysical Research Communications* 46 (6): 2127–33.